CHROMATOGRAPHY OF PARTICLE SUSPENSIONS

by

© Aamir Husain, B.Tech., M.Eng.

A Thesis

Submitted to the School of Graduate Studies
in Partial Fulfilment of the Requirements
for the degree

Doctor of Philosophy

McMaster University
October, 1980

This thesis is dedicated

to my wife, Rasheeda

Doctor of Philosophy
(Chemical Engineering)

McMaster University
Hamilton, Ontario

Title	:	Chromatography of Particle Suspensions
Author	:	Aamir Husain, B.Tech. (I.I.T., Kharagpur, India); M.Eng. (McMaster University)
Supervisors	:	Dr. A.E. Hamielec, Dr. J. Vlachopoulos
Number of Pages	:	xviii, 210.

ABSTRACT

In recent years, a number of chromatographic techniques have been reported to measure the size of submicron particles. Little of the published work has dealt with the quantitative estimation of particle size, efforts, largely, having been directed in demonstrating the capability to resolve colloid peaks. Ability to make quantitative measurements is a prime requirement for any analytical tool and this is the problem that is addressed in this work.

Common to all the chromatographic techniques is the phenomenon of axial dispersion which disperses a colloid over a finite interval centered around its mean residence time or retention volume. The response to a pulse of monodispersed colloid is a bell shaped chromatogram, the shape of which along with the peak separation capability of the instrument, determine for a given detector, the type of analysis by which raw measured data have to be processed. The analysis may be of two types. The first, applies correction factors to moments calculated directly from the measured chromatogram to account for axial dispersion, while, the second approach allows a calculation of the moments of the diameter distribution of particles which at any instant occupy the detector cell. Besides developing the various methods for treating chromatographic data in detail, the problem of determining the response to a pulse of monodispersed colloid has been attempted. Experimentally, such information can be determined only with some difficulty, owing to the unavailability of very narrow distribution

standards.

Experiments were conducted using a size exclusion chromatograph equipped with a turbidity detector. The performance of the turbidity detector was critically evaluated. A column calibration procedure has been attempted which minimises material loss, significantly reduces the extent of axial dispersion and improves peak separation. The theoretical analyses discussed earlier were applied to experimental chromatograms of polystyrene latices with very encouraging results.

ACKNOWLEDGEMENTS

The author wishes to thank:

Drs. A.E. Hamielec and J. Vlachopoulos for their supervision,

Dr. T.B. MacRury for making available some of his data,

My friend and colleague, Dr. L.H. Garcia for some useful discussions,

Mrs. Amy Stott for her care and patience in typing this thesis,

Family members for their affection and moral support,

My friends, Kalpana Raina and Tariq Rizvi for their invaluable help in proof-reading this manuscript,

The Department of Chemical Engineering, McMaster University and the Petroleum Research Fund for providing financial assistance,

My wife, for her patience and understanding.

TABLE OF CONTENTS

LIST OF FIGURES

LIST OF TABLES

NOMENCLATURE

a	Radius of particle
A	Area, Optical density
c	Concentration
C	Concentration, Cross-section
d	Diffusion coefficient
D	Diameter of particle
$\bar{D}$	Diameter of packing particle
f	Diameter frequency distribution
F	Force, measured chromatogram
$\bar{F}$	Laplace transform of F, the measured chromatogram
G	Instrumental spreading function
$\bar{G}$	Laplace transform of G
I	Intensity of light beam
K	Extinction coefficient
K_{abs}	Absorption coefficient
K_{sca}	Scattering coefficient
ℓ	Optical path length
L	Length of capillary
M_k	kth moment of the diameter frequency distribution
n	Number of capillaries
N	Number concentration of particles
P	Pressure
Q	Flow-rate

r	Radial distance
R	Radius of capillary
R_F	Separation factor
$\bar{t}$	Mean residence time
T	Temperature
v	velocity, retention volume
$\bar{v}$	average velocity
V	Volume
w	width of channel
W	True chromatogram
$\bar{W}$	Laplace transform of W
y	Mean retention volume
z	Axial distance

Greek Letters

ϵ	Absorbance
η	Viscosity, refractive index
κ	Boltzmann's constant
λ	Wavelength of light
ρ	Density
τ	Turbidity
ϕ	Interaction energy, volume fraction

Subscripts

c	Correct
f	Fluid

ic	Capillaries representing the interstitial volume
m	Medium
n	Number average
p	Particle
pc	Capillaries representing the pore volume
s	System, surface average
ss	Specific surface average
t	Turbidity average
uc	Uncorrect
v	Volume average
w	Weight average

CHAPTER 1

INTRODUCTION TO THE CHROMATOGRAPHY OF PARTICLE SUSPENSIONS

1.1 GENERAL BACKGROUND

The importance of an accurate measurement of particle size and particle size distribution needs hardly be mentioned. The control of particle size by means of reproducible, accurate and fairly simple analysis is of primary importance in far reaching technological areas. Techniques such as electron microscopy, light scattering, centrifugation and small angle x-ray scattering have been used to determine particle size distributions of colloidal dispersions but are time consuming and unsuitable as online quality control methods. Different methods for particle size measurement have been discussed in several sources [Groves (1974),(1978),(1980); Groves et al (1968),(1972); Allen (1975)] and will not be discussed here. The main concern here is to examine various methods based on chromatographic principles, that have evolved in recent years, for the size measurement of particle suspensions in the submicron range.

Chromatography has until recently been concerned exclusively with the separation of matter at the molecular level. One result of this restriction to the molecular domain is that, from a practical point of view, chromatographic methods invariably deal with species in solution. Recently , however, chromatographic separations have been reported where the materials resolved are in suspension rather than in solution. Four major areas of particle chromatography have evolved; non-porous packed

systems - hydrodynamic chromatography (HDC), porous packed systems - size exclusion chromatogrphy (SEC), open capillary tubular systems - capillary chromatography (CPC), and field-flow fractionation (FFF). The first reported investigations on HDC, SEC and CPC appeared in the works of Small (1974), Krebs and Wunderlich (1971), and Noel et al (1978) respectively. FFF has been pioneered by Giddings who has published extensively on the subject. Unlike in HDC and SEC, separation in CPC and FFF occur in one phase instead of two. All these chromatographic systems basically involve an assembly consisting of a mobile phase reservoir, pump, pressure gauge, sample injection valve, column(s), detector, flow-rate gauge and recorder (Fig. 1.1).

In HDC, particle separation arises predominantly from an interaction between the finite particle size and the mobile phase interstitial velocity profile. This results in a size gradation such that the larger particles elute ahead of the smaller particles followed by the eluant. The eluant is generally ionic. At low ionic strength, separation occurs solely according to size as described, while, at high ionic strength, a reversal of flow separation may occur, with the smaller particles eluting first and in addition, separation becomes possible not only based on differences in size but also in composition. The high ionic strength limit of HDC has been termed potential barrier chromatography [Ruckenstein (1976)].

The object of using porous packing, SEC, has been to improve resolution over the non-porous HDC system by super-imposing a steric exclusion effect on the flow separation. Particles smaller than the

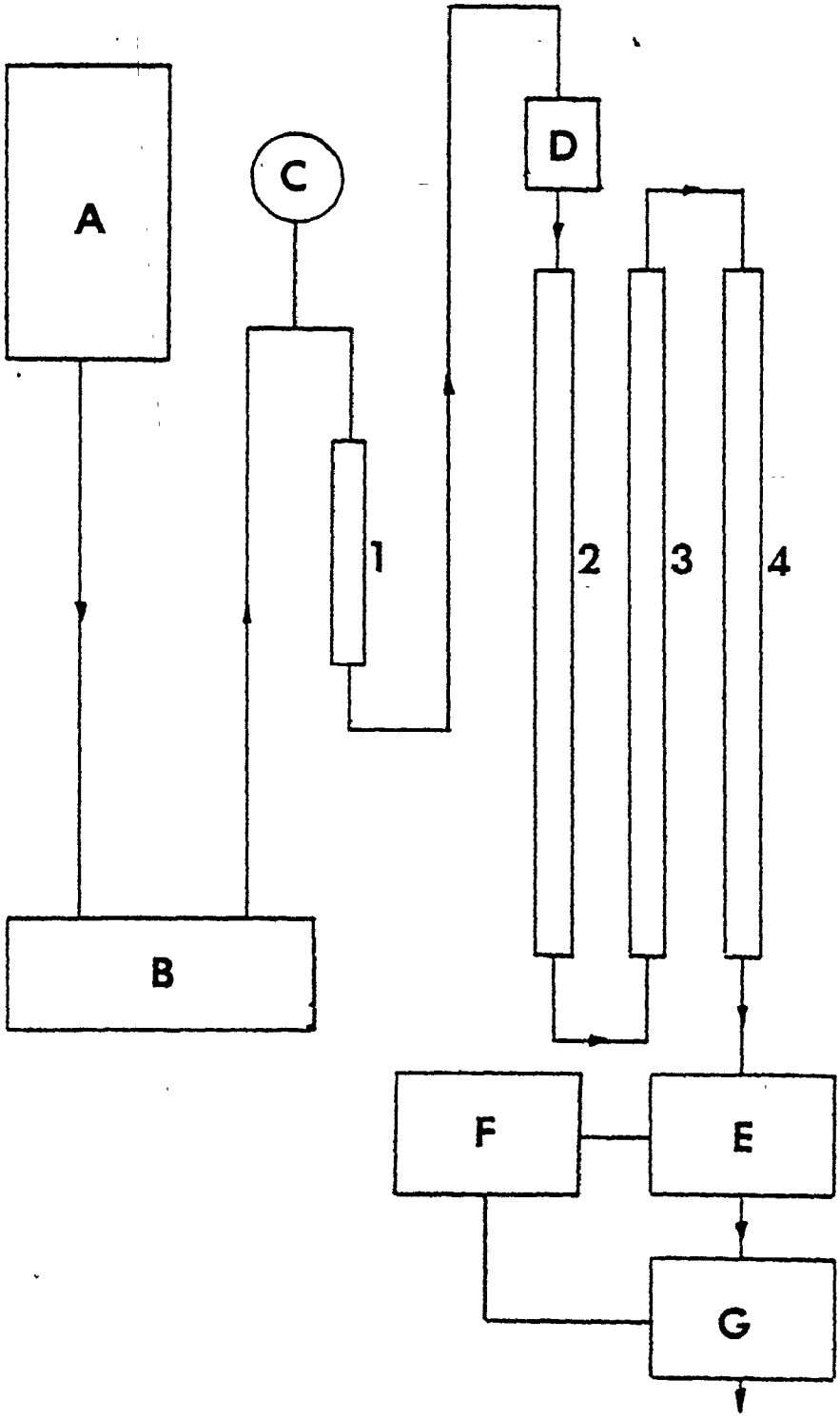

Fig. 1.1 Schematic diagram of chromatographic apparatus. A. Reservoir B. Pump C. Pressure gauge D. Sample injection valve E. Detector F. Recorder G. Flow-rate gauge. Column 1 serves as a prefilter and to dampen pressure pulses. Columns 2, 3, & 4 are the separation columns.

pore diameter can diffuse into the pores giving a second and more efficient mechanism of retardation and size separation.

Particle separation by CPC is a promising method for fractionation of particles, particularly for sizes greater than 1 μ. Separation is achieved in narrow cylindrical capillaries of approximately 0.4 mm diameter, which is considerably larger than the equivalent capillary diameter of the packed beds in HDC or SEC. As with the packed beds, larger particles travel through the capillary at a faster rate; in contrast to HDC or SEC where the separation involves Brownian motion of submicron particles, CPC shows increased resolution for particles greater than 1 μ due to non-Brownian effects.

As the name suggests, FFF uses the coupling of a body force field with a flow profile to achieve differential migration. The carrier velocity should be slow enough such that laminar flow is ensured and the channel width is required to be small in order to give pronounced velocity differences with small differences in distance from the wall. The force field which can be electrical, magnetic, gravitational, thermal etc. in nature, causes the solute molecules to accumulate in a layer of unique thickness near one channel wall. The solute is then transported by flow along the channel at a rate fixed by the mean thickness of the layer. Small particles migrate in advance of large particles and emerge from the channel first, in contrast to the elution behaviour in the other systems. As the field strength is increased, the particles are pushed with increasing firmness against the wall. Steric FFF is realized when the mean Brownian displacement from the wall

becomes less than the particle radius and larger particles begin to elute first due to a purely hydrodynamic effect. Two sub-techniques, sedimentation and flow FFF have shown the greatest promise for particle separation and characterization.

1.2 PEAK SEPARATION AND PEAK BROADENING

The passage of an injected sample through the columns and detector generates an output trace on the recorder called a chromatogram. For several reasons, to be outlined, a chromatogram can never fully represent the distribution of colloid sizes in the injected sample. Instrumental spreading or axial dispersion causes elution of a single species to occur over a range of retention volumes. The chromatogram of the sample is the superposition of these distributions. When the number of species are few, one might obtain a chromatogram involving many obvious but overlapping peaks. However, with a large number of species, the peaks of individual species are not evident; one usually obtains a unimodal chromatogram and sometimes a more complex one. Interpretation of a chromatogram must, therefore, account for this superposition and involves an evaluation of instrumental spreading and correction of the detector response to obtain the true concentrations of the component species.

When the sample injected is monodispersed, peak broadening occurs solely due to axial dispersion; for a polydispersed sample, additional broadening results from the desirable process of size separation. The chromatograms of monodispersed samples may be used to construct a

calibration curve relating the particle size with its peak retention volume. As shown in Fig. 1.2, such a calibration curve will result in superficially larger and smaller particle sizes corresponding to the leading and trailing edges of the chromatogram, respectively. Hence, the need to correct the detector response.

Axial dispersion can conveniently be separated into two independent and additive contributions, namely, extra-column dispersion and column dispersion which is dominant. Extra-column dispersion is confined to dispersion stemming from a finite pulse input and occurring in the injection value, tubing and detector cell. For a column packed with porous packing material, column dispersion results from interstitial dispersion, i.e., dispersion in the mobile phase and pore dispersion, i.e., dispersion arising from permeation of the colloids into the pores. Obviously, for an HDC column, pore dispersion does not exist. For a CPC or FFF system, it is probably immaterial to distinguish between column and extra-column dispersion. It is reasonable to expect that axial dispersion will be most pronounced in a SEC column, lesser in a HDC column and least in a CPC or FFF system. The main sources of interstitial dispersion in SEC of polymer molecules are longitudinal diffusion, eddy diffusion and flow velocity variations caused by non-uniform packing [Friis and Hamielec (1975)]. It may be expected that these factors also operate when colloids are chromatographed.

In Chapter 2, theories are developed to predict the rate of particle transport through a column, i.e., the calibration curve. So

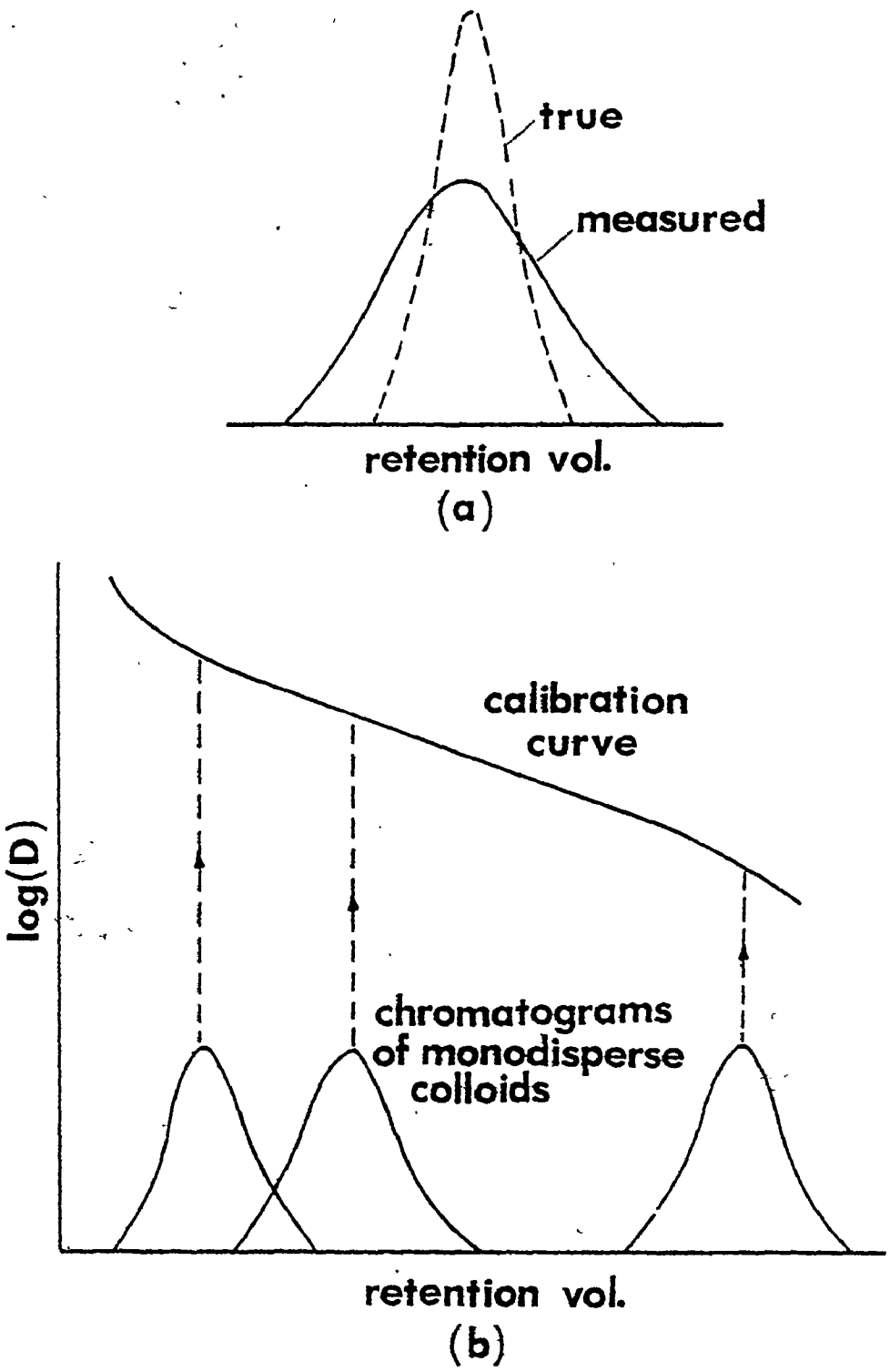

Fig. 1.2 Peak separation and peak broadening.

far no theory has been reported to predict the effect of axial dispersion on the shape of the chromatogram of a monodispersed sample. This information is necessary to correct the detector response. An empirical approach to handle this problem will be developed in Chapter 4.

1.3 SCOPE OF PRESENT WORK

Axial dispersion is a serious imperfection in the analysis of particle sizes by chromatography. Without regard to axial dispersion, measured particle sizes may be considerably underestimated. The main emphasis of this work is to evaluate currently available methods and to develop new methods of sufficient generality which allow the detector response to be suitably corrected so that meaningful size information is obtained. Experimental work involved the use of a size exclusion chromatograph equipped with a turbidity detector.

CHAPTER 2

AN ANALYSIS OF FLOW SEPARATION IN THE CHROMATOGRAPHY OF PARTICLE SUSPENSIONS

2.1 INTRODUCTION

Aside from the obvious importance in providing an insight into the causes of resolution loss in chromatographic processes, the dynamics of chromatographic separation are interesting and intriguing because of the complex nature of the process. The nature of column chromatography brings together the mechanics of fluid flow, the thermodynamics of solutions and transport through porous media, as in the case of size exclusion chromatography. The partition characteristics, as well as the transport properties of the different components of the colloid between the stationary and mobile phases, result in different retention volumes for each component in the column. The consequence of this phenomenon is the separation of the components as individual peaks or as the envelop chromatogram of the incompletely resolved peaks of the components of the sample. Aside from its ability to separate a heterogeneous system into its individual components, the column has other characteristics which tend to negate this primary purpose. As a consequence of axial dispersion, separated peaks are axially dispersed resulting in peak broadening.

In the subsequent discussion in this Chapter, attention will be focussed on various competing mechanisms for colloidal separation by chromatographic techniques. Theories are outlined which allow a

prediction of the rate of particle transport, i.e., peak separation. The complexity of peak broadening has to-date precluded a theoretical analysis.

2.2 MECHANISM OF SEPARATION

In this section, the mechanics of fluid flow through narrow cylindrical conduits are considered. The discussion is aimed to elucidate the mechanisms by which a colloidal suspension undergoes size separation as it flows through the column. In any one type of chromatography, particle transport may be governed by one or a combination of these mechanisms. Thus for HDC and SEC, the hydrodynamic, the ionic and van der Waals effects are of considerable importance, while in FFF, the hydrodynamic effect and the effect of the applied force field, control the migration of colloid particles. The tubular pinch effect is invoked to explain the colloidal behaviour in CPC. Let us now briefly consider each of these mechanisms.

2.2.1 The Hydrodynamic Effect [Small (1974); Small et al (1976)]

Consider a capillary tube of radius R, as in Fig. 2.1, through which a carrier solvent undergoes Poiseuille flow. A colloidal particle, injected into such a channel, will by Brownian motion make radial excursions normal to the direction of flow, sampling and adopting velocities across the capillary and will thereby, display a mean velocity similar to the fluid but with the important limitation that, the size of the particle prevents it from adopting the slower velocities

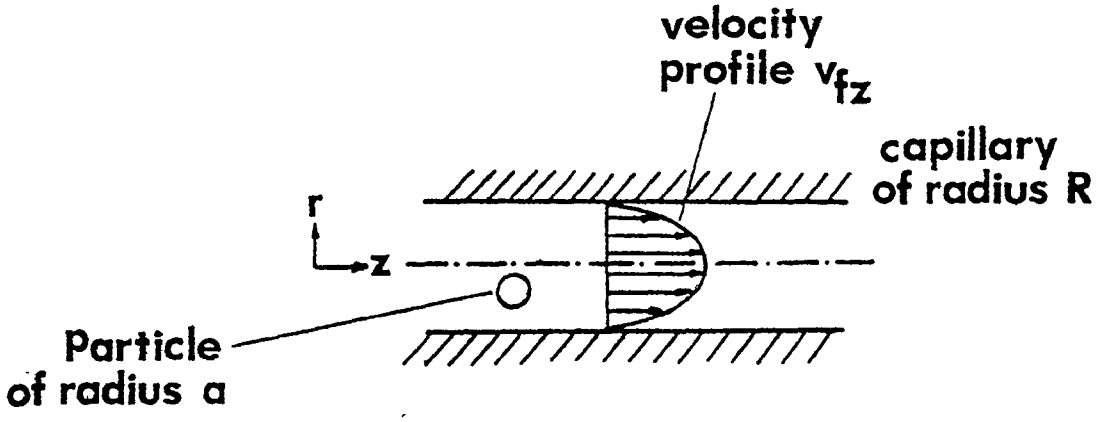

Fig. 2.1 Schematic of a spherical solute particle immersed in Poiseuille flow of aqueous carrier solution through a long cylindrical capillary.

close to the interface. Furthermore, the larger the particle, the more it is rejected from these sluggish regions and hence, the greater its mean velocity. Consequently, the particle will move through the capillary with a mean velocity which exceeds the mean velocity of the fluid by a factor that increases with increasing ratio of particle to capillary radius.

2.2.2 The Ionic Strength Effect [Small (1974); Small et al (1976)]

Consider the electrostatic interaction between the colloid and the capillary wall both of which have associated electrical double layers. In the case of the latex particles, the double layer is attributable to fixed anionic surface charges, as well as adsorbed surfactant anions. If a glass capillary is considered, then it is known to have a negative surface charge. The resulting electrostatic repulsion between the colloid and the capillary determines how closely the former can approach the latter and in accordance with accepted theories of double layer interaction, this distance at closest approach should increase with decreasing ionic strength. Thus, at low ionic strength, the colloid particle will be repelled from the wall and will experience the faster moving core fluid with a resulting increase in its velocity.

2.2.3 Van der Waals Effect [Small (1974); Small et al (1976)]

As the ionic concentration of the fluid is increased, double layer repulsion diminishes and the colloid can approach the wall more

closely. Van der Waals interaction between the particle and wall becomes more important as the distance of closest approach decreases and has a retarding effect on the velocity of the particle. This effect would be in opposition to the hydrodynamic and electrostatic effects. Since van der Waals interaction increases with increasing particle size, one would also expect the retardation to be greater for a larger particle size.

2.2.4 The Tubular Pinch Effect

It has generally been observed that, when rigid spheres are transported in a Poiseuille flow through a straight cylindrical tube, they undergo radial displacement and move along trajectories which asymptotically approach straight lines, parallel to the tube axis, at a fixed distance between the latter and the wall. Segre and Silberberg (1962) proposed the term 'tubular pinch' to describe this focussing of particles into an annular ring. They showed that a neutrally bouyant sphere is subject to radial forces that carry it to an equilibrium position at approximately a distance of six-tenths the tube radius from the axis. The origin of the force causing this radial displacement or focussing is in the inertia of the moving liquid. The radial equilibrium position is a function of the liquid velocity and the ratio of particle to tube radius. Walz and Grün (1973) showed that when the liquid velocity is increased in a tube, particles assume equilibrium positions nearer to the tube wall.

2.2.5 The Effect of An Applied Force Field [Giddings (1978)]

Consider a thin rectangular channel. As a dilute particle suspension moves down the channel, an external gradient or force field applied perpendicularly to the channel axis interacts with the particles, forcing them into a characteristic equilibrium distribution layer against one wall. This layer is of different thickness for each distinct particulate species, depending on the physical basis of the coupling between the field and the species and on the diffusion coefficient of that species.

Flow along the channel axis displaces the particles downstream. Because the flow is parabolic, its velocity is greatest near the center of the channel. Thus, particles with a thick layer extending into the center will be swept out of the channel first, while, species forced into a narrow layer in the relatively quiescent flow regions near the channel wall will be significantly retained. This is the basis for selective retention and produces, in general, a retention spectrum in which small particles are eluted first and large particles last.

2.3 THEORY OF PEAK SEPARATION IN HYDRODYNAMIC CHROMATOGRAPHY

The flow of colloidal particles through packed beds is affected by such factors as the size of the colloid and packing and the flow-rate and composition of the eluant. The rate of migration of the colloid peak may be conveniently expressed by a dimensionless quantity, the R_F number. R_F is simply the ratio of the rate of migration of the colloid peak to the rate of eluant flow (or a marker species) in the void volume

of the column. A summary of observations to-date on how R_F depends on column operating conditions is now given.

Fig. 2.2 shows Small's (1974) data on the rate of transport of polystyrene latices through ion exchange beds of different diameter D. The fact that R_F clearly increases with increasing diameter of the latex particles, D, provides the basis for a chromatographic size separation. As the particle size of the packing is decreased, the potential for size separation improves, as indicated by the increasing slope of the R_F versus D plots. Most significantly, R_F is always greater than unity or the latex particles move more rapidly through the bed than the eluant.

The dependence of R_F on ionic strength of the eluant is shown in Fig. 2.3. The ionic strength in the eluant was varied by the addition of increasing amounts of electrolyte and in all cases R_F was found to increase with decreasing ionic strength. In curves A and B, the dependence of R_F on D is reduced and indeed in the highest ionic strength is actually reversed for the higher particle size latices. In curve A, data for the two largest latices are not shown simply because neither of these appeared in the effluent but were deposited in the column.

The data in Fig. 2.3, when re-plotted [McHugh et al (1976)] as log D versus Δv, the difference in retention volumes of the eluant and latex, are shown in Fig. 2.4. With the exception of curves A & B, a series of parallel lines result, indicating that the resolution is independent of ionic strength over this range. When the ionic strength was varied by addition of ionic surfactant, similar results were

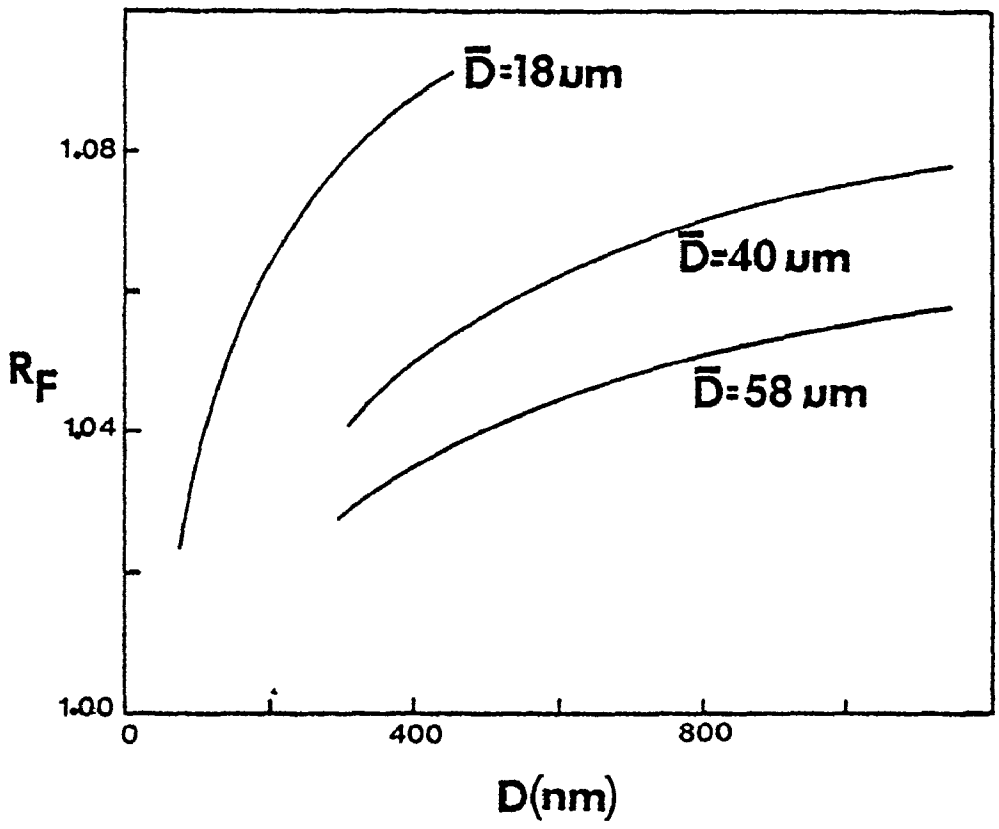

Fig. 2.2 The dependence of R_F on latex particle diameter and packing diameter $\bar{D}$.

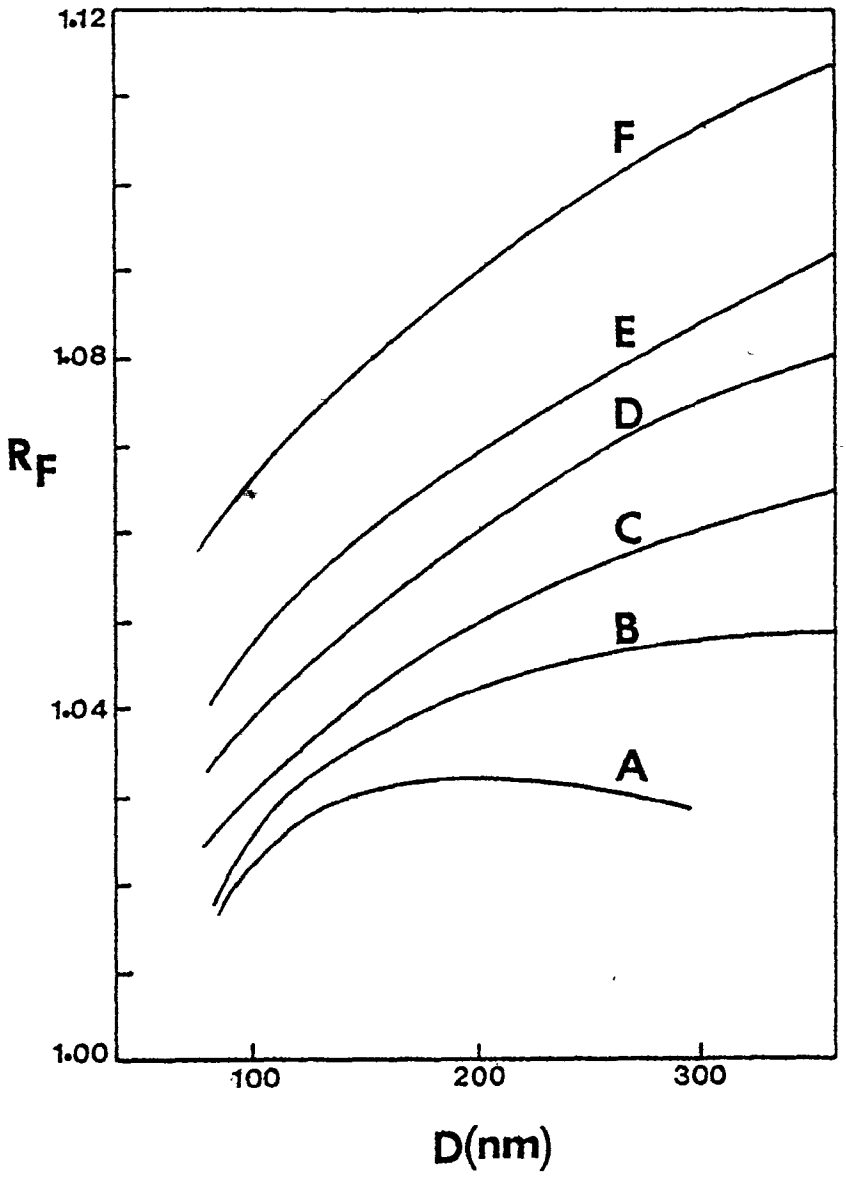

Fig. 2.3 The effect of the ionic strength of the eluant on the R_F of polystyrene latices. Eluant concentration moles per liter of NaCl. A, 1.76×10^{-1}; B, 9×10^{-2}; C, 2.96×10^{-2}; D, 4.6×10^{-3}; E, 1.7×10^{-3}; F, 4.25×10^{-4}.

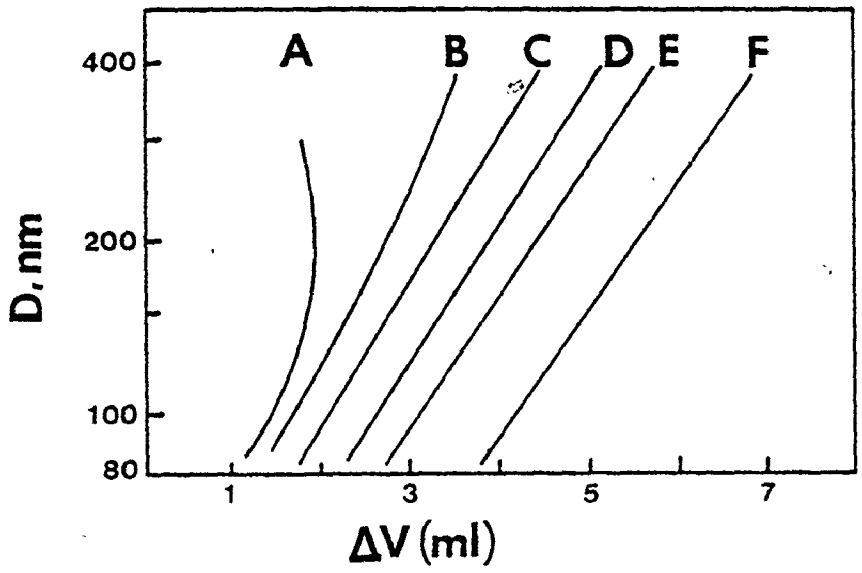

Fig. 2.4 The data in Fig. 2.3 replotted as particle diameter versus NaCl Normality : A = 1.76×10^{-1}, B = 9×10^{-2}, C = 2.96×10^{-2}, D = 4.6×10^{-3}, E = 1.7×10^{-3} F = 4.25×10^{-4}.

obtained.

Two approaches have been taken to model the role of the colloidal forces in hydrodynamic chromatography. The capillary model first proposed by Small (1974) and developed in several sources since [McHugh et al (1976); Stoisits et al (1976); Silebi and McHugh (1978); Prieve and Hoysan (1978)], considers the interstitial space as a system of interconnecting parallel capillaries of equal size. In the second approach, proposed by Buffham (1978), the speed of the chromatographic transients are calculated from the behaviour of a colloidal suspension in equilibrium in the vicinity of a plane interface. Expressed in this form, the theory is independent of the geometry of the particulate material that constitutes the HDC column. Both approaches are now outlined; the analysis in terms of a capillary model given by Silebi and McHugh is developed and is reinforced with the ideas of Prieve and Hoysan who presented a very similar treatment.

The Capillary Model

A solute particle does not spend the same fraction of its total residence time at each radial position. If interactions between particles are negligible, the residence time distribution for the solute during a transient will be the same as in the case where the solute is continuously injected. From an analysis of the particle continuity equation in the presence of a radial force field, for the case of continuous injection, it can be shown that the radial concentration distribution is a Boltzmann.

$$C(r) \propto \exp [- \phi(r)/\kappa T] \tag{2.1}$$

where $\phi(r)$, the particle-wall total interaction energy is given by the superposition of the repulsive potentials arising from the double layer and Born repulsive forces and van der Waals attractive potential.

$$\phi = \phi_{DL} + \phi_{B} + \phi_{VW} \tag{2.2}$$

The average particle velocity can be calculated by weighting the local particle velocity $v_{pz}(r)$ at a given radial position by the concentration at that position to give

$$\bar{v}_p = \frac{\int_0^{R-a} v_{pz}(r) \exp[-\phi(r)/\kappa T] \, r \, dr}{\int_0^{R-a} \exp[- \phi(r)/\kappa T] \, r \, dr} \tag{2.3}$$

where the upper integration limit is due to the consideration that the particle cannot approach the capillary wall closer than its radius.

$v_{pz}(r)$, in general, is different from the undisturbed fluid velocity, $v_{fz}(r)$, at the particle centre. This is due to the couple arising from the force imbalance on the particle, which experiences a higher velocity on its side closest to the centre of the capillary compared to its side closest to the wall. This wall effect results in a modified form of the Poiseuille equation

$$v_{pz}(r) = 2\bar{v}_f[1 - (r/R)^2 - \gamma(a/R)^2] \tag{2.4}$$

where γ is the wall effect parameter.

For an ionic marker, ϕ_B and ϕ_{VW} are negligible and its average velocity is obtained by taking the limits of $\phi(r)$ and $v_{pz}(r)$ as a tends to zero.

$$\bar{v}_m = \frac{\int_0^R 2\bar{v}_f \left[1 - (r/R)^2\right] \exp\left[-\phi(r)/\kappa T\right]_{a\to 0} \, r \, dr}{\int_0^R \exp\left[-\phi(r)/\kappa T\right]_{a\to 0} \, r \, dr} \tag{2.5}$$

R_F is then calculated from its definition

$$R_F = \bar{v}_p/\bar{v}_m \tag{2.6}$$

In Table 2.1, a comparison is made between the various analyses reported using the capillary model and the above analysis. Eqns. (2.1)-(2.6) adequately predict the data shown in Figs. 2.2 and 2.3. Before attempting to discuss these data and other model predictions in view of the various effects considered, the analysis presented by Buffham (1978) will be presented.

The Equilibrium Theory of Buffham

Buffham assumes that the HDC column is in equilibrium internally and with the feed stream in which the colloid is present at a low concentration, C. The speed of the chromatographic transient is related to the equilibrium behaviour but it is not assumed that the column is in equilibrium during a transient.

Since the mobile phase is non-uniform in the steady state because

of hydrodynamic effects and colloidal forces, the average residence time of the particle is given by

$$\bar{t}_p = \int_V c \, dV / QC \qquad (2.7)$$

where the integral of the local concentration, c is taken over the

Table 2.1 Analyses Reported By Various Workers Using the Capillary Model Compared to Silebi's Treatment

Reference	Comments
Stoisits et al (1976)	Interaction energy term not considered, i.e., $\phi(r)=0$ Wall effect neglected, i.e., $\gamma=0$. The ionic strength effect on R_F cannot be predicted
McHugh et al (1976)	The thickness of the excluded region was considered to exceed the particle radius due to double layer repulsion. The ionic marker was also considered to be excluded from a region very close to the wall. The radial concentration profile was assumed uniform so that the exponential terms in eqns. (2.3) and (2.5) were set equal to unity.
Prieve and Hoysan (1978)	As in McHugh's work, the effect of double layer repulsion on the thickness of the excluded region was accounted for. The marker was not considered ionic, however.

volume, V of the mobile phase. For a perfect marker, the interstitial and feed concentrations are identical and therefore

$$\bar{t}_m = V/Q \qquad (2.8)$$

It follows, therefore, that

$$R_F = \bar{t}_m/\bar{t}_p = V/[\int_V c/C \, dV] \qquad (2.9)$$

The colloid particles are distributed in the mobile phase at steady state in accordance with the colloïdal forces between the particles and the packing. Owing to the large R/a ratio, the packed bed is modelled as a system of colloid particles immersed in a semi-infinite fluid and bounded by a plane interface. Accordingly,

$$R_F = V/[\, A \int_0^\infty (c/C) \, dh] \qquad (2.10)$$

where h is the distance from the interface and A, the surface area of the packing. Equilibrium considerations in the presence of a force field leads to a Boltzmann concentration distribution as before:

$$c/C = \exp[\, - \phi(h)/\kappa T] \qquad (2.11)$$

Eqn. (2.11) predicts an infinite concentration at the interface (due to van der Waals forces), which rapidly falls to less than 10^{-60} as h increases from zero. As h is increased further, the concentration increases, c/C eventually exceeds unity, attains a maximum and then decays to unity. Figs. 2.5(a) & (b) illustrate the deep concentration minimum close to the interface and the profile deeper into the liquid.

Eqns. (2.10) and (2.11) can be used to calculate R_F as a function of particle diameter for varying concentrations of electrolyte and

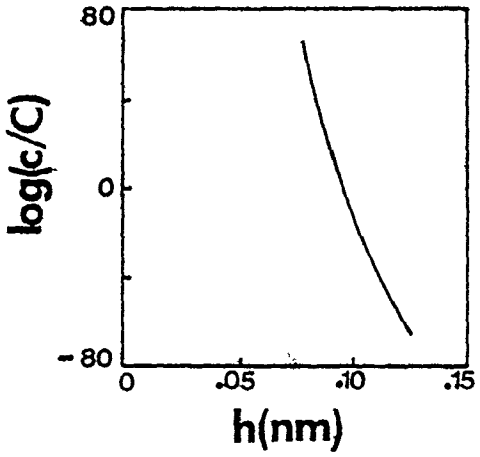

Fig. 2.5(a) Colloid concentration profile close to the interface.

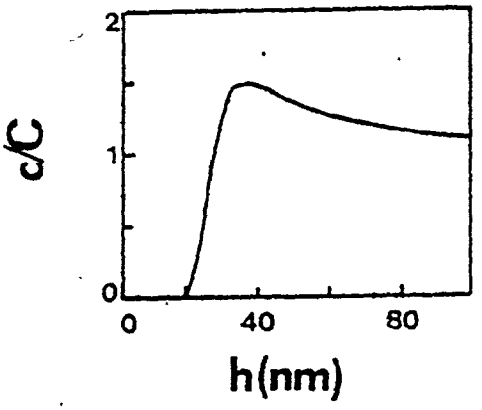

Fig. 2.5(b) Colloid concentration profile far from the interface.

packing diameter. Model predictions compare favourably with Small's data.

In the light of the capillary model for HDC, the various experimental phenomena are now discussed: colloidal forces can either enhance or hinder the average particle velocity depending on the ionic strength. Decreasing the ionic strength increases the exclusion volume; the average velocity increases with particle radius in accordance with the exclusion principle. On the other hand, at high ionic strength, the average velocity may decrease with particle radius in opposition to the exclusion principle and may become less than the average fluid velocity. This behaviour at high ionic strength coincides with the appearance of a deep secondary minimum in $\phi(r)$. As a result, particles tend to spend a greater fraction of their time in this low energy, low velocity position than at other positions. Larger particles spend a greater fraction of their time in this well than smaller particles, so that, the average velocity of larger particles may be slower. The interesting dependence of R_F on packing diameter is purely a hydrodynamic effect.

The equilibrium theory explains the ionic effect by virtue of the dependence of the concentration profile on the double layer repulsive potential. The hydraulic radius, R(=V/A), accounts for the effect of the packing diameter. Since, the integral in eqn. (2.10) is independent of R, the equation predicts an increase in R_F with increasing R or packing diameter. This clearly is in opposition to the observed effect and marks the distinct failing of the equilibrium approach.

At low ionic strength, both theories predict the independence of

R_F from material parameters associated with the colloid and the packing material, thus, indicating the feasibility of universal calibration. At higher ionic strength, one finds, owing to the reduced double layer repulsion, a predominance of van der Waals attraction and thus, an increasing sensitivity of the R_F versus D relationship to material parameters. Thus at low ionic strength, HDC can be used as a particle sizing technique, while, at higher ionic concentrations, it will separate colloids of the same particle size but different chemical properties.

2.4 THEORY OF PEAK SEPARATION IN SIZE EXCLUSION CHROMATOGRAPHY

In addition to the factors governing the separation of colloids in HDC, the use of porous packing introduces the possibility of size separation due to steric exclusion from the pores. Due to the complex flow patterns in porous packed beds, the attendant difficulty in predicting the migration of a colloid peak is obvious. Nagy (1979) attempted to simplify this problem by using very large pores relative to the size of the colloids being separated. Their analysis, therefore, assumes that all particles enter the pores and accordingly, describes one extreme of SEC where permeation by all species occurs.

Fig. 2.6 shows Nagy's data (1979) obtained using a porous column with a mean pore size of 2.5 μ (the latter is considerably greater than the maximum particle size analysed). No electrolyte was used and the ionic strength was varied by using surfactant alone, at concentrations below and above the critical micelle concentration. The qualitative

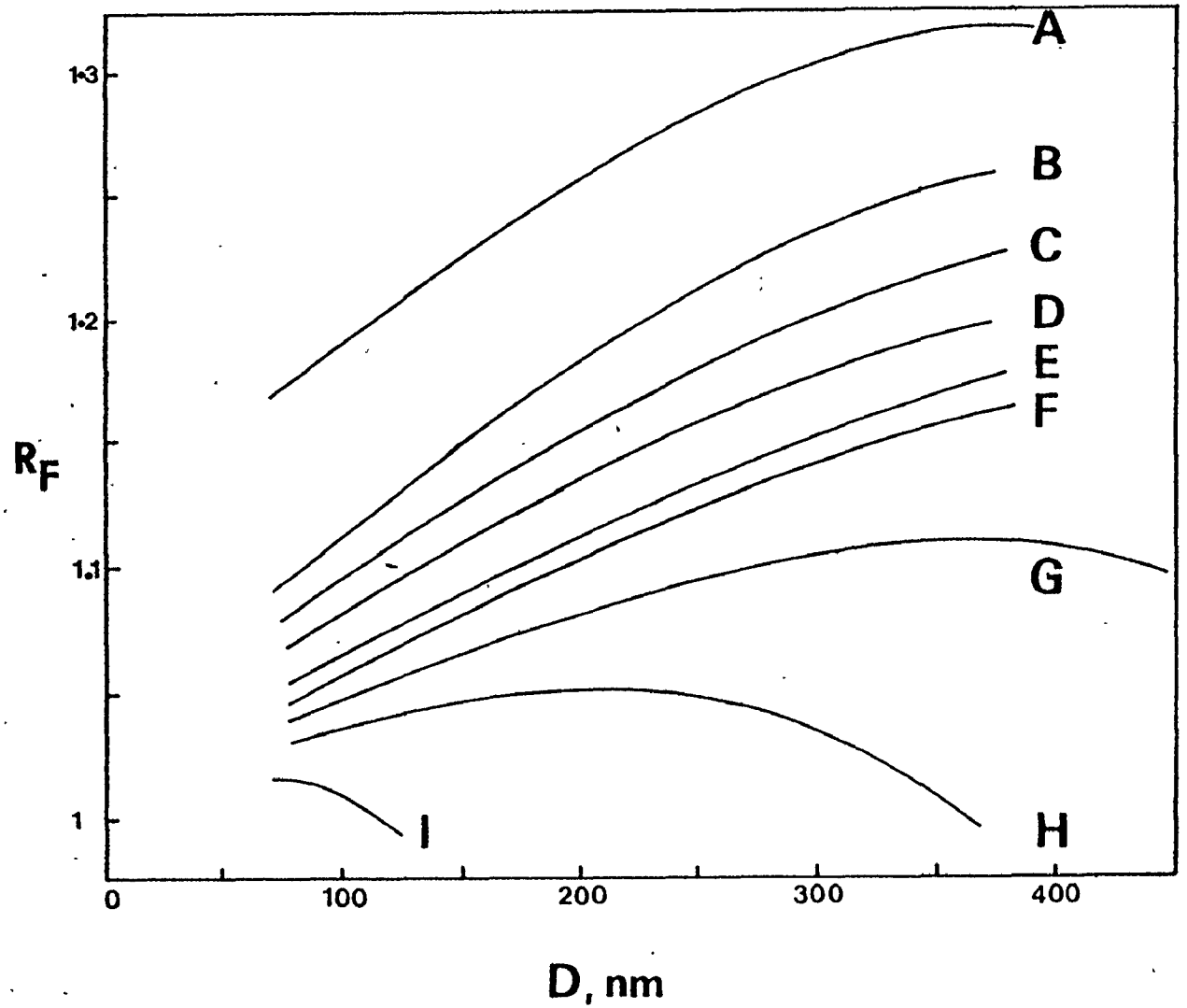

Fig. 2.6 Ionic strength effects for a porous Fractosil system. Total ionic strengths: A = 0.00022M SLS, B = 0.00055M SLS, C = 0.00103M SLS, D = 0.00129M AMA, E = 0.00515 AMA, F = 0.0101M AMA, G = 0.0210M SLS, H = 0.035M SLS, I = 0.105M SLS. (SLS - Sodium lauryl sulfate; AMA - Aerosol MA).

features of these data are similar to those observed in HDC, though, the R_F values are larger due to partial penetration of the pores by the particles.

Nagy (1979) modelled his data using a flow-through bank model as shown in Fig. 2.7. The large tubes in a given bank represent the totality of interstitial regions at the same level in the column, while, the small tubes represent the totality of the pores within the packing at the same level. The space between banks of zero volume serves as a mixing region for altering particle trajectories. The probability of a particle entering a tube at any bank is assumed equal to the ratio of flow through all such tubes to the total flow rate through all tubes. The principle result of their analysis predicts that

$$1/R_F = (V_{pc}/V)/R_{F,pc} + (V_{ic}/V)/R_{F,ic} \qquad (2.12)$$

where $R_{F,ic}$ and $R_{F,pc}$, the separation factors corresponding to the interstitial capillary and pore respectively, are calculated as before. V_{pc}, V_{ic} and V represent, respectively, the pore, interstitial and total void volume.

It is now shown that the result in eqn. (2.12) can be obtained using a simpler model which regards the tubes as being continuous. The peak retention volume of the colloid peak, V_p is given by

$$V_p = n_{pc} Q_{pc} \bar{t}_{pc} + n_{ic} Q_{ic} \bar{t}_{ic} \qquad (2.13)$$

where n, Q and $\bar{t}$ are the tube number, flow rate, and the average

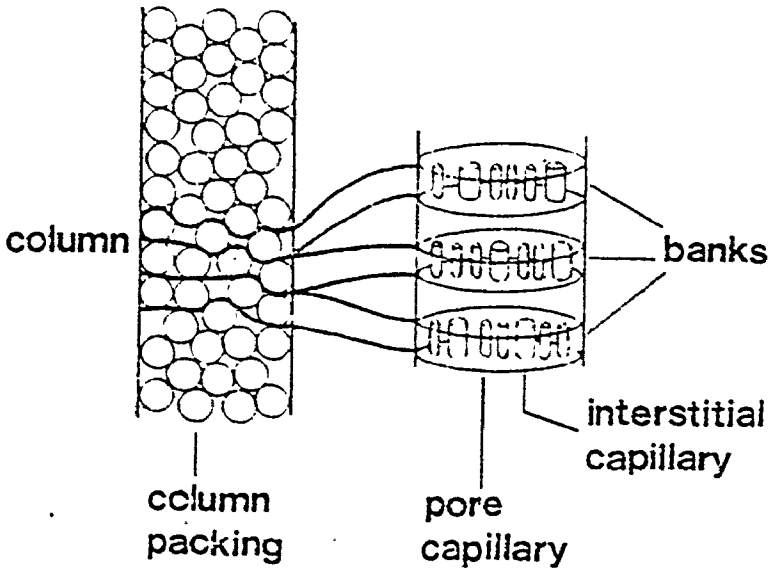

Fig. 2.7 A bank model of a SEC column.

residence time, respectively. It follows, therefore,

$$1/R_F = (n_{pc} Q_{pc} \bar{t}_{pc} + n_{ic} Q_{ic} \bar{t}_{ic})/V_m \qquad (2.14)$$

where V_m is the retention volume of the marker peak and is equal to V. If the length of the column is L and cross-sectional area of a capillary, A, then

$$\begin{aligned} 1/R_F &= L/V_m [n_{pc} Q_{pc}/(\bar{v}_p)_{pc} + n_{ic} Q_{ic}/(\bar{v}_p)_{ic}] \\ &= L/V_m [n_{pc} A_{pc} (\bar{v}_m/\bar{v}_p)_{pc} + n_{ic} A_{ic} (\bar{v}_m/\bar{v}_p)_{ic}] \\ &= (n_{pc} A_{pc} L/V_m)/R_{F,pc} + (n_{ic} A_{ic} L/V_m)/R_{F,ic} \\ &= (V_{pc}/V)/R_{F,pc} + (V_{ic}/V)/R_{F,ic} \end{aligned} \qquad (2.15)$$

This result is the same as that derived by Nagy, eqn. (2.12) using the more complicated bank model. The apparent equivalence of the two models is intriguing; however, this is a direct consequence of assigning the probability of a particle traveling through a tube as equal to the ratio of flow through all such tubes to the total flow rate through all tubes. It is not surprising that predictions based on eqn. (2.12) agree rather poorly with the experimental data in Fig. 2.6, since, a parallel array of large and small tubes which allows no fluid intermixing is hardly representative of the flow process in a packed column.

Nagy cites several reasons, chief among which is the slow diffusion coefficients of colloids, to justify the use of a flow model as opposed to a diffusion model. As pointed out by Small (1977), if a

bank model is considered, on physical grounds, separation by flow would seem unlikely, since, very little fluid would flow through the extremely fine pores of the packing when the much less restricted pathway around the particles is available to it. It is beyond the scope of this work to consider alternate models. It is, however, suggested that, since the equilibrium theory proposed by Buffham (1978) for HDC is essentially independent of the complex flow geometry, it may be possible to extend the treatment to predict SEC behaviour. Further work in this direction would undoubtedly be facilitated by a critical review by Casassa (1971) who has examined the various models proposed to explain peak migration in SEC.

2.5 THE TRANSPORT OF PARTICLES IN CAPILLARY CHROMATOGRAPHY

Recently, Noel et al (1978) reported a liquid chromatographic separation in a capillary tubing of particles ranging from 0.5 to 30 μ. Retention volumes were inversely related to particle diameter for materials of diverse composition, as shown in Fig. 2.8. The resolution of particles was dependent on column diameter and length and both the velocity and viscosity of the mobile phase (methanol or dilute ethylene glycol in water). A reduction in column diameter or length increased resolution; the effect of increased length is attributed to increased particle-wall interaction. A minimum flowrate was observed below which particles did not focus and resolution decayed rapidly. Also the peak width for particles exceeding 1μ decreased with an increase in velocity contrary to the behaviour for submicron particles. An increased mobile

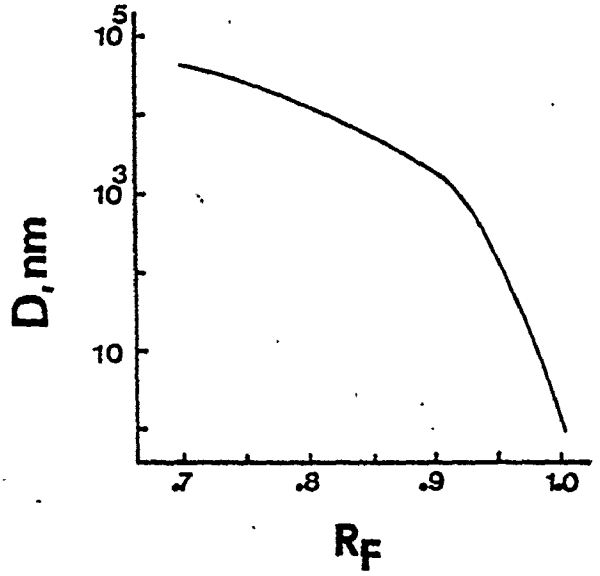

Fig. 2.8 Calibration curve for a CPC column: length 500 ft. x 0.02 in. I.D.; mobile phase, 1% ethylene glycol in water; flow-rate, 125 ml/h.

phase viscosity caused a marked deterioration in resolution of particles less than 1μ, while, it had practically no effect on large diameter particles.

The particles and tube radii used in the capillary flow experiments are much smaller than those used in the studies undertaken by Segre and Silberberg (1962). As a consequence, it cannot be assumed that all of the data derived from their macrosystems apply to the separation of microparticulates in capillaries. However, any particle that is radially segregated in a capillary should have a retention behaviour that is predicted by laminar flow equations. Accordingly, if the wall effect is neglected, the velocity of a radially segregated particle will be the same as the liquid at that position, i.e.,

$$v_{pz}(r) = \Delta P R^2 [1 - (r/R)^2]/4\eta L \qquad (2.15)$$

Combining eqn. (2.15) with a linear particle diameter-retention time calibration curve,

$$\ell nD = D_1 t + D_2 = D_1 \frac{L}{v_{pz}(r)} + D_2 \qquad (2.16)$$

where D_1 and D_2 are calibration constants, one obtains

$$r/R = \{1 - 4D_1 \eta L^2/[\Delta P R^2(\ell nD - D_2)]\} \qquad (2.17)$$

Eqn. (2.17) predicts that, small particles are located at a radial position between sixth-tenths and seven-tenths of the tube radius and

that, large particles focus in an annulus near the tube axis, in agreement with the observations of Segre and Silberberg (1962) and Oliver (1962). Although, there is insufficient evidence to conclude that particle resolution in capillary chromatography is the result of the 'tubular pinch effect', the data of Noel et al (1978), at least, imply it. Brownian motion plays an increasingly important role for particles less than 1 μ and they are probably separated by a hydrodynamic mechanism.

2.6 AN ANALYSIS OF SEPARATION IN FIELD FLOW FRACTIONATION

In the following analysis, an expression for R_F is derived which is generally valid for all FFF systems. The theoretical prediction of R_F has been found to be in reasonable agreement with experiments for the various FFF systems. It is beyond the scope of this thesis to consider FFF in detail.

In the absence of flow, a force acting on a particle will induce an average drift velocity $\bar{v}$, along axis x. At steady state, the flux of particles normal to the field is zero and hence

$$dc/dx = -\bar{v}c/d \qquad (2.18)$$

where d is the diffusion coefficient of the particle. The solution of eqn. (2.18) leads to an exponential concentration distribution in the equilibrium layer

$$c/c_0 = \exp(-x/\ell) \tag{2.19}$$

where c_0 is the concentration at the wall, x is the distance above the wall and $\ell = d/\bar{v}$ is a characteristic parameter called the mean layer thickness. The laminar liquid velocity across the channel width, w is given by

$$v_f(x) = 6\bar{v}_f [x/w - (x/w)^2] \tag{2.20}$$

The average particle velocity is calculated as

$$\bar{v}_p = \int_0^w c(x)\, v_f(x)\, dx \,/\, \int_0^w c(x)dx \tag{2.21}$$

It follows, therefore, that

$$R_F = \bar{v}_p/\bar{v}_f = 6\lambda[\coth(1/2\lambda) - 2\lambda] \tag{2.22}$$

where,

$$\lambda = \ell/w \tag{2.23}$$

Under conditions of high retention, eqn. (2.22) reduces to

$$R_F = 6\lambda \tag{2.24}$$

The parameter λ is related to the underlying physical chemistry of the

system through the relationship

$$\lambda = d/\bar{v}w = \kappa T/Fw \qquad (2.25)$$

where F is the effective force exerted on a single particle by the field. F and hence, λ take different forms depending upon the applied field. Since, particles cannot approach the wall of the channel closer than one particle radius, an approximate correction term is introduced in eqn. (2.24) which then becomes

$$R_F = 6\lambda + 6\alpha \qquad (2.26)$$

where α is the ratio of particle radius to channel width w.

λ controls selectivity and separation in normal FFF where R_F is less than 1.0. However, in the high field limit of normal FFF (steric FFF), the mean Brownian displacement from the wall becomes less than the particle radius. In this domain, particles extend out into the flow stream primarily because of their own finite size. α becomes controlling and R_F exceeds unity. The situation becomes akin to that in HDC with one important qualification: in steric FFF, unlike in HDC, the particles are held close to the wall resulting in higher selectivity.

Fig. 2.9 demonstrates the ability of sedimentation FFF (centrifugal force applied) to separate monodispersed samples of polystyrene latices over a ten fold size range. The separation is indeed phenomenal.

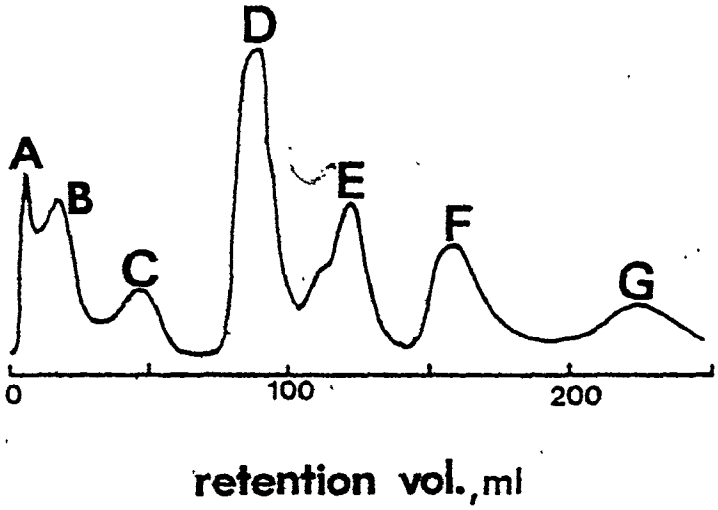

Fig. 2.9 Separation of polystyrene latices by sedimentation FFF.

A. 91 nm B. 176 nm C. 234 nm
D. 357 nm E. 481 nm F. 765 nm G. 982 nm

CHAPTER 3

DETECTION OF COLLOIDAL PARTICLES

3.1 INTRODUCTION

One of the most widely used detectors in the chromatography of colloidal particles has been the turbidity detector operating in the uv range. Depending upon the choice of wavelength, the resulting signal is due either to a combination of scattering and chemical absorption effects or principally due to scattering effects. The detector signal is dependent on the particle size, concentration and extinction coefficient, leading in the worst situation to a sixth order dependence on particle diameter for very small particles. This is to be contrasted to the case of differential refractometry where the detector generates a signal proportional to particle concentration or the third power of the diameter. In this chapter, the theoretical considerations governing the generation of the signal in both the turbidity and the refractive-index detectors are explored. Their optimum mode of operation is indicated as are their relative merits and demerits.

3.2 EXTINCTION OF LIGHT BY COLLOIDAL PARTICLES

3.2.1 Absorbance and Turbidity of a Dispersed System of Spheres

In the most general case, particles may absorb as well as scatter light. In the Beer-Lambert equation, the intensity of the transmitted

light, I_t, relative to the intensity of the incident light I_0 is given by

$$(I_t/I_0)_{abs} = \exp(-\varepsilon \ell) \tag{3.1}$$

where ε is the absorbance of the material and ℓ, the path length. Eqn. (3.1) describes the attenuation of a light beam due to absorption alone. For nonabsorbing systems, the turbidity τ, is a concept analogous to the absorbance, i.e.,

$$(I_t/I_0)_{sca} = \exp(-\tau \ell) \tag{3.2}$$

For a system which displays absorption and scattering simultaneously, the following composite relationship applies

$$(I_t/I_0) = \exp[-(\varepsilon+\tau)\ell] \tag{3.3}$$

The experimental extinction in a system which exhibits these two effects equals the sum of ε and τ. For a system of N dispersed particles per unit volume, ε and τ are given by

$$\varepsilon = N \pi D^2 K_{abs}/4 \tag{3.4}$$

$$\tau = N \pi D^2 K_{sca}/4 \tag{3.5}$$

where K_{abs} and K_{sca} are respectively, the coefficients for absorption and scattering. The geometrical cross-section of the dispersed spheres, $\pi D^2/4$ times the coefficient, defines a quantity known as the cross-section, C

$$C_{abs} = \pi D^2 K_{abs}/4 \tag{3.6}$$

$$C_{sca} = \pi D^2 K_{sca}/4 \tag{3.7}$$

The cross-sections represent the blocking power of a particle as far as transmission of incident light is concerned. Expressing eqns. (3.4) and (3.5) in terms of the volume fraction, ϕ of the spheres one obtains

$$\varepsilon/\phi = \pi D^2 K_{abs}/4V \tag{3.8}$$

$$\tau/\phi = \pi D^2 K_{sca}/4V \tag{3.9}$$

where V is the volume of one sphere. If the particle concentration is expressed in terms of c, the total weight of the spheres in 100 g of system, then the above equations take the form

$$(\varepsilon/c) = 0.01\ (\rho_s/\rho_p)\ (\varepsilon/\phi) \tag{3.10}$$

$$(\tau/c) = 0.01\ (\rho_s/\rho_p)\ (\tau/\phi) \tag{3.11}$$

where ρ_p and ρ_s are respectively, the densities of particle and system. The experimentally measured quantity is $\ell n\ (I_0/I_t)$. It follows from the above equations that,

$$\ell n(I_0/I_t) = 0.01(\rho_s/\rho_p)\ (3/2D)\ (K_{abs} + K_{sca})\ \ell\ c \qquad (3.12)$$

Therefore, the slope of the experimentally determined $\ell n(I_0/I_t)$ versus c data yields information on the total extinction coefficient, K ($=K_{abs} + K_{sca}$); if particles are nonabsorbing, then K_{sca} alone is measured. The coefficients are measured at sufficiently low concentrations where complications due to multiple scattering are non-existent and the $\ell n(I_0/I_t)$ versus c data are linear through the origin.

3.2.2 Theoretical Estimation of Scattering and Absorption Coefficients

The magnitudes of the scattering and absorption coefficients are dependent on the wavelength of light, the size of the particles and the refractive index of both particle and medium. The light scattering of colloidal spheres can be treated on the basis of two theories - Rayleigh (1881) and Mie (1908). The results of such an analysis are generally reported as a function of a size parameter α and a refractive index ratio m, where α and m are defined to be

$$\alpha = \pi\ D/\lambda \qquad (3.13)$$

$$m = n_p/n_m \qquad (3.14)$$

λ is the wavelength of light in the medium and is related to the wavelength in vacuum, λ_0 by

$$\lambda = \lambda_0/n_m \tag{3.15}$$

The Rayleigh theory yields accurate results for non-absorbing particles at any practically conceivable m provided $\alpha \leq 0.4$. The most general theory by Mie is free from any restriction as to α and m values. Unlike Rayleigh theory, it applies to absorbing particles; provision for absorption is introduced by defining the refractive index of an absorbing material as a complex number $n_1 - in_2$ where $i = \sqrt{(-1)}$. For nonabsorbing materials, n_2 equals zero. Both n_1 and n_2 are wavelength dependent characteristics of the material; n_2 obviously increases as the wavelength of an absorption peak is approached. The idea of representing the refractive index of an absorbing material by a complex number has been elegantly dealt with by Hiemenz (1977).

Rayleigh theory yields a simple expression for K_{sca} given by

$$K_{sca} = 8\alpha^4[(m^2 - 1)/(m^2 + 2)]^2/3 \tag{3.16}$$

The coefficients derived from Mie theory have the form

$$K_{sca} = (2/\alpha^2) \sum_{n=1}^{\infty} (2n+1)(|a_n|^2 + |b_n|^2) \tag{3.17}$$

$$K = K_{sca} + K_{abs} = (2/\alpha^2) \sum_{n=1}^{\infty} (2n+1)\, R_e\, (a_n + b_n) \tag{3.18}$$

where

$$a_n = \frac{\psi_n(\alpha)\,\psi_n'(\alpha m) - m\,\psi_n(\alpha m)\,\psi_n'(\alpha)}{\zeta_n(\alpha)\,\psi_n'(\alpha m) - m\,\psi_n(\alpha m)\,\zeta_n'(\alpha)} \tag{3.19}$$

$$b_n = \frac{m\,\psi_n(\alpha)\,\psi_n'(\alpha m) - \psi_n(\alpha m)\,\psi_n'(\alpha)}{m\,\psi_n(\alpha)\,\psi_n'(\alpha m) - \psi_n(\alpha m)\,\zeta_n'(\alpha)} \tag{3.20}$$

$$\zeta_n(\alpha) = \psi_n(\alpha) + i\,\chi_n(\alpha) \tag{3.21}$$

$$\psi_n(\alpha) = (\pi\,\alpha/2)^{1/2}\,J_{n+1/2}(\alpha) \tag{3.22}$$

$$\chi_n(\alpha) = -(\pi\,\alpha/2)^{1/2}\,N_{n+1/2}(\alpha) \tag{3.23}$$

$J_{n+1/2}(\alpha)$ and $N_{n+1/2}(\alpha)$ are half order integral Bessel and Neuman functions.

The oscillatory character of the scattering coefficient is shown in Fig. 3.1. The coefficient approaches the value of 2.0 at large α values, indicating that the scattering cross-section is then twice as large as the geometrical cross-section. Fig. 3.2 shows the strong effect of m on K_{sca} at small and intermediate α values. The numerical value of K_{sca} at the first maximum is larger and the maximum occurs at a lower α value, the larger the value of m. These differences become increasingly smaller, until at a sufficiently large α, m has no longer any effect on K_{sca}. An important conclusion reached by Heller and Pangonis (1957) is that, the smaller the particle size, the larger the maximal specific scattering power (τ/c) attainable with a given material at a given wavelength, provided the relative refractive index is increased to a correspondingly larger value. Mie theory calculations

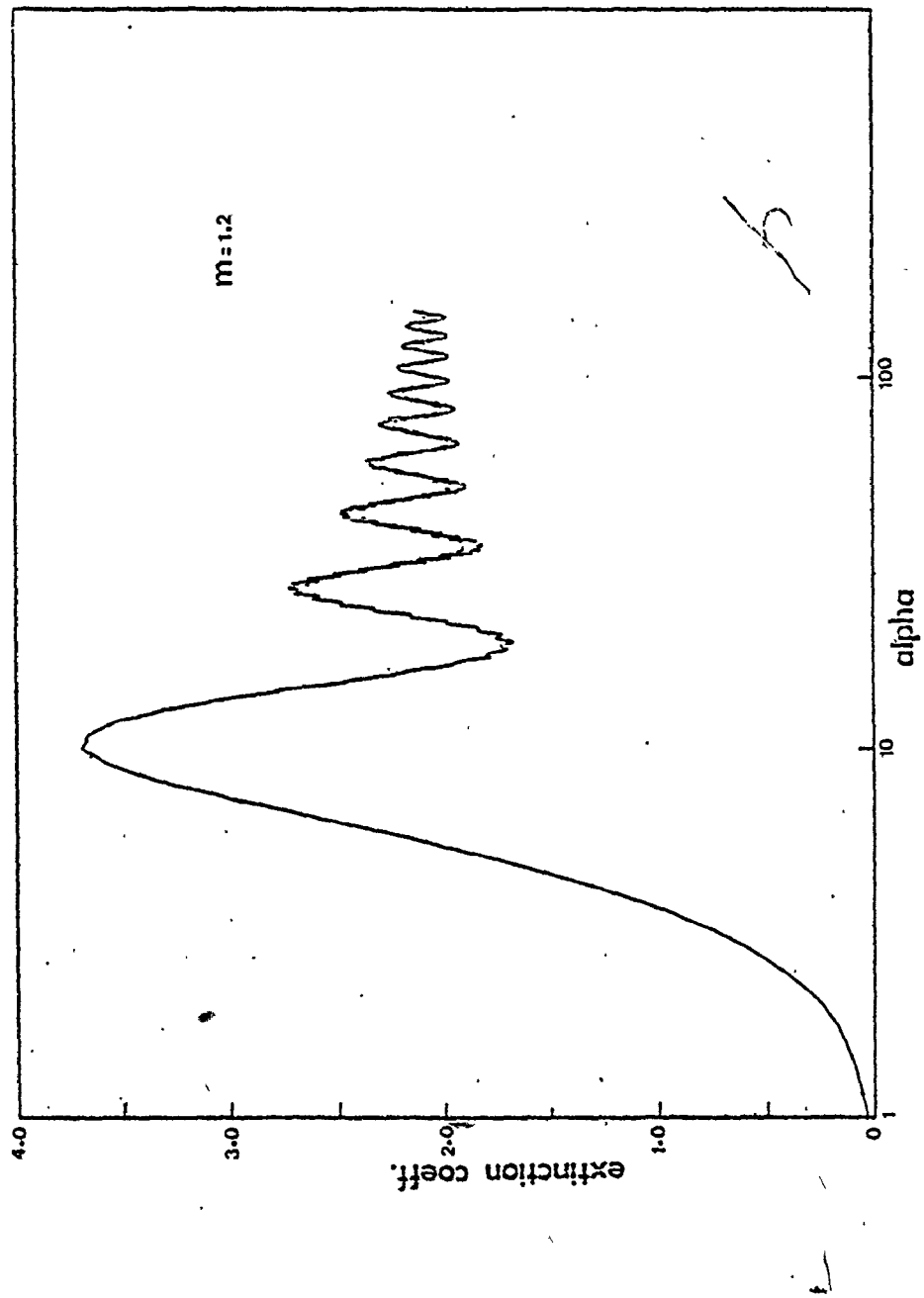

Fig. 3.1 Oscillatory character of the extinction coefficient.

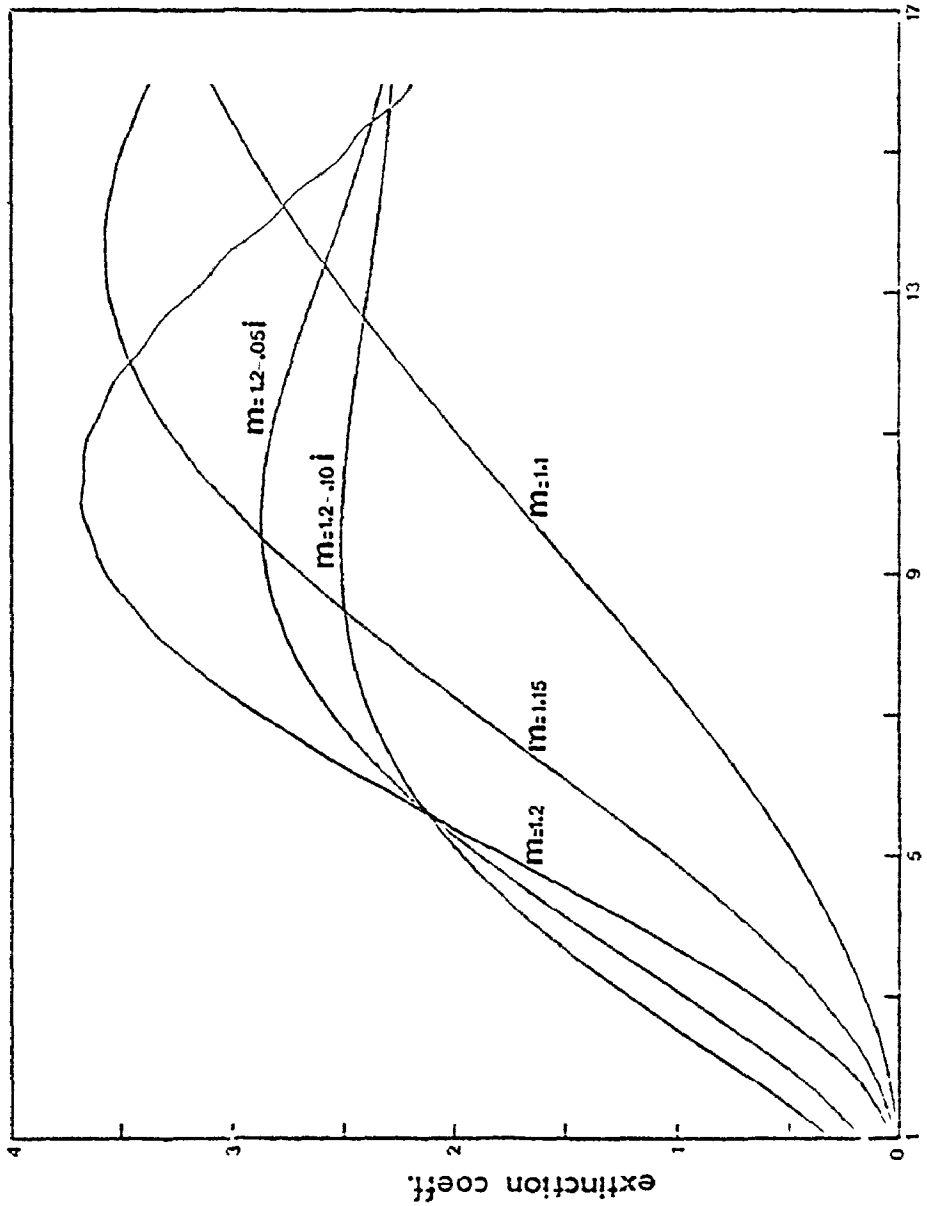

Fig. 3.2 The extinction coefficient.

were done using a subroutine written by Dave (1968).

The range of rigorous validity of Rayleigh theory is very small. Heller (1965) assessed its more important range of practical validity using Mie data as a reference. His results are shown in Table 3.1 where Δ_α, the percent deviation, is defined as

$$\Delta_\alpha = 100\ (\alpha_R - \alpha_m)/\alpha_R \tag{3.24}$$

Table 3.1 Percent deviation Δ_α

	$\alpha = \pi D/\lambda$					
m	0.2	0.4	0.6	0.8	1.0	1.2
1.00	-0.55	-2.1	-4.6	-8.0	-11.9	...
1.05	-0.40	-1.8	-4.1	-7.2	-10.9	...
1.10	-0.40	-1.6	-3.6	-6.4	-9.9	...
1.15	-0.35	-1.3	-3.0	-5.6	-8.9	-13.0
1.20	-0.25	-1.1	-2.5	-4.9	-7.9	-12.0
1.25	-0.20	-0.8	-2.0	-4.0	-6.9	-11.0
1.30	-0.15	-0.6	-1.5	-3.2	-5.8	-10.0
1.33	-0.15	-0.5	-1.4	-2.85	-5.2	- 9.4

It is observed that Δ_α decreases with increasing m for all α. Analytical expressions for the specific turbidity [Heller (1957)], τ/c, which approximate the Mie functions are given in Table 3.2. Their range of applicability are specified in Table 3.3.

Fig. 3.2 indicates the considerable enhancement in the small particle extinction coefficient due to chemical absorption. This feature is of great practical significance and will be discussed in the

Table 3.2 Approximate Expressions for the Specific Turbidity, τ/c ($\Delta_\alpha < 5$, ρ_s/ρ_p assumed equal to unity)

1. First Approx. $\ln[(\tau/c)\lambda] = A + B/\alpha + (C + D/\alpha)\ln(m-1)$

α Range	A	B	C	D
0.8 - 2.0	-0.3079	-1.060	2.084	-0.0564
1.8 - 3.0	0.0021	-1.642	2.084	-0.0564
2.6 ->6.0	0.0021	-1.642	1.944	0.3643

2. Second Approx. $\ln[(\tau/c)\lambda] = A + B/\alpha + (C + D \ln \alpha)\ln(m-1)$

α Range	A	B	C	D
1.2 - 1.8	-0.3079	-1.060	2.000	0.1486
2.2 ->6.0	0.0021	-1.642	2.125	-0.1486

Table 3.3 Range of Validity of First Approximation in Table 3.2.

A. Limiting upper m value if Δ_α is not to exceed the specified deviation			B. Limiting upper α value if Δ_α is not to exceed the specified deviation		
α	5%	10%	m	5%	10%
1.0	>1.30	>1.30	1.05	6.15	6.75
2.0	>1.30	>1.30	1.10	5.45	7.30
3.0	>1.30	>1.30	1.15	6.10	8.25
4.0	1.20	1.27	1.20	4.00	5.05
5.0	1.16	1.20	1.25	3.50	4.15
6.0	1.15	1.17	1.30	3.30	3.80
7.0	1.16	1.16			
8.0	1.14	1.15			

next section in context to its application to chromatography. Generally speaking, the extinction coefficient is an oscillating function of α; for nonabsorbing particles, the amount of oscillation is more pronounced the larger m is, while if the particles are light absorbers, the amount of oscillation in the curves decreases with increasing value of the imaginary component of the refractive index; the limiting value of the

extinction coefficient at large α, with or without absorption is 2.0.

3.2.3 Particle Size Distribution by Turbidity Spectra

It follows from eqn. (3.5), that the turbidity of a polydispersed latex is given by

$$\tau = N \int_0^\infty \pi/4 \; D^2 \; K_{sca}(\alpha,m) f(D) \; dD \tag{3.25}$$

where f(D) is the normalized particle size distribution function. The latex concentration is given by

$$c = \rho_p N \int_0^\infty \pi/6 \; D^3 \; f(D) \; dD \tag{3.26}$$

From the above equations, it follows that

$$\frac{\tau}{c} = \frac{3}{2\rho_p} \; \frac{\int_0^\infty D^2 \; K_{sca}(\alpha,m) f(D) \; dD}{\int_0^\infty D^3 f(D) \; dD} \tag{3.27}$$

$$\frac{\tau_{\lambda 1}}{\tau_{\lambda 2}} = \frac{\int_0^\infty D^2 K_{sca}(\alpha_1,m_1) f(D) \; dD}{\int_0^\infty D^2 K_{sca}(\alpha_2,m_2) f(D) \; dD} \tag{3.28}$$

Note that eqns. (3.27) and (3.28) are independent of N and can be used to solve for f(D) if it has a known form. The lognormal distribution occurs naturally in many latex systems; it is given by

$$f(D) = 1/(\sqrt{2\pi} \; \bar{\sigma} \; D) \exp\{-1/2 \; [(\ln D - \mu)/\bar{\sigma}]^2\} \tag{3.29}$$

Therefore, if specific turbidity data at least at two wavelengths or turbidity data at least at three wavelengths are measured, then in principle μ and $\bar{\sigma}$ can both be solved for. Limitations exist for very small particles where Rayleigh scattering occurs and for very large particles where K_{sca} tends to 2.0; in both extremeties eqns. (3.27) and (3.28) become insensitive to f(D). Additionally, with one extra piece of information, the refractive index of the latex may also be calculated; its value is not necessarily the same as the refractive index of a film formed from the latex.

A review of various techniques for calculating f(D) by turbidity spectra is found in the book by Kerker (1969). Recently, Zollars (1980) established the uniqueness of the solution for f(D) using turbidity spectra and pointed out that multivalued solutions are artifacts of poor numerical search techniques. An application of turbidity spectra to chromatography will be developed in Chapter 4. For absorbing systems, K_{sca} in the above equations may simply be replaced by the total extinction coefficient, K.

3.2.4 Turbidimetric Detection in Chromatography

It follows from eqns. (3.5) and (3.16) that the turbidity for very small particles which behave as Rayleigh scatterers is proportional to the sixth power of the particle diameter. For larger particles obeying Mie scattering theory, the corresponding dependence is lower. As a consequence of the above, the small particle signal is comparitively weak, though it can be augmented by using shorter

wavelengths. However, for obtaining particle size distributions, the relative signal is of greater importance. Silebi's (1979) calculations indicate that a change of wavelength or refractive index has a small influence on the relative signal for nonabsorbing particles. The relative signal is improved for absorbing particles due to a significant enhancement of the extinction coefficient of the smaller particles. These theoretical observations were confirmed by Nagy (1979) who chromatographed mixtures of polystyrene latices at 220 and 254 nm (controversy exists concerning whether particles absorb at 254 nm; at 220 nm, however, strong absorption occurs). One of Nagy's results, shown in Fig. 3.3, demonstrates the dramatic improvement in the 88 nm peak measured at a wavelength of 220 nm compared to that at 254 nm.

3.2.5 Sources of Error in Turbidity Measurements [Heller and Tabibian (1957)]

Appreciable error may result if instruments which are perfectly suitable for ordinary absorption measurements are used for turbidity measurements without proper modifications and precautions. There are three principle sources of error in turbidity measurements: 1) interference of laterally scattered light 2) the corona effect 3) effect of the solid angle. These effects are now described. Consider the schematic shown in Fig. 3.4.

Laterally scattered light may leave the cell and may by diffuse reflection from the inner walls of the cell housing, even though they are blackened, reach the photomultiplier tube, (see the schematic pencil

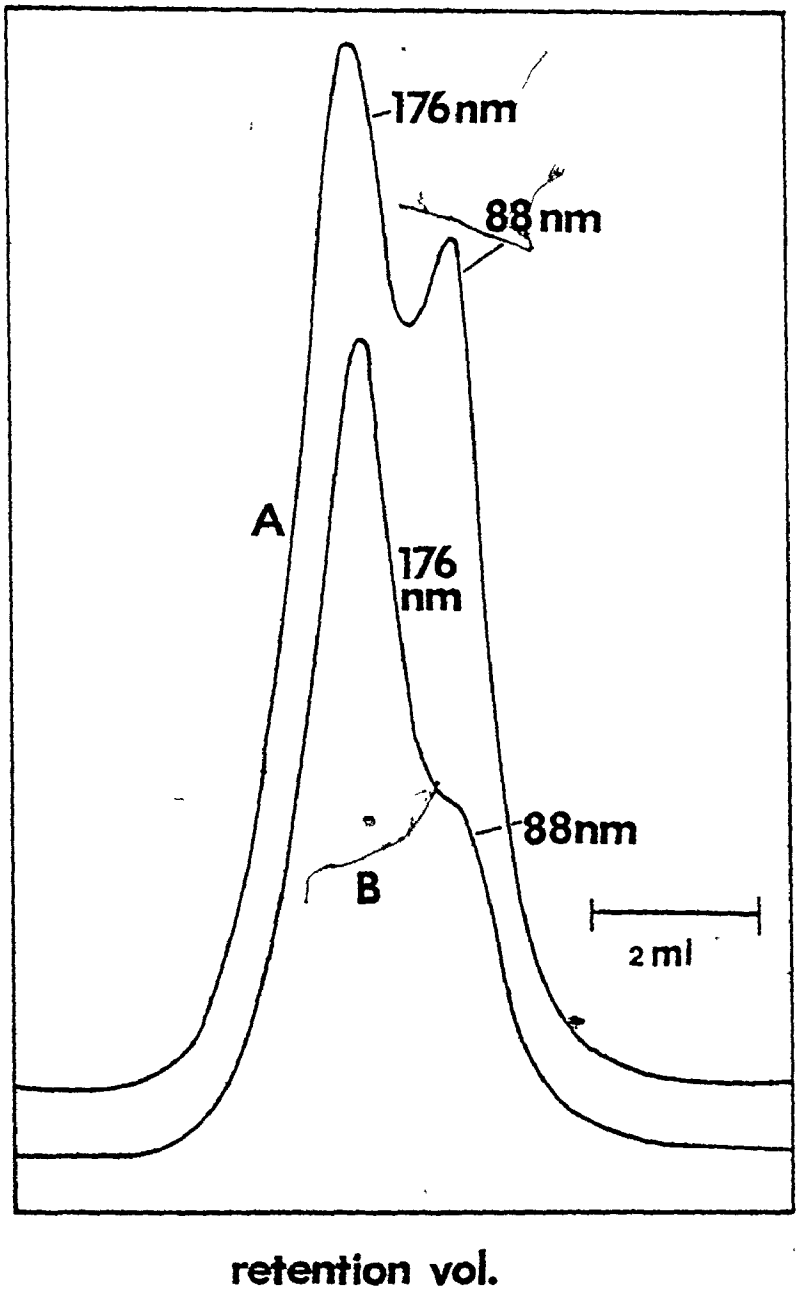

Fig. 3.3 HDC separation of a bimodal mixture of 88 nm and 176 nm polystyrene latices.

A. response at 220 nm B. response at 254 nm

of diffuse reflected light, ℓ_d in Fig. 3.4) resulting in an apparent turbidity smaller than the true one. In turbidity measurements it is, therefore, advisable to use cells whose lateral walls have been blackened. The intensity of the stray light, although, small compared to that of the primary beam, is strong enough to falsify the concentration dependence of the turbidity.

The secondary scattered light, ℓ_s, originates within those portions of the cell not traversed by the primary beam, ℓ_p. On a photographic plate, the secondary scattered light manifests itself as a corona around the primary beam. The corona can easily be excluded by placing at the exit end of the cell a diaphram with an opening only slightly larger than the diameter of the beam. The luminosity of the corona approaches zero at infinite dilution.

Primary scattered light, originating in the central cell section traversed by the primary beam, also interferes with turbidity measurements. A central volume element $\Delta v'$, located near the exit end of the cell, (not shown in figure) will emit a cone of scattered light represented by ω in Fig. 3.4. This angle and with it the amount of scattered light entering the photocell is determined by both its distance from the scattering volume element and the aperture of the diaphram 2. Since the scattered light contains contributions of all the elements in the cylindrical volume illuminated by the primary beam, the integral effect is by no means negligible. This solid angle effect can be minimized by reducing the aperture of the photocell to slightly less than the diameter of the primary beam.

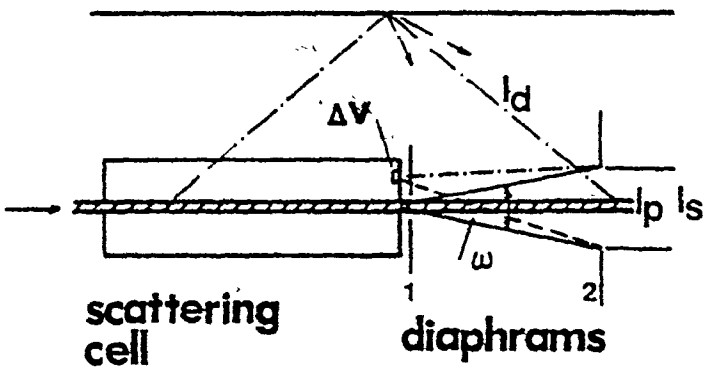

Fig. 3.4 Sources of error in turbidity measurements.

By far, the major portion of the light flux reaching the photocell is accounted for by the primary beam, ℓ_p. However, the stray and scattered light intensities are strong enough to falsify the concentration dependence of turbidity, if the relatively simple precautions outlined above are not adopted.

3.3 REFRACTION OF LIGHT BY COLLOIDAL PARTICLES

3.3.1 Mixture Rules for Index of Refraction

Table 3.4 scrutinizes the interrelations of some important refractive index mixture rules used for determining the refractive index of a solute. The mixture rules of widest applicability are the Lorentz-Lorenz and the Wiener equations [Heller (1965)]. These apply only in the case of particles which are small compared to the wavelength of incident light. Such a restriction, limits their application to a small fraction of the colloidal range. Zimm and Dandliker (1954) derived a more general refractive index expression based on the Mie theory. Their expression for the dispersion refractive index, n_s is given by

$$\frac{dn_s}{dc} = \frac{3n_m}{2\alpha^3\rho_p} \mathrm{Re}\left\{ \sum_{n=1}^{\infty} \frac{2n+1}{2n(n+1)} (a_n - b_n) \right\} \qquad (3.30)$$

where c is the weight concentration in g/cm^3. Eqn. (3.30) does not contain the restriction that α be small and allows calculation of the effect of light scattering on the refractive index of a colloidal dispersion. In the limit as $\alpha \to 0$, eqn. (3.30) reduces to

$$\frac{dn_s}{dc} = \frac{3n_m(m^2-1)}{2(m^2+1)\rho_p} \qquad (3.31)$$

a result derivable from Heller's equation (1965).

Nakagaki and Heller (1956) confirmed the validity of eqn. (3.30) for particle diameters as large as 500 nm. More recently, Silebi (1979) obtained good agreement of measured data with eqn. (3.31) for particles as large as 350 nm. Both measurements were made with polystyrene latices at a wavelength of 546.1 nm. Subsequent data measured by Nagy (1979) indicate that, dn_s/dc reverses in sign with increasing particle size. Its implication is that, the signal has a zero value for some intermediate particle size. Interpretation of Nagy's data is complicated due to the use of a broad wavelength source. However, the calculations of Zimm and Dandliker and those of Nakagaki and Heller indicate that, depending on the value of m, the signal may either increase with α or decrease and eventually change sign.

3.3.2 Differential Refractometry Detection in Chromatography

Differential refractometry shows a less dramatic dependence on particle size (third order) than turbidimetry of nonabsorbing particles. The advantage of differential refractometry is negated by the requirement of a higher sample concentration compared to the amount necessary for a photometric detection due to the limited sensitivity of available differential refractometers. With the advent of more sensitive detectors, this draw-back will likely be overcome.

Table 3.4 Mixture Rules for Index of Refraction

	Equation	Remarks
1. Lorentz-Lorenz	$\frac{n_s^2-1}{n_s^2+2} = \phi_m \frac{n_m^2-1}{n_m^2+2} + \phi_p \frac{n_p^2-1}{n_p^2+2}$	Volume additivity is not assumed. If $n_s \to n_m$ (dilute solution) and $n_p \to n_m$, equation reduces to Dale-Gladstone's equation. If volume additivity is assumed and $n_m \to 1.0$, equation reduces to Wiener's equation.
2. Wiener	$\frac{n_s^2 - n_m^2}{n_s^2 + 2n_m^2} = \phi_p \frac{n_p^2 - n_m^2}{n_p^2 + 2n_m^2}$	Volume additivity is assumed. If $n_s \to n_m$ (dilute solution) equation reduces to Heller's equation.
3. Heller	$\frac{n_s - n_m}{n_m} = \frac{3}{2} \phi_p \frac{m^2-1}{m^2+2}$	Volume additivity is assumed. If $n_p \to n_m$, equation reduces to Dale-Gladstone's and Biot's equations assuming volume additivity.
4. Dale-Gladstone	$n_s - 1 = \phi_m(n_m-1)+\phi_p(n_p-1)$	Volume additivity is not assumed. If such an assumption is made, equation reduces to Biot's equation.
5. Arago and Biot	$n_s = \phi_m n_m + \phi_p n_p$	Volume additivity is not assumed.

n_s = refractive index of system , n_p = refractive index of particle , n_m = refractive index of medium, ϕ_p = volume fraction of particles, ϕ_m = volume fraction of medium.

CHAPTER 4

CHROMATOGRAM INTERPRETATION - CALCULATION OF PARTICLE SIZE DISTRIBUTION

4.1 INTRODUCTION

As discussed in Chapter 1, axial dispersion is a serious imperfection in the analysis of particle sizes by chromatography. In the absence of a suitable theory which can predict axial dispersion effects, the only practical alternative to correct chromatographic data for axial dispersion is to use experimental calibration procedures. It is necessary first to establish a relationship between the experimental chromatogram, F(v) and the function W(y) representing the chromatogram that would be obtained in the absence of axial dispersion.

The chromatogram height F(v), for a single species can be expressed as

$$F(v) = W\, G(v) \tag{4.1}$$

where W is the area of the chromatogram and G(v) is the normalized instrumental spreading function of that species. For a polydispersed sample with n species, F(v) is given by a linear summation of the individual species contributions, i.e.,

$$F(v) = \sum_{i=1}^{n} W_i\, G_i(v) \tag{4.2}$$

where W_i and $G_i(v)$ represent the area and normalized spreading function for species i. When the number of species is very large, W_i can be replaced by a continuous distribution function W(y), where y is the mean retention volume. F(v) can be expressed as

$$F(v) = \int_0^\infty W(y)G(v,y)dy \qquad (4.3)$$

where, G(v,y) is the normalized spreading function of a species with mean retention volume, y. Eqn. (4.3) is frequently referred to as Tung's axial dispersion equation. Note that the lower limit in the above integral may have to be considered as $-\infty$ in certain forms of its solution.

The solution of eqn. (4.3) for W(y) requires an appropriate form for the spreading function and a determination of the numerical values of its parameters. Further, to convert W(y) into a size distribution requires a relationship between the mean retention volume y and particle diameter, D.

The function G(v,y) is frequently considered to be uniform, i.e.,

$$G(v,y) = G(v-y) \qquad (4.4)$$

This considerably simplifies the mathematical treatment of eqn. (4.3). A commonly used form for G(v-y) is the Gaussian function given as

$$G(v-y) = G_0(v-y) = \sqrt{1/(2\pi\sigma^2)}\ \exp[-(v-y)^2/(2\sigma^2)] \qquad (4.5)$$

The Gaussian function is inadequate, however, when single species chromatograms are skewed. Provder and Rosen (1970) suggested using a general statistical spreading function to account for skewed single species chromatograms. It is given as

$$G(v-y) = G_0(v-y)\ [1 + \sum_{n=3}^{\infty} A_n\ H_n(x)/n!] \qquad (4.6)$$

where

$$x = (v-y)/\sigma \qquad (4.7)$$

$H_n(x)$ are the Hermite polynomials and the coefficients, A_n, are functions of the nth order moments, μ_n, of G(v-y) about y. A special case of eqn. (4.6) is called the Edgeworth series and is obtained when $A_6 = 10\ A_3^2$ and $A_n=0$ for $n\geq 7$. $H_n(x)$ and A_n for n upto 6 are given in Table 4.1. The first two coefficients are of direct statistical significance: A_3 provides an absolute statistical measure of skewness while A_4 is a measure of the flattening or kurtosis of the spreading function.

The determination of parameter values of a spreading function is treated in Chapter 5. Consider now, the relationship between D and y, the particle diameter-retention volume calibration curve. Calibration curves which are nonlinear in ln D over the retention volume range of

TABLE 4.1 n^{th} Order Hermite Polynomials And Coefficients A_n

n	$H_n(x)$	A_n
3	$x^3 - 3x$	$\mu_3/\mu_2^{3/2}$
4	$x^4 - 6x^2 + 3$	$\mu_4/\mu_2^2 - 3$
5	$x^5 - 10\,x^3 + 15\,x$	$\mu_5/\mu_2^{5/2} - 10\,\mu_3/\mu_2^{3/2}$
6	$x^6 - 15\,x^4 + 45\,x^2 - 15$	$\mu_6/\mu_2^3 - 15\,\mu_4/\mu_2^2 + 30$

interest, are generally expressed as

$$\ln D(y) = A - By + Cy^2 \qquad (4.8)$$

Frequently, C=0, resulting in a linear calibration curve which may alternately be written as

$$D(y) = D_1 \exp(-D_2 y) \qquad (4.9)$$

where D_1, $D_2 > 0$ and $D_2 = B$.

Eqn. (4.3) may be solved numerically or analytically. The numerical solution yields the distribution function W(y) or the diameter frequency distribution, while an analytical solution allows only the calculation of moments of the diameter frequency distribution. Both forms of solution are now investigated.

4.2 NUMERICAL SOLUTION OF THE AXIAL DISPERSION EQUATION-SOLVING FOR THE DISTRIBUTION FUNCTION

Several numerical methods have been reported in the literature for the solution of the integral equation. These have been reviewed by Friis and Hamielec (1975) and more recently evaluated by Silebi and McHugh (1979) for their application to particle chromatography. Unfortunately the evaluation by Silebi and McHugh was made using experimental chromatograms and in view of the uncertainty in their measurement and the spreading functions being precisely not known, their conclusions must be regarded with caution. However, common with previous evaluations, they observed that a method, due to Ishige et al (1971), performed better than other available methods. A principle drawback of Ishige's method noted by these workers is its tendency to over-estimate the small particle size population relative to a large particle size population when the two are present together; a modification was suggested to overcome this drawback.

In this section, Ishige's method (his method 2) is described. Using synthesized chromatograms, the method and some of its variations are critically evaluated.

Ishige's method uses the fact that any response $F^*(v)$ always has a broader distribution than the input distribution, $W(y)$. Hence, if a distribution $F_i(v)$ is broader than $F^*(v)$, the assumed $W_i(y)$ must be sharpened to give a response closer to $F^*(v)$. Using $F^*(v)$ as the initial guess for $W(y)$, subsequent improved estimates were calculated by

$$W_{i+1} = (F^*/F_i)W_i \qquad (4.10)$$

where F_i is the chromatogram calculated using W_i. The procedure is repeated until F_i satisfies a convergence criteria. The method is illustrated in Fig. 4.1. Note that W_i is always normalized before use.

Silebi et al argued that eqn. (4.10) consideres the contribution at each retention volume as due only to particles at that volume and did not include contributions from neighbouring sizes. Accordingly, they suggested the algorithm

$$W_{i+1} = \prod_{k=-n'}^{k=n'} (F^*_{i+k}/F_{i+k})^{\gamma_{i,k}} W_i \qquad (4.11)$$

where the normalized weighting exponents, $\gamma_{i,k}$, are taken from the relative contributions of the sizes within a specified neighbourhood of the retention volume under consideration.

A variation of eqn. (4.10) which accelerates convergence is given as

$$W_{i+1} = (F^*/F_i)^{\alpha} W_i \qquad (4.12)$$

where, $\alpha > 1$. For the purpose of illustration, α values of 1.5, 2.0 and F_i/F^* are chosen; the last choice applies a varying correction factor across the chromatogram, the correction increasing in severity with increasing deviation between the measured and calculated chromatograms.

The algorithms, eqns. (4.10)-(4.12) were evaluated by comparing

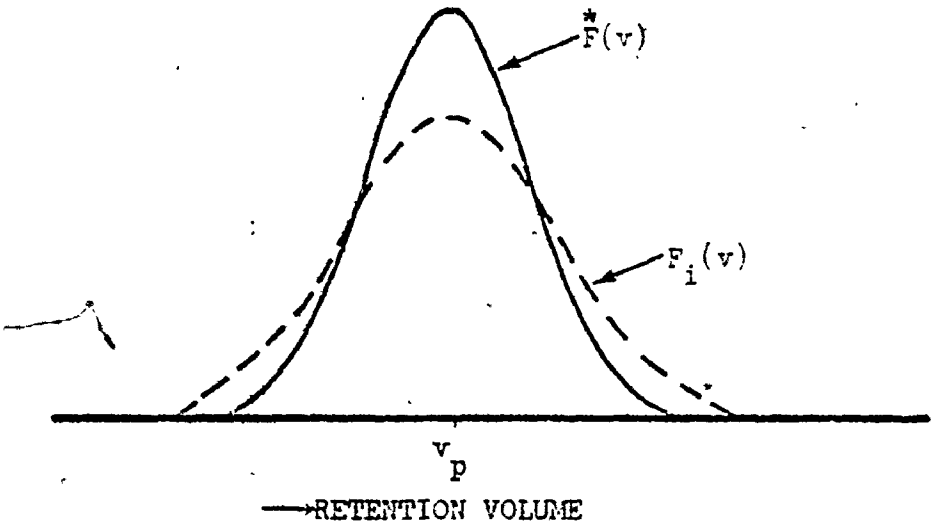

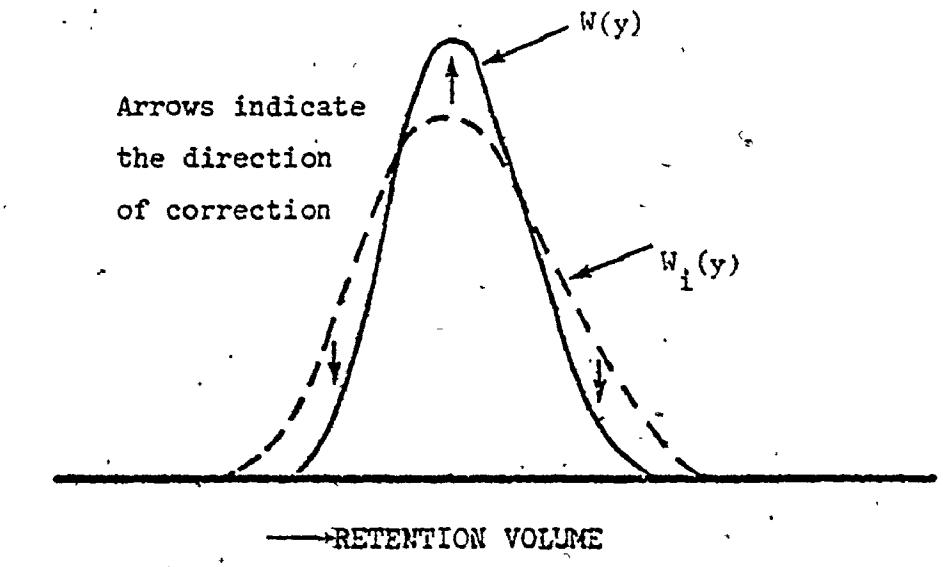

Fig. 4.1 Graphical illustration of the algorithm [eqn.(4.10)]

the recovered W(y) for various synthesized chromatograms. For convenience, examples from the literature were used with one exception, where mixtures of two narrow particle size distribution samples were considered. The results are shown in Tables 4.2-4.5 and Fig. 4.2. The recovered W(y) for all cases using any of the above procedures were comparable though, in some cases they deviated significantly from the true W(y). In all cases, however, calculated diameter averages were in good agreement with assumed values. It is obvious from the results that: 1) the procedure suggested by Silebi and McHugh is computationally very inefficient. It over-estimates the small particle population to the same extent that Ishige's procedure or any of its other variations do. 2) as expected, when $\alpha>1$, convergence is accelerated, in some cases computation time being significantly lower. In some cases, where oscillations occur in the recovered W(y), the problem may be overcome by a suitable choice of α. 3) Fig. 4.2 illustrates the fallacy of numerically recovering W(y) when the true W(y) is a discrete rather than a continuous distribution.

Even though diameter averages can be calculated with fairly good accuracy, in general, the poor recovery of W(y) that are obtained from any of the above methods and by extension the earlier reported methods (since these were shown to be inferior to Ishige's method), detracts from the use of numerical procedures to estimate the size distribution frequency. Calculation of diameter averages can be accomplished more economically by analytical considerations of eqn. (4.3). These are developed in great detail in Section 4.4.

Table 4.2 Numerical Recovery of W(y)

Original W(y)	2 Peak W(y), Tung (1969)		
G(v-y)	Gaussian, σ^2= 0.5	Gaussian, σ^2=2.0	Gaussian, σ^2= 4.0
F*(v)	Bimodal	Bimodal	Unimodal
Algorithm+	1 2 3 4 5	1 2 3 4 5	1 2 3 4 5
No. of iterations	2 2 2 4 2	4 6 3 4 4	7 10 5 4 7
Tolerance attained ($\times 10^{-4}$)	57 73 64 73 47	90 67 55 87 77	94 96 78 73 81
Execution time relative to Ishige's method	1.0 1.1 1.0 1.2 1.0	1.0 1.6 0.9 1.0 1.0	1.0 1.9 0.8 0.7 1.0
Most efficient algorithm	Eqn.(4.12), $\alpha = F_i/F^*$	Eqn.(4.12), α = 1.5	Eqn.(4.12), α = 2.0

+ 1, Ishige's ; 2, Silebi's ; 3, α=1.5 ; 4, α=2/0 ; 5, $\alpha=F_1/F^*$

Table 4.3 Numerical Recovery of W(y)

Original W(y)	3 Peak W(y) (recovered from Case 1A data of Ishige)														
G(v-y)	Gaussian σ^2= 0.5					Gaussian, σ^2= 1.0					Gaussian, σ^2=2.0					Provder & Rosen's Spreading Function c^2= 1.0, A_3= 1.0				
F*(v)	3 Peaks					3 Peaks					Unimodal					3 peaks				
Algorithm+	1	2	3	4	5	1	2	3	4	5	1	2	3	4	5	1	2	3	4	5
No. of iterations	5	6	3	10	5	5	7	4	11	5	14	29	10	7	13	11	11	8	9	11
Tolerance attained ($\times 10^{-4}$)	71	92	91	90	64	86	82	56	96	79	96	98	89	98	98	88	91	85	72	91
Execution time relative to Ishige's method	1.0	1.3	0.9	1.3	1.0	1.0	1.5	1.0	1.4	1.0	3.0	0.8	0.6	1.0	1.0	1.0	1.0	0.8	0.9	1.0
Most efficient algorithm	Eqn.(4.12) α=1.5 & F_i/F^*					Eqn.(4.12) α=1.5					Eqn.(4.12) α=1.5 & 2.0					Eqn.(4.12) α=1.5 & 2.0				

+ 1, Ishige's ; 2, Silebi's ; 3, α=1.5 ; 4, α=2.0 ; 5, $\alpha=F_i/F^*$

Table 4.4 Numerical Recovery of W(y)

Original W(y)	2 Peaks and a shoulder
G(v-y)	Gaussian, $\sigma^2 = 1$
F*(v)	F*(v) given to 3 significant digits (case 2A data of Ishige)

Algorithm	Remarks
Ishige's $\alpha = 1.5$ $\alpha = F_i/F^*$	Oscillations in main portion of recovered W(y)
Silebi's	Converged in 10 iterations to a tolerance of 0.0096. Recovered W(y) is smooth and shows evidence of 2 peaks though the second peak position is in error. Recovery is comparable to that obtained with F*(v) specified to 4 significant digits.
$\alpha=2$	Recovery is similar to that in Silebi's method. A convergence to a tolerance of .0095 was obtained in 5 iterations, however.

Table 4.5 Numerical Recovery of W(y)

Original W(y)	2 Peak W(y) composed of a mixture of 176/109 nm particles in the ratio 1:n														
G(v-y)	Gaussian, $\sigma^2 = 0.5\ m\ell^2$														
F*(v)	2 Peak F*(v)														
n	3					1					1/3				
Algorithm+	1	2	3	4	5	1	2	3	4	5	1	2	3	4	5
No. of iterations	276	516	184	25	302	254	511	170	7	274	240	579	161	7	265
Tolerance attained ($\times 10^{-4}$)	133	132	133	461	131	154	147	154	984	151	161	145	161	994	159
Execution time relative to Ishige's method	1.00	3.10	0.68	0.13	1.10	1.00	3.30	0.68	0.07	1.10	1.00	4.00	0.69	0.08	1.10
n, calculated	4.80	4.85	4.80	4.60	4.80	1.60	1.60	1.60	1.40	1.60	0.53	0.53	0.53	0.41	0.53
Most efficient algorithm	Eqn.(4.12), $\alpha=2.0$					Eqn.(4.12), $\alpha=2.0$					Eqn.(4.12), $\alpha=2.0$				

+ 1, Ishige's ; 2, Silebi's ; 3, =1.5 ; 4, =2.0 ; 5, $=F_i/F^*$

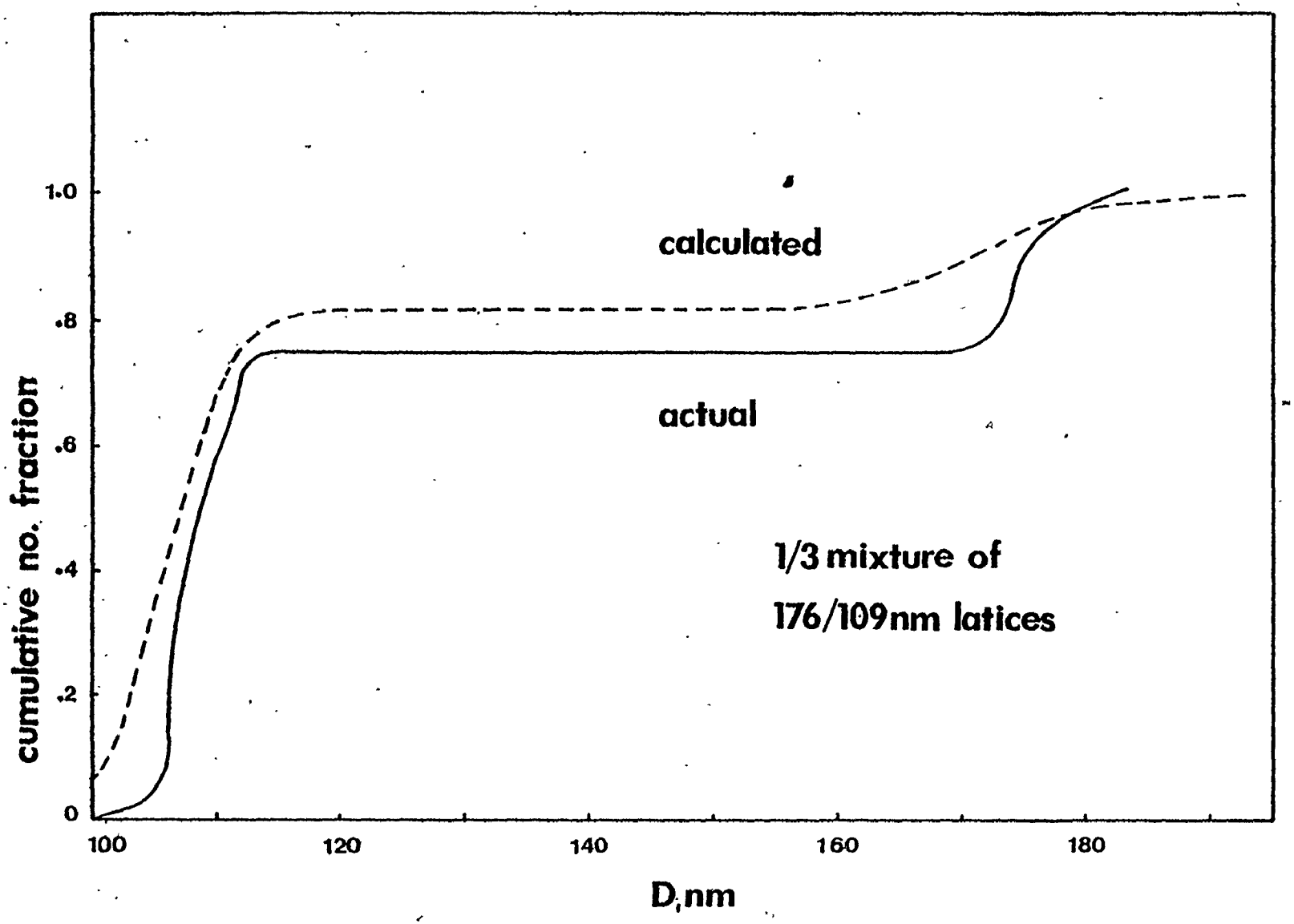

Fig. 4.2 A comparison of the distribution calculated from eqn.(4.12), (α=2.0) with the assumed distribution for a bimodal mixture of particles.

4.3 NUMERICAL SOLUTION OF THE AXIAL DISPERSION EQUATION-SOLVING FOR THE SPREADING FUNCTION

When W(y) is composed of essentially single sized species, then the measured chromatogram is in fact the spreading function for that species. The statistical properties of such a function are size or retention volume dependent and, hence, attempts to estimate the spreading function have involved the use of narrow distribution standards. When the standards are ultra-narrow, then it is justified to assume that the measured chromatogram reflects the spreading characteristics of the chromatographic columns. Most available standards are, however, not sufficiently monodispersed and the identification of the spreading function, in general, requires a knowledge of their size distribution. One exception is the reverse flow technique, proposed by Tung, Moore and Knight (1966); it allows an estimate of the spreading function independent of the size distribution function of the injected standards.

The reverse flow technique is based on the assumption that, when the flow is reversed, the process of size separation is reversed also, while, instrumental spreading continues to broaden the peak. With this technique, a standard sample is allowed to flow through half of the column length; the direction of flow is then reversed. The resulting chromatogram reflects the spreading characteristics of that half of the column. The process is repeated for the other half. When a Gaussian spreading function is assumed, its variance σ^2 is related to σ_1^2 and σ_2^2, the variances of the measured chromatograms, by the following

relationship:

$$\sigma^2 = (\sigma_1^2 + \sigma_2^2)/2 \qquad (4.13)$$

A less tedious procedure [Tung and Runyon (1969)] involves fitting the leading edge of the chromatogram with a Gaussian function with variance, σ_c^2. If σ^2 (as determined by the reverse flow technique) and σ_c^2 are equal within experimental error, then it is inferred that the leading edge of the chromatogram is monodispersed. Otherwise, the assumption of a Gaussian W(y) together with the calibration curve information, leads to an estimation of the size distribution of the leading edge. Such information is then used for an unknown column to estimate its spreading characteristics. This procedure assumes that the leading edge of the chromatogram is composed of similar sized species irrespective of a column's resolution. This, clearly, cannot be expected to hold in general.

A more direct approach and widely used, involves the use of moment equations derivable from eqn. (4.3). The parameters of the spreading function, either Gaussian or skewed, are calculated from a knowledge of the averages of the size distribution, typically, the number and the weight average. The spreading function generated from such estimates may not necessarily represent the actual spreading characteristic of the column and correlations of the spreading function parameters with retention volume must be regarded with caution.

Recently, Berger (1979) suggested a calculation procedure based

on the simultaneous solution of eqn. (4.3) and

$$C_n(v) = \int_{-\infty}^{\infty} \{W(y)\ G(v_n,y)\ \Delta y\}\ G(v,y)\ dy \qquad (4.14)$$

where $C_n(v)$ is the chromatogram of the re-injected fraction collected at the retention volume, v_n. No restriction was placed on the form of $G(v,y)$ except that it is uniform.

In this section, a simple numerical procedure is presented for estimating the spreading function from eqn. (4.3). It is assumed that $W(y)$ is known. For a latex sample, such information can be obtained by electron microscopy. When a sample has a narrow distribution, parameters of the calculated $G(v,y)$ may be related to the mean size. However, when the sample is broad, the calculated $G(v,y)$ is an effective spreading function which may be used to calculate $W(y)$ for an unknown sample having a similar width.

The procedure used is similar to that of Ishige et al (1971) for calculating $W(y)$. It is assessed using synthesized chromatograms. Application to experimental chromatograms of Dow polystyrene latices is shown in Chapter 5. For a turbidity detector,

$$W(y) \propto N(y)\ K(y)\ D^2(y) \qquad (4.15)$$

where N and K are the number concentration and extinction coefficient respectively of a particle of size D having a mean retention volume y. For a linear calibration curve,

$$D(y) = D_1 \exp(-D_2 y) \tag{4.9}$$

$$dD(y) = -D_2 D(y)\, dy \tag{4.16}$$

where D_1 and D_2 are the calibration constants. N(y) is related to the particle size distribution, f(D), as follows:

$$f(D)\, dD = \frac{-N(y)\, dy}{\int_0^\infty N(y)\, dy} \tag{4.17}$$

where f(D) dD is the fraction of particles in the size range D to D + dD. The negative sign in eqn. (4.17) is due to the negative slope of the calibration curve. It follows from the above equations that,

$$W(y) \propto f(D)\, K(y)\, D^3(y) \tag{4.18}$$

Substituting eqn. (4.18) in eqn. (4.3) yields

$$\tilde{F}(v) \propto \int_0^\infty f(D)\, K(y)\, D^3(y)\, G(v,y)\, dy \tag{4.19}$$

A discrete form of eqn. (4.19) is more suited when the function, f(D), is discontinuous and is given as

$$F(v) \propto \sum_{\text{over all } D} f(D)\, K(y)\, D^2(y)\, G(v,y) \tag{4.20}$$

Extensions of the above equations to a nonlinear calibration curve are straight-forward.

Consider the numerical solution of eqn. (4.3) or any of its forms, eqn. (4.19) or (4.20). It is assumed that the spreading function is uniform; it is, therefore, necessary to solve only for one distribution function.

If one, initially, sets the spreading function (corresponding to $y = v_p$) equal to the measured chromatogram F(v), i.e.,

$$G_1(v - v_p) = F(v) \tag{4.21}$$

then since the spreading function is assumed uniform, it follows that

$$G_1(v - y) = F(v_p + v - y) \quad \text{(see Fig. 4.3)} \tag{4.22}$$

v_p is the peak retention volume of the measured chromatogram. Eqns. (4.21) and (4.22) provide an excellent initial guess for the spreading function, since, the chromatogram of narrow standards largely reflect the spreading characteristics of the instrument. Subsequent improved estimates of the spreading function are obtained as follows:

$$G_{i+1} = (F/F_i)G_i \tag{4.23}$$

The procedure in eqn. (4.23) is repeated until convergence occurs. If

$$P = \int_0^\infty | F(v) - F_1(v) | \, dv \tag{4.24}$$

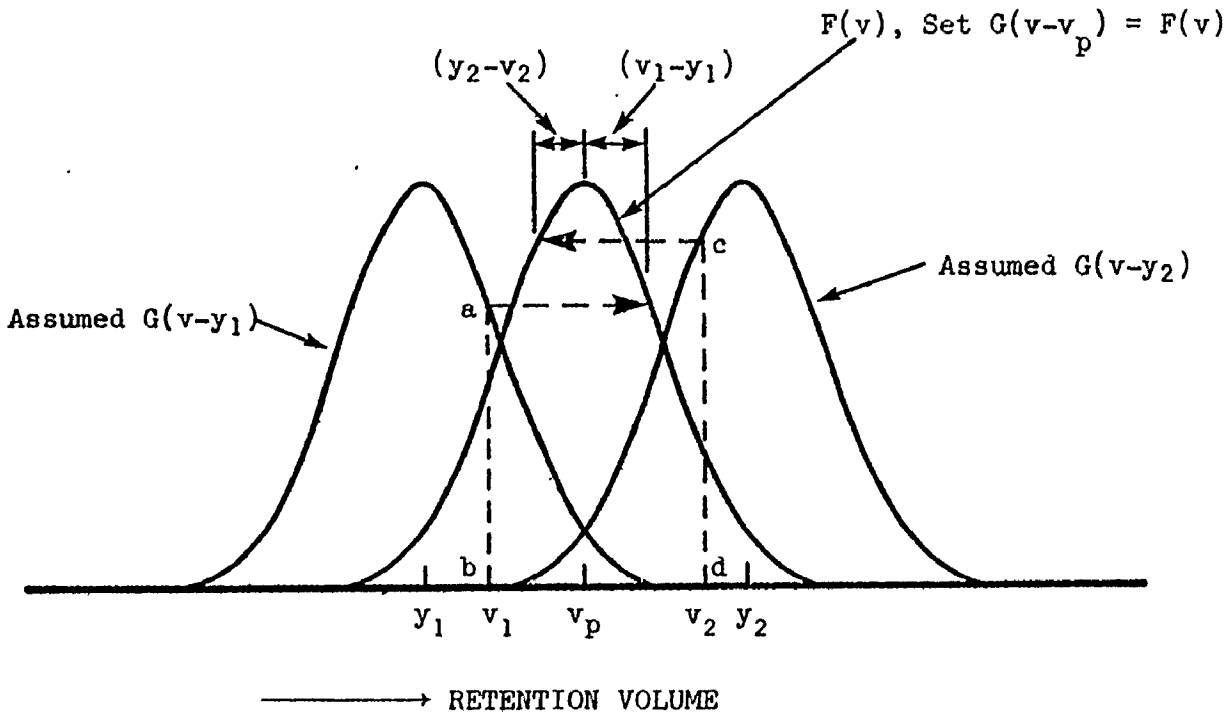

Example:

$$G(v_1 - y_1) \equiv ab \equiv F(v_p + v_1 - y_1)$$

$$G(v_2 - y_2) \equiv cd \equiv F(v_p + v_2 - y_2)$$

Fig. 4.3 The initial estimate for the spreading function.

is less than a given tolerance (a tolerance of 0.01 was set in the calculations) or if the value of P for the i^{th} iteration exceeds the value at the previous iteration, without the tolerance being satisfied, then, the calculations are terminated. It is to be noted, that, each new estimate of the spreading function must be normalized.

The procedure stated in eqn. (4.23) was evaluated by synthesizing F(v) using an assumed spreading function and an assumed W(y). The spreading function was either a Gaussian or a skewed function obtained by setting all coefficients except A_3 equal to zero in the statistical shape function proposed by Provder and Rosen (1970). To calculate W(y), electron microscopy data of Dow polystyrene latices were used and the extinction coefficients were calculated using either Rayleigh or Mie theory. The results are presented in Figs. 4.4–4.11 where the estimated spreading function is compared with the actual function.

The values of the parameter σ^2 used in the computations span a wide range with a value of 0.5 ml^2 being representative of columns used in hydrodynamic chromatography, while, larger values are encountered in size exclusion chromatography. Significant skewing is introduced by setting $A_3 = 1.0$. It is evident from the results, that, the calculated spreading functions compare very favourably with the assumed functions over the entire range of retention volumes.

Also shown in the plots are the ratios of the chromatogram heights calculated according to Mie theory to those calculated according to Rayleigh theory. These indicate a rather low sensitivity of the

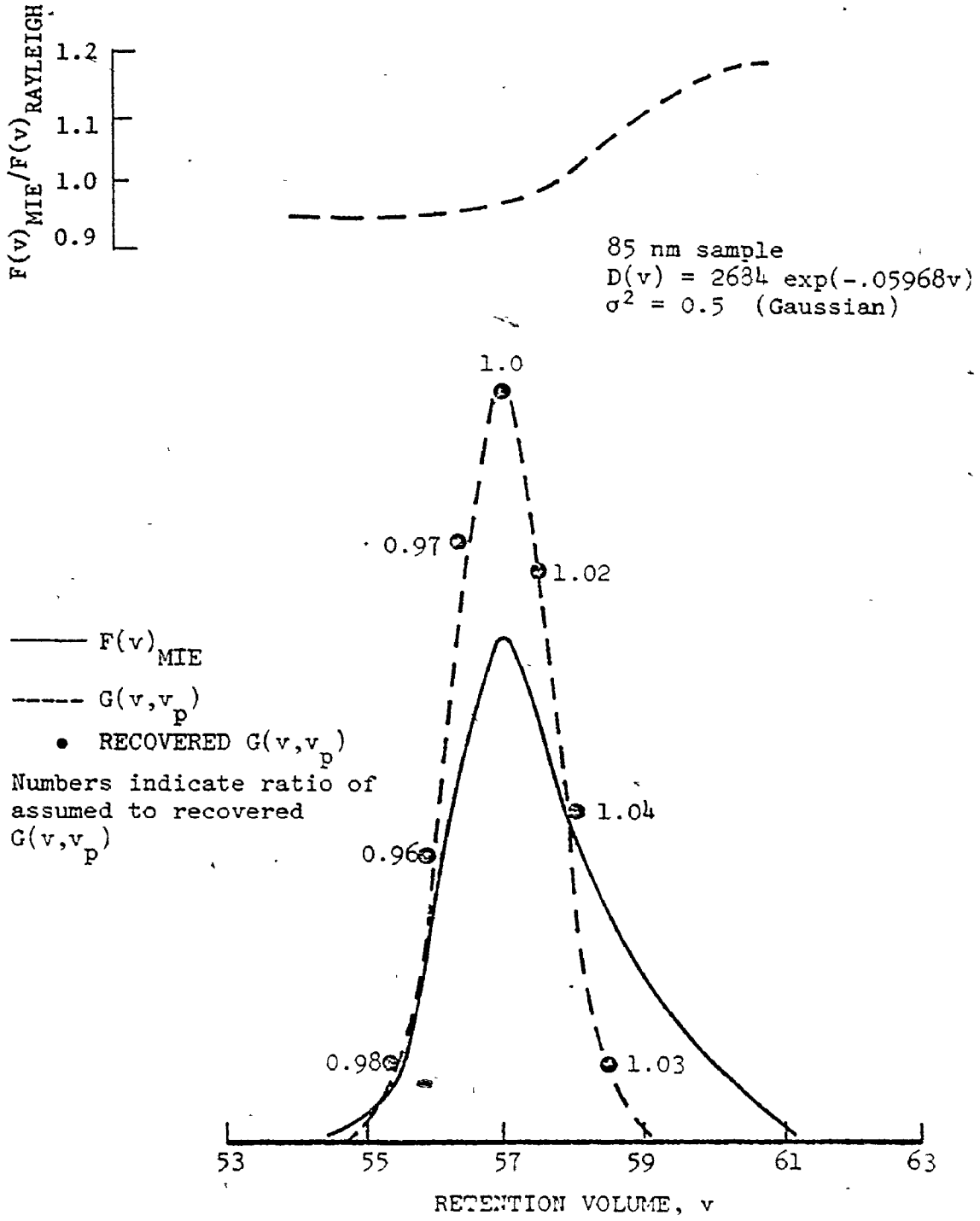

Fig. 4.4 Comparison of assumed and calculated spreading functions.

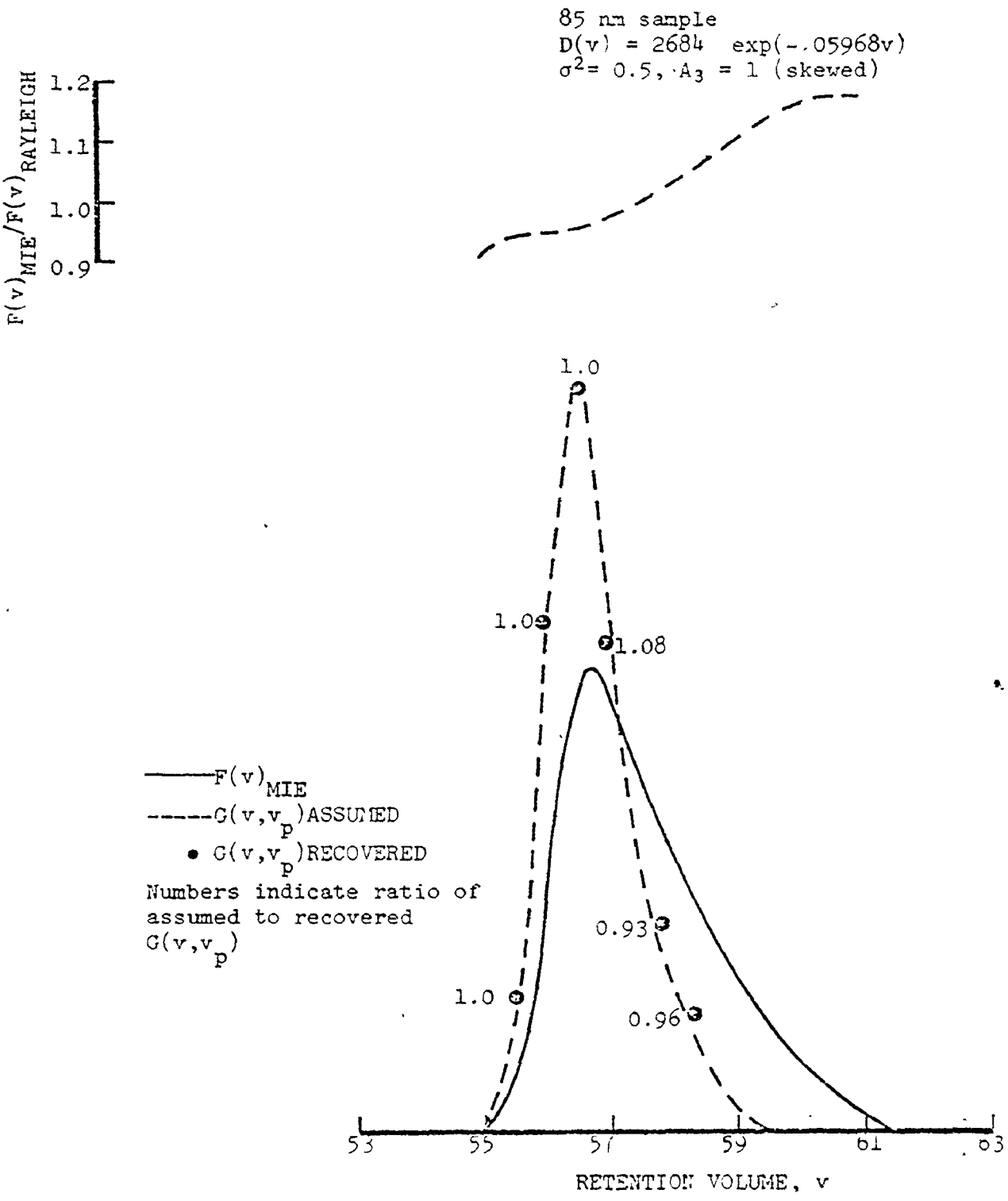

Fig. 4.5 Comparison of assumed and calculated spreading functions.

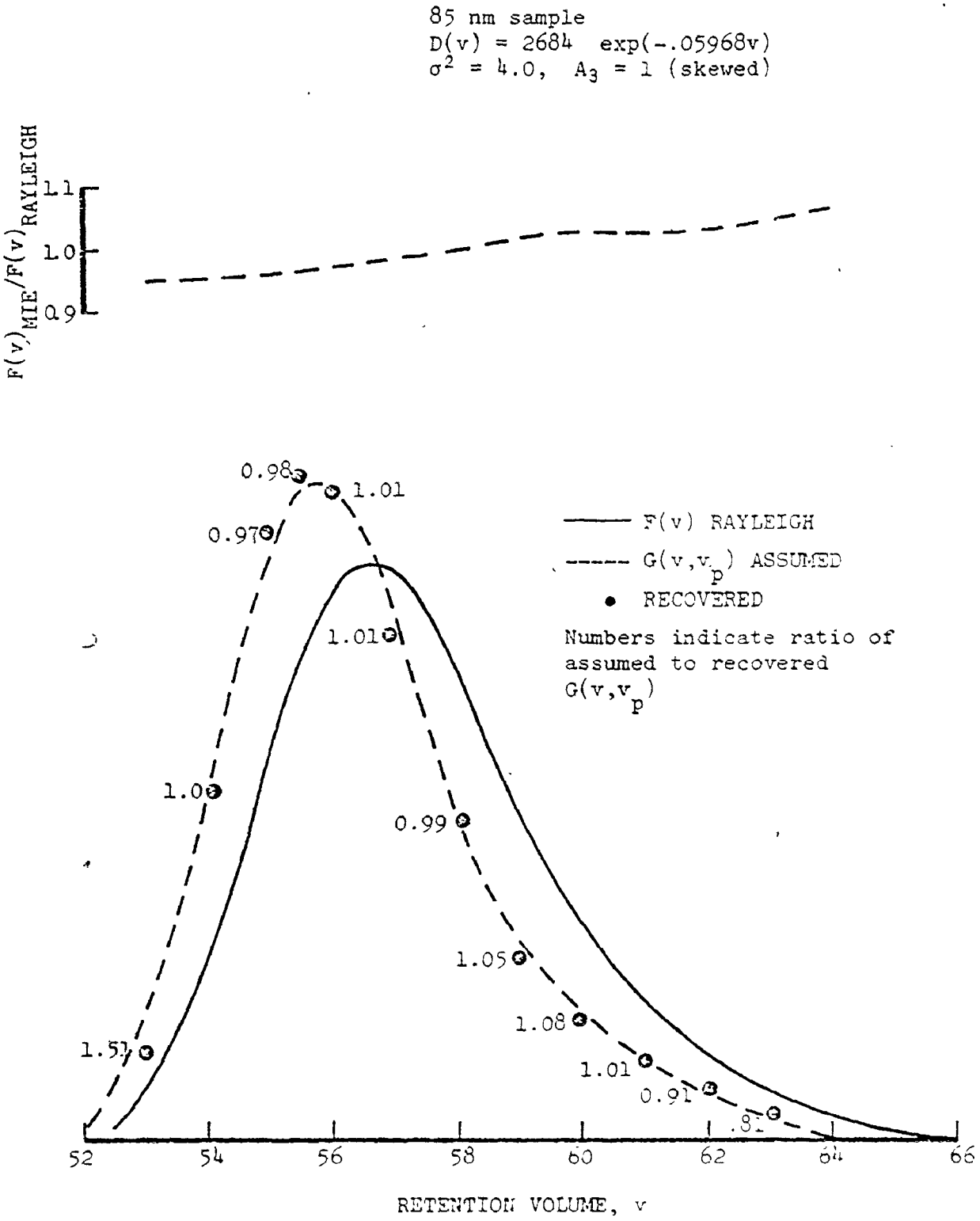

Fig. 4.6 Comparison of assumed and calculated spreading functions.

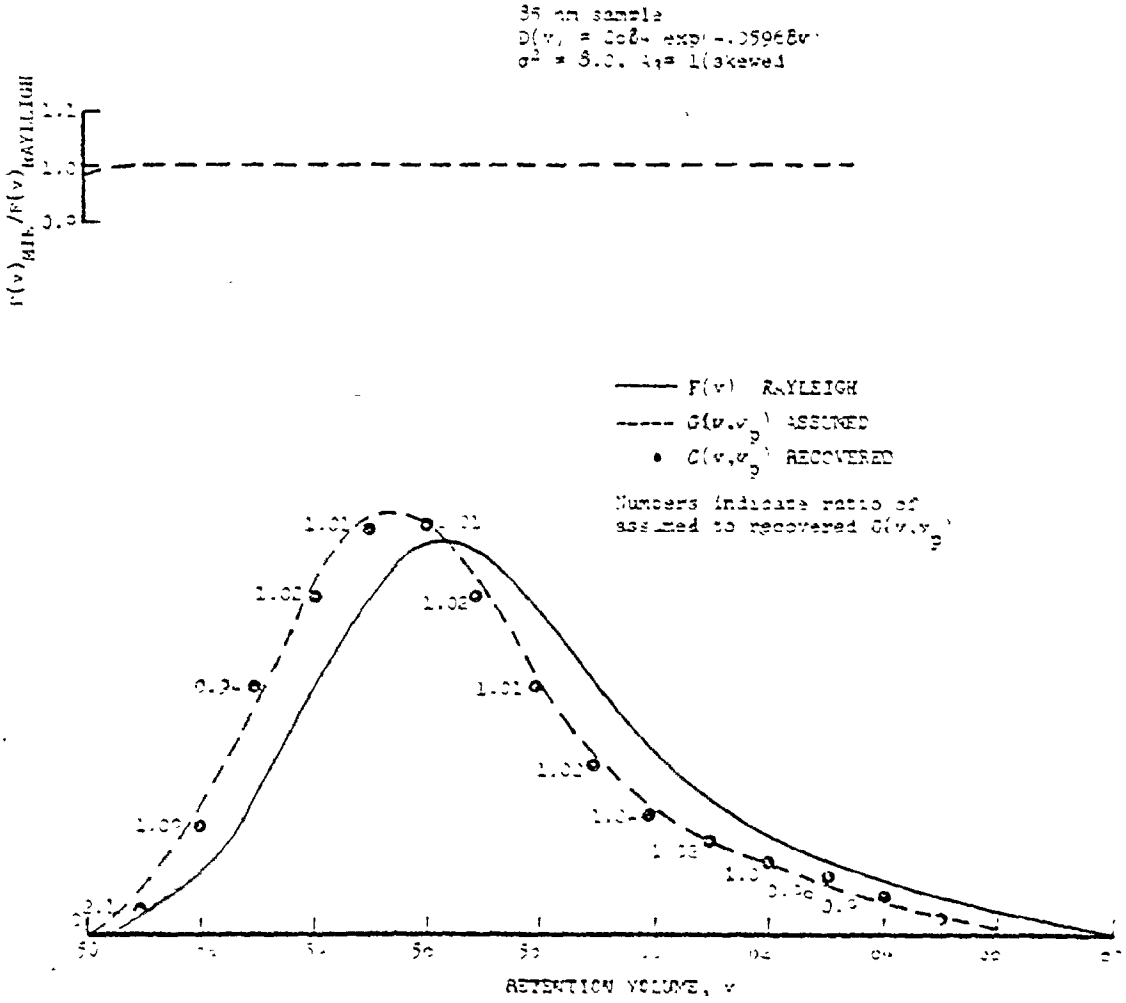

Fig. 4.7 Comparison of assumed and calculated spreading functions.

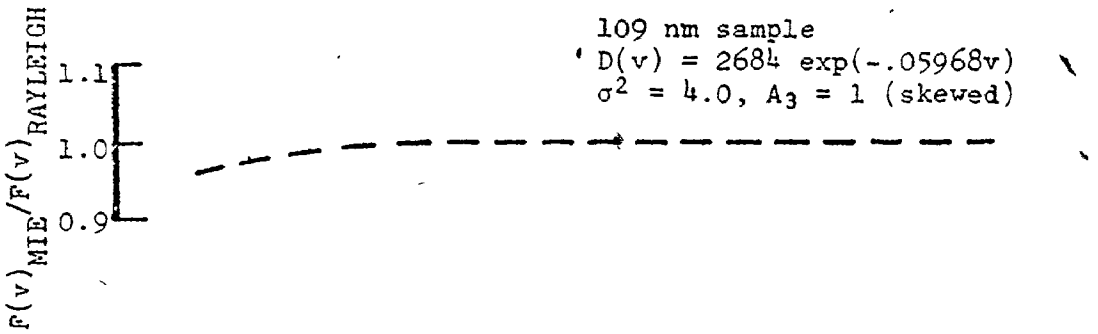

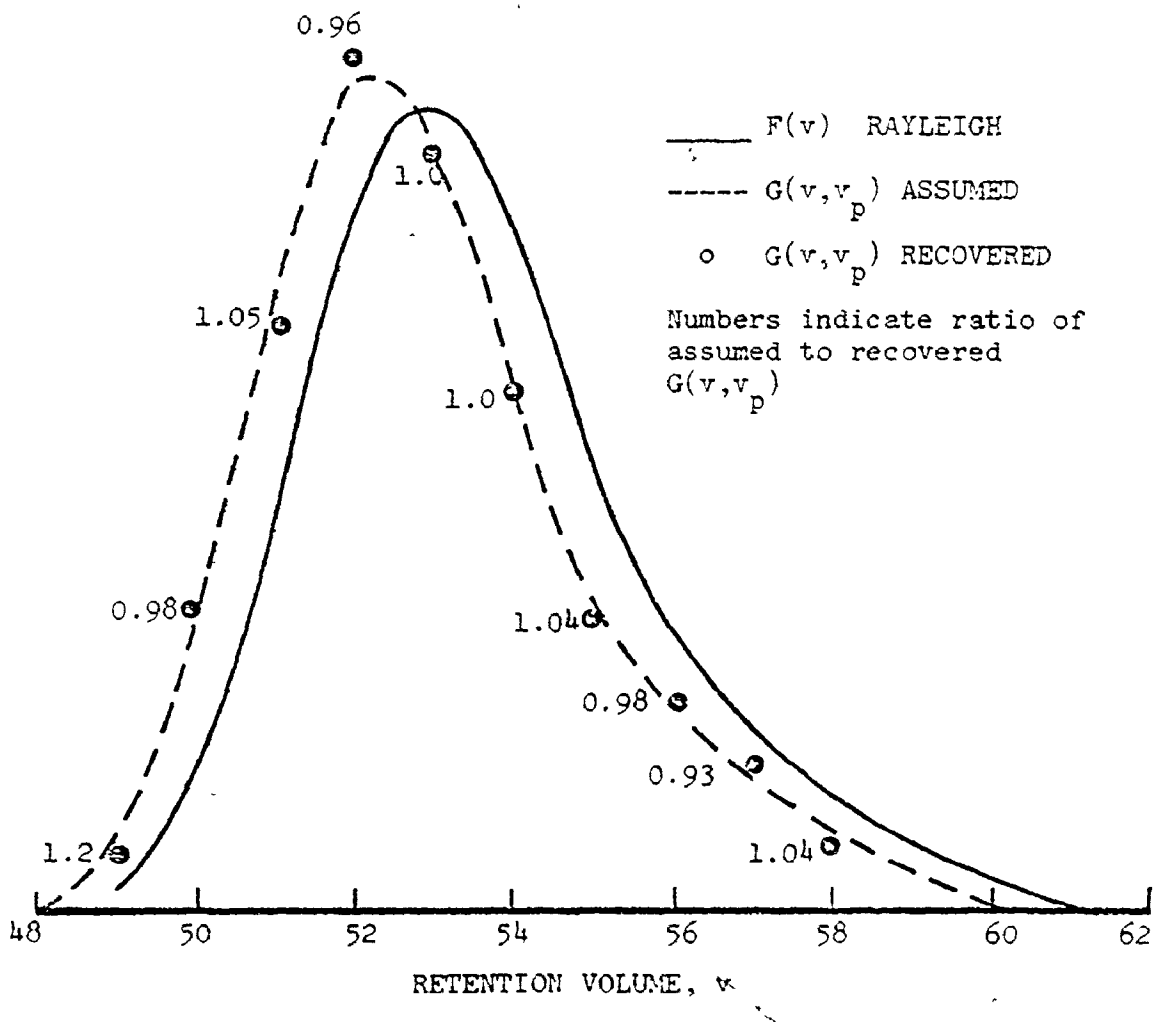

Fig. 4.8 Comparison of assumed and calculated spreading functions.

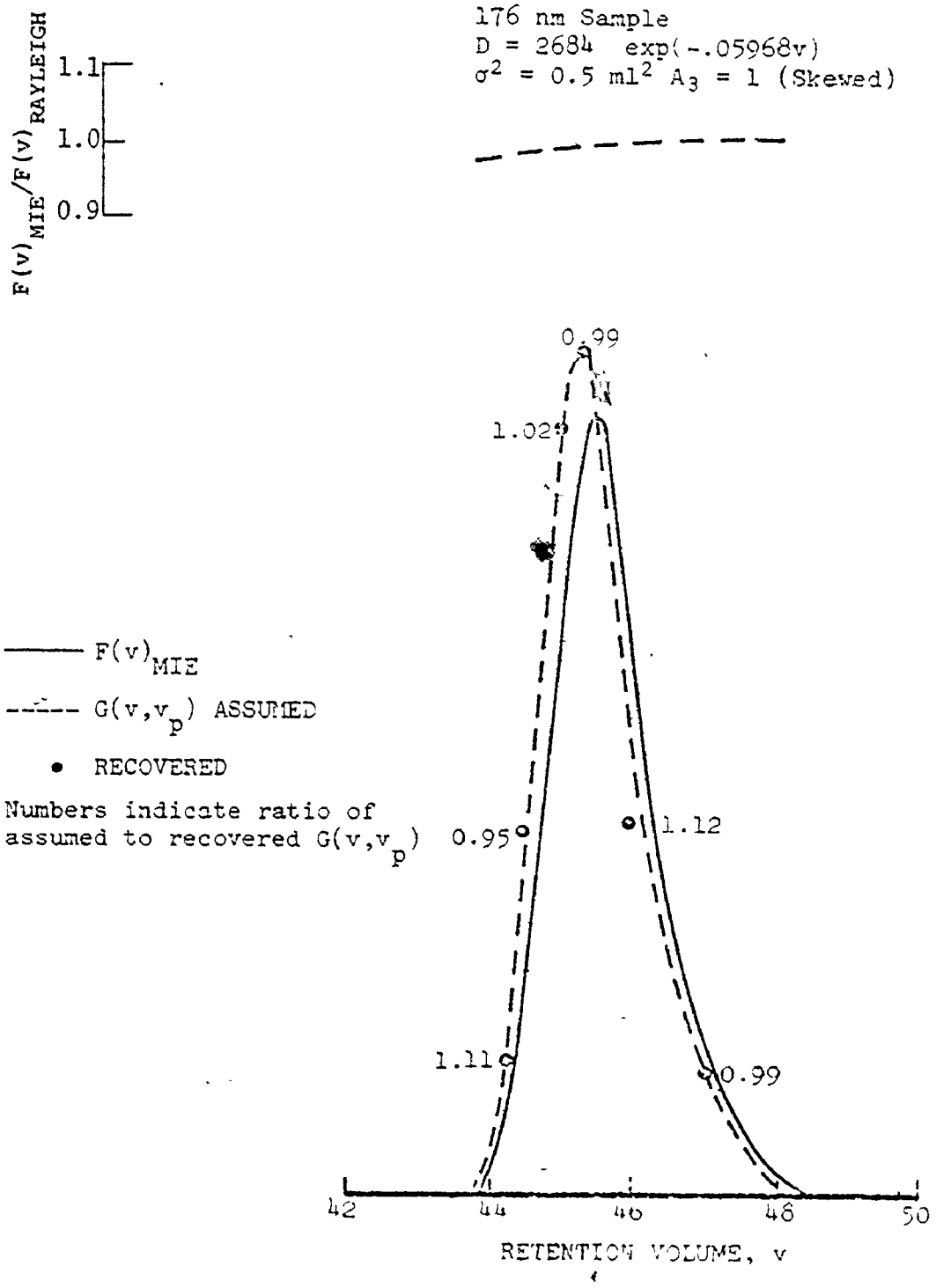

Fig. 4.9 Comparison of assumed and calculated spreading functions.

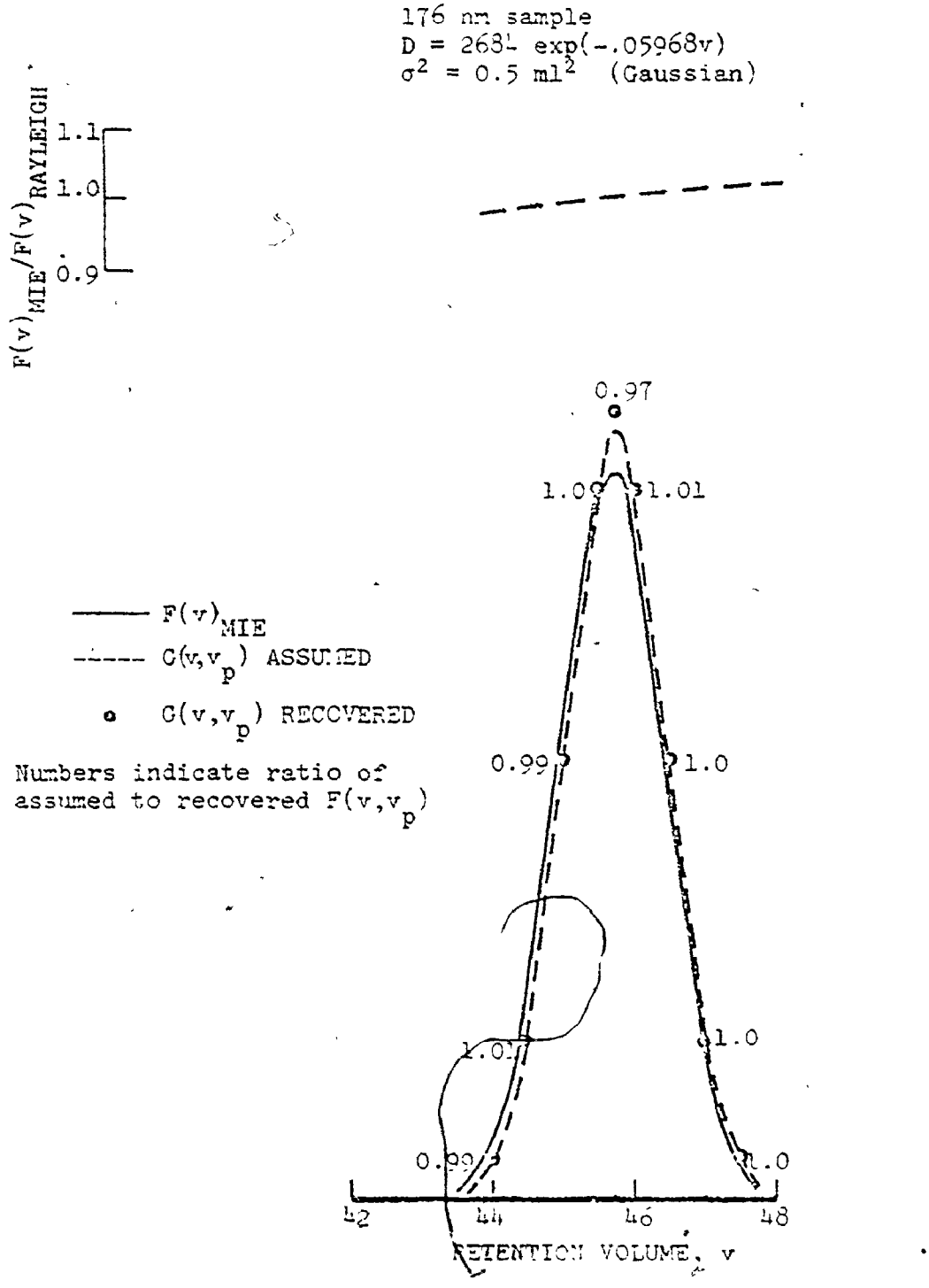

Fig. 4.10 Comparison of assumed and calculated spreading functions.

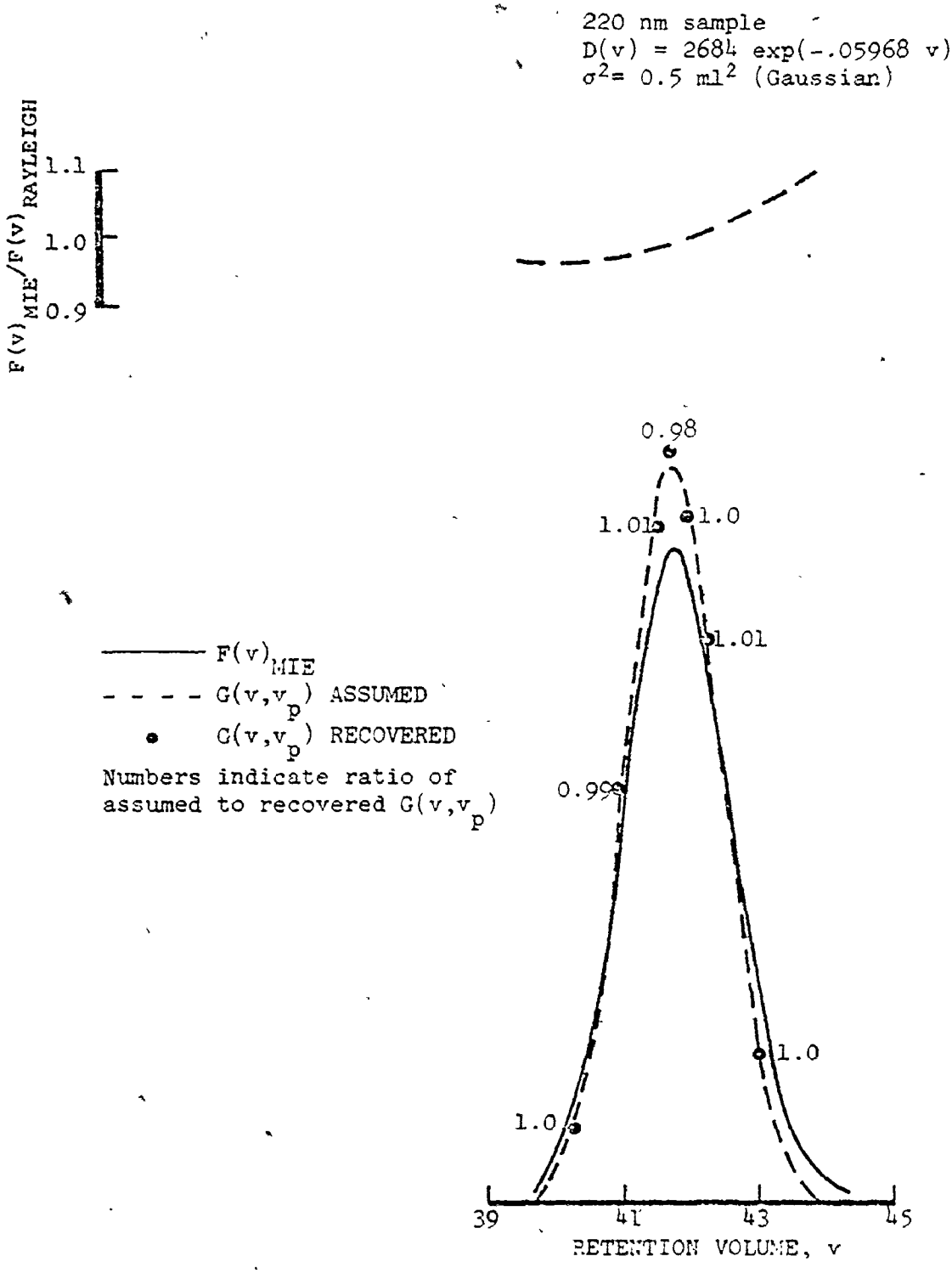

Fig. 4.11 Comparison of assumed and calculated spreading functions.

calculated narrow distribution chromatograms to the light scattering theory applied.

When applied to experimental chromatograms of narrow particle standards, the calculated spreading function data allows an independent assessment of the adequacy of functions (Gaussian or the statistical shape function) assumed to describe them. The method suggested here can form the basis for a systematic investigation of the variation of spreading function parameters with retention volume over a wide range of operating conditions. It should be stressed that parameters calculated in this manner, represent their actual values, rather than manipulated variables such as are obtained when searching for their values with the help of moment equations (Section 4.4).

4.4 ANALYTICAL SOLUTION OF THE AXIAL DISPERSION EQUATION-SOLVING FOR THE MOMENTS OF THE SIZE DISTRIBUTION FUNCTION

In this section, three analytical methods of varying generality for solving Tung's integral equation are presented. Method 1 was developed by Hamielec and Singh (1979) while Methods 2 and 3 have been developed during the course of this study. These methods, of which Method 3 is most general, should find extensive application in the analysis of chromatograms obtained by the various forms of particle chromatography. Each of the methods is now discussed in detail.

4.4.1 Laplace Transform Method of Hamielec and Singh-Method 1

Taking the Laplace transform of the convolution integral

resulting from the substitution of eqn. (4.4) in eqn. (4.3), yields

$$\bar{F}(s) = \bar{W}(s)\,\bar{G}(s) \tag{4.25}$$

If all coefficients except A_3 in eqn. (4.6) are zero then,

$$\bar{G}(s) = \exp(s^2\sigma^2/2)(1 - \sigma^3 s^3 A_3/6) \tag{4.26}$$

For a turbidity detector in the Rayleigh scattering regime,

$$F(v) \propto N(v)\,D^6(v) \tag{4.27}$$

where N(v) is the number concentration of particles of diameter D(v) at retention volume, v. The corresponding equation for a refractive index detector is similar but with a third order diameter dependence. In general, therefore, the detector signal is of the form:

$$F(v) \propto N(v)\,D^{\gamma}(v) \tag{4.28}$$

The uncorrected frequency distribution is given by

$$f(D)\,dD = -N(v)\,dv \,/\, \int_0^{\infty} N(v)\,dv \tag{4.29}$$

where the negative sign appears due to the inverse relationship of the diameter with retention volume. Ln D(v) is usually linearly related

with retention volume and hence can be expressed as

$$D(v) = D_1 \exp(-D_2 v) \tag{4.9}$$

where D_1 and D_2 are constants. The various diameter averages (see Appendix A.1 for their definitions) may be expressed in terms of Laplace transforms, for e.g.,

$$D_n(uc) = D_1 \bar{F}[(1-\gamma)D_2] \; / \; \bar{F}(-\gamma D_2) \tag{4.30}$$

$$D_n(c) = D_1 \bar{W}[(1-\gamma)D_2] \; / \; \bar{W}(-\gamma D_2) \tag{4.31}$$

Subscripts, uc and c, represent uncorrected and corrected diameter averages. It follows from eqns. (4.30) and (4.31) that

$$\frac{D_n(c)}{D_n(uc)} = \frac{\bar{G}(-\gamma D_2)}{\bar{G}[(1-\gamma)D_2]} = \exp[(\gamma-1/2)D_2^2 \sigma^2][\frac{1 + \gamma^3 \alpha D_2^3}{1-(1-\gamma)^3 \alpha D_2^3}] \tag{4.32}$$

where

$$\alpha = \sigma^3 A_3/6 \tag{4.33}$$

The right hand side of eqn. (4.32) represents a correction factor for the number average diameter. The correction factor is comprised of an exponential term representing an axial dispersion correction for Gaussian spreading and a second term representing a skewing correction. Similar correction factors for the other diameter averages are given in Table 4.6. Therefore, to calculate the corrected diameter averages, the uncorrected diameter averages calculated directly from the chromatogram

Table 4.6 Axial Dispersion Correction Factors ($B' \equiv D_2$)

Diameter Average t	Correction Factor: General Detector	Turbidity Detector ($\gamma=6$) $\alpha=0$	Refractive Index Detector ($\gamma=3$) $\alpha=0$
$D_n(c)/D_n(uc)$	$\exp[(\gamma-1/2)B'^2\sigma^2]\dfrac{(1+\gamma^3\alpha B'^3)}{[1-(1-\gamma)^3\alpha B'^3]}$	$\exp(11\ B'^2\sigma^2/2)$	$\exp(5\ B'^2\sigma^2/2)$
$D_s(c)/D_s(uc)$	$\exp[(\gamma-1)B'^2\sigma^2]\ \dfrac{(1+\gamma^3\alpha B'^3)^{1/2}}{[1-(2-\gamma)^3\alpha\ B'^3]^{1/2}}$	$\exp(10\ B'^2\sigma^2/2)$	$\exp(4\ B'^2\sigma^2/2)$
$D_v(c)/D_v(uc)$	$\exp[(\gamma-3/2)B'^2\sigma^2]\dfrac{(1+\gamma^3\alpha\ B'^3)^{1/3}}{[1-(3-\gamma)^3\alpha\ B'^3]^{1/3}}$	$\exp(9\ B'^2\sigma^2/2)$	$\exp(3\ B'^2\sigma^2/2)$
$D_{ss}(c)/D_{ss}(uc)$	$\exp[(\gamma-5/2)B'^2\sigma^2]\dfrac{[1-(2-\gamma)^3\alpha\ B'^3]}{[1-(3-\gamma)^3\alpha B'^3]}$	$\exp(7\ B'^2\sigma^2/2)$	$\exp(B'^2\sigma^2/2)$
$D_w(c)/D_w(uc)$	$\exp[(\gamma-7/2)B'^2\sigma^2]\dfrac{[1-(3-\gamma)^3\alpha\ B'^3]}{[1-(4-\gamma)^3\alpha\ B'^3]}$	$\exp(5\ B'^2\sigma^2/2)$	$\exp(-B'^2\sigma^2/2)$
$D_t(c)/D_t(uc)$	$\exp[(\gamma-9/2)B'^2\sigma^2]\dfrac{[1-(3-\gamma)^3\alpha\ B'^3]^{1/3}}{[1-(6-\gamma)^3\alpha\ B'^3]^{1/3}}$	$\exp(3\ B'^2\sigma^2/2)$	$\exp(-3\ B'^2\sigma^2/2)$

are multiplied by appropriate correction factors. It is clear that the correction factors are specific for each detector type.

4.4.2 A New Method for Calculating Moments of the Size Distribution as a Function of Retention Volume - Method 2

Since Rayleigh scattering theory applies only to particles at the low end of the colloidal range, the previous formulae for the turbidity detector are rather restrictive in their application. The following analysis considers a turbidity detector in the Mie scattering regime. Moments of the frequency distribution and the number of particles in the detector cell are evaluated as a function of retention volume. This enables all relevant diameter averages for the sample to be calculated. The development parallels that of Yau et al (1977) for molecular weight analysis by size exclusion chromatography.

Due to column dispersion, the contents of the detector cell at any retention volume are polydispersed, and may be considered as made up of all species at retention volume y which are dispersed to v. Accordingly, for a turbidity detector, the following proportionality holds:

$$W(y)\, G(v,y) \propto N(v,y)\, K(y)\, D^2(y) \text{ at retention volume } v \qquad (4.34)$$

where K(y) and N(v,y) are respectively, the extinction coefficient and number concentration of particles with mean retention volume, y at retention volume, v.

The corrected frequency distribution, f(v,D), at v may then be expressed as

$$f(v,D)\,dD = -\frac{N(v,y)dy}{\int_0^\infty N(v,y)dy} \tag{4.35}$$

From eqn. (4.34), it follows that,

$$f(v,D)\,dD = -\frac{W(y)\,G(v,y)\,\{K(y)\,D^2(y)\}^{-1}dy}{\int_0^\infty W(y)\,G(v,y)\,\{K(y)\,D^2(y)\}^{-1}dy} \tag{4.36}$$

It follows from their definitions (Appendix A.1) that the average diameters of the particles eluting at v may be expressed as

$$D_n(v) = \{\int_0^\infty N(v,y)\,D(y)\,dy\} / \{\int_0^\infty N(v,y)\,dy\} \tag{4.37}$$

$$D_s(v) = \{\int_0^\infty N(v,y)\,D^2(y)\,dy\}^{1/2} / \{\int_0^\infty N(v,y)\,dy\}^{1/2} \tag{4.38}$$

$$D_v(v) = \{\int_0^\infty N(v,y)\,D^3(y)\,dy\}^{1/3} / \{\int_0^\infty N(v,y)\,dy\}^{1/3} \tag{4.39}$$

$$D_{ss}(v) = \{\int_0^\infty N(v,y)\,D^3(y)\,dy\} / \{\int_0^\infty N(v,y)\,D^2(y)\,dy\} \tag{4.40}$$

$$D_w(v) = \{\int_0^\infty N(v,y)\,D^4(y)\,dy\} / \{\int_0^\infty N(v,y)\,D^3(y)\,dy\} \tag{4.41}$$

$$D_t(v) = \{ \int_0^\infty N(v,y)\, D^6(y)\, dy \}^{1/3} / \{ \int_0^\infty N(v,y)\, D^3(y)\, dy \}^{1/3} \quad (4.42)$$

In the above expressions, when N(v,y) is replaced by N(v) (the total number of particles eluting at v), and D(y) in each equation is replaced by the corresponding diameter average, diameter averages for the entire sample are obtained. The integrals in the above expressions are all of the form

$$I(\gamma) = \int_0^\infty W(y)\, G(v,y)\, \{K(y)\, D^2(y)\}^{-1}\, D^\gamma(y)\, dy \quad (4.43)$$

so that

$$D_n(v) = I(1)/I(0) \quad (4.44)$$

$$D_s(v) = \{I(2)/I(0)\}^{1/2} \quad (4.45)$$

$$D_v(v) = \{I(3)/I(0)\}^{1/3} \quad (4.46)$$

$$D_{ss}(v) = I(3)/I(2) \quad (4.47)$$

$$D_w(v) = I(4)/I(3) \quad (4.48)$$

$$D_t(v) = \{I(6)/I(3)\}^{1/3} \quad (4.49)$$

In the following analysis, an analytical solution for eqn. (4.43) is developed. The cases for a linear and a nonlinear calibration curve are treated separately. Both yield solutions of similar form.

Linear Calibration Curve

For a linear particle diameter-retention volume calibration

curve, D(y) may be expressed as

$$D(y) = D_1 \exp(-D_2 y) \tag{4.9}$$

while $K^{-1}(y)$ may be adequately fitted by an expression of the type

$$K^{-1}(y) = \sum_{i=1}^{n} \{A_i \exp(B_i y)\} \tag{4.50}$$

The product $\{K(y)\ D^2(y)\}^{-1}\ D^\gamma(y)$ is then equivalent to

$$\{K(y)\ D^2(y)\}^{-1}\ D^\gamma(y) = \sum_{i=1}^{n} \{C_i \exp(-E_i y)\} \tag{4.51}$$

where $C_i = A_i\ D_1^{\gamma-2}$ and $E_i = -\{B_i + (2-\gamma)D_2\}$ (4.52)

Nonlinear Calibration Curve

A nonlinear particle diameter-retention volume calibration curve D(y), may be expressed as

$$D(y) = \sum_{i=1}^{p} D_i \tag{4.53}$$

where $D_i = D_{i,1} \exp(-D_{i,2} y)$ (4.54)

It follows that, $D^\gamma(y)$ is given by

$$D^{\gamma}(y) = \sum^{m} \frac{\gamma !}{\gamma_1 ! \, \gamma_2 ! \, \ldots . \gamma_p !} D_1^{\gamma_1} D_2^{\gamma_2} \ldots . D_p^{\gamma_p} \qquad (4.55)$$

where the sum is taken over all non-negative integers γ_1, γ_2, ... γ_p for which, $\gamma_1 + \gamma_2 .. + \gamma_p = \gamma$. The number of terms in the summation is denoted by m. The product $\{K(y) \; D^2(y)\}^{-1}$ in eqn. (4.43) may be represented as

$$\{K(y) \; D^2(y)\}^{-1} = \sum_{i=1}^{n} \{A_i \exp(B_i \; y)\} \qquad (4.56)$$

so that $K^{-1}(y) \; D^{\gamma-2}(y)$ is given by

$$K^{-1}(y) \; D^{\gamma-2}(y) = \sum_{i=1}^{mxn} C_i \exp(-E_i \; y) \qquad (4.57)$$

where C_i and E_i are related to the coefficients in eqns. (4.55) and (4.56). Eqn. (4.43) may, therefore, be written as

$$I(\gamma) = \sum_i C_i \int_0^{\infty} W(y) \; G(v,y) \; \exp(-E_i \; y) dy \qquad (4.58)$$

Assuming the spreading function to be uniform and Gaussian, one obtains after some simplification,

$$I(\gamma) = \sum_i [C_i \exp\{-E_i v + (E_i\sigma)^2/2\} \int_0^\infty W(y) \frac{1}{\sqrt{2\pi\sigma^2}} \exp(-\{(v - E_i\sigma^2) - y\}^2/2\sigma^2)dy] \quad (4.59)$$

The integral in the above expression may be recognized as $F(v - E_i\sigma^2)$ by comparison with eqns. (4.3)-(4.5). Therefore,

$$I(\gamma) = \sum_i C_i \exp\{-E_i v + (E_i\sigma)^2/2\} F(v - E_i\sigma^2) \quad (4.60)$$

Eqn. (4.60) can, now, be used to evaluate the various diameter averages given by eqns. (4.44)-(4.49). To evaluate the same for the total sample, one needs to evaluate N(v). From eqn. (4.35), it follows that,

$$N(v) \propto \int_0^\infty W(y)\, G(v,y)\{K(y)\, D^2(y)\}^{-1} dy \propto I(0) \quad (4.61)$$

For a detector where,

$$W(y)\, G(v,y) \propto N(v,y)\, D^\gamma(y), \text{ at retention volume } v \quad (4.62)$$

the integrals involved in calculating the corrected diameter averages are also of the form of eqn. (4.58) and may be similarly evaluated. For a refractometer, γ has a value equal to 3 while for the turbidity detector in the Rayleigh scattering regime, it is 6. Therefore, the method outlined above is quite general and may be used to calculate diameter averages, corrected for axial dispersion, for a general

detector.

It is easy to show that eqn. (4.60) is valid not only for a Gaussian spreading function but for a whole family of functions of the form

$$G(v,y) = G_0(v-y)\ \phi(y) \tag{4.63}$$

where $\phi(y)$ is any function of y. This may be viewed in two ways. First, by lumping W(y) and $\phi(y)$ together as an altered W(y), eqn. (4.60) is consistent with the notion that moments of a distribution are not unique. A second viewpoint and a more practical one is that the preceding analysis is not restricted to a Gaussian spreading function but encompasses non-Gaussian functions of the form given above. This conclusion should be applicable to the formalism developed by Hamielec et al (1978) since, it can be shown that for a general detector represented by eqn. (4.62), the present analysis leads to similar correction factors as given in Table 4.6. Consider, for example, the number average diameter, calculated for a turbidity detector according to Rayleigh theory.

$$D_n(uc) = \int_{-\infty}^{\infty} F(v)\ D^{-5}(v)\ dv \ / \int_{-\infty}^{\infty} F(v)\ D^{-6}(v)\ dv \tag{4.64}$$

$$D_n(c) = \int_{-\infty}^{\infty} N(v)\ D_n(v)\ dv \ / \int_{-\infty}^{\infty} N(v)\ dv \tag{4.65}$$

Eqn. (4.65) is equivalent to

$$D_n(c) = \int_{-\infty}^{\infty} I(1)\, dv \;/\; \int_{-\infty}^{\infty} I(0)\, dv \qquad (4.66)$$

It follows from eqn. (4.60) that,

$$I(1) \propto D_1^{-5} \exp(5D_2 v + 25D_2^2\sigma^2/2)\; F(v+5D_2\sigma^2) \qquad (4.67)$$

$$I(0) \propto D_1^{-6} \exp(6D_2 v + 36D_2^2\sigma^2/2)\; F(v+6D_2\sigma^2) \qquad (4.68)$$

Substituting eqns. (4.64),(4.67) and (4.68) in eqn. (4.66) and simplifying, yields the desired result:

$$D_n(c) = \exp(11\, D_2^2\sigma^2/2)\; D_n(uc) \qquad (4.69)$$

Note that the lower integration limit in eqns. (4.64)-(4.66) is $-\infty$ rather than 0. This is necessary to obtain the result in eqn. (4.69). Hence, the present analysis yields results consistent with the theoretical treatment of Hamielec et al. Also, formulae derived for Gaussian spreading functions, in general, are applicable to non-Gaussian functions of the form given by eqn. (4.63).

For a linear calibration curve, Fig. 4.12 demonstrates the excellent fit to the extinction coefficient data calculated from Mie theory. K(y) can typically vary over six decades across a broad chromatogram. A nonlinear estimation routine is used to estimate the

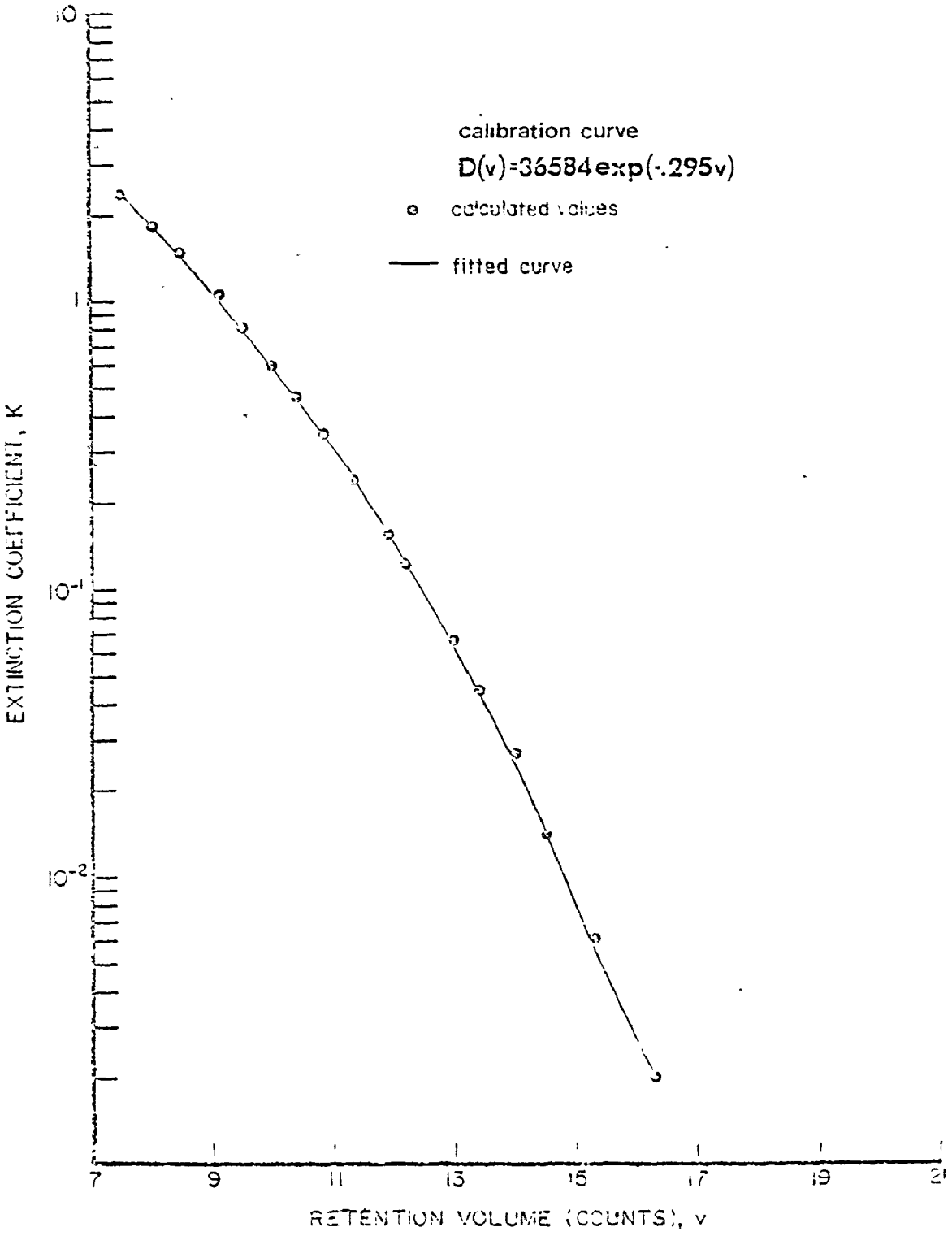

Fig. 4.12 Fit of extinction coefficient data for polystyrene particles in water at a wavelength in vacuum of 254 nm (Particles are considered to be non-absorbing; also wavelength dependence of refractive index is not taken into account).

parameters of the fit. Alternately, a multivariable search routine can be used to minimise

$$\sum_{\text{over all } y} \{\hat{K}(y) / K(y) - 1\}^2 \qquad (4.70)$$

where $\hat{K}(y)$ is an estimate of $K(y)$.

A typical variation of diameter averages with retention volume for a unimodal size distribution is shown in Fig. 4.13. Axial dispersion causes the diameter averages at low retention volumes to be lower than the corresponding calibration diameters; the reverse occurs at the high retention volume end. Consider the effect of truncating the tails of a synthesized chromatogram. Curve ABCD in Fig. 4.14 represents the path along which a diameter average varies, for a chromatogram synthesized from a unimodal $W(y)$ and a given spreading function, with the diameter averages based on the portion of the chromatogram between retention volumes X and Y, chromatogram heights beyond X and Y being considered nonzero, however. In an experimental chromatogram, the latter would be indistinguishable from the baseline. Along ABCD, $D_n < D_s < D_v < D_{ss} < D_w < D_t$. When chromatogram heights beyond X and Y are set equal to zero, the path becomes A'BCD'. Along A'B and CD', the order of the diameter averages are, generally, reversed. This anomaly occurs due to the nature of the moment equation where, each term under the summation is multiplied by the ordinate $F(v-E_i\sigma^2)$. At retention volumes in the neighbourhood of Y, evaluation of smaller moments

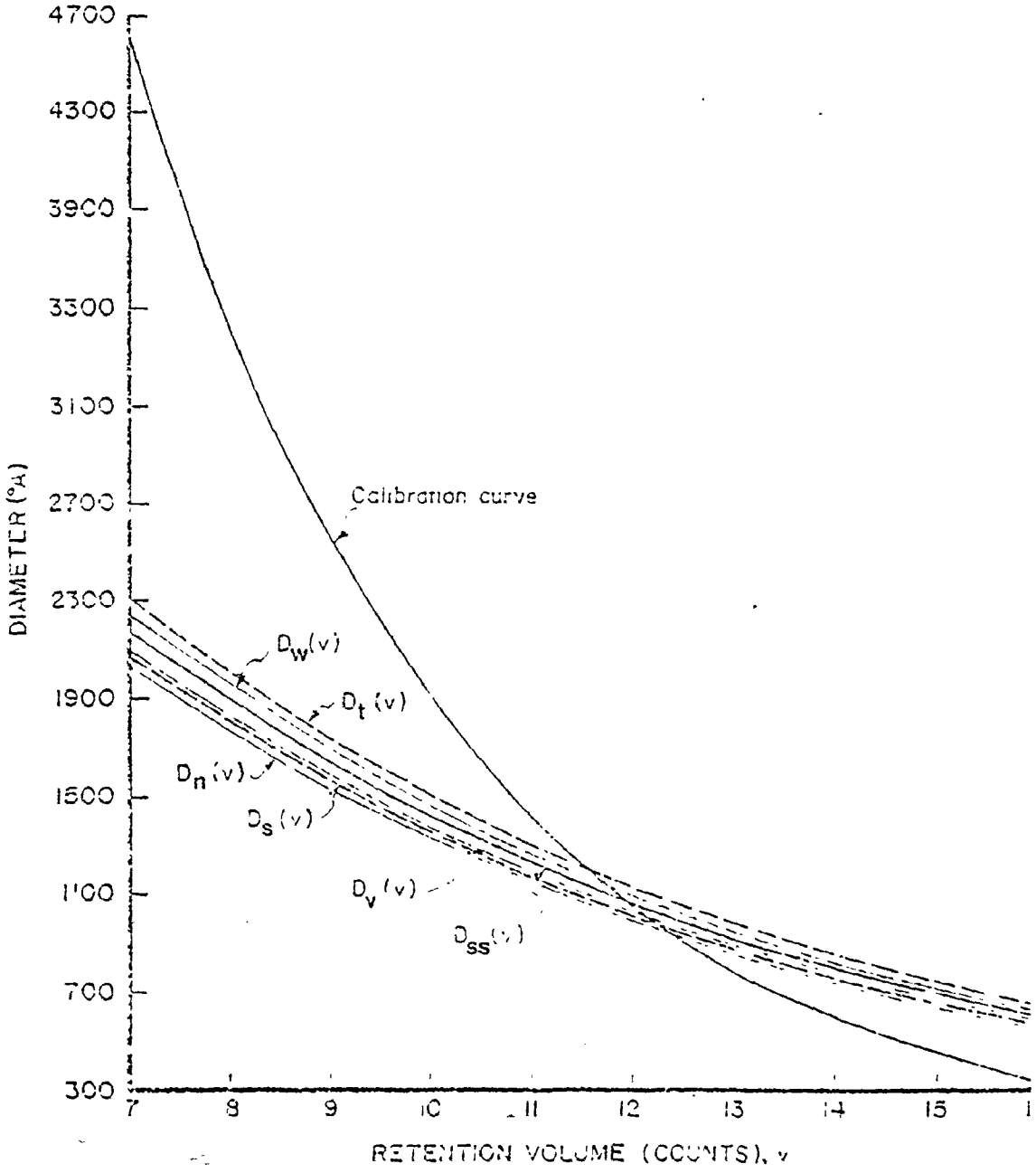

Fig. 4.13 Variation of particle diameter averages with retention volume.

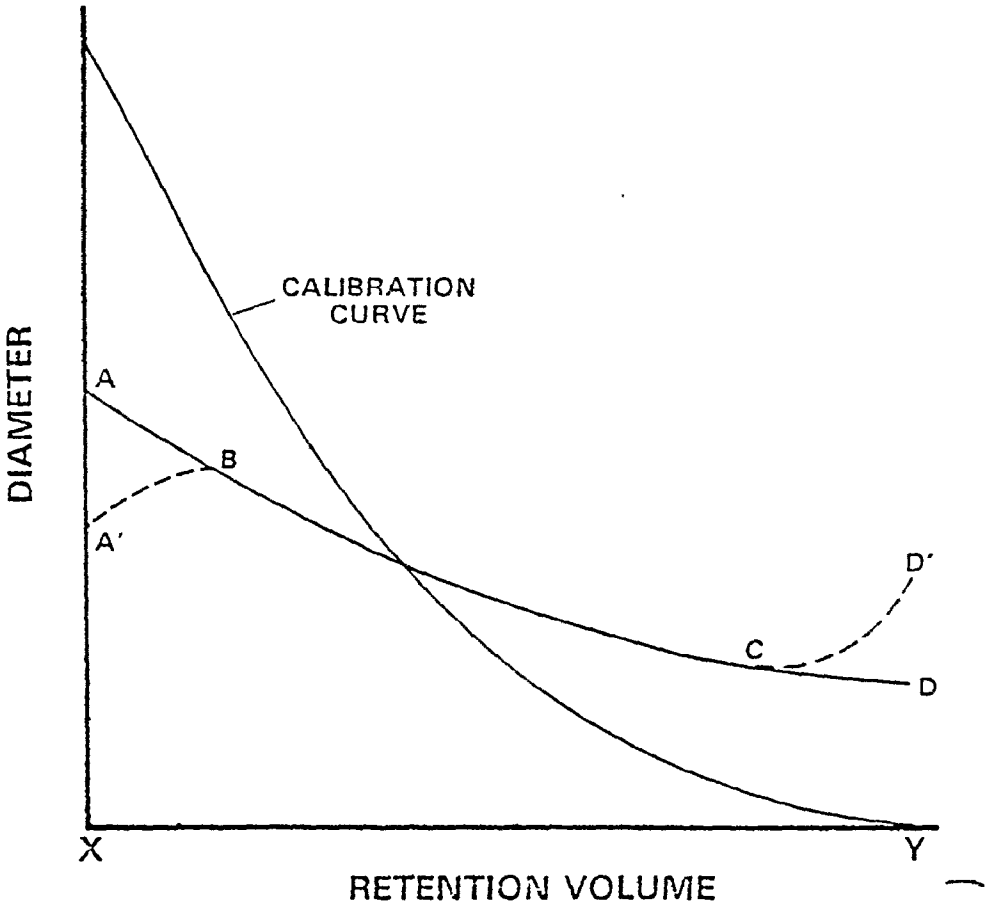

Fig. 4.14 Illustration of the numerical error in the application of Method 2.

requires ordinates at retention volumes beyond this neighbourhood (higher v), while in the vicinity of X, evaluation of higher moments requires ordinates at retention volumes beyond the neighbourhood of X (lower v). Departure from ABCD with opposite trends at the respective ends are thus exhibited. The effects cancel each other to a certain extent. The points B and C approach A and D respectively, as σ^2 is decreased.

It is to be noted that, the equations developed in this section are given in terms of a single adjustable parameter, σ^2. In some practical situations, the spreading function may not be representable by the form given by eqn. (4.63); evidence to such an effect may be inferred from the difficulty of obtaining meaningful diameter averages from chromatograms of narrow particle standards, using a single σ^2 value. In such a situation, it is advantageous to develop an analytical solution using the more general shape function, eqn. (4.6). This is now considered.

4.4.3 A New Generalized Method for Calculating Moments of the Size Distribution - Method 3

Provder and Rosen's (1970) statistical shape function may be rewritten in the form (truncated beyond n=6)

$$G(v-y) = G_0(v-y)\ a_0\left(1 + \sum_{n=1}^{6} a_n (v-y)^n/\sigma^n\right) \qquad (4.71)$$

where

$$a_0 = 1 + A_4/8 - A_6/48 \tag{4.72}$$

$$a_1 a_0 = -A_3/2 + A_5/8 \tag{4.73}$$

$$a_2 a_0 = A_6/16 - A_4/4 \tag{4.74}$$

$$a_3 a_0 = A_3/6 - A_5/12 \tag{4.75}$$

$$a_4 a_0 = -A_6/48 + A_4/24 \tag{4.76}$$

$$a_5 a_0 = A_5/120 \tag{4.77}$$

$$a_6 a_0 = A_6/720 \tag{4.78}$$

Analytical solutions of the moment equations are now developed. The term a_0 is not carried through the analysis since it cancels out in the moment expressions. The lower integration limit is set equal to $-\infty$. Two detector types are considered, namely,

Type 1 : $$F(v) \propto N(v)\, D^{\gamma}(v) \tag{4.28}$$

Type 2 : $$F(v) \propto N(v)\, D^{2}(v)\, K(v) \tag{4.79}$$

As noted earlier, Type 1 represents both the refractive index detector ($\gamma=3$) and the turbidity detector scattering according to Rayleigh theory ($\gamma=6$). Type 2 includes the turbidity detector scattering according to Mie theory. It follows from eqns. (4.28) and (4.79) and the definition of a moment

$$M_k = \int_{-\infty}^{\infty} D^k f(D)\, dD \tag{4.80}$$

that,

$$\text{Type 1:}\quad M_k(uc) = \int_{-\infty}^{\infty} F(v)\, D(v)^{k-\gamma}\, dv \Big/ \int_{-\infty}^{\infty} F(v)\, D(v)^{-\gamma}\, dv \tag{4.81}$$

$$\text{Type 2:}\quad M_k(uc) = \int_{-\infty}^{\infty} F(v)\, D(v)^{k-2}\, K(v)^{-1}\, dv \Big/ \int_{-\infty}^{\infty} F(v) D(v)^{-2} K(v)^{-1} dv \tag{4.82}$$

$M_k(c)$ are similarly defined by replacing F(v) by W(y). The equations are of the form:

$$M_k(\ ) = \bar{M}_k(\ )/\bar{M}_0(\ ) \tag{4.83}$$

If $\phi_k(v)$ is defined as

$$\text{Type 1:}\quad \phi_k(v) = D(v)^{k-\gamma} \tag{4.84}$$

$$\text{Type 2:}\quad \phi_k(v) = D(v)^{k-2}\, K(v)^{-1} \tag{4.85}$$

then,

$$\bar{M}_k(uc) = \int_{-\infty}^{\infty} F(v)\phi_k(v)\, dv \tag{4.86}$$

Figini (1979) recently proposed the solution of an equation similar to eqn. (4.86). Rewriting it with the help of eqns. (4.3) and (4.4) yields

$$\overline{M}_k(uc) = \int_{-\infty}^{\infty} W(y)\, I_k(y)\, dy \qquad (4.87)$$

where,

$$I_k(y) = \int_{-\infty}^{\infty} \phi_k(v)\, G(v-y)\, dv \qquad (4.88)$$

Consider a nonlinear particle diameter-retention volume calibration curve given by

$$\ln D(v) = A' - B'v + C'v^2 \qquad (4.8)$$

(Previously used symbols D_1 and D_2 are respectively equal to exp A' and B'). The fit of extinction coefficients K(v) calculated from Mie theory is represented, similarly, by

$$\ln K(v) = A'' - B''v + C''v^2 \qquad (4.89)$$

It follows from eqns. (4.84), (4.85), (4.8) and (4.89) that,

$$\phi_k(v) = \exp(kA - kBv + kCv^2) \qquad (4.90)$$

where

Detector	kA	kB	kC	
Type 1	$(k-\gamma)A'$	$(k-\gamma)B'$	$(k-\gamma)C'$	(4.91)
Type 2	$(k-2)A'-A''$	$(k-2)B'-B''$	$(k-2)C'-C''$	(4.92)

Table 4.7 Coefficients $Q_{n,k}$ in Eqn. (4.96)(subscript k on α and P are omitted for convenience)

Coefficient	Expression
$Q_{0,k}$	$\sqrt{P}\ \{1-\alpha P\frac{a_1}{\sigma}+P(\sigma^2+\alpha^2P)\frac{a_2}{\sigma^2}-\alpha P^2(3\sigma^2+\alpha^2P)\frac{a_3}{\sigma^3}+P^2[\alpha^2P\ (6\sigma^2+\alpha^2P)+3\sigma^4]\ \frac{a_4}{\sigma^4}$ $-\alpha P^3(\alpha^4P^2+10\ \alpha^2\sigma^2P+15\ \sigma^4)\frac{a_5}{\sigma^5}+[P^4\alpha^2(\alpha^4P^2+15\ \alpha^2\sigma^2P+45\ \sigma^4)+15\ P^3\sigma^6]\ \frac{a_6}{\sigma^6}\ \}$
$Q_{1,k}$	$\sqrt{P(P-1)}\ \{\frac{a_1}{\sigma}-2\alpha P\frac{a_2}{\sigma^2}+3P(\sigma^2+\alpha^2P)\frac{a_3}{\sigma^3}-4\alpha P^2(3\sigma^2+P\alpha^2)\frac{a_4}{\sigma^4}$ $+5P^2(3\sigma^4+6\sigma^2\alpha^2P+\alpha^4P^2)\frac{a_5}{\sigma^5}-6\alpha P^3(15\sigma^4+10\sigma^2\alpha^2P+\alpha^4P^2)\frac{a_6}{\sigma^6}\ \}$
$Q_{2,k}$	$\sqrt{P(P-1)^2}\ \{\frac{a_2}{\sigma^2}-3\alpha P\frac{a_3}{\sigma^3}+6P(\sigma^2+\alpha^2P)\frac{a_4}{\sigma^4}-10\alpha P^2(3\sigma^2+P\alpha^2)\frac{a_5}{\sigma^5}$ $+15P^2[\alpha^2P\ (6\sigma^2+\alpha^2P)+3\sigma^4]\frac{a_6}{\sigma^6}\ \}$
$Q_{3,k}$	$\sqrt{P(P-1)^3}\ \{\frac{a_3}{\sigma^3}-4\alpha P\frac{a_4}{\sigma^4}+10\ P(\sigma^2+\alpha^2P)\frac{a_5}{\sigma^5}-20\ \alpha P^2(3\sigma^2+P\alpha^2)\frac{a_6}{\sigma^6}\}$
$Q_{4,k}$	$\sqrt{P(P-1)^4}\ \{\frac{a_4}{\sigma^4}-5\ \alpha P\frac{a_5}{\sigma^5}+15\ P(\sigma^2+\alpha^2P)\frac{a_6}{\sigma^6}\ \}$
$Q_{5,k}$	$\sqrt{P(P-1)^5}\ \{\frac{a_5}{\sigma^5}-6\ \alpha P\frac{a_6}{\sigma^6}\ \}$
$Q_{6,k}$	$\sqrt{P(P-1)^6}\ \frac{a_6}{\sigma^6}$

Since, in the final moment equations, A, B and C do not appear except as their product with k, the above equations are valid for all values of k_σ including k=0. Let,

$$P_k = (1 - 2\,kC\sigma^2)^{-1} \tag{4.93}$$

$$\alpha_k = kB\sigma^2 \tag{4.94}$$

$$R_k = \sigma^2 P_k[(kB)^2/2 - 2(kA)(kC)] \tag{4.95}$$

then, the solution of eqn. (4.88) is given by

$$I_k(y) = \exp(R_k)\ \phi_k^{P_k}(y) \sum_{n=0}^{6} Q_{n,k}\ y^n \tag{4.96}$$

where the coefficients $Q_{n,k}$ are given in Table 4.7. The integrals required to obtain the above solution are given in the Appendix. Note, that when P_k=1, $Q_{n,k}$(n=1,...6) vanish and $Q_{0,k}$ simplifies to

$$Q_{0,k} = 1 + \sum_{n=3}^{n=6} (-1)^n\ P_k^n\ (\alpha_k/\sigma)^n\ A_n/n! \tag{4.97}$$

The upper limit in the summation may be higher if additional terms are considered in the shape function. It follows from eqns. (4.83), (4.87) and (4.96) that,

$$M_k(uc) = \exp(R_k - R_0)\ \frac{\sum_{n=0}^{6} [Q_{n,k} \int_{-\infty}^{\infty} y^n\ W(y)\ \phi_k^{P_k}(y)\ dy]}{\sum_{n=0}^{6} [Q_{n,0} \int_{-\infty}^{\infty} y^n\ W(y)\ \phi_0^{P_0}(y)\ dy]} \tag{4.98}$$

Consider the simplifications of eqn. (4.98) for each detector type

Type 1, Case A: kC=0, i.e., linear calibration curve, and generalized spreading function

Since,

$$kC = 0 \tag{4.99}$$

therefore,

$$P_k = 1 \tag{4.100}$$

$$Q_{n,k} = 0 \quad n = 1, 2 \ldots \tag{4.101}$$

Hence,

$$M_k(c)/M_k(uc) = \exp[\sigma^2 k (\gamma - k/2) B'^2] Q_{0,0}/Q_{0,k} \tag{4.102}$$

$Q_{0,k}$ is given according to eqn. (4.97). For a Gaussian spreading function, this equation yields the results derived by Hamielec et al (1978).

Type 1, Case B: kC≠0, i.e., nonlinear calibration curve and Gaussian spreading function

When the spreading function is Gaussian,

$$Q_{0,k} = \sqrt{P_k} \tag{4.103}$$

$$Q_{n,k} = 0 \quad n=1, 2 \ldots \tag{4.104}$$

Therefore

$$\frac{M(c)}{\dfrac{[(k-\gamma)P_k + \gamma]}{[(1-P_0)\gamma]}\,\dfrac{M(c)}{M_k(uc)}} = \exp(R_0 - R_k)\sqrt{(P_0/P_k)} \tag{4.105}$$

It is obvious that a direct relationship between the k^{th} corrected and uncorrected moments is not obtained.

Type 1, Case C: $kC \neq 0$, i.e., nonlinear calibration curve, and generalised spreading function

Let

$$\overline{y_k^n} = \int_{-\infty}^{\infty} y_n \, W(y) \phi_k^{P_k}(y) \, dy \Big/ \int_{-\infty}^{\infty} W(y) \, \phi_k^{P_k}(y) \, dy \qquad (4.106)$$

Then

$$\frac{M(c)\,[(k-\gamma)P_k+\gamma]}{\overline{M(c)\,[(1-P_0)\gamma]}^{M_k(uc)}} = \exp(R_0-R_k)\frac{\sum_{n=0}^{6} Q_{n,0}\,\overline{y_0^n}}{\sum_{n=0}^{6} Q_{n,k}\,\overline{y_k^n}} \qquad (4.107)$$

Since $\overline{y_k^n}$ is defined in terms of the unknown distribution $W(y)$, the practical use of eqn. (4.107) depends upon obtaining a suitable approximation for $\overline{y_k^n}$. This will be discussed later.

Type 2, Case A: $kC=0$, i.e., linear calibration curve, linear extinction coefficient fit, and generalized spreading function

Eqns. (4.99)-(4.101) are applicable and hence,

$$M_k(c)/M_k(uc) = \exp[\sigma^2 kB'(-kB'/2+2B'+B'')]Q_{0,0}/Q_{0,k} \qquad (4.108)$$

It is significant to note that, as in the case of the other detectors, a simple correction factor has been derived for the turbidity detector in the Mie scattering regime. A linear calibration curve is not uncommon in chromatography. The condition of a linear extinction coefficient fit is more difficult to satisfy; however, if the spreading function is not excessively broad, this condition may be approached. Relationships for some important diameter averages are given in Table 4.8. Note that, when B"=4B' (Rayleigh scattering), the formulae for the diameter averages reduce to those derived by Hamielec et al (1978).

Type 2, Case B: kC≠0 and Gaussian spreading function

Eqns. (4.103) and (4.104) are applicable and hence,

$$M_k(uc) = \exp(R_k - R_0)\sqrt{(P_k/P_0)}\int_{-\infty}^{\infty} W(y)\,\phi_k^{P_k}(y)\,dy \Big/ \int_{-\infty}^{\infty} W(y)\phi_0^{P_0}(y)\,dy \qquad (4.109)$$

Let,

$$P_k = 1 + f_k \qquad (4.110)$$

Therefore,

$$\int_{-\infty}^{\infty} W(y)\,\phi_k^{P_k}(y)\,dy \equiv \int_{-\infty}^{\infty} W(y)\,\phi_k(y)\,\phi_k^{f_k}(y)\,dy \qquad (4.111)$$

If $\phi_k^{f_k}(y)$ is approximated as

$$\phi_k^{f_k}(y) = [D(y)\,K^{-1}(y)]^{f_k(k-2)} \propto \text{constant}\,[D(y)\,D(y)]^{-\beta f_k(k-2)} \qquad (4.112)$$

Table 4.8 Axial Dispersion Correction Factors for the Turbidity Detector in the Mie Scattering Region (Linear Calibration Curve, Linear Extinction Coefficient Fit and Generalized Spreading Function)

Diamter Average	Correction Factor*
$D_n(c)/D_n(uc)$	$\exp[\sigma^2 B'(3B'/2+B'')]Q_{0,0}/Q_{0,1}$
$D_s(c)/D_s(uc)$	$\exp[\sigma^2 B'(B' + B'')][Q_{0,0}/Q_{0,2}]^{1/2}$
$D_v(c)/D_v(uc)$	$\exp[\sigma^2 B'(B'/2+B'')][Q_{0,0}/Q_{0,3}]^{1/3}$
$D_{ss}(c)/D_{ss}(uc)$	$\exp[\sigma^2 B'(-B'/2+B'')] Q_{0,2}/Q_{0,3}$
$D_w(c)/D_w(uc)$	$\exp[\sigma^2 B'(-3B'/2+B'')] Q_{0,3}/Q_{0,4}$
$D_t(c)/D_t(uc)$	$\exp[\sigma^2 B'(-5B'/2+B'')][Q_{0,3}/Q_{0,6}]^{1/3}$

* $Q_{0,k}$ $\quad 1+ \sum_{n=3}(-1)^n(\alpha_k/\sigma)^n A_n/n!$ (upper summation limit not specified)

where the extinction coefficient is assumed proportional to $D^{\beta}(y)$, then

$$\int_{-\infty}^{\infty} W(y)\ \phi_k^{P_k}(y)\ dy = \text{constant}\ \overline{M}(c)_{(k+g_k)} \tag{4.113}$$

where,

$$g_k = (k-2-\beta)f_k \tag{4.114}$$

If β in eqn. (4.112) is independent of k, eqn. (4.109) simplifies to

$$M_k(uc) = \exp(R_k-R_0)\sqrt{P_k/P_0}\ \overline{M}(c)_{(k+g_k)}\ /\overline{M}(c)_{g_0}$$

$$= \exp(R_k-R_0)\sqrt{P_k/P_0}\ M(c)_{k+g_k}\ /M(c)_{g_0} \tag{4.115}$$

or alternately,

$$\frac{M(c)_{(k+g_k)}}{M(c)_{g_0}\ M_k(uc)} = \exp(R_0-R_k)\sqrt{P_0/P_k} \tag{4.116}$$

To apply this equation, $k+g_k$ is set successively equal to 0, 1, 2 ... and solved for k. Using the corresponding uncorrected moments, the ratios $M_0(c)/M_{g_0}(c)$, $M_1(c)/M_{g_0}(c)$, $M_2(c)/M_{g_0}(c)$ etc. can be calculated and hence $M_1(c)$, $M_2(c)$ etc., since $M_0(c) = 1$.

This approximate method is apparently simpler than the treatment outlined in Section 4.4.2. However, it lacks the attractive feature of the previous method namely, a calculation of the size variation across the chromatogram. When Rayleigh scattering theory is applicable, β is

identically equal to 4, $B''=4B'$, $f_k = g_k=0$ and eqn. (4.116) yields the formulae derived by Hamielec et al (1978). Note that, when Rayleigh scattering theory is not applicable, β may still be approximated as 4; however, now, $B''\neq 4B'$, $f_k\neq 0$, $g_k\neq 0$.

Type 2, Case C: $kC\neq 0$ and generalised spreading function

In accordance with the development for Case B, one obtains

$$\frac{M(c)_{(k+g_k)}}{M(c)_{g_0}\, M_k(uc)} = \exp(R_0-R_k)\, \frac{\sum_{n=0}^{6} Q_{n,0}\, \overline{y_0^n}}{\sum_{n=0}^{6} Q_{n,k}\, \overline{y_k^n}} \qquad (4.117)$$

It is seen from the preceding analysis that, a direct relationship exists between $M_k(c)$ and $M_k(uc)$ only when $kC=0$; otherwise, $M_k(uc)$ is related to a ratio of true moments. In terms of application, this presents, however, no difficulty.

Calculation of $\overline{y_k^n}$ and choice of β

When W(y) is narrow, it is reasonable to approximate $\overline{y_k^n}$ by v_p^n where, v_p is the peak retention volume. This is shown later for the experimental chromatograms of narrow particle standards. It is conceivable that when W(y) is broad and axial dispersion relatively small, $\overline{y_k^n}$ may be calculated by replacing W(y) in eqn. (4.106) by the actual chromatogram. Alternately, $\overline{y_k^n}$ may be set equal to $\bar{v}_n$ where $\bar{v}$ is

the mean retention volume based on the actual chromatogram.

If Rayleigh scattering theory is applicable, then, the value of β is identically equal to 4. Otherwise, it is less than 4 and varies with the particle size range. A value in the range, $2<\beta<4$ is proposed.

The above suggestions were evaluated using synthesized chromatograms for a turbidity detector in the Mie scattering regime [eqns. (4.116) and (4.117)]. It was more convenient to compare uncorrected diameter averages with those calculated directly from F(v). The results are shown in Tables 4.9 and 4.10. The calculations of the diameter averages for a specific value of β, with and without the approximation $\overline{y_k^n} \approx \bar{v}^n$, were almost identical and are not shown. It is observed that, calculations based on the moment equation, for $\beta=2$, 3 and 4, do not differ significantly from each other and agree closely with those calculated from F(v) directly. The assumption of $P_k = 1$ [eqns. (4.116) and (4.117) reduce to eqn. (4.108)] leads to significantly erroneous results, even though, the actual value of P_k is only slightly different from unity. In other case studies made, where a value of P_k as high as 1.2 was used, the above approximations were found to be equally valid.

Application of some of the equations derived in this section is demonstrated in Chapter 5. This section is concluded by briefly comparing all the analytical methods discussed so far. The comparison is given in Table 4.11. It is appropriate to mention here that, though, the spreading function parameters are considered independent of retention volume in deriving solutions to the integral equation, in

Table 4.9 Evaluation of the Moment Equations [Eqns. (4.116) and (4.117)] for the Type 2 Detector

Calibration curve	:	$A' = 8.0158$ $B' = 0.1707$ $C' = 0$
Extinction coefficient fit	:	$A'' = 1.2674$ $B'' = -0.2042$ $C'' = -0.0166$
$W(y)$	:	Gaussian with mean retention volume 20 and variance 2
P_k	:	1.071

$G(v-y)$	:	Gaussian , $\sigma^2 = 2.0$					$\sigma^2 = 2.0; a_1 = -0.4$; $a_i = 0$, $i=2,\ldots 6$					
Diameter Average		D_n	D_s	D_v	D_{ss}	D_w	D_t	D_n	D_s	D_v	D_{ss}	D_w	D_t
Uncorrected													
1. From $F(v)$		56.7	60.6	64.8	74.1	84.7	96.8	69.5	73.1	77.2	85.9	96.4	108.6
2. From moment equation ($\beta=2$)		57.0	61.0	65.3	74.7	85.3	97.4	68.5	72.3	76.4	85.4	96.0	108.4
3. From moment equation ($\beta=3$)		56.8	60.7	65.0	74.3	84.9	97.0	68.2	71.9	76.0	85.0	95.6	107.9
4. From moment equation ($\beta=4$)		56.5	60.4	64.6	74.0	84.5	96.5	67.9	71.6	75.7	84.6	95.1	107.4
5. From moment equation assuming $P_k=1$		75.4	82.7	82.5	96.1	108.4	122.1	83.3	91.0	90.4	104.4	117.0	131.2
Correct or True													
6. From $W(y)$		76.8	79.2	81.8	87.1	92.6	98.5	76.8	73.1	77.2	85.9	96.4	108.6

Table 4.10 Evaluation of Moment Equations [Eqns. (4.116) and (4.117)] for the Type 2 Detector

Calibration curve	:	$A' = 8.0158$ $B' = 0.1707$ $C' = 0$	
Extinction coefficient fit	:	$A''_2 = 1.2674$ $B'' = -0.2042$ $C'' = -0.0166$	
G(v-y)	:	$\sigma^2 = 2.0$; $a_1 = -0.4$; $a_i = 0$, i=2 ... 6	
P_k	:	1.071	
W(y)	:	Lognormal with parameters, ℓn 20 and 0.01	2 Peak W(y) composed of 2 Gaussian peaks having means, 18.0 and 22.0 ; variance, 2.0

Diameter Average	D_n	D_s	D_v	D_{ss}	D_w	D_t	D_n	D_s	D_v	D_{ss}	D_w	D_t
Uncorrected												
1. From F(v)	65.5	69.6	74.1	83.8	94.8	107.1	64.7	67.1	70.4	77.5	89.9	108.0
2. From moment equation (β=2)	64.2	68.5	73.0	83.1	94.4	106.9	63.4	65.9	69.2	76.4	88.9	107.1
3. From moment equation (β=3)	63.7	68.0	72.6	82.7	94.0	106.4	63.3	65.7	69.0	76.0	88.2	106.2
4. From moment equation (β=4)	63.3	67.6	72.2	82.2	93.5	105.9	63.1	65.5	68.7	75.6	87.5	105.3
5. From moment equation assuming P_k=1	78.8	87.5	86.3	102.0	115.2	129.5	77.1	82.9	82.7	94.5	109.2	129.6
Corrected or True												
6. From W(y)	72.6	75.7	78.7	85.0	91.2	97.2	71.0	72.5	74.5	78.8	86.4	97.3

practice, they are slowly varying functions. When applying these equations to experimental chromatograms, however, error resulting from use of constant average parameter values is not likely to be significant.

Table 4.11 A Comparison of the Analytical Methods for Solving the Integral Equation.

Attributes	Method 1	Method 2	Method 3
Can handle nonlinear calibration curve	No	Yes	Yes
Can handle generalized spreading function	Yes	No	Yes
Can treat the turbidity detector using Mie theory	No	Yes	Yes
Possible to treat chemical absorption	No	Yes	Yes
Solution obtained as a function of retention volume	No	Yes	No

4.5 AN ABSOLUTE PARTICLE SIZE DETECTOR BASED ON TURBIDITY SPECTRA ANALYSIS

In the chromatography of suspensions, axial dispersion phenomenon is rather pronounced, chiefly, due to the small diffusion coefficients of the particles. This requires significant axial dispersion corrections to obtain absolute particle size distributions and particle diameter averages; various correction procedures developed in previous sections may be used in this regard. Alternately, as suggested by

Hamielec (1978), the coupling of a chromatograph with an absolute detector such as one based on turbidity-spectra analysis, can provide an absolute measure of the size distribution of the detector cell contents as a function of retention volume. It is then possible to obtain size distribution information of the injected sample. The theoretical basis for such a detector follows from eqn. (3.25), which is rewritten as

$$F(v) \propto N(v) \int_0^\infty K(v) D^2(v) f(v,D)\, dD \qquad (4.118)$$

In principle, the measurement of turbidity as a function of wavelength, should permit one to solve eqn. (4.118) for N(v) and the parameters of the frequency distribution, f(v,D). Due to axial dispersion, the contents of the detector cell will be a mixture of different sized particles. It is reasonable to expect that, with adequate resolution, the distribution would be narrow, unimodal and representable by a two parameter distribution function, even though the size distribution of the total sample may be complex. In some instances, it may be of interest to measure the refractive index of the particles and relate this to a material property. For example, the refractive index might be used to give a measure of the copolymer composition of latex particles. One could, therefore, treat the refractive index ratio, m as an unknown.

It follows from eqn. (4.118) that, the turbidity ratio at two wavelengths, $F_{\lambda_i}(v)/F_{\lambda_1}(v)$ is given by

$$F_{\lambda_i}(v)/F_{\lambda_1}(v) = \int_0^\infty K_{\lambda_i}(v)\, D^2(v)\, f(v,D)dD \Big/ \int_0^\infty K_{\lambda_1}(v)\, D^2(v) f(v,D)dD \qquad (4.119)$$

If further, $f(v,D)$ is assumed to be lognormal with parameters $\mu(v)$ and $\bar{\sigma}^2(v)$, then,

$$\frac{F_{\lambda_i}(v)}{F_{\lambda_1}(v)} = \frac{\int_0^\infty K_{\lambda_i}(v)\, D(v)\, \exp\{-[\ell nD(v) - \mu(v)]^2/2\bar{\sigma}^2(v)\}dD}{\int_0^\infty K_{\lambda_1}(v)\, D(v)\, \exp\{-[\ell nD(v) - \mu(v)]^2/2\bar{\sigma}^2(v)\}dD}$$

$$= f_i'(v) \qquad (4.120)$$

The parameters, $\mu(v)$ and $\bar{\sigma}^2(v)$ may be obtained by minimizing the criterion

$$\Psi = \sum_{i=2}^{I} \left| F_{\lambda_i}(v)/F_{\lambda_1}(v) - f_i'(v) \right| \qquad (4.121)$$

where, I is the total number of wavelengths scanned. Due to the inverse particle diameter-retention volume relationship, the search is constrained by the requirement that,

$$\mu(v_{i+1}) < \mu(v_i) \quad \text{for } v_{i+1} > v_i \qquad (4.122)$$

Any suitable multivariable search method may be used. The search procedure used in this study was based on a Hook and Jeeves direct search method. Without any loss of accuracy, it was possible to assume in all cases that $\bar{\sigma}^2(v)$ is constant across the chromatogram. This significantly reduces computational effort, requiring a two variable

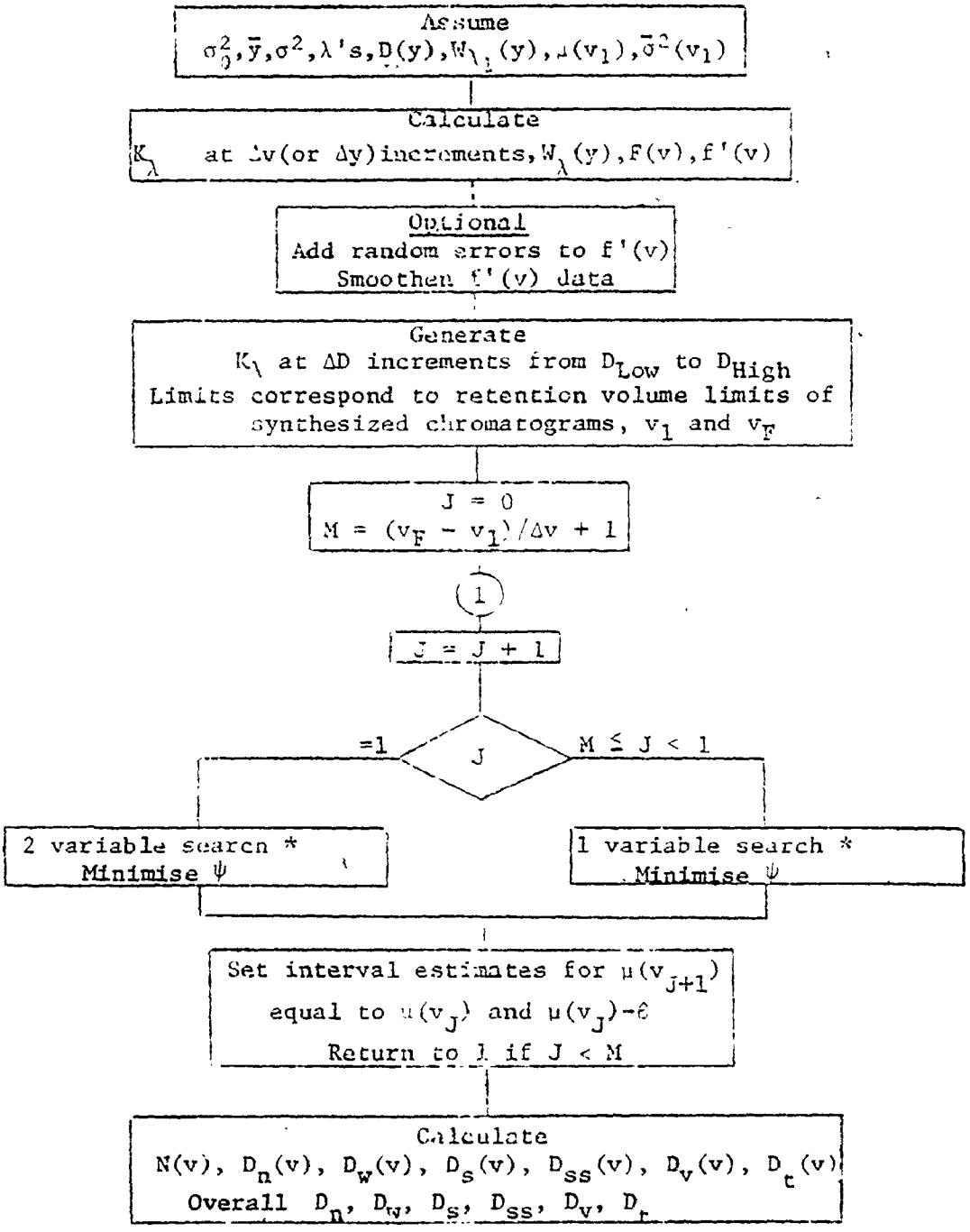

* When calculating the integrals in eqn.(4.120) , the integration is done between appropriate cut-off diameters corresponding to current values of search variables.

Fig. 4.15 Computer flow-sheet for calculating particle diameter averages using the absolute detector

search only at the initial retention volume, followed by a single variable search at all other retention volumes. The computational scheme is given in Fig. 4.15.

A Simulation Study to Evaluate the Absolute Detector

So far it has tacitly been assumed that, the lognormal distribution is the appropriate one to use. This supposition can be tested by comparing f(v,D) from eqn. (4.118) with f(v,D) given by eqn. (4.36), which is stated here again for convenience

$$f(v,D)dD = - \frac{W(y)\ G(v,y)\ \{K(y)\ D^2(y)\ \}^{-1}dy}{\int_0^\infty W(y)\ G(v,y)\{K(y)D^2(y)\ \}^{-1}dy} \qquad (4.36)$$

Since,

$$W(y) \propto N(y)\ K(y)\ D^2(y) \qquad (4.123)$$

it follows that,

$$W_{\lambda_i}(y) = K_{\lambda_i}(y)\ W_{\lambda_1}(y)/K_{\lambda_1}(y) \qquad (4.124)$$

Therefore, if $W_{\lambda_1}(y)$ is assumed, eqn.(4.124) allows W(y) at other wavelengths to be estimated. Hence, if the spreading function is known, the ratio $F_{\lambda_i}(v)/F_{\lambda_1}(v)$ can be calculated.

Results

Without any loss of generality, the particles were assumed to be

nonabsorbing in the wavelength range scanned, 2540-4500°A. A suspension of polystyrene particles in aqueous media was considered. Up to ten turbidity ratios were used in the minimization step. Both linear and nonlinear calibration curves were treated. σ^2, the variance of the Gaussian instrumental spreading function was varied across the chromatograms.

The results for Case 1 and all relevant simulation data are given in Table 4.12. $W_{1^\lambda}(y)$ is assumed to be Gaussian with mean, $\bar{y}$ and variance, σ_0^2. When a two variable search for $\mu(v)$ and $\bar{\sigma}^2(v)$ was performed at each count across the chromatogram, $\bar{\sigma}^2(v)$ was found to oscillate about a mean value. Therefore, it was decided to treat $\bar{\sigma}^2(v)$ as a constant across the chromatogram and its value was determined by a two variable search at the starting count. As shown in Table 4.12 $\mu(v)$ consistently decreases from 7.74 at count 7 to 6.04 at count 16 corresponding to the negative slope of the calibration curve. The results in Table 4.12 and Fig. 4.16 where the size distribution is plotted, provide adequate justification for the assumption of a lognormal distribution function.

It would seriously limit the applicability of this method if the search procedure was overly sensitive to initial parameter estimates. This fortunately is not the case. Poor estimates may, however, lead to an erroneous solution.

Fig. 4.17 shows some calculated individual species chromatograms. (Only portions of the chromatograms are drawn, sufficient to identify the peak retention volume. Curves are not drawn to scale). A point on

Table 4.12 The Absolute Detector - Simulation Results for Case 1 (Linear Calibration Curve)

σ_0^2=1.25 count^2, $\bar{y}$=11.5 count, σ^2=0.75 count^2, $\bar{\sigma}^2(v)$=0.0405, D=36584.0exp(-0.295 y)

		$D_n(v)$		$D_s(v)$		$D_v(v)$		$D_{ss}(v)$		$D_w(v)$		$D_t(v)$ (^oA)	
v	$\mu(v)$	1	2	1	2	1	2	1	2	1	2	1	2
7	7.74	2448	2336	2500	2384	2552	2433	2661	2533	2772	2638	2884	2747
8	7.61	2022	2059	2066	2101	2110	2144	2201	2233	2296	2325	2395	2421
9	7.42	1668	1704	1704	1739	1741	1775	1817	1848	1896	1924	1978	2004
10	7.25	1378	1438	1407	1467	1437	1497	1499	1559	1564	1623	1632	1691
11	7.10	1142	1238	1166	1264	1190	1290	1241	1343	1293	1398	1348	1456
12	6.88	945	997	965	1017	986	1038	1028	1081	1072	1126	1118	1172
13	6.65	777	791	795	808	812	824	848	858	885	894	924	930
14	6.48	639	668	653	681	667	695	697	724	728	754	760	785
15	6.30	528	554	539	565	550	577	574	601	598	626	625	651
16	6.04	449	429	456	438	464	447	480	465	498	485	518	505

Overall	D_n	D_s	D_v	D_{ss}	D_w	D_t
1 Eqn. (4.36)	767	812	860	966	1086	1222
2 Eqn. (4.120)	792	838	889	1001	1131	1275
% Deviation	3.3	3.2	3.4	3.6	4.1	4.3

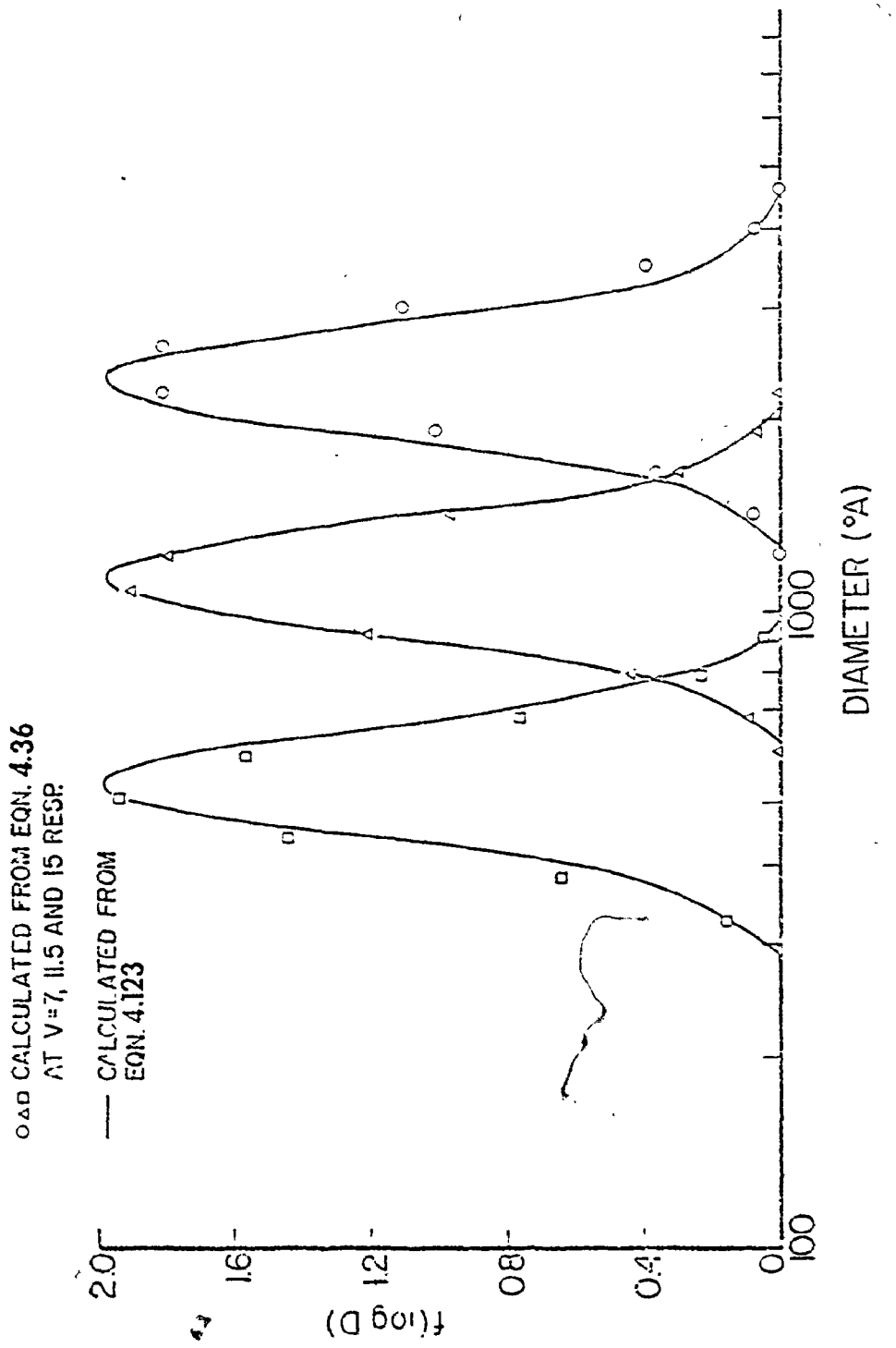

Fig. 4.16 The absolute detector - size distribution calculated as a function of retention volume.

the chromatograms is calculated from the product $f(v,D)xN(v)$ for a known D. When the peak retention volumes are plotted against corresponding diameters, the points lie close to the assumed calibration curve. This procedure is suggested to ascertain the correctness of the solution.

Table 4.13 summarises the results for Cases 2 and 3. These differ from Case 1 in the magnitude of the particle diameters. The data for Case 3 is typical of capillary chromatography, the retention volume

Table 4.13 The Absolute Detector-Simulation Results for Cases 2 & 3 (Linear Calibration Curve)

Case 2 σ_0^2 = 1.25 count^2, $\bar{y}$ = 11.5 count, σ^2 = 0.75 count^2, 1 count=5mℓ, $D = 8 \times 10^4 \exp(-0.295y)$. Bracketted numbers were obtained when σ^2 was varied linearly from 0.75 (v=7) to 1.25 (v=16).

	D_n	D_s	D_v	D_{ss}	D_w	D_t (°A)
Eqn. (4.36)	1814 (1822)	1921 (1928)	2037 (2043)	2291 (2297)	2587 (2593)	2929 (2935)
Eqn. (4.120)	1789 (1760)	1911 (1888)	2042 (2028)	2332 (2340)	2669 (2707)	3053 (3132)
% Deviation	1.4 (3.4)	0.5 (2.1)	0.2 (0.7)	1.8 (1.9)	3.2 (0.7)	4.2 (6.7)

Case 3 σ_0^2 = 1.25 sec^2, $\bar{y}$ = 905 sec, σ^2 was varied linearly from 30 (t=855) to 45 (t=955)sec^2, $D = 2.56 \times 10^{13} \exp(-0.0248\ t)$

	D_n	D_s	D_v	D_{ss}	D_w	D_t (°A)
Eqn. (4.36)	3579	3728	3884	4216	4579	4975
Eqn. (4.120)	3616	3769	3929	4271	4645	5056
% Deviation	1.0	1.1	1.2	1.3	1.4	1.6

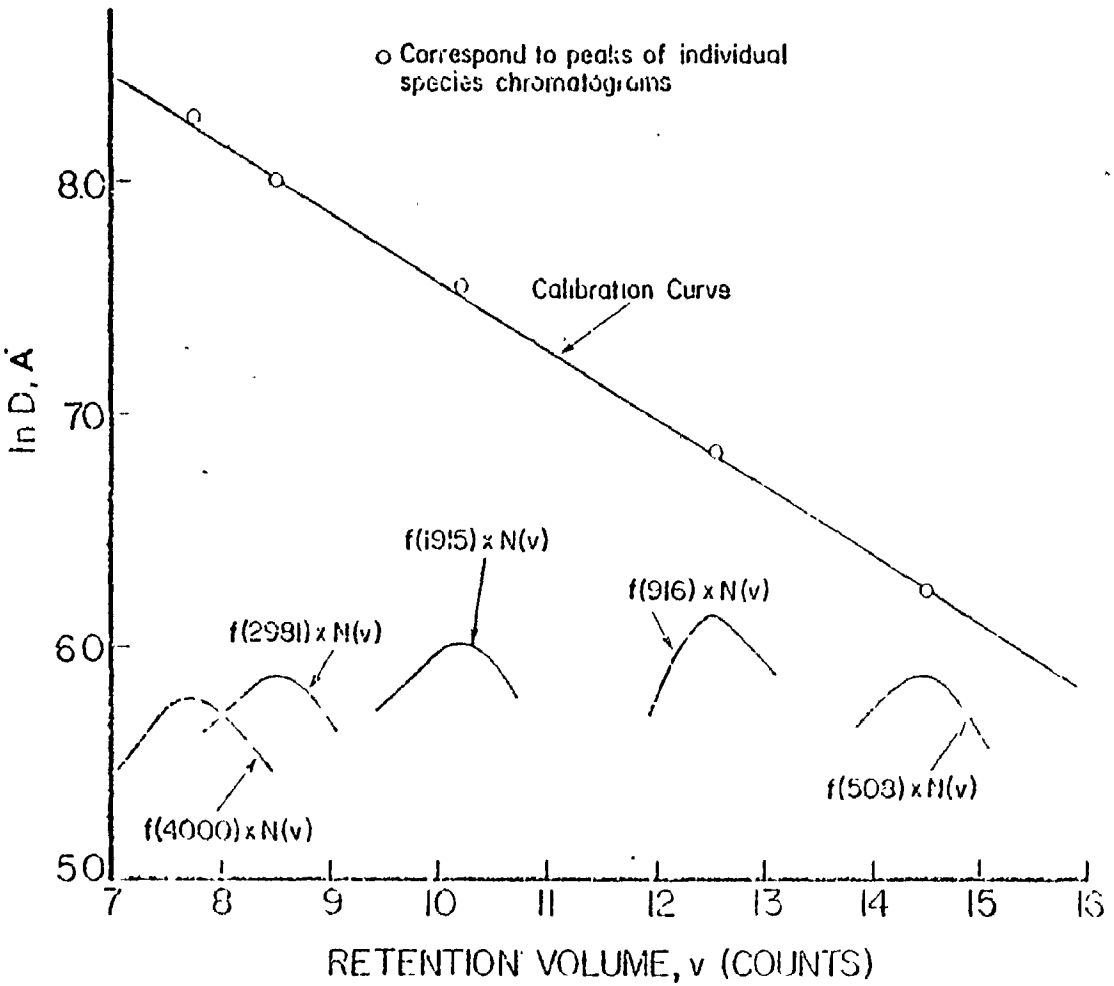

Fig. 4.17 The absolute detector - plot showing agreement of calculated peak retention volumes with assumed calibration curve.

axis being replaced by a time axis for convenience. It is interesting to note from the results of Case 2 that, a nonuniform σ^2 has little effect on calculated diameter averages. Evident from Table 4.13 is the excellent agreement between diameter averages computed from eqns. (4.36) and (4.120).

The results of cases 4 and 5, which involve a nonlinear calibration curve, are given in Table 4.14. In Case 4, nonlinearity in the calibration curve is restricted to the higher diameter end, while it

Table 4.14 The Absolute Detector-Simulation Results for Cases 4 & 5 (Nonlinear Calibration Curve)

Case 4 σ_0^2 = 1.25 count^2, $\bar{y}$ = 11.5 count, σ^2 = 0.75 count^2, 1 count=5mℓ

$D = 36584\exp(-0.295y)+3\times10^{12}\exp(-3y)$

	D_n	D_s	D_v	D_{ss}	D_w	D_t (^oA)
Eqn. (4.36)	767	812	860	966	1086	1223
Eqn. (4.120)	763	814	869	991	1134	1295
% Deviation	0.5	0.3	1.0	2.6	4.4	5.9

Case 5 σ_0^2 = 1.25 count^2, $\bar{y}$ = 11.5 count, σ^2 = 0.75 count^2, 1 count=5mℓ

$D = 1.75\times10^{6}\exp(-0.8543y)+3.51\times10^{3}\exp(-0.0531y)-1.521\exp(0.4138y)$

	D_n	D_s	D_v	D_{ss}	D_w	D_t (^oA)
Eqn. (4.36)	1537	1587	1629	1706	1773	1844
Eqn. (4.120)	1357	1413	1473	1601	1743	1900
% Deviation	11.7	11.0	9.6	6.2	1.7	3.0

occurs at both ends in Case 5.* Imperfect resolution may lead to a bimodal distribution in the detector cell, even when the input sample is unimodal. This was observed at higher retention volumes for Case 5, which explains the larger discrepancy between calculated D_n, D_s and D_v from eqns. (4.36) and (4.120).

To evaluate the robustness of the search procedure when the data have experimental error, random errors (a mean of zero and standard deviation, σ_e) were added to the turbidity ratio data of Case 1. The data, subsequently smoothened, is shown in Fig. 4.18 for different values of σ_e. Results in Table 4.15 indicate substantially the same values of diameter averages as those calculated for Case 1.

Table 4.15 The Absolute Detector - Effect of Random Error in Turbidity Data on Diameter Averages

	D_n	D_s	D_v	D_{ss}	D_w	D_t ($^{\circ}$A)
Case 1 (σ_e=0)	792	838	889	1001	1131	1275
Case 6 (σ_e=0.01)	791	835	883	988	1110	1250
Case 7 (σ_e=0.02)	798	838	882	977	1088	1215

Discussion

In all the simulation cases, chromatograms at any one wavelength were derived from a Gaussian W(y) at λ=2540 Å. These chromatograms are not Gaussian and those at higher wavelengths are skewed towards the low diameter tail. Therefore, the validity of a lognormal representation of the size distribution in the detector must not be linked with any

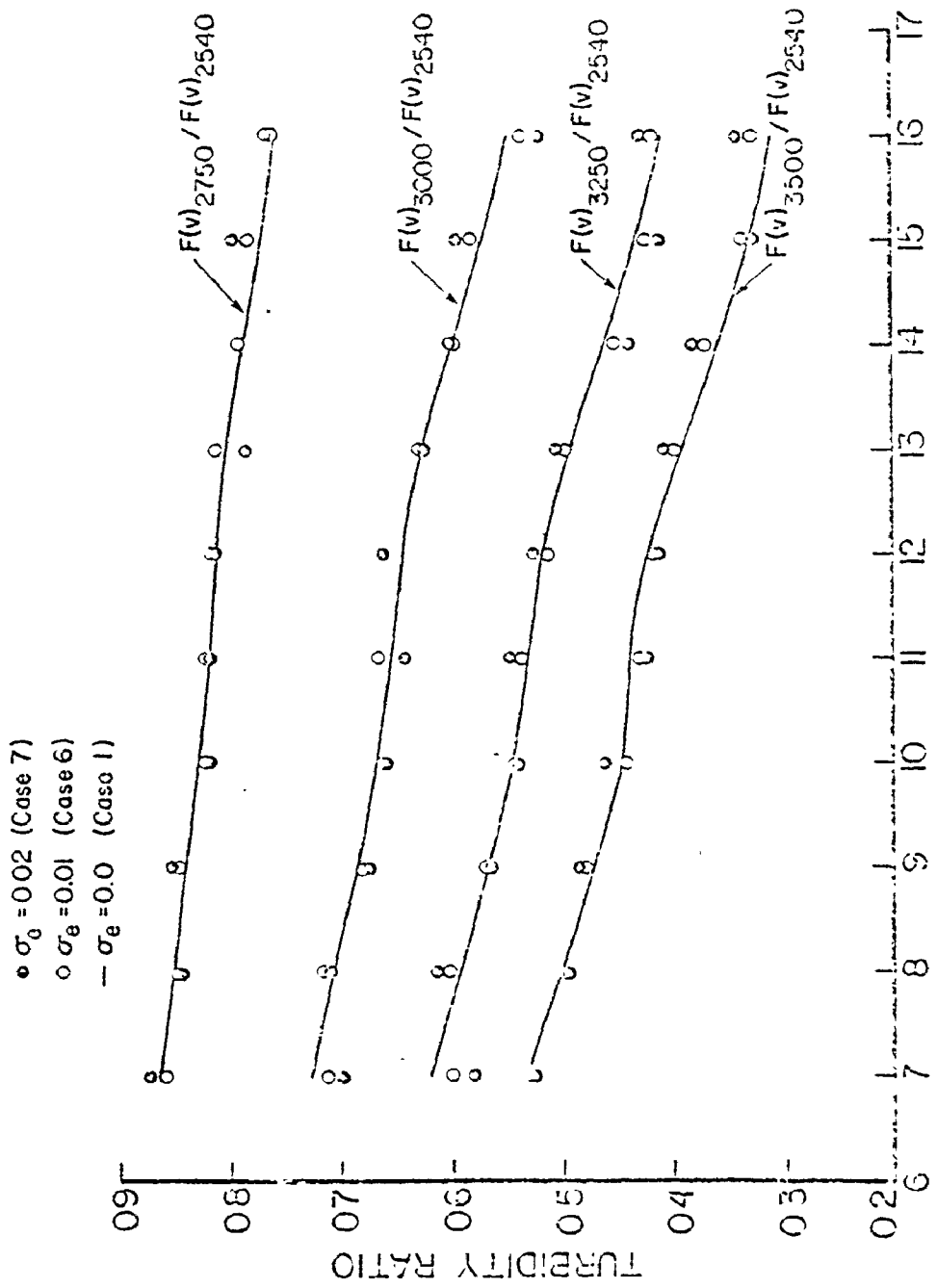

Fig. 4.18 The absolute detector - turbidity ratio data for cases 1, 6 & 7.

specific form of a chromatogram and appears to be general. (This was additionally confirmed by simulating cases where W(y) at λ=2540 ^{o}A was assumed lognormal). These comments apply to unimodal chromatograms when the resolution of the instrument is adequate. Caution must be excercised when the calibration curve is nonlinear.

Results for the cases discussed earlier do not differ significantly from those evaluated using a two variable search at each retention volume. This is due to the relatively large magnitude of the parameter $\mu(v)$ compared to $\bar{\sigma}^{2}(v)$, so that a small discrepancy in the value of $\bar{\sigma}^{2}(v)$ has little effect. This useful approximation results in a considerable saving of computation time which were typically of the order of 300-400 secs. (CDC 6400).

CHAPTER 5

PARTICLE SIZE ANALYSIS USING SIZE EXCLUSION CHROMATOGRAPHY

5.1 INTRODUCTION-REVIEW OF PREVIOUS INVESTIGATIONS ON SIZE EXLUSION CHROMATOGRAPHY OF PARTICLES

Krebs and Wunderlich (1971) were the first to report a separation of poly-methyl methacrylate and polystyrene latices using silica gel having very large pores (500-50,000 ^{o}A). This was followed by the work of Gaylor and James (1975), who fractionated polymeric latices and inorganic colloidal silica, using columns packed with porous glass and water compatible polymeric porous gels. Their experimental work included examination of various packing types as well as chromatogram reproducibility. Investigations into the use of a differential refractometer showed the signal response to be highly dependent on both chemical composition and particle size. Coll et al (1975) experimenting with porous glass packing (CPG, 500-3000 ^{o}A pore size), found it necessary to add electrolyte (potassium nitrate) as well as surfactant (Aerosol OT) to the aqueous eluant. In the absence of electrolyte latex particles could not sample the pore volume. Peak broadening was extensive and system resolution did not approach that normally observed with SEC of polymer molecules.

Hamielec and Singh (1978) presented the first comprehensive theoretical and experimental investigation of SEC. Using the carrier solvent suggested by Coll et al and porous glass and silica packing

(100-30,000 ^{o}A), they established the universality of the particle diameter-retention volume calibration using latices of different composition. The slope of the calibration curve was essentially independent of the mobile phase flowrate, however, it was dependent on the packing size, the slope being smaller (corresponding to a better resolution), for a reduced packing size. The effect on peak variance of the mobile phase flowrate and latex particle size is shown in Table 5.1. Analytical expressions were derived for a general detector which corrected the diameter averages calculated from the chromatogram for imperfect resolution. One of the detectors considered was a turbidity detector in the Rayleigh scattering regime. They had marginal success in predicting particle diameter averages for injected latices. In a separate publication [Singh and Hamielec (1978)] these authors reported the use of SEC for monitoring the growth of particle size in emulsion polymerization.

Table 5.1 Peak Broadening Data of Hamielec and Singh for Polystyrene Latices

Mobile Phase Flowrate (mℓ/min)	Chromatogram Variance (mℓ^2) PS-1000^{o}A	PS-2340^{o}A	PS-3120^{o}A
0.94	23.09	20.66	19.39
2.58	29.75	28.69	27.88
7.50	34.47	32.89	29.34

Nagy (1979) performed an extensive investigation of the chromatography of polystyrene latices using porous glass packing materials - CPG (500-10,000^{o}A pore size) and Fractosil (25,000^{o}A pore

size). The Fractosil system enabled a significant increase in pore penetration by all particle diameters and represents, more appropriately, permeation rather than exclusion chromatography. In a distinct departure from previous practice, only emulsifier (ionic) was added to the aqueous eluant resulting in significantly reduced colloid loss within the packed bed. Particle loss was attributed to entrapment within the porous matrix, resulting in skewed chromatograms. Material balance calculations reveal that small particle sizes are completely recovered while significant sample loss occurs for the larger particle sizes. Ionic strength effects observed with the Fractosil system are shown in Fig. 2.6. While these effects are similar to those in HDC and may be explained analogously, R_F factors are higher; when size exclusion occurs as with the CPG columns, R_F factors even larger were observed. This is due to the fact that latices, to a varying extent depending upon the pore size, experience a fraction of the total pore volume while the entire pore volume is accessible to the marker species. Attempts to model the data in Fig. 2.6 were rather unsuccessful.

Johnston et al (1979) recently investigated the feasibility of SEC for particle size measurement, using CPG columns (1000 & 3000°A pores) and polystyrene latices. They observed a similar ionic strength effect as described by Nagy. A reduction in packing size caused a small increase in R_F while significantly increasing sample loss. A linear calibration curve was obtained in the size range 60-300 nm using a single 3000°A pore column capable of resolving latices with mean diameter ratios as low as 1:3. In general, peak variance increases with

particle size, reaches a maximum and then starts to decrease, consistent with the behaviour observed in SEC of polymer molecules. The data in Table 5.1 shows only the decreasing trend. Using the analytical method developed in Section 4.4.2, the measured weight average diameter was found in good agreement with measurements based on light scattering.

So far, all the investigations have been largely concerned with polymeric latices of diameters greater than 20 nm and packing sizes greater than 40 μ. Kirkland (1979) investigated the properties of small porous silica microspheres (less than 10 μ particle size and less than 75 nm pores) and superficially porous particle (solid core, porous crust, particle size less than 25 μ) for characterizing inorganic silica sols in the range 1-50 nm. The effect of increased flowrate on peak broadening as measured by the plate height and the ionic strength effect were similar to those observed in earlier investigations. Columns using both types of packing materials exhibited relatively high resolution because of rapid equilibrium of slowly diffusing colloids with the pores. Silica sols greater than 80 nm were retained within the pore structures into which they were able to permeate. However, larger silica sols were unable to permeate the pores and eluted normally. Of course, if a colloid size approaches the size of the interstitial pores, then, it is permanently retained as a result of simple filtration.

The principle results of the above investigations are now summarised.

Peak Separation

1. The particle diameter-retention volume calibration curve, in

general, is composed of two linear segments - the segment at low retention volumes, beyond the exclusion limit of the porous packing, corresponds to HDC size separation, while the segment at high retention volumes corresponds to SEC size separation.

2. The calibration curve is insensitive to flowrate variations.
3. Increasing the ionic strength of the aqueous eluant causes a shift in the calibration curve to higher retention volumes due to increased pore permeability. At low ionic strength, a universal calibration is obtained.
4. A smaller packing size improves peak separation.

Peak Broadening

1. Peak broadening, in general, increases with colloid size, reaches a maximum and then starts to decrease as the exclusion limit of the pores is approached.
2. Peak broadening increases with an increase in flowrate.
3. Increasing the ionic strength, increases dispersion due to increased accessibility of the pores.
4. A well designed packing, such as one where the particle has a solid core and a porous crust, can significantly reduce dispersion. For CPG type of packing material, peak breadening can be excessive.
5. The chromatogram of narrow standards are generally skewed, the extent of skewing increasing with particle size. Skewing possibly results from the entrapment of particles within the porous matrix.

5.2 EXPERIMENTAL

5.2.1 Equipment

The apparatus employed for chromatographing particle suspensions has been schematically represented in Chapter 1. The instrumentation consists of 1) pump 2) sample injection valve 3) packed columns 4) detector 5) volume counter 6) strip chart recorder. Details follow.

Pump A positive displacement pump (Milton Roy Mini Pump) with an adjustable delivery volume was used. This pump was designed to handle back pressures of up to 5000 psi. Pressure fluctuations were damped out with an inline pulse damper.

Sample injection valve A conventional six port two way injection valve manufactured by Disc Instruments Inc. was used. The volume of the sample loop was 0.4 mℓ approximately.

Packed columns The columns used were dry packed using a packing apparatus purchased from Mandle Scientific. The packing employed was CPG of pore sizes 1000, 2000 and 3000 ^{o}A and 200-400 mesh size.

Detector The detector was a Pharmacia UV spectrophotometer with a cell of 1 cm path length and operating wavelengths of 254, 280 and 350 nm.

Volume counter A Water's liquid volume indicator with a 1mℓ siphon was used to monitor eluant volume. At the low flow rates used, the siphon

dump volume required no correction.

Carrier fluid The carrier fluid was deionized water containing 1 gm/ℓ each of sodium nitrate and Aerosol OT. Compared to the use of potassium nitrate suggested by Coll et al (1975), the carrier solvent used had much better clarity and at room temperature, the electrolyte has no tendency to precipitate the surfactant.

Particle standards Polystyrene latices with a narrow size distribution were used. These were purchased from two sources - Dow and Polysciences. The average diameter of the Dow latices were 85, 109, 176, 209, 220 and 312 nm while those of Polysciences were 57, 98, 183 and 275 nm. The frequency data of the Dow latices measured by electron microscopy are given in Appendix A.3.

Sample injection procedure Sample preparations were made by dispersing a few drops of standard latices in 100 mℓ of carrier fluid. An ultrasonic bath was used as a dispersing aid. Solute charges were typically less than 0.01 wt. %.

5.2.2 Calibration of Columns

Three columns of 3000 Å pore size and one each of 2000 Å and 1000 Å were packed. They were individually calibrated. All the three 3000 Å columns showed similar peak separation characteristics for particle sizes between 312 nm and 57 nm. However, peak broadening was much

larger for one of the 3000 Å columns. This column was discarded. Of the remaining two 3000 Å columns, one was subjected to the following:

The column was disconnected from the chromatograph and mounted on the packing apparatus which was then activated. This cause the packing in the column to further settle. Additional packing material was then added. The column was once again calibrated. The improvement in the calibration curve was not significant. A significant loss of the larger particle size colloids occurred in the column following this additional treatment. This is clearly shown in Fig. 5.1 for a 312 nm sample. Note the shift in peak position probably caused by loss of pore volume due to attrition between particles of the glass packing. This additional treatment was subsequently abandoned.

The 1000 Å column did not show any resolution between 312 nm and 57 nm particle sizes. The calibration curves for the 2000 Å, 3000 Å columns and their combination are shown in Fig. 5.2. The 57 nm particle standard appears to have been erroneously characterized by the supplier. This was subsequently confirmed by electron microscopy. The 2000 Å column exhibited a sharp upturn in its calibration curve close to its exclusion limit. It is to be noted that while data points corresponding to 312 and 275 nm diameter particles appear on individual column calibration curves, they are not indicated for the calibration curve of the combination. This is because these larger diameter particles were completely retained in the packed columns, thus generating no detector response. The percentage recoveries of these particles from individual columns were considerably less than 100%, resulting in their complete

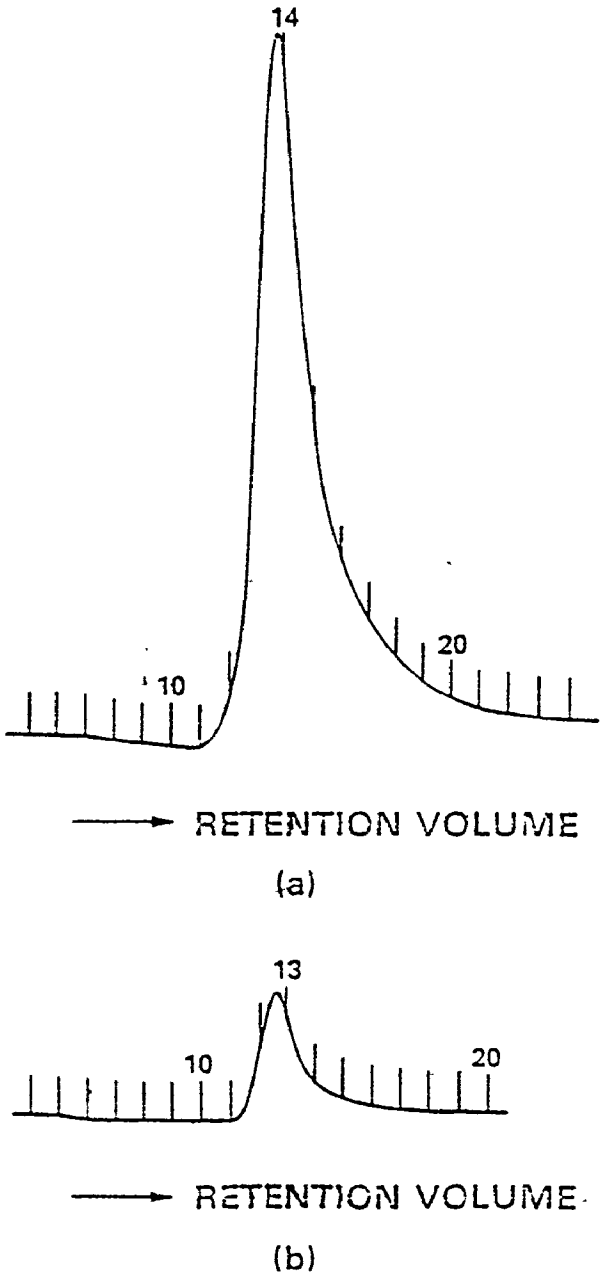

Fig. 5.1 Chromatogram of 312 nm sample (a) before treatment and (b) after treatment.

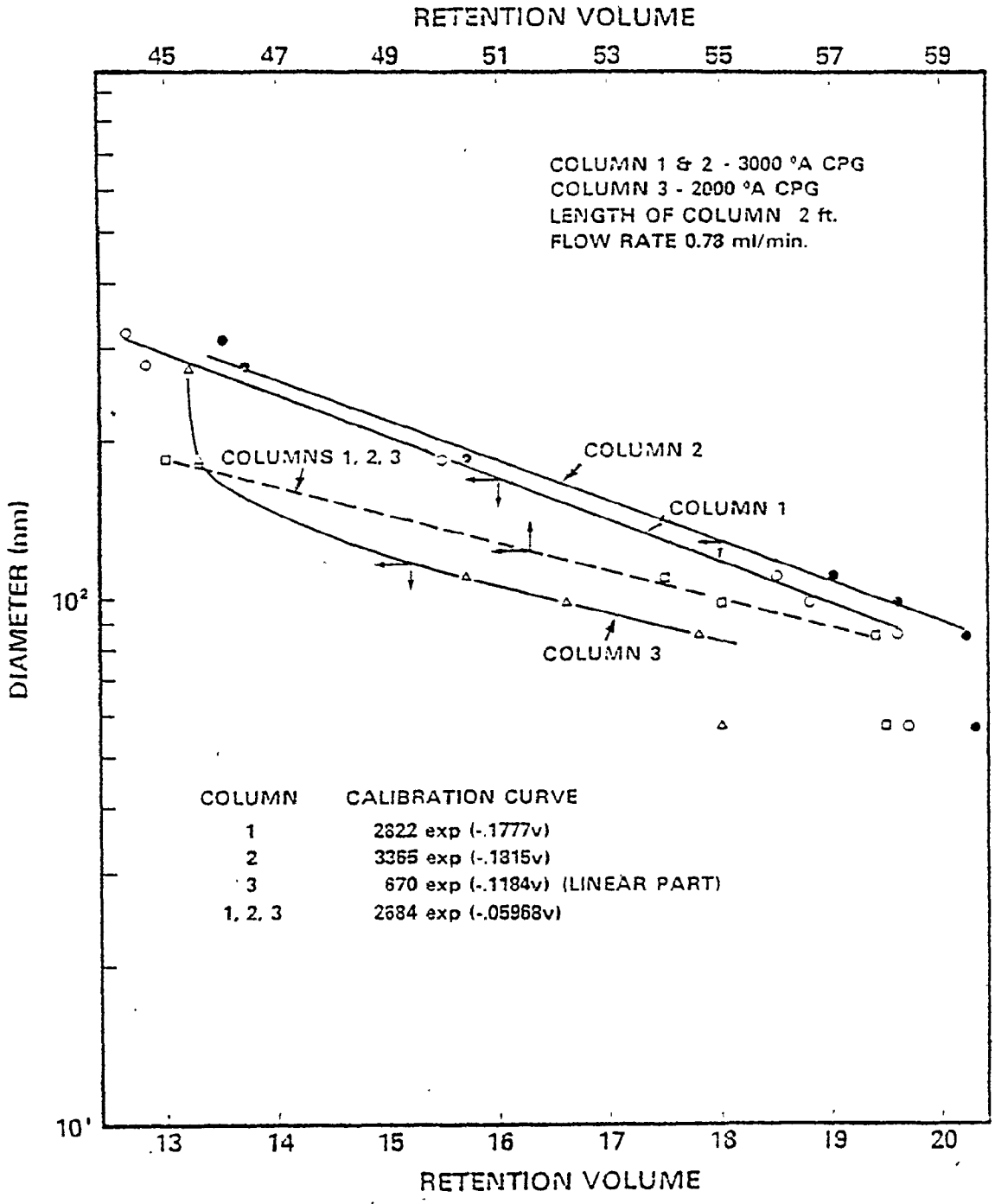

Fig. 5.2 Particle diameter-retention volume calibration curves.

loss when the columns were combined in series.

At this stage it is useful to make a comparison of the present calibration procedure with that of previous workers. Coll et al (1975) employed a set of 5 columns with a total length of 6 m packed with CPG 3000, 2000, 2000, 1000 and 500 Å porous glass. They obtained a linear calibration curve in the range 200 to 25 nm. They did not calibrate each column individually and it is very likely that the 1000 and 500 °A columns contributed insignificantly to peak separation. Hamielec and Singh (1978) investigated peak separation using several column combinations. Like their predecessors, columns were not calibrated one at a time. Their best calibration curve obtained using two 4 ft columns packed with CPG 2500 and 1500 Å porous glass, respectively, had a slope of 0.0928 ml^{-1}. Using 2 columns (CPG 1000 Å and CPG 3000 °A) of unspecified length, Johnston et al (1979) measured a slope of 0.0436. Their ionic strength was even lower than that of the earlier workers. In the present work it has been able to obtain a slope of 0.05968 ml^{-1} with 6 ft of packed column. To discriminate between columns, the appropriate criterion for comparison is the product $(D_2\sigma)^2$. While identical conditions were not used, the peak variances of the polystyrene latices measured in the present work were considerably smaller than those reported earlier [Hamielec and Singh (1978)], leading to lower $(D_2\sigma)^2$ values. The merit in individual column calibration is the elimination of columns with poor resolution (high D_2) and large peak broadening (high σ^2). Finally, Hamielec et al could detect particles up to ~500 nm while the upper limit in the present work is less than 275

nm. This appears to be related to the packing density of the columns; the denser a packed bed, lower the maximum particle size that can elute from it.

5.2.3 Calibration of Detector

The detector was calibrated by pumping solutions of sodium dichromate of known absorbance through the sample port of the detector. The solutions were prepared in the carrier fluid which served as reference. The recorder response was measured as the ultimate height reached on the chart paper above the baseline, when the sample fluid was switched to a sodium dichromate solution of known absorbance. The calibration was insensitive to flowrate variations.

The data shown in Fig. 5.3 indicate a linear response at wavelengths of 254 and 350 nm. However, at 280 nm a distinct departure from linearity occurred at low sample absorbance. This nonlinearity has implications in particle size measurement.

5.2.4 Particle Standards - How Monodispersed Are They?

The electron microscopy frequency data of Dow polystyrene latices is given in the Appendix A.3. The micrographs of the Polysciences latices are shown in Figs. 5.4-5.7. Contrary to the claims of the suppliers, these latices are not truly monodispersed, the micrograph of the 275 nm sample in fact revealing two distinct particle populations.

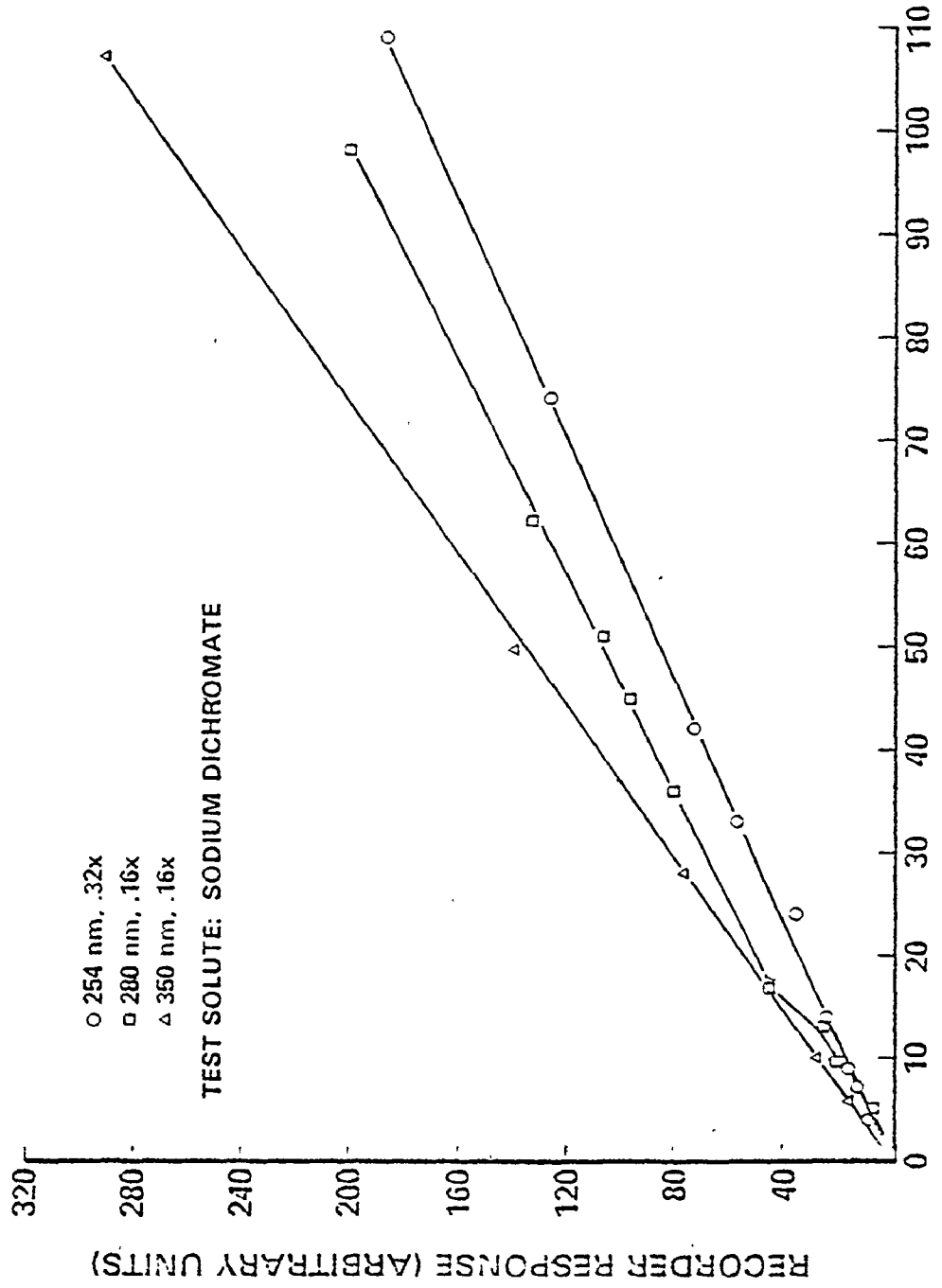

Fig. 5.3 Calibration curves of detector at wavelengths 254, 280 and 350 nm.

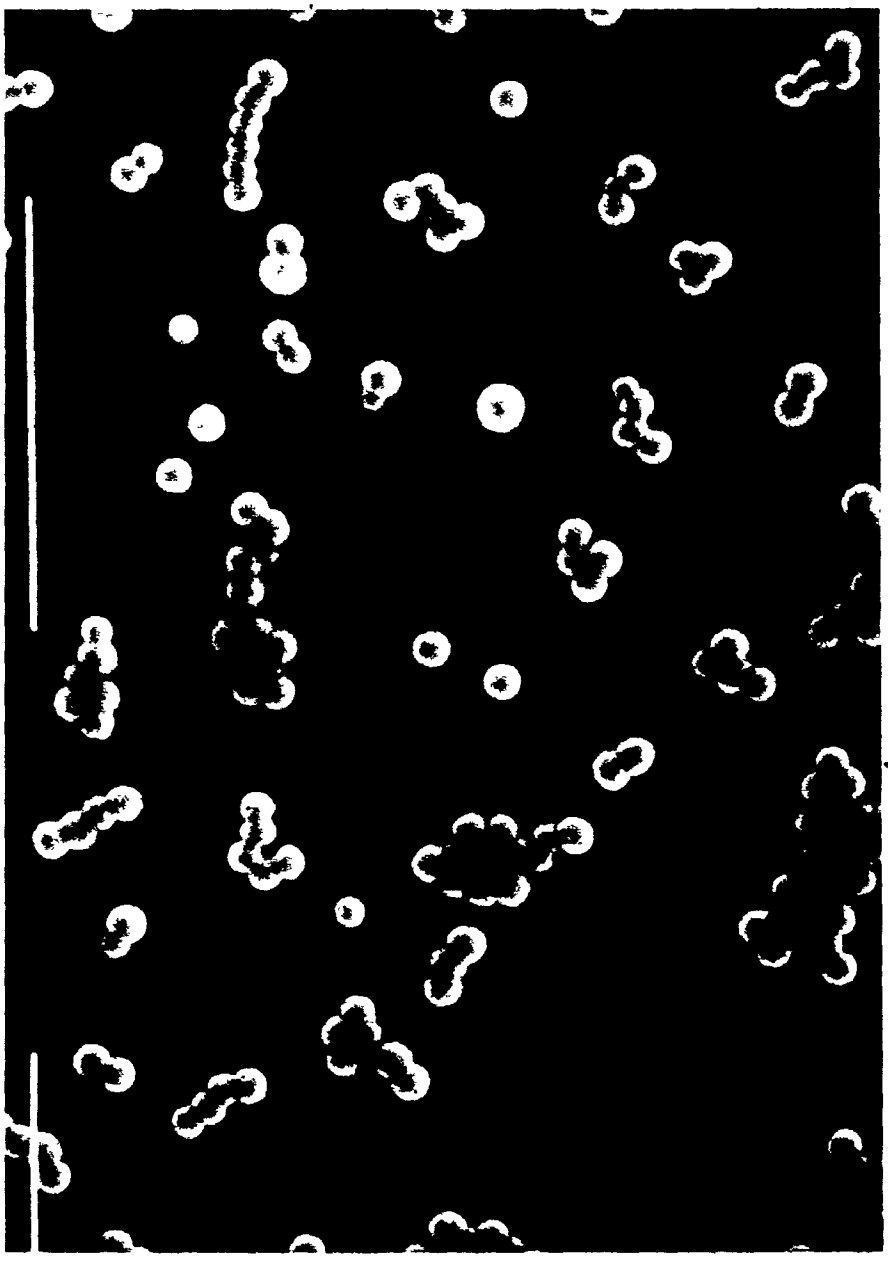

Fig. 5.4 Scanning electron micrograph of 57 nm Polysciences polystyrene latex

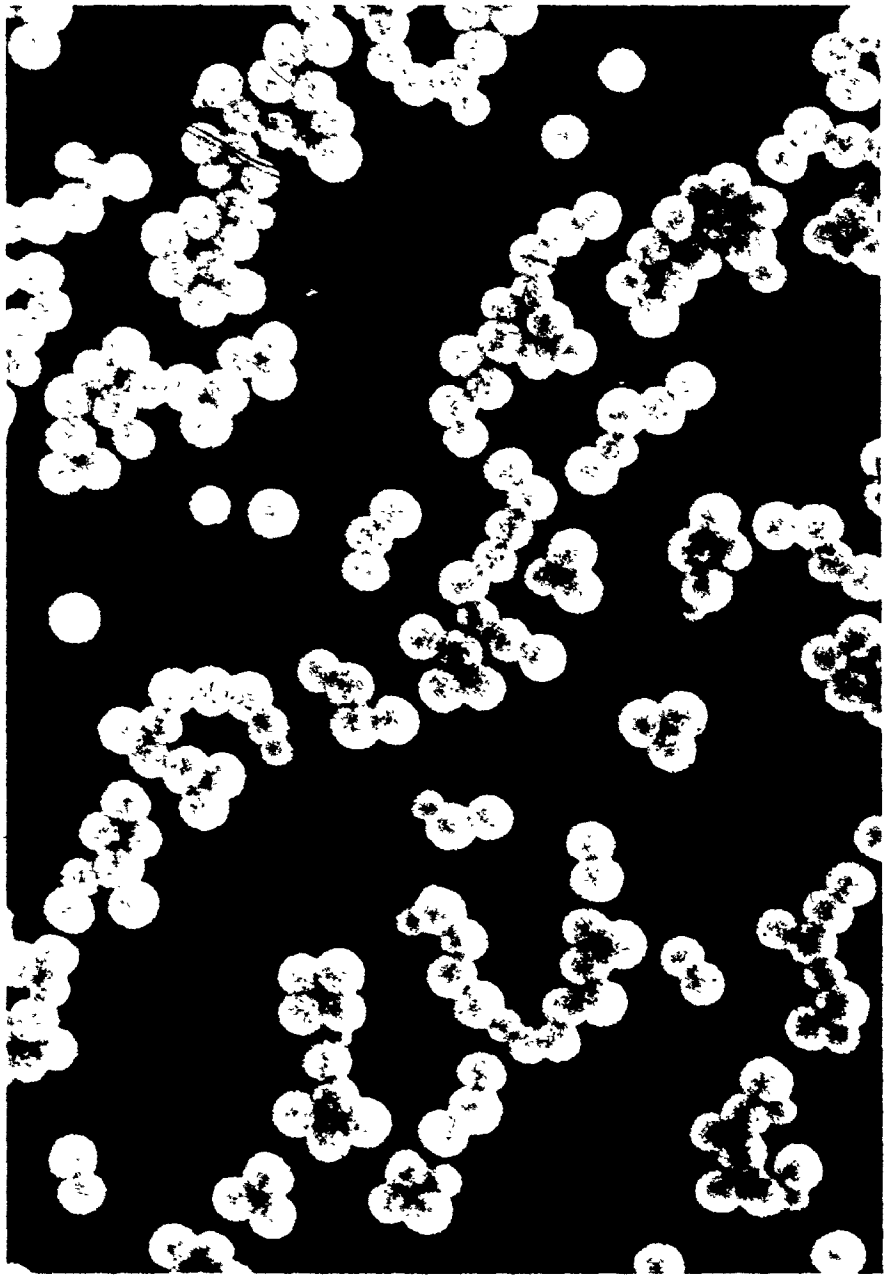

Fig. 5.5 Scanning electron micrograph of 98 nm Polysciences polystyrene latex

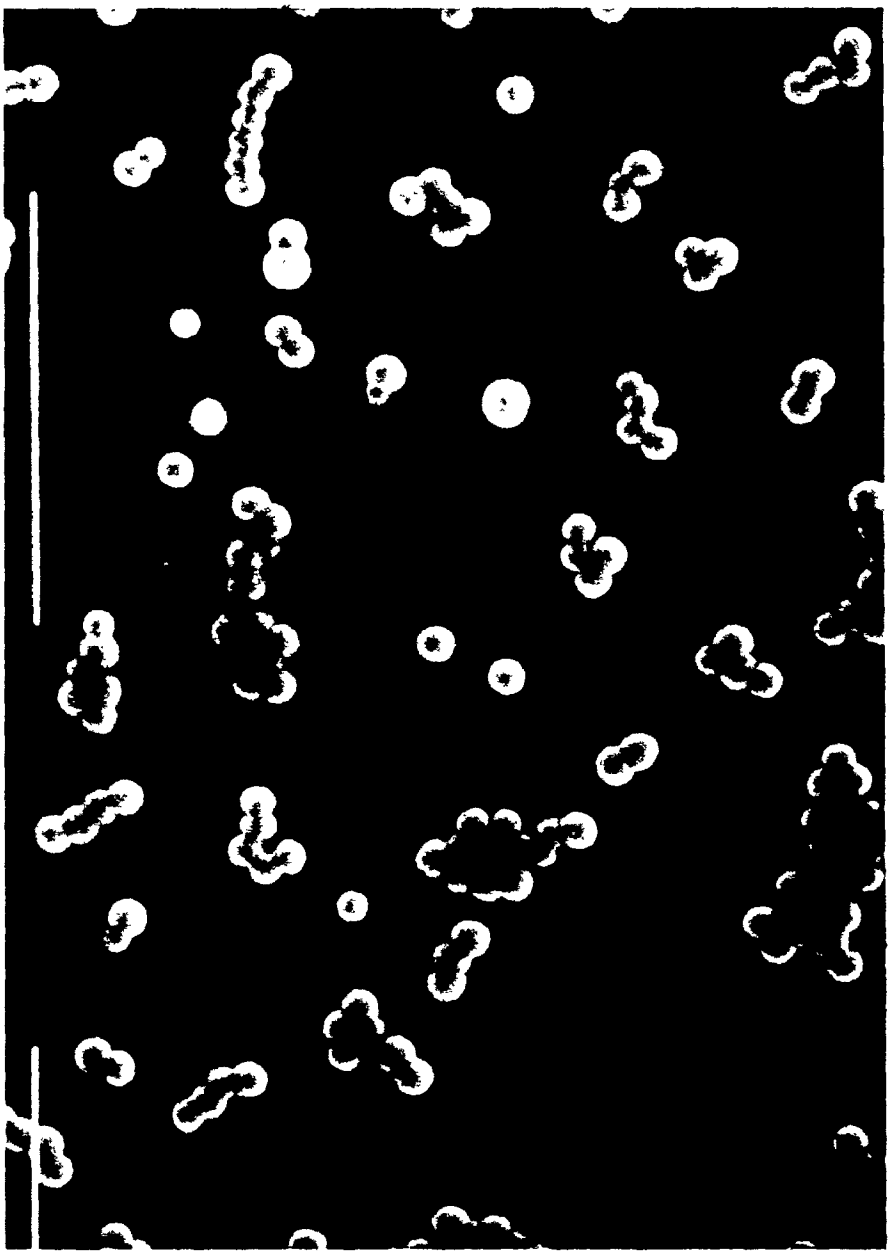

Fig. 5.6 Scanning electron micrograph of 183 nm Polysciences polystyrene latex

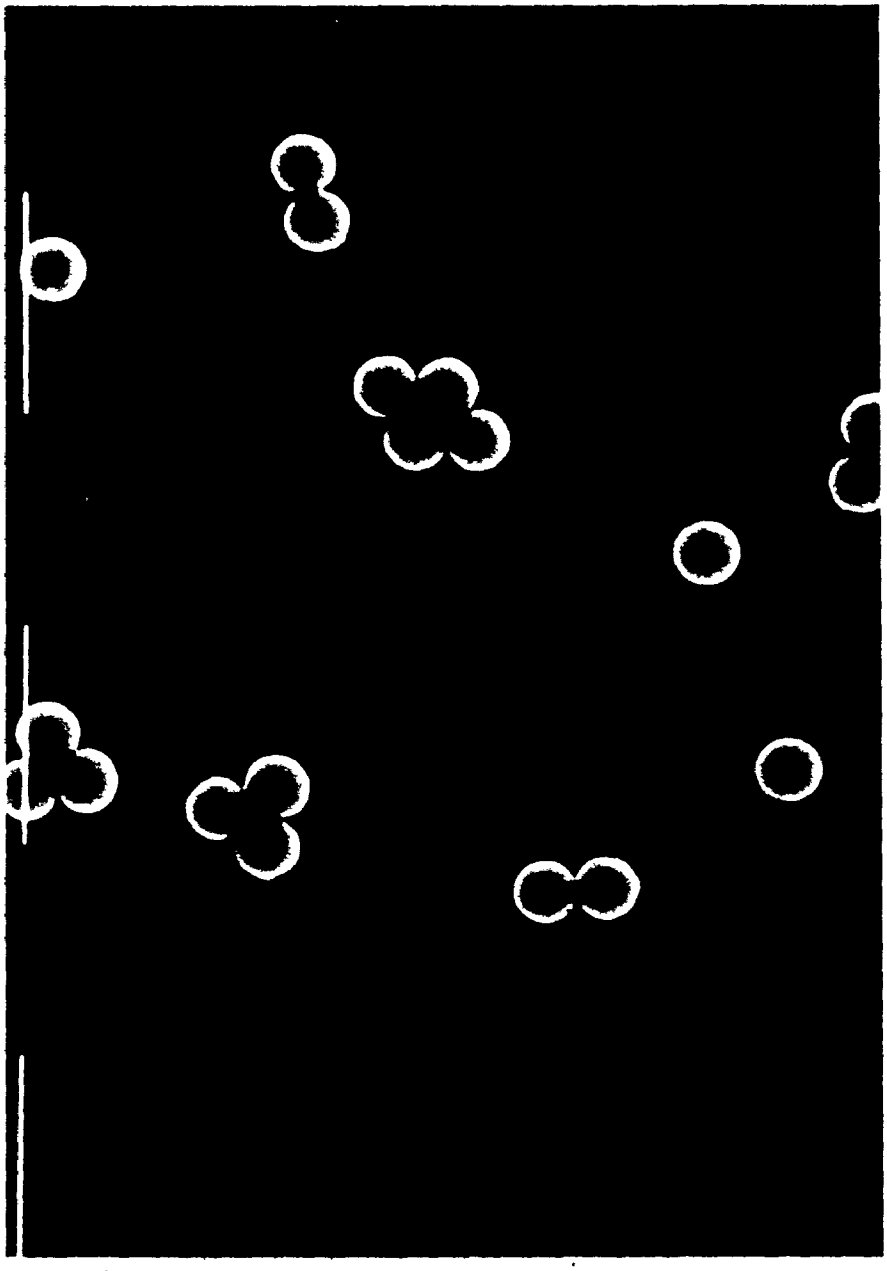

Fig. 5.7 Scanning electron micrograph of 275 nm Polysciences polystyrene latex

Calculation of the average diameters, D_n to D_t for the Dow latices indicate them to be virtually identical. This probably is also true for the Polysciences latices. Therefore, the fact that the latices are not truly monodispersed should apparently have no bearing on the diameter-retention volume calibration. However, as observed in the synthesized chromatograms, Figs. 4.4-4.11, the peak position that would be measured in the event of true monodispersity of the latices can under certain conditions be significantly different from the peak position of the F(v) chromatogram.

Evident from Figs. 4.4-4.11, is the considerable difference between the shape of the spreading function and the F(v) chromatogram. It indicates the fallacy of seeking a correlation between the mean retention volume of the latices and the statistical properties of their chromatograms, rather than those of the spreading functions such as one attempted by Johnston et al (1979).

5.2.5 Measurement of Extinction Coefficients

Heller and Tabibian (1975) noted that errors, due to laterally scattered light and the corona effect, as large as to cause a 30% reduction in measured turbidity, may result 'if instruments which are perfectly suitable for ordinary absorption measurements are used for turbidity measurements without proper modifications'. To evaluate the performance of the turbidity detector used in the present study, particle suspensions of various concentrations of several polystyrene latex standards were prepared. Their extinction coefficients were

measured using both a bench-top UV spectrophotometer (Beckman, Model 25) and the online detector (Pharmacia).

In the absence of multiple scattering, eqn. (3.12) describes the experimental extinction of light by colloidal particles. It is re-written here as

$$\frac{1}{\ell} \ln(I_o/I_t) = \frac{2.303}{\ell} A = 0.015 \frac{\rho_s}{\rho_p} \frac{K c}{D} \qquad (5.1)$$

where A is the optical density. A versus c data collected from a Beckman spectrophotometer then yields the value of K for a known D at any specific wavelength.

To measure K using the online detector, the packed columns were replaced by a suitable length of 1/16 in O.D. stainless steel tubing and peak areas corresponding to injections of various particle suspensions and sodium dichromate solutions were recorded on chart paper. The following analysis was then applied.

The recorder response F(v) is related to the optical density in the detector cell, A'(v) by

$$F(v) = \xi A'(v) \quad \text{(when response is linear)} \qquad (5.2)$$

Therefore,

$$\int_0^\infty F(v)\, dv = \xi \int_0^\infty A'(v)\, dv = \xi A V_s \qquad (5.3)$$

where A is the optical density of the injected sample and V_s is the sample volume. The product ξV_s may be estimated from the slope of a

peak area versus A plot for sodium dichromate. For known weight concentrations of particle suspensions injected, A is considered the unknown; A versus c data are then obtained from a measurement of their peak areas and hence, K calcualted from eqn. (5.1). It should be noted from eqn. (5.3) that, in the absence of optical effects noted earlier, peak area versus optical density data for the various sized particles and sodium dichromate solute must fall on the same straight line.

The data from the Beckman spectrophotometer measured at three different wavelengths, 254, 280 and 350 nm are shown in Figs. 5.8-5.10. Figs. 5.11-5.14 indicate the data measured using the online detector. The measured and calculated extinction coefficients are given in Table 5.2 (see Appendix A.2 for tables of scattering coefficients). The data shown in Figs. 5.11-5.14 indicate that, while, the smaller particles (85, 98 and 109 nm) are indistinguishable from the dissolved solute (sodium dichromate) in as far as detector behaviour is concerned, the detector response differs significantly for the larger diameter particles. The reduced peak areas and hence turbidities measured for the larger particles are consistent with the findings of Heller and Tabibian that, the corona effect and the interference effect of laterally scattered light cause a reduction in measured turbidity, the effects being more pronounced for larger particles and causing a departure from the linear dependence of turbidity on concentration, at concentrations lower than those at which, it would occur in the absence of such effects.

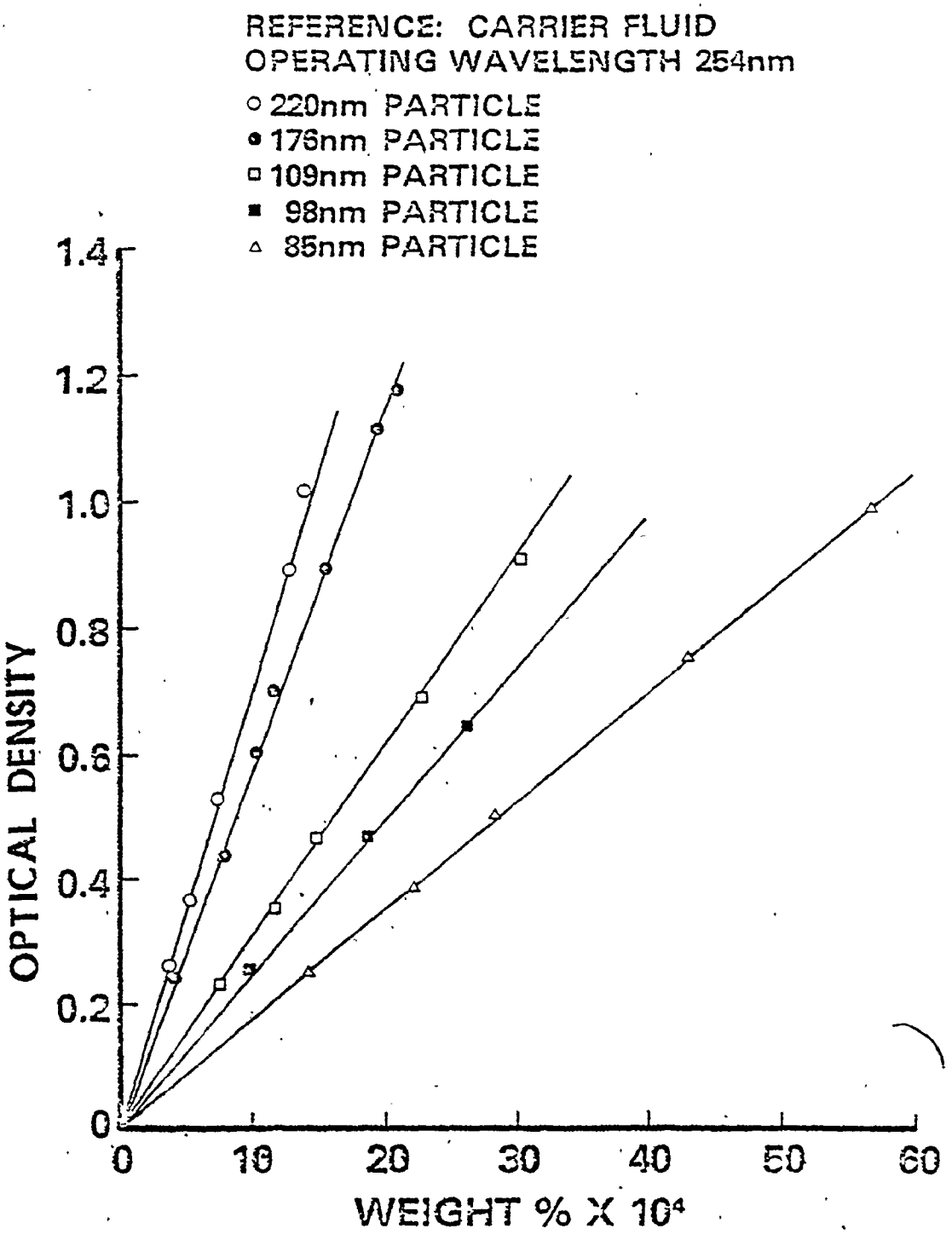

Fig. 5.8 Optical density versus weight percent of standard latices at 254 nm.

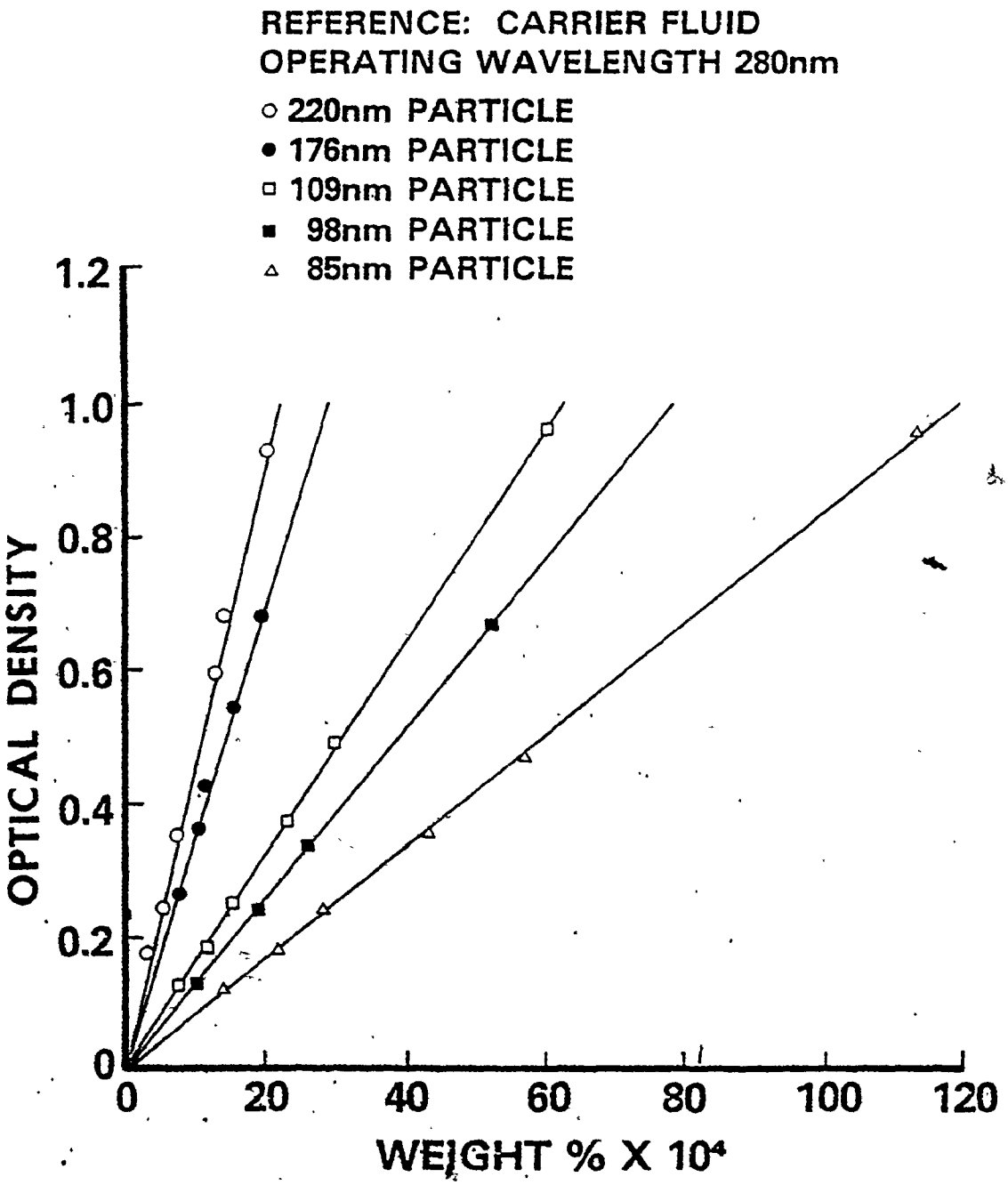

Fig. 5.9 Optical density versus weight percent of standard latices at 280 nm.

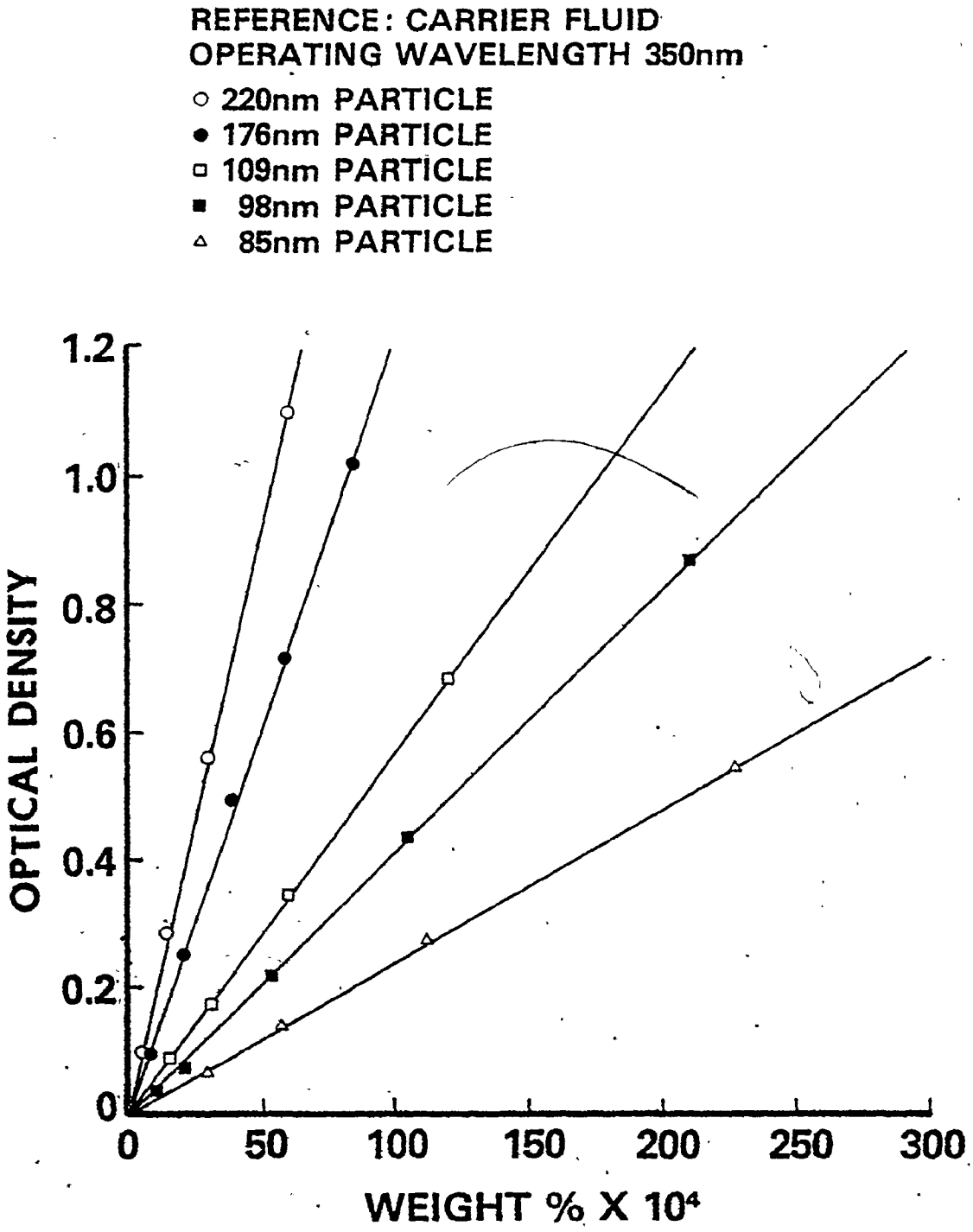

Fig. 5.10 Optical density versus weight percent of standard latices at 350 nm.

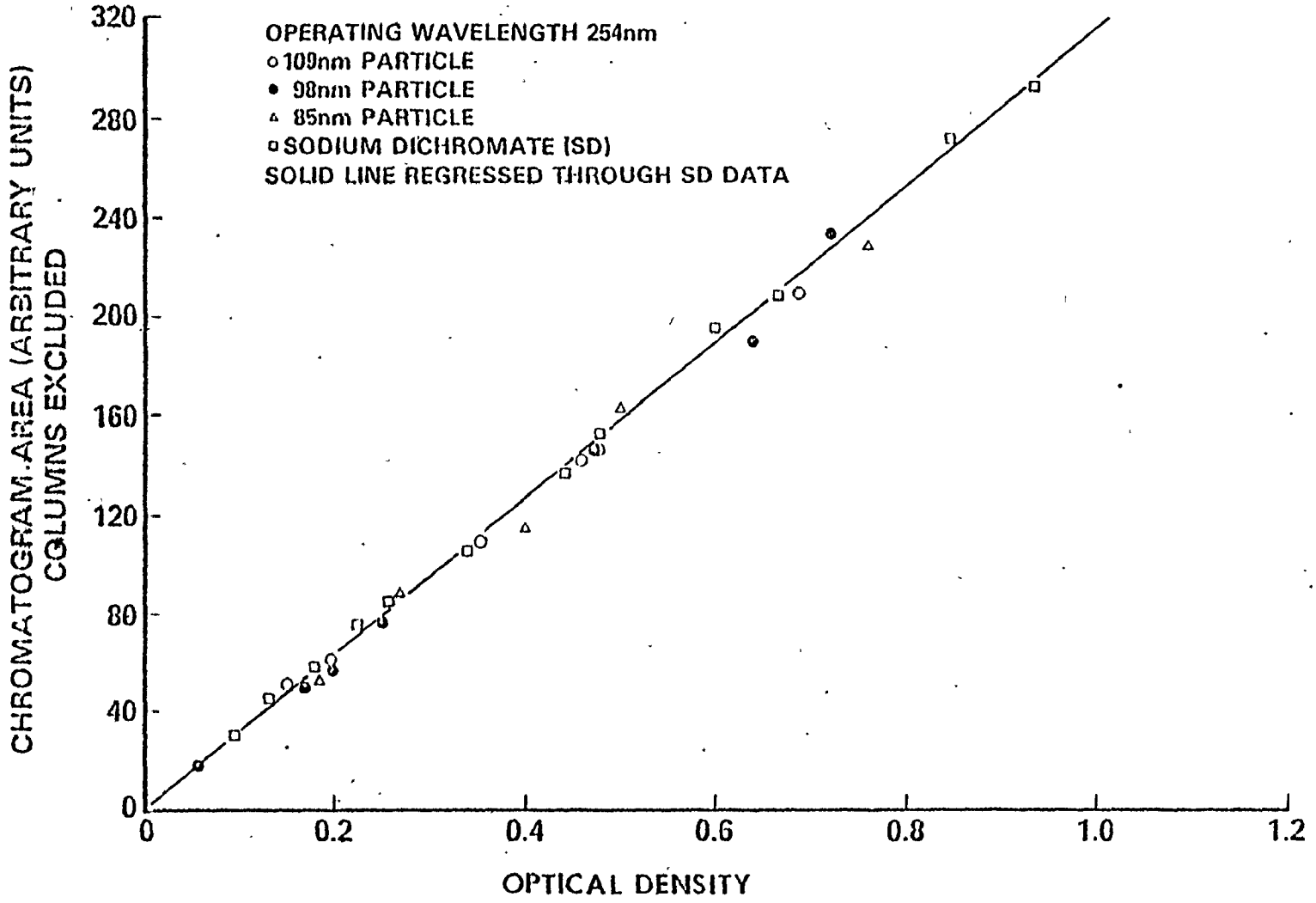

Fig. 5.11 Comparison of detector response of 85, 98 and 109 nm latices with that of sodium dichromate.

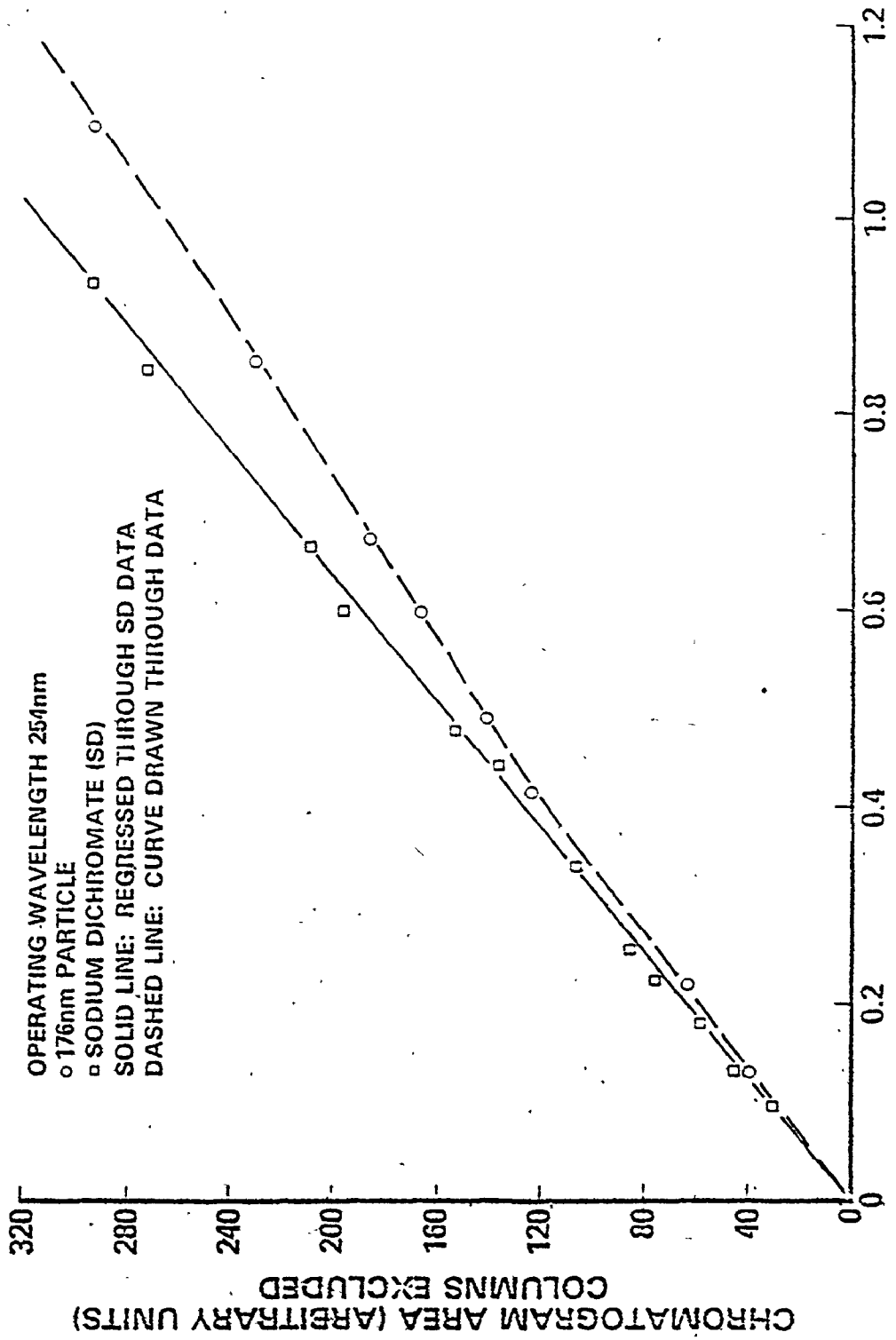

Fig. 5.12 Comparison of detector response of 176 nm latex with that of sodium dichromate.

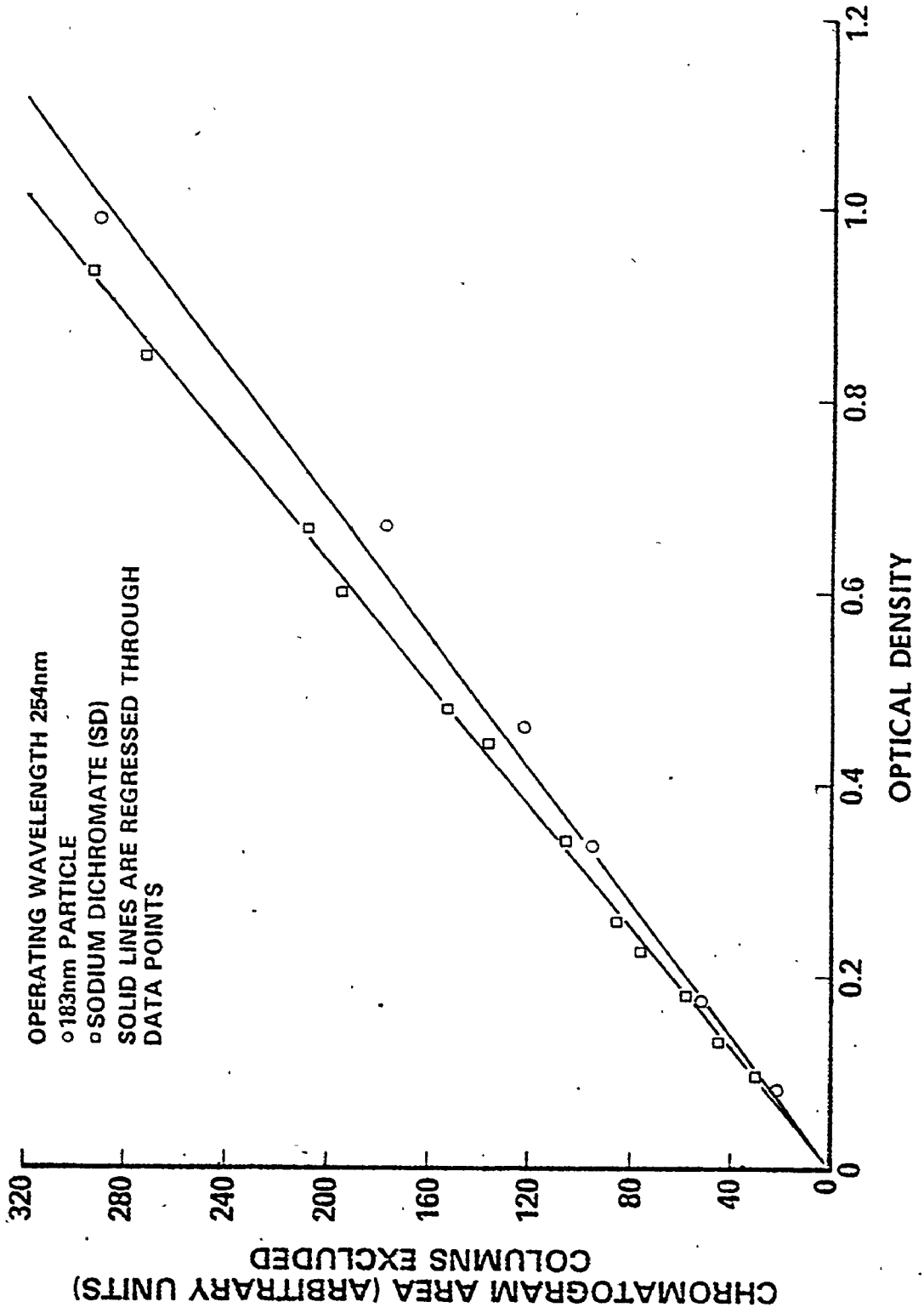

Fig. 5.13 Comparison of detector response of 183 nm latex with that of sodium dichromate.

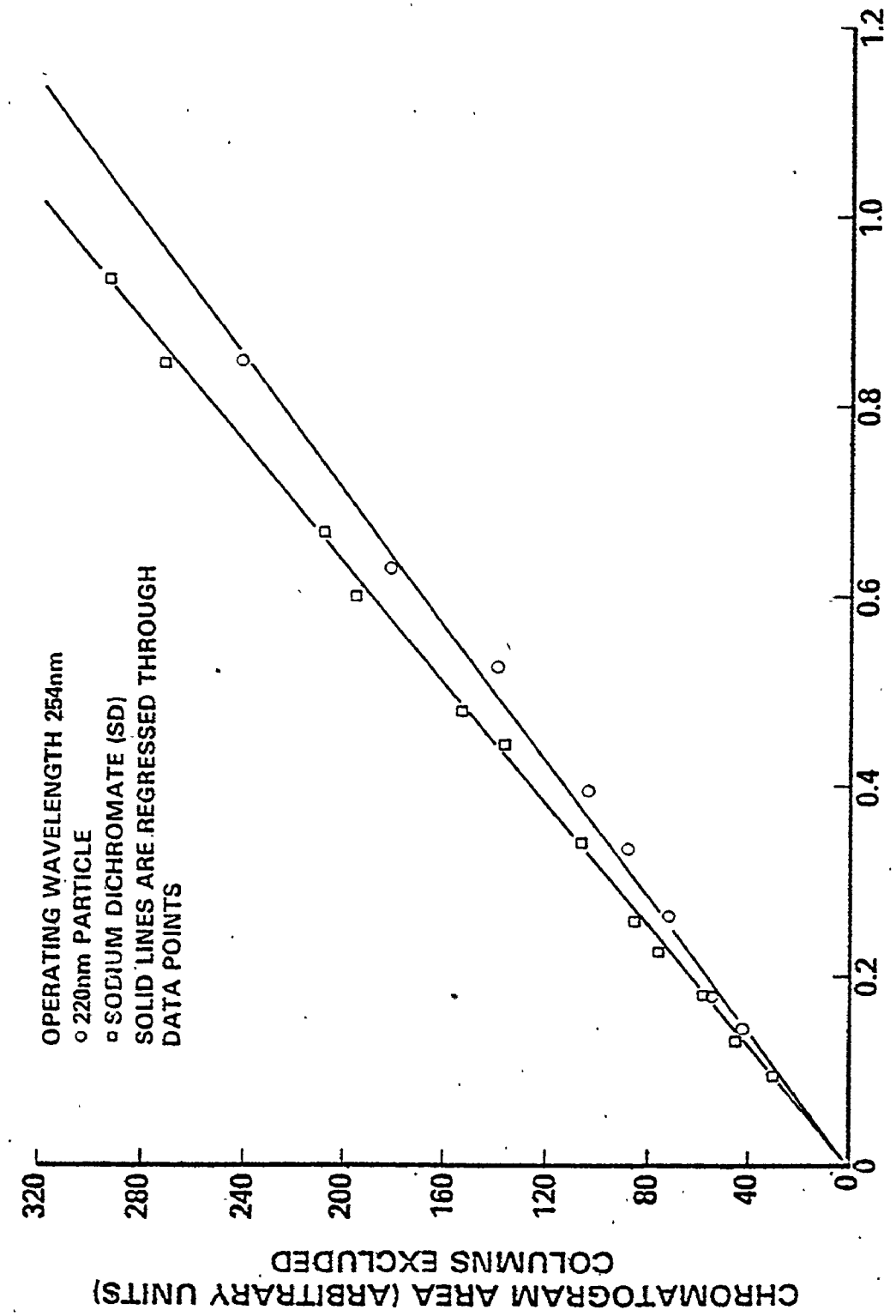

Fig. 5.14 Comparison of detector response of 220 nm latex with that of sodium dichromate.

Table 5.2 Comparison of Measured and Calculated Extinction Coefficients

Wavelength (nm)		Diameter (nm)					
		85	98	109	176	183	220
254	Mie theory+	0.1755	0.2530	0.3330	1.0686	1.1636	1.6600
	Beckman	0.2372	0.3801	0.5260	1.5850	1.8330	2.4030
	Online detector	0.2264	0.3898	0.5054 (0.72*)	1.3280 (1.89*)	1.6640	2.1460
280	Mie theory+	0.1188	0.1755	0.2299	0.7831	0.8468	1.2518
	Beckman	0.1121	0.2008	0.2796	0.9606	1.1710	1.5590
350	Mie theory+	0.0472	0.0749	0.1030	0.3639	0.4056	0.6378
	Beckman	0.0327	0.0654	0.1000	0.3467	0.4830	0.6547
	Online detector	-	-	-	0.312	-	0.6295

+Refractive index of polystyrene [Kerker(1969)] $= 1.5683 + 10.087 \cdot 10^{-11} / \lambda_0^2$.
Refractive index of water [Kerker (1969)] $= 1.3240 + 3.046 \cdot 10^{-11} / \lambda_0^2$.
where, λ_0 is the wavelength in vacuum (cm).
*Measured from data of Silebi and McHugh (1979).

Table 5.2 compares the measured values of extinction coefficients with calculated values from theory at wavelengths of 254, 280 and 350 nm. The lower values of the extinction coefficients measured using the online detector compared to those using the Beckman instrument, are due to the optical effects discussed above. The disagreement between the extinction coefficients calculated from Mie theory (for nonabsorbing

spheres) and the measured values using the Beckman instrument is very significant, particularly at 254 and 280 nm.

Silebi and McHugh (1979) concluded from the investigation of their detector response that, instrument errors were not present and Mie theory for nonabsorbing particles was applicable in evaluating the turbidity signal. However, it appears that their measured values of extinction cross-section are consistently larger than calculated values, despite a deceptively close agreement indicated on a log (extinction cross-section) versus log (diameter) plot. Values of extinction coefficient calculated from their data are also shown in Table 5.2.

In an attempt to resolve the discrepancy between calculated and measured extinction coefficients, one may consider the following factors:

1. Polystyrene particles absorb light at 254 nm.
2. The particles contain residual styrene monomer which strongly absorbs light at a wavelength of 254 and 280 nm.
3. Additives in the latex formulations such as emulsifier etc. absorb in the UV range.
4. The latex particles are not monodispersed.

Accordingly, SEC analysis of latex samples (dried and dissolved in tetrahydrofuran) were carried out. The carrier solvent was tetrahydrofuran and peaks were monitored by a Waters' dual absorbance detector at wavelengths of 254 and 340 nm. The latter detection wavelength was the closest to 350 nm available.

Fig. 5.15 shows the SEC traces for the 312 nm Dow latex sample.

Note the response at 340 nm is at twenty-five times the sensitivity of the response at 254 nm and hence, considerably exaggerated in comparison. At 254 nm two peaks are clearly noted, a polymer peak and a secondary peak whose retention volume corresponds to that of styrene monomer. At 340 nm, since neither monomer nor polymer absorb, the observed peak is attributable to the presence of additives such as emulsifier.

For the other Dow samples (85, 109, 176 and 220 nm), the response shown in Fig. 5.16 was typical. Note the hump in the trailing end of the SEC trace. At 340 nm, there was a distinct response though much smaller than that observed for the 312 nm sample.

The SEC traces for the 98 and 183 nm Polysciences samples are shown in Figs. 5.17 and 5.18. These are similar to the responses of the 312 nm particle though at 340 nm the effect was considerably smaller and comparable to the other Dow samples.

These observations were later confirmed by Shull (1979) according to whom

1. Residual styrene content in the particles is less than 1/2 wt %.
2. Tetrahydrofuran may cause the leaching of oligomers from the latex particles. This is evident in Fig. 5.17 as the slight hump between the two peaks.
3. The surfactant used in preparing the latices does not absorb in the range 250-300 nm.

On the basis of the above observations, it is concluded that at 350 nm the discrepancy between calculated and measured extinction coefficients

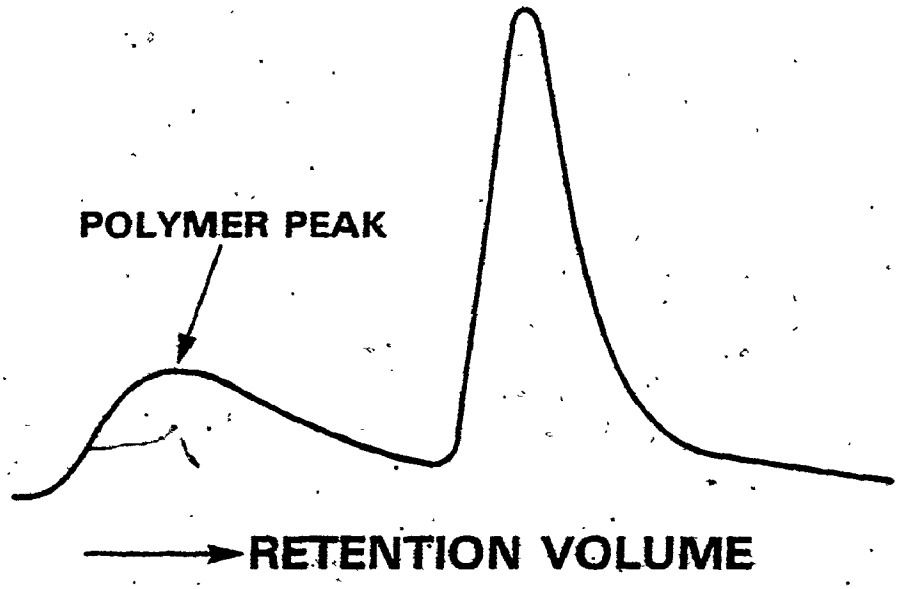

(a)

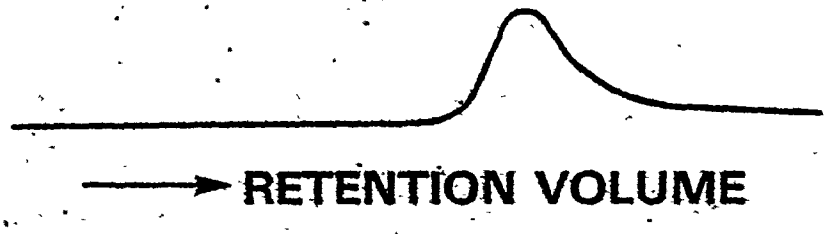

(b)

Fig. 5.15 SEC analysis of 312 nm Dow latex sample: SE Dupont silica columns (a) response at 254 nm wavelength (full scale 0.5A)(b) response at 340 nm wavelength (full scale 0.02A).

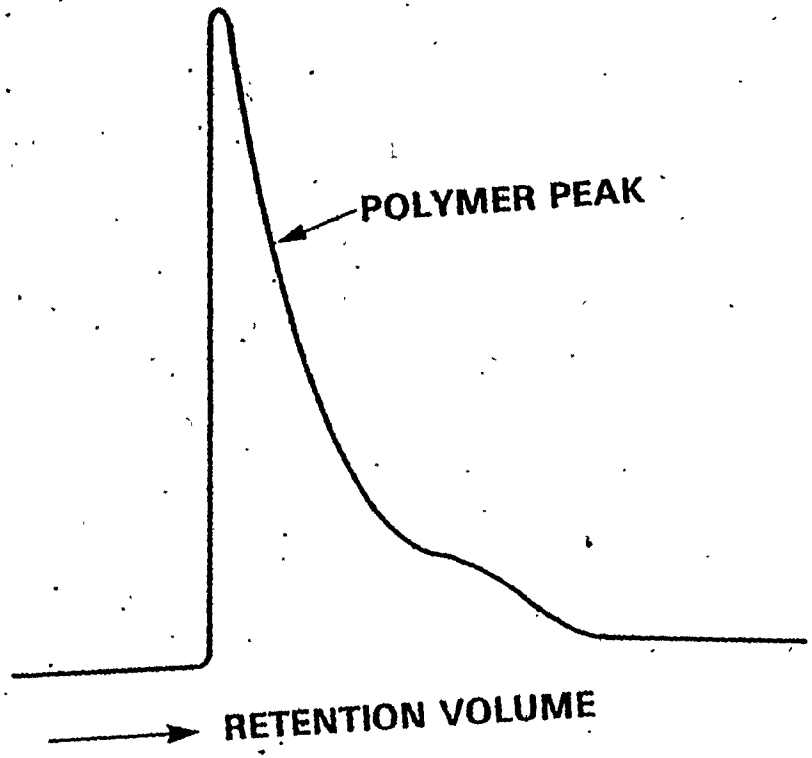

Fig. 5.16 SEC analysis of 220 nm Dow latex sample : E-linear Waters' silica columns. Response at 254 nm wavelength (full scale 0.5A).

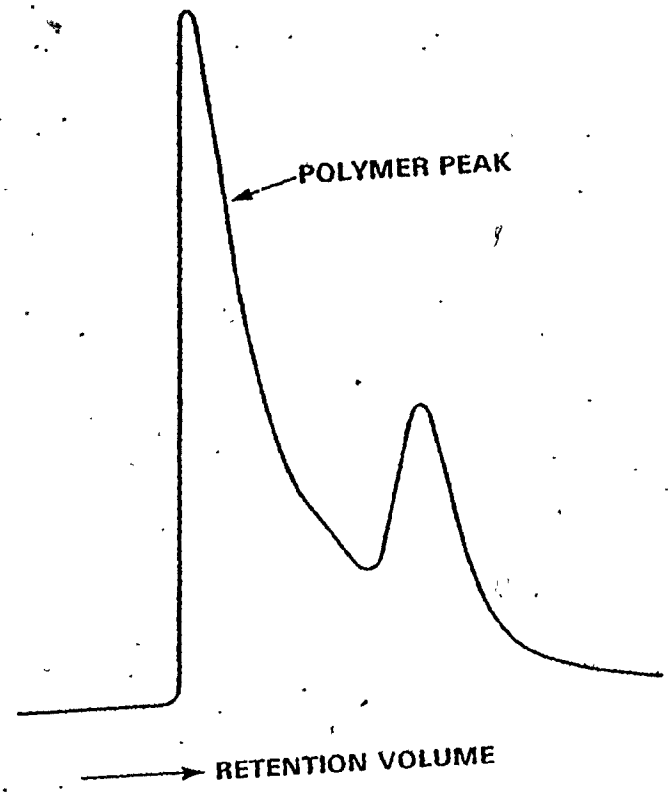

Fig. 5.17 SEC analysis of 98 nm Polysciences latex sample: E-linear Waters' silica columns. Response at 254 nm wavelength (full scale 0.5A).

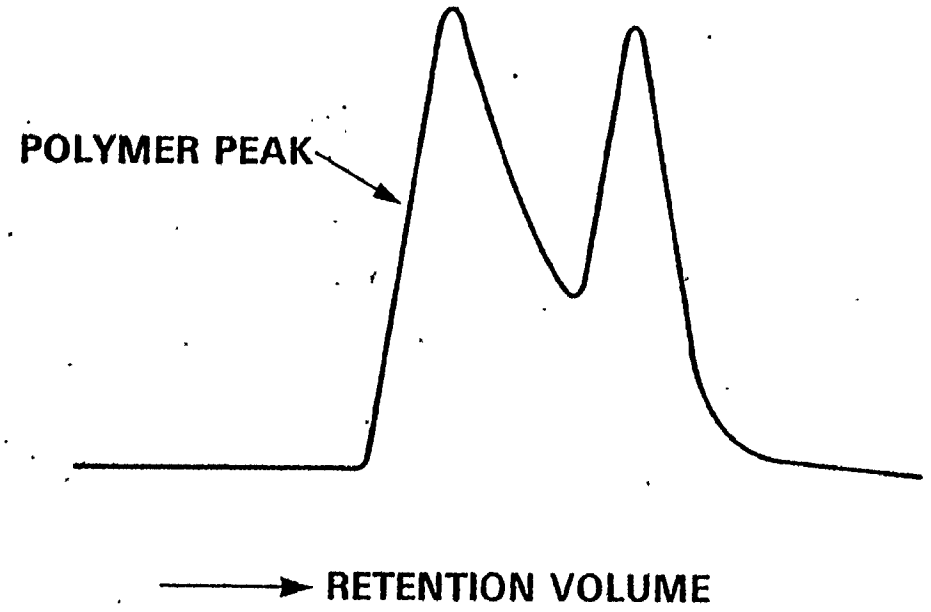

Fig. 5.18 SEC analysis of 183 nm Polysciences latex sample: E-linear Waters' silica columns. Response at 254 nm wavelength (full scale 0.5A).

may be attributed to the presence of additives in the latex formulations and polydispersity of the latices. Whether or not, polystyrene latices absorb at 254 nm, can only be established once the contributions to the extinction coefficients from the additives, residual monomer and oligomers if any, are assessed. A combination of the aforementioned are probably responsible for departure from theory at 254 and 280 nm.

5.2.6 Particle Recovery

From eqn. (5.3) it follows that the number of particles, N_{out} which elute from a column for a known injection, of concentration c_o (particles/cc), are given by

$$N_{out} = \frac{2.303 \int_0^\infty F(v)\, dv}{\xi\, \ell\, \frac{\pi}{4} D^2} \tag{5.4}$$

The number of particles injected is given by $c_o V_s$. Therefore, the number percent recovery R, is calculated as

$$R = \frac{2.303 \int_0^\infty F(v)\, dv}{\xi\, \ell\, c_o\, V_s\, \frac{\pi}{4} D^2} \times 100 \tag{5.5}$$

Alternatively, it follows from eqn. (5.4) that R may be evaluated as

$$R = \frac{\left(\int_0^\infty F(v)\, dv \right)_c}{\left(\int_0^\infty F(v)\, dv \right)_{wc}} \times 100 \tag{5.6}$$

where the integrals in the numerator and denominator represent peak areas for the same sample obtained with and without the columns, respectively. A correction factor must be incorporated in eqn. (5.5) to account for instrumental errors. Eqn. (5.6) is valid in such an event, however, as long as the chromatogram area versus optical density curve is linear.

Particle recoveries calculated according to eqn. (5.6) indicated essentially 100% recoveries for the 85, 98 and 109 nm samples. However, the recovery for the 183 nm sample was only 41%.

When particle recovery is very poor, successive injections of the same sample in a normal run (with columns) generate increasing peak areas. For instance, the following peak areas were measured for a sample: 44.6, 49.3, 49.6, 49.2 and 51.4. After a considerable time elapse during which no sample was injected, peak areas measured were 43.4, ..., 48.1, ... Apparently a gradual buildup of particles occurs within the packed bed due to successive injections; this buildup is reduced if sample injection is discontinued and when injection is restarted, a peak area lower than the previous is measured, which once again starts to increase with additional injections. Therefore, in such a situation, it is not possible to measure meaningfully the percent recovery for a sample. Furthermore, if two samples of different particle size are successively injected, the peak area measured for the second sample may partly be the result of the previous injection of the first sample.

5.2.7 Measurement of Particle Diameter Averages

In spite of the disagreement between measured and calculated extinction coefficients, it is of interest to examine the diameter averages obtained using Mie and Rayleigh theories. Two sets of data are examined. The first set was treated assuming the spreading functions were Gaussian or modified Gaussian, eqn. (4.63). Methods 1 and 2 were applied and in accordance with Method 2, the extinction coefficients calculated from Mie theory were fitted against retention volume by a sum of exponentials. Excellent fit was obtained. The second data set could not adequately be treated assuming a Gaussian or a modified Gaussian spreading function. Method 3 was applied to these data assuming the truncated Provder and Rosen's shape function was an adequate description of instrumental spreading. Application of Method 3 requires the extinction coefficients calculated from Mie theory to be fitted by the quadratic in retention volume, eqn. (4.89). An adequate fit was obtained.

Data Treatment of Set 1

Fig. 5.19 shows the chromatograms for the 85, 98, 109 and 183 nm particles measured at a wavelength of 254 nm. While skewing exists in all the chromatograms, it is most pronounced for the largest particle size. Chromatograms of mixtures of latices are shown in Fig. 5.20. The calibration data and measured variances are shown in Table 5.3. It must be noted that while the calibration curve spans a retention volume range of 13 ml, the chromatograms span about twice this volume. The extension of the calibration curve beyond a retention volume of 58 ml may

overestimate particle diameters if the resolution of the high retention volume end falls off rapidly, while its extension to retention volumes of less than 45 ml may likewise underestimate particle diameters, if the exclusion limit of the pores is approached. Further, the low retention volume ends of the chromatograms may correspond to particles that are larger than the maximum size that would elute from the columns. The latter consideration is, however, of no consequence as long as the extension of the linear calibration is safely done.

Table 5.3 Calibration Data and Measured Variances (Set 1)

Sample (nm)	Peak Retention Volume (ml)	Measured Variance (ml^2) Wavelength (nm) 254	280	350
85	58	12.42	12.97	12.66
98	55	12.56	13.58	13.58
109	54	13.26	13.42	13.05
183	45	14.15	-	13.96

Tables 5.4-5.6 contain the results of the particle size analysis for data measured at the three different wavelengths. The value of σ^2 was set equal to the measured variance. It could very well have been obtained by solving the expression for any one diameter average; different values would have been obtained depending on the theory used. Here, no attempt is made to force fit the data. The diameter averages, D_n to D_t are arranged in increasing order of magnitude which is also the order of decreasing imperfect resolution correction factors. Observe the relatively small differences between uncorrected diameter averages

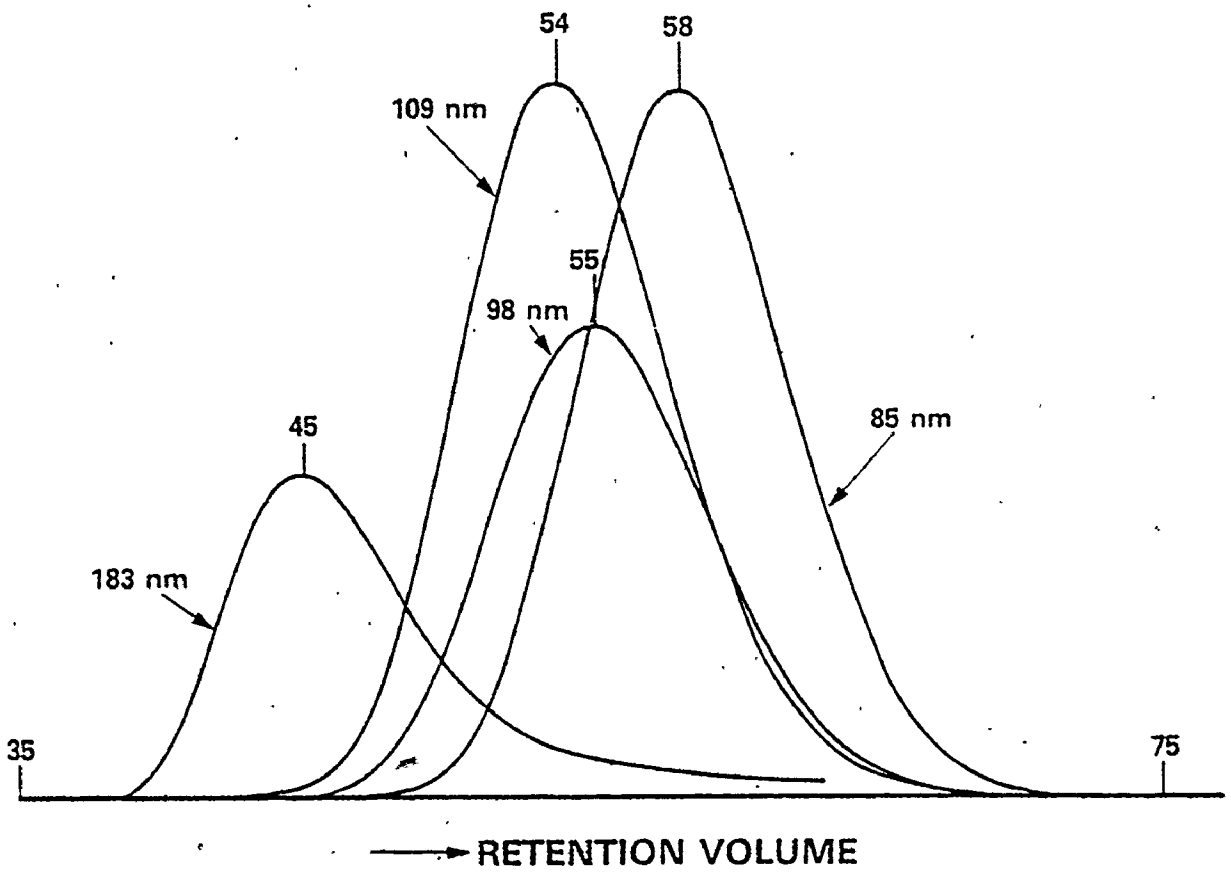

Fig. 5.19 Chromatograms of standard latices measured at 254 nm wavelength (Data set 1).

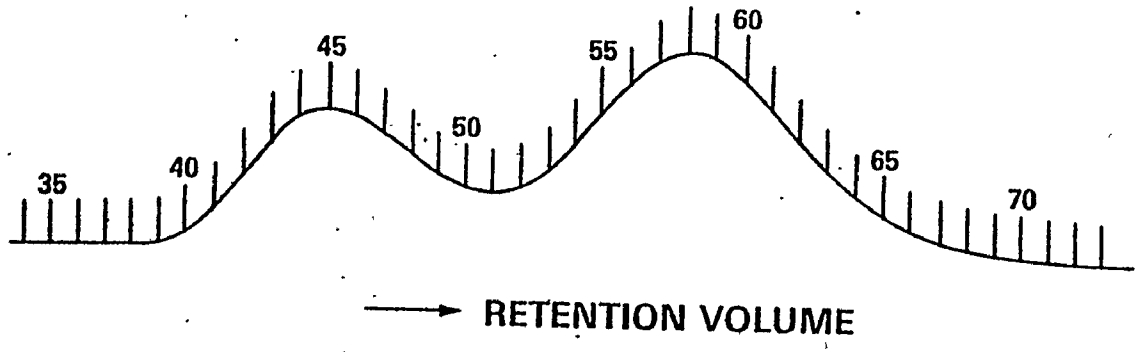

MIXTURE 1: MIXTURE OF 183 AND 85 nm LATICES

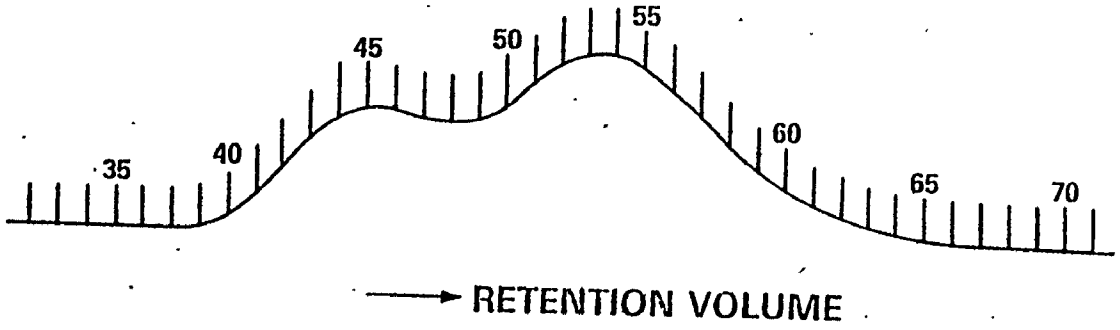

MIXTURE 2: MIXTURE OF 183 AND 109 nm LATICES

Fig. 5.20 Chromatograms of mixtures 1 and 2 measured at 254 nm wavelength (Data set 1).

Table 5.4. Diameter Average for Latex Particles Measured at 254 nm (Data Set 1)

For each sample,
Row 1. Uncorrected diameter averages from Rayleigh theory (Appendix A.1)
Row 2. Uncorrected diameter averages from Mie theory (Appendix A.1)
Row 3. Diameter averages in row 1 corrected using Rayleigh correction factors (Table 4.5)
Row 4. Diameter averages in row 2 corrected using Rayleigh correction factors (Table 4.5)
Row 5. Corrected diameter averages from Mie theory (Method 2, Section 4.4.2)

Sample	Variance $\sigma^2(ml^2)$	D_n	D_s	D_v	D_{ss}	D_w	D_t (nm)
		63.1	64.7	66.3	69.7	73.2	76.7
		65.6	67.3	69.1	72.7	76.4	80.2
85	12.423	80.5	80.7	80.9	81.3	81.7	82.0
		83.7	84.0	84.3	84.9	85.4	85.7
		80.7	80.8	81.1	81.7	81.9	82.1
		74.8	76.6	78.5	82.5	86.8	91.0
		78.4	80.5	82.6	87.0	91.6	96.1
98	12.560	95.6	95.8	96.1	96.5	97.0	97.4
		100.3	100.6	101.0	101.8	102.4	102.7
		95.8	96.0	96.3	96.9	97.4	97.7
		76.2	78.7	81.2	86.4	91.6	96.6
		81.1	83.8	86.5	92.1	97.6	102.8
109	13.258	98.9	99.6	100.4	101.9	103.1	103.7
		105.2	106.2	107.0	108.7	109.8	110.7
		100.2	101.0	101.7	103.2	103.7	104.1
		105.6	111.0	116.7	129.1	141.6	152.3
		121.9	128.3	134.6	148.0	159.3	168.2
183	14.152	139.3	142.8	146.5	154.0	160.6	164.3
		160.8	165.1	168.8	176.5	180.7	181.4
		150.9	154.4	157.3	163.6	167.8	169.9

calculated from Rayleigh and Mie theories. In view of the low value of $(D_2\sigma)^2$, the magnitude of the correction factors is fairly small. The measured diameter averages for all but the 183 nm sample are in

excellent agreement with their reported values. They increase from D_n to D_t in the order expected. For the 183 nm sample, though D_{ss}, D_w and D_t are fairly close, D_n, D_s and D_v, are rather low. This appears to be related to the pronounced skewing of the chromatogram.

In terms of the accuracy of measurement, it appears from Tables 5.4-5.6 that detection of a narrow distribution particle mixture at 350 or 280 nm is just as advantageous as detection at 254 nm. However, for a broad particle size distribution sample, detection at 254 nm or lower, where particles absorb, provides a distinct improvement in small particle detection as discussed in Chapter 3.

Table 5.5 Diameter Averages for Latex Particles Measured at 280 nm (Data Set 1)

For each sample,

Row 1. Uncorrected diameter averages from Mie theory (Appendix A.1)
Row 2. Diameter averages in row 1 corrected using Rayleigh correction factors (Table 4.5)
Row 3. Corrected diameter averages from Mie theory (Method 2, Section 4.4.2)

Sample	Variance $\sigma^2(ml^2)$	D_n	D_s	D_v	D_{ss}	D_w	D_t (nm)
		63.8	65.7	94.4	95.1	96.0	96.5
85	12.966	82.3	82.7	83.2	84.1	84.9	85.3
		79.8	80.2	80.6	81.3	81.8	82.2
		74.3	76.6	79.0	84.0	89.1	94.0
98	13.575	96.9	97.6	98.2	99.5	100.5	101.1
		94.2	94.2	94.4	95.1	96.0	96.5
		81.1	83.7	86.4	91.9	97.3	102.6
109	13.421	105.5	106.4	107.1	108.6	109.7	110.2
		101.1	101.8	102.3	103.3	104.1	104.4

Table 5.6 Diameter Averages for Latex Particles Measured at 350 nm (Data Set 1)

For each sample,
Row 1. Uncorrected diameter averages from Mie theory (Appendix A.1)
Row 2. Diameter averages in row 1 corrected using Rayleigh correction factors (Table 4.5)
Row 3. Corrected diameter averages from Mie theory (Method 2, Section 4.4.2)

Sample	Variance $\sigma^2(ml^2)$	D_n	D_s	D_v	D_{ss}	D_w	D_t (nm)
		64.3	66.0	67.8	71.4	75.2	79.1
85	12.66	82.5	82.7	83.0	83.6	84.2	84.6
		81.4	81.2	81.2	81.6	82.3	82.5
		73.1	75.4	77.9	82.9	88.0	93.0
98	13.580	95.4	96.1	96.8	98.2	99.3	100.0
		92.8	93.4	93.8	94.9	96.0	96.3
		81.0	83.3	85.7	90.6	95.7	100.8
109	13.050	104.6	105.1	105.6	106.6	107.5	108.1
		101.1	101.6	101.9	102.6	103.5	103.8
		123.9	129.3	134.7	146.2	156.8	165.8
183	13.964	162.8	165.8	168.5	174.0	177.6	178.6
		154.1	156.5	158.7	164.0	168.1	169.5

Now, consider the two binary mixtures shown in Fig. 5.20. Mixture 1 was a mixture of 183 and 85 nm particles in the weight ratio of 38.73/61.27, while, mixture 2 was a mixture of 183 and 109 nm particles in the weight ratio of 51.05/48.95.

The diameter averages calculated from the mixture rule are given in Table 5.7. While the true values for each mixture appear in the first row, the values that would be obtained from the analysis of the bimodal

chromatograms should be compared with the third row entries, since, these account not only for the less than satisfactory calculations for the 183 nm sample chromatogram, but also for the incomplete recovery of the 183 nm particles.

Table 5.7 Diameter Averages of Mixtures of Latex Particles Based on Mixture Rule (Data Set 1)

For each mixture,
Row 1. Calculated assuming all diameter averages for each latex are equal to the size reported by supplier. For example, $D_n = D_s = D_v = D_{ss} = D_w = D_t = 85$ for 85 nm sample.
Row 2. Calculated from diameter averages for each latex as given by Mie Theory. For example, $D_n = 80.7$, $D_s = 80.8$, etc. (Table 5.4) for 85 nm sample.
Row 3. Calculated as in row 2 but accounting for incomplete recovery of 183 nm particles.

Mixture	D_n	D_s	D_v	D_{ss}	D_w	D_t
	90.8	93.8	98.0	107.2	123.0	140.1
1	84.9	86.9	90.2	98.3	112.2	128.4
	82.6	83.6	85.4	89.7	98.1	111.8
	122.4	125.6	129.4	137.4	146.8	155.5
2	109.4	112.5	116.1	124.7	134.7	143.8
	104.6	106.7	109.1	114.8	122.0	130.6

The diameter averages of the mixtures evaluated using Mie Theory are presented in Table 5.8. For each mixture, they are computed for σ^2 values corresponding to those of individual components and their mean. The averages fortunately are not very sensitive to the value of σ^2. Computed values with mean σ^2 for each mixture compare very favourably with corresponding third row entries in Table 5.7. Similar results were

obtained when Rayleigh scattering theory was considered.

Table 5.8 Diameter Averages of Mixtures of Latex Particles Calculated Using Mie Theory (Data Set 1)

Mixture	Variance $\sigma^2(ml^2)$	D_n	D_s	D_v	D_{ss}	D_w	D_t
	12.423	81.2	82.2	84.0	88.3	96.8	110.5
1	14.152	83.6	84.6	86.0	89.8	98.7	113.4
	13.288	82.2	83.2	85.0	89.3	97.7	111.8
	13.258	107.4	109.1	110.8	114.9	121.6	129.5
2	14.152	108.8	110.4	111.8	115.7	122.3	130.3
	13.705	107.9	109.6	111.1	115.2	121.9	130.0

Considering the inapplicability of either Rayleigh or Mie theory,* it is indeed surprising that the calculated diameter averages are in such good agreement with expected values. Eqn. (4.60) derived using Mie theory throws some light on this anomaly. Consider that $K^{-1}(y)$ in eqn.(4.50) is multiplied by δ where δ is a constant independent of y. In a very approximate sense, this describes the variation of measured extinction coefficient with y; its consequence is to introduce a constant multiplying factor δ in eqn. (4.60). The latter, however, has no effect on the evaluation of the diameter averages.

Data Treatment of Set 2

Fig. 5.21 shows the chromatograms for the 85, 109, 176 and 220 nm particles measured at a wavelength of 254 nm. The calibration data and measured variances are shown in Table 5.9.

---

* When absorption is neglected.

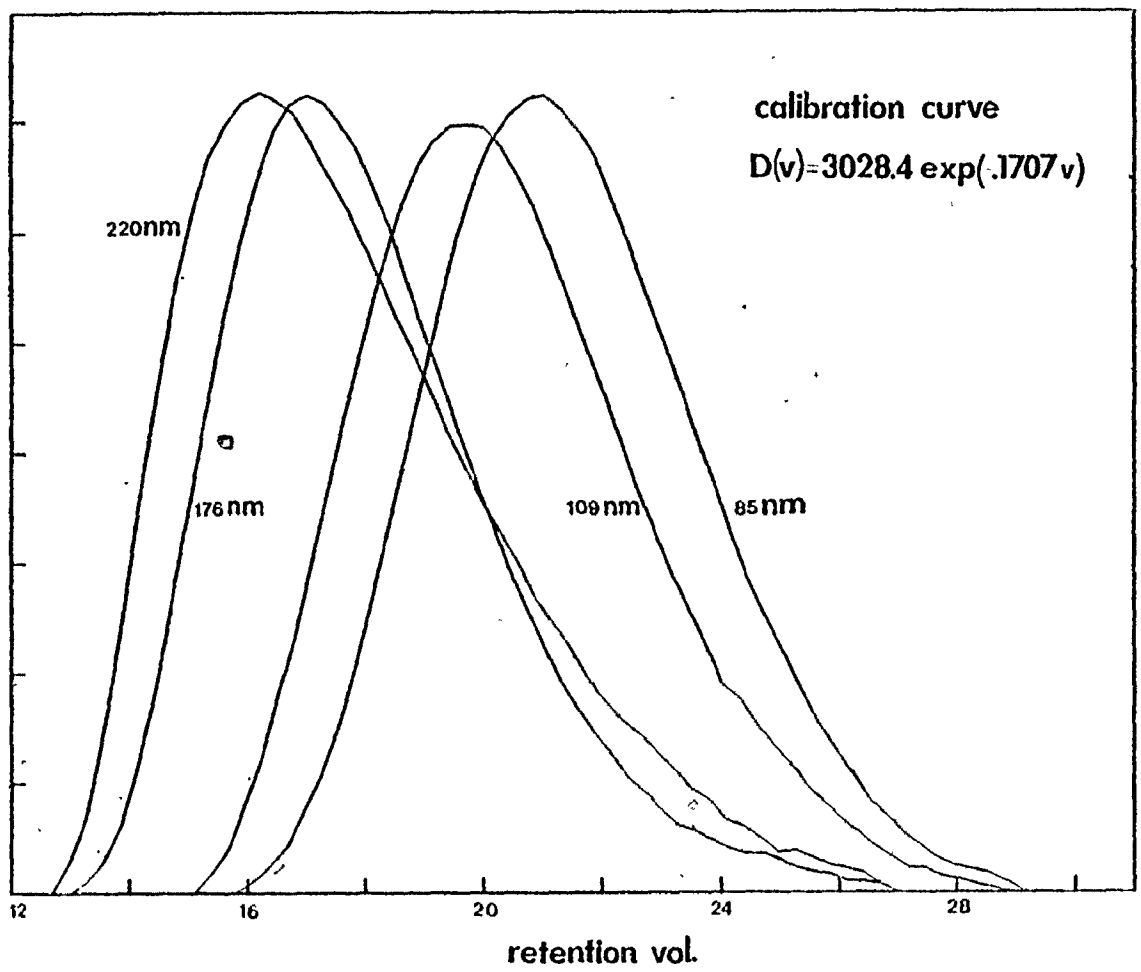

Fig. 5.21 Chromatograms of standard latices measured at 254 nm wavelength (Data set 2).

Table 5.9 Calibration Data and Measured Variances (Data Set 2)

Sample	85	109	176	220
Peak Retention Volume$_2$(mℓ)	21.02	19.70	17.00	15.35
Measured Variance (mℓ^2)	5.15	5.59	5.37	3.58

The uncorrected diameter averages are given in Table 5.10. For the smaller diameter latices, calculations based on Mie and Rayleigh theories, particularly for the lower diameter averages, do not differ considerably from each other. Observe that inspite of the lower values of the measured variance compared to Data Set 1, the axial dispersion correction would have to be significantly larger due to pronounced skewing. The correction equations are now applied.

Table 5.10. Uncorrected Diameter Averages Calculated Using Rayleigh and Mie Theories (Data Set 2)

Row 1 calculated from Rayleigh theory, Row 2 calculated from Mie theory

Sample	D_n	D_s	D_v	D_{ss}	D_w	D_t
85	33.2	35.1	37.5	42.8	50.6	60.1
	34.1	36.5	39.5	46.3	56.5	68.4
109	35.7	38.0	41.0	47.5	57.6	70.2
	37.3	40.3	44.3	53.6	67.8	83.8
176	46.4	49.8	54.5	65.2	83.0	104.0
	51.2	57.1	65.0	84.4	111.4	135.0
220	89.3	94.1	100.0	112.8	130.3	149.9
	104.9	113.1	122.3	143.2	166.3	186.3

A. Application of Rayleigh Correction Factors

The relationship between the corrected and the uncorrected moment is given by

$$M_k(c)/M_k(uc) = \exp[\sigma^2 k(6 - k/2)\, B'^2]\; Q_{0,0}/Q_{0,k} \qquad (4.102)$$

where,

$$Q_{0,k} = 1 + \sum_{n=3} (-1)^n (\alpha_k/\sigma)^n A_n/n! \qquad (4.97)$$

$$\alpha_k = (k-6)\, B'\, \sigma^2 \qquad (4.91 \text{ \& } 4.94)$$

Considering only the coefficients A_3 and A_4 and setting

$$\varepsilon_1 = (B'\sigma)^3 A_3/6 \qquad (5.7)$$

$$\varepsilon_2 = (B'\sigma)^4 A_4/24 \qquad (5.8)$$

the following relationships can be derived.

$$D_n(c) = D_n(uc) \exp(11\, \sigma^2 B'^2/2) \frac{(1+216\,\varepsilon_1 + 1296\,\varepsilon_2)}{(1+125\,\varepsilon_1 + 625\,\varepsilon_2)} \qquad (5.9)$$

$$\frac{[D_n(c)/D_n(uc)]^{10/11}}{D_s(c)/D_s(uc)} = \left(\frac{1+216\varepsilon_1+1296\varepsilon_2}{1+125\varepsilon_1+625\varepsilon_2}\right)^{10/11} \left(\frac{1+64\varepsilon_1+256\varepsilon_2}{1+216\varepsilon_1+1296\varepsilon_2}\right)^{1/2} \qquad (5.10)$$

$$\frac{[D_n(d)/D_n(uc)]^{9/11}}{D_v(c)/D_v(uc)} = \left(\frac{1+216\varepsilon_1+1296\varepsilon_2}{1+125\varepsilon_1+625\varepsilon_2}\right)^{9/11} \left(\frac{1+27\varepsilon_1+81\varepsilon_2}{1+216\varepsilon_1+1296\varepsilon_2}\right)^{1/3} \qquad (5.11)$$

If both A_3 and A_4 are nonzero, then eqns. (5.10) and (5.11) are solved

for ε_1 and ε_2 and σ^2 is estimated from eqn. (5.9). If A_4 is considered zero, then only eqns. (5.9) and (5.10) are solved. Calculation results are shown in Table 5.11. It is obvious from these results that the parameter A_3 and A_4 are significant; the significance of A_5 and A_6 could not be tested due to a difficulty in solving the additional equations. However, the calculated results with the two shape parameters are quite satisfactory. An alternate scheme to calculate σ^2 and A_n from the moment equations is developed later and does not have the present difficulty.

Table 5.11 Diameter Averages for Latex Particles Measured at 254nm (Data Set 2) - Application of Rayleigh Correction Factors

Sample	σ^2	A_3	A_4	D_n	D_s	D_v	D_{ss}	D_w	D_t
85	3.67	1.944	0.	85.2	84.7	83.9	82.3	79.1	77.1
	5.12	1.812	-2.134	85.2	86.4	87.1	88.5	86.7	82.2
109	4.51	1.919	0.	108.7	108.1	107.1	105.2	100.5	95.8
	5.90	1.896	-1.975	108.7	109.7	110.3	111.7	109.3	101.8
176	5.75	1.603	0.	175.6	173.8	172.6	170.3	164.4	152.9
	6.87	1.719	-1.467	175.6	175.2	175.9	177.2	175.5	160.6
220	3.13	3.629	0.	220.2	221.6	221.5	221.2	209.5	194.6
	4.15	3.277	-3.429	220.2	223.2	225.3	229.5	222.3	203.4

B. Application of Mie Correction Factors

The pertinent equation to be solved is

$$\frac{M(c)}{(k+g_k)} \Big/ M_{g_0}(c)\, M_k(\omega) = \exp(R_0 - R_k) \frac{\sum_{n=0}^{6} Q_{n,0}\, \overline{y_o^n}}{\sum_{n=0}^{6} Q_{n,k}\, \overline{y_k^n}} \qquad (4.117)$$

where the various terms are as defined in Section 4.4.3. Consider now, the solution of the above equation. Two cases were treated: In the first case, the parameters of the spreading function were obtained by the numerical recovery of G(v-y) as described in Section 4.3. In the second case, the parameters were considered variables and their values were obtained by solving eqn. (4.117).

The measured chromatograms and the corresponding spreading functions are shown in Figs. 5.22-5.24. For the 220 nm sample, the estimated spreading function did not differ markedly from the experimental chromatogram and hence this result is not graphed. The values of the parameters σ^2, A_3, A_4 and A_5 are given in Table 5.12. Fig. 5.25 illustrates the fit obtained for the 85 nm sample using the

Table 5.12 Parameters of the Statistical Shape Function (Data Set 2)

Sample	σ^2	A_3	A_4	A_5
85	5.13	0.396	-0.0992	-0.7733
109	5.62	0.509	-0.0137	-1.0376
176	5.34	0.737	0.4830	-0.6978
220	3.58	0.716	0.0930	-1.7240

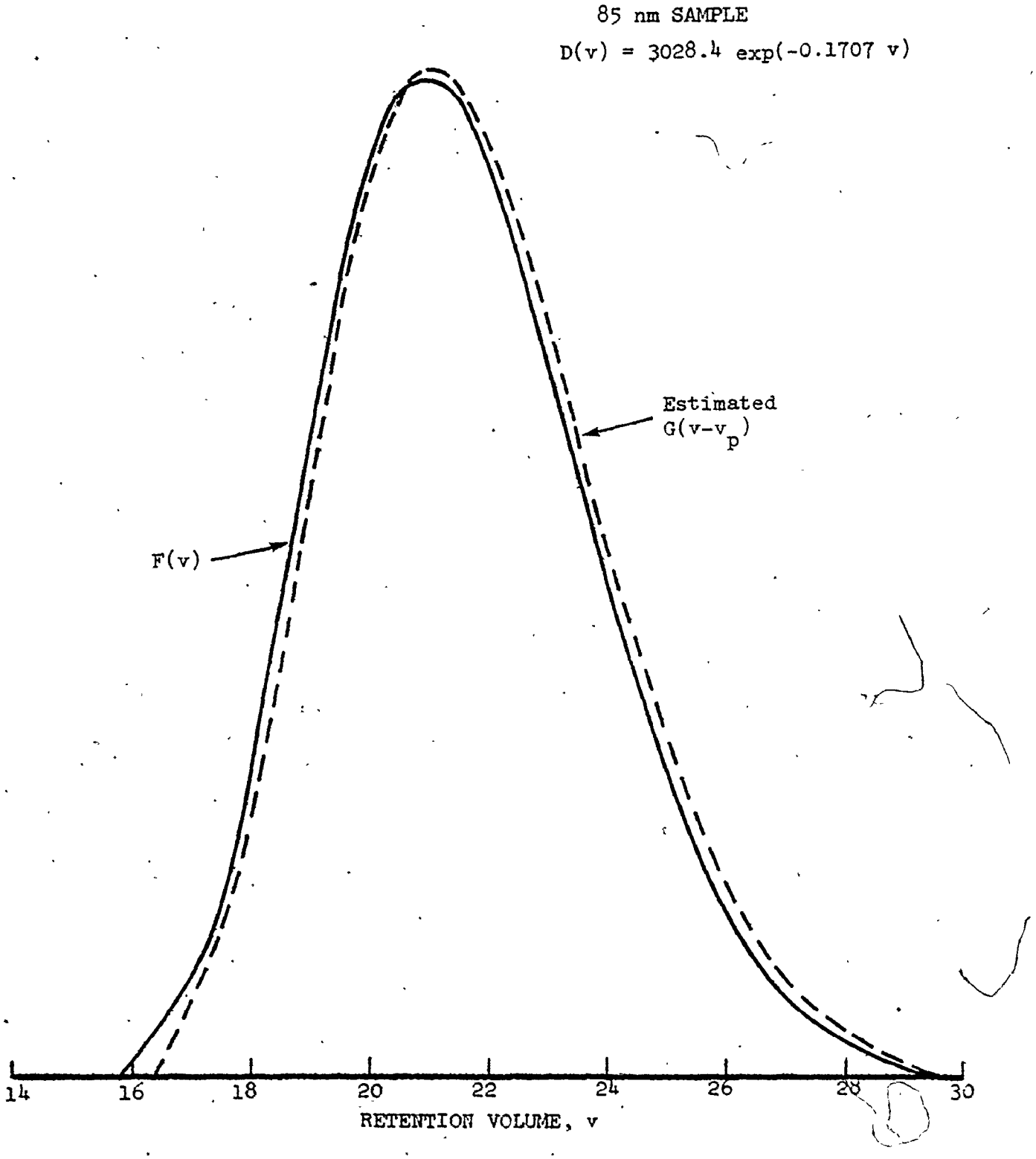

Fig. 5.22 Estimation of the spreading function from experimental chromatogram.

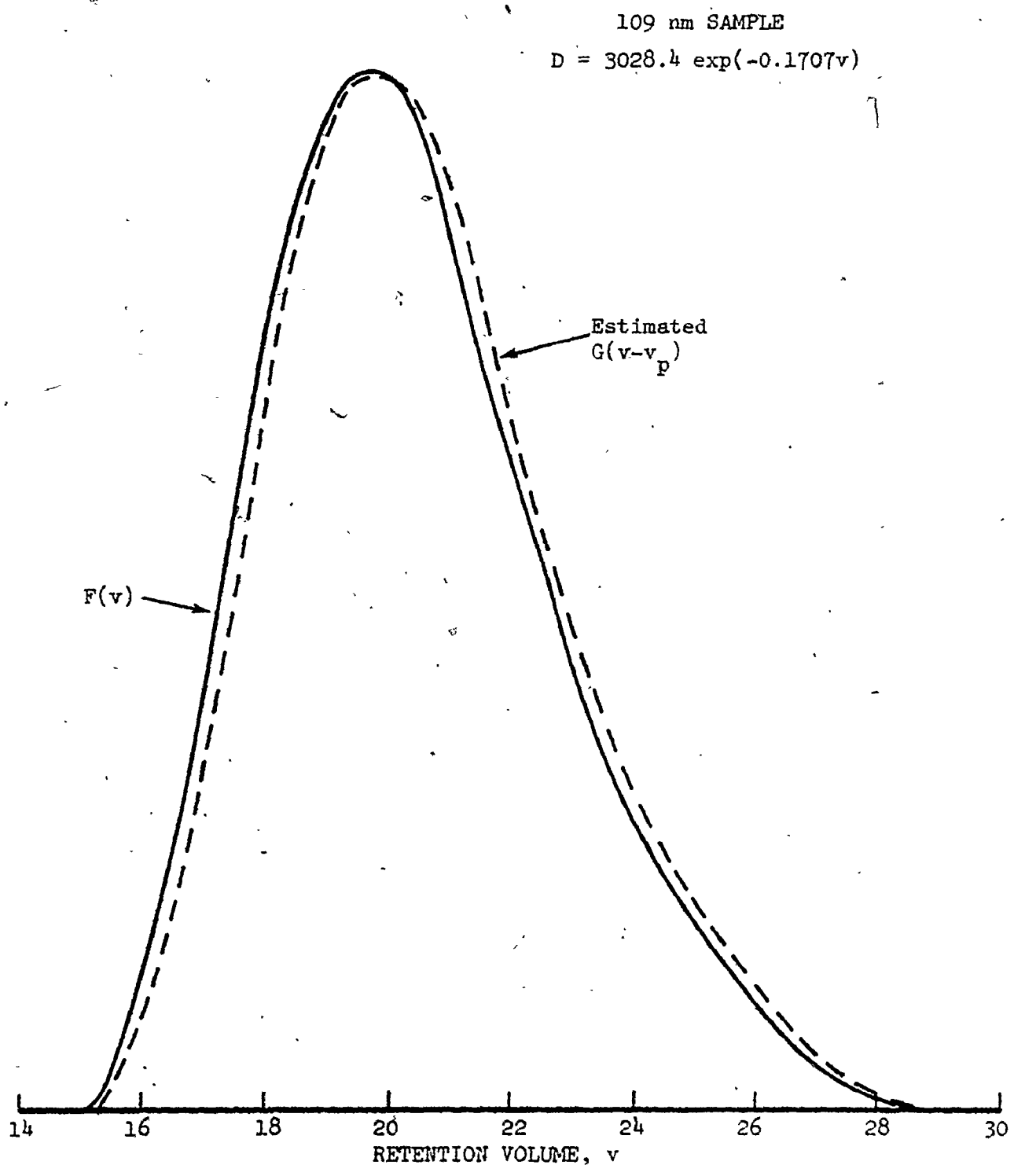

Fig. 5.23 Estimation of the spreading function from experimental chromatogram.

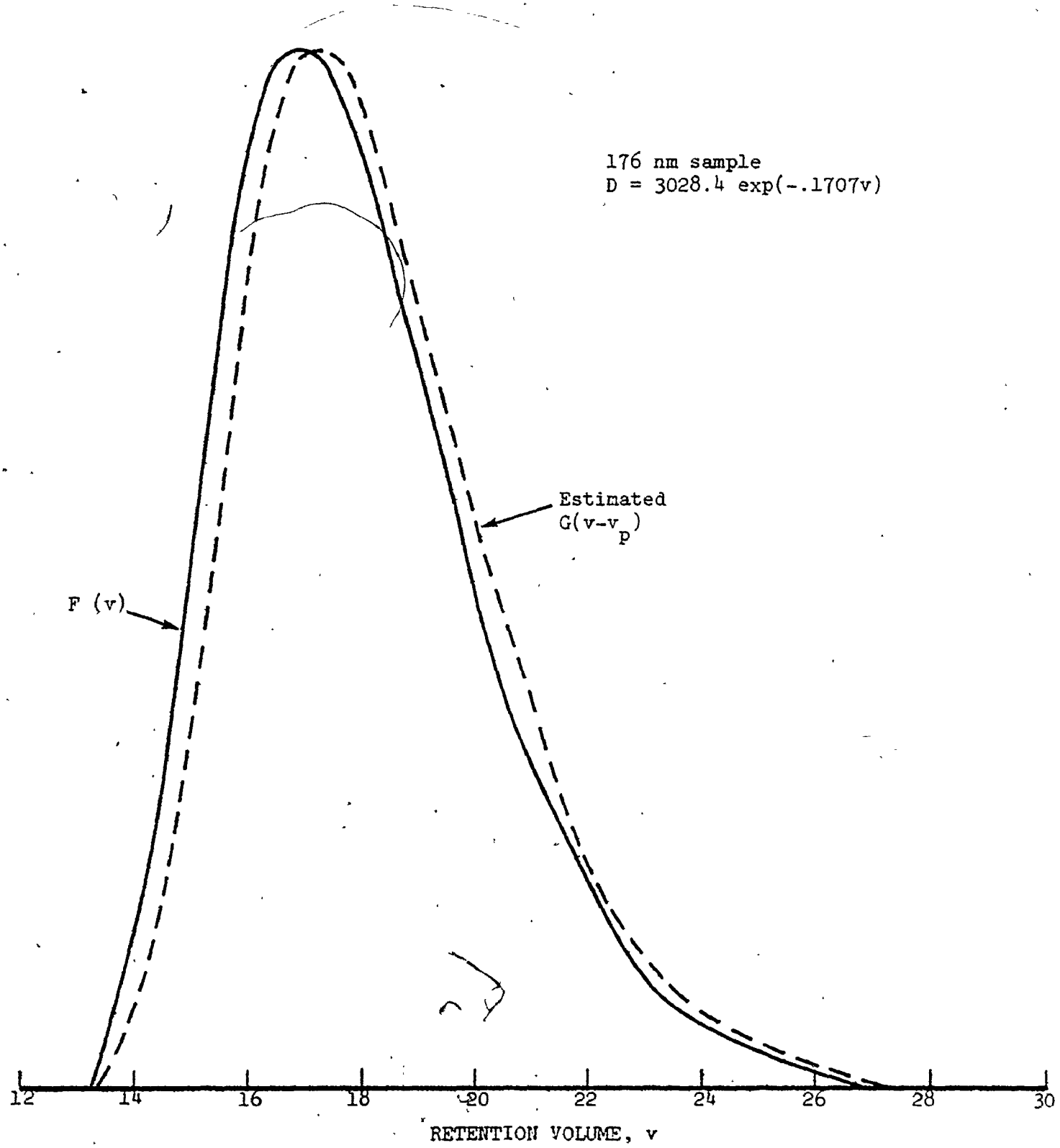

Fig. 5.24 Estimation of the spreading function from experimental chromatogram.

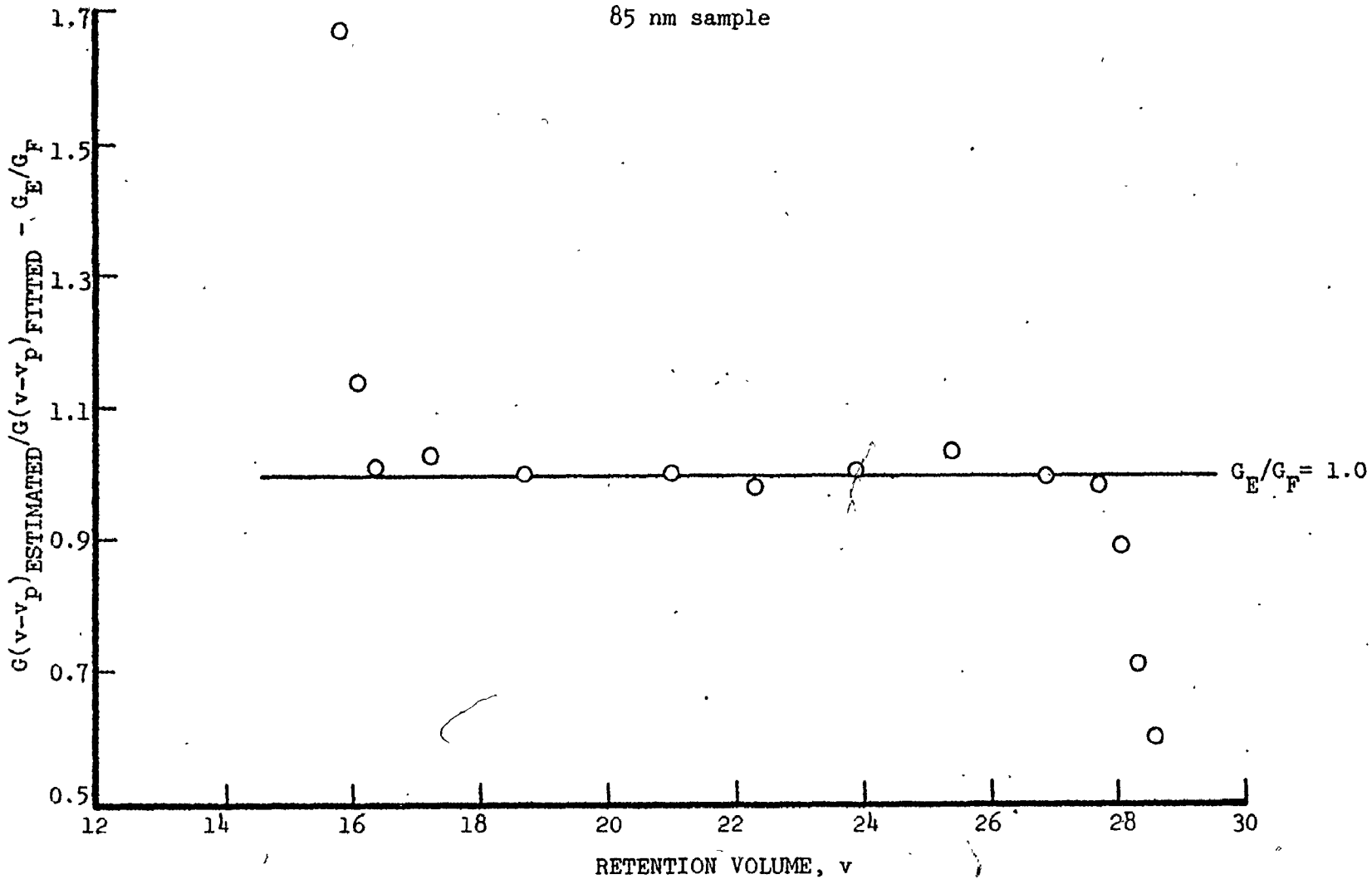

Fig. 5.25 Fit of the estimated instrumental spreading function to Provder and Rosen's shape function.

Edgeworth series. The central portion is adequately represented while the low and high retention volume ends are respectively, underestimated and overesti- mated. The fits for the 109, 176 and 220 nm samples were similar though, poorer. Table 5.13 summarises the results of the fitting.

Table 5.13 Fit of the Spreading Function Data by the Edgeworth Series (Data Set 2)

Sample	Span of the lower retention volume end where $G_E/G_F > 1.1$ (%)	Span of the central portion of the spreading function where $0.9 < G_E/G_F < 1.1$ (%)	Span of the higher retention volume end where $G_E/G_F < 0.9$ (%)
85	4.1	79.6	16.3
109	6.2	73.0	21.8
176	12.4	66.2	21.4
220	10.3	70.0	19.7

G_E/G_F denotes the ratio of the estimated G(v-y) to the fitted G(v-y)

It was mentioned in Chapter 4 that when W(y) is narrow, $\overline{y_k^n}$ may be approximated by v_p^n, where v_p is the peak elution volume. Table 5.14 compares $\overline{y_k^n}$, calculated rigorously according to eqn. (4.106) and its approximation. Excellent agreement is observed. Note that $\overline{y_k^n}$ is essentially independent of k.

As discussed in Chapter 4, the choice of ß must be made contingent on the value of the constant in

$$\int_{-\infty}^{\infty} W(y)\, \phi_k^{P_k}(y)\, dy = \text{constant}\, \bar{M}(c)^{(k+g_k)} \qquad (4.113)$$

being independent of k. Table 5.15 indicates that β values in the range 0.75-4.25 are adequate. The calculations were done using the electron microscopy frequency data in Appendix A.3.

Table 5.14 Estimation of $\overline{y_k^n}$ (the range corresponds to k=0 to 24)

	85 nm	109 nm	176 nm	220 nm
n=1				
Eqn.(4.106)	20.9-20.6	19.5-19.4	16.7-16.6	15.4-15.3
v_P^n	21.0	19.7	17.0	15.4
n=6				
Eqn.(4.106)	$8.52-7.66\times10^7$	$5.50-5.29\times10^7$	$2.16-2.13\times10^7$	$1.32-1.28\times10^7$
v_P^n	8.63×10^7	5.85×10^7	2.41×10^7	1.31×10^7

Table 5.15 Estimation of the Value of the Constant in Eqn. (4.113)(Range Corresponds to k=0 to 6)

	85 nm	109 nm	176 nm	220 nm
β=0.75	2.83- 2.80	2.89- 2.88	2.27- 2.27	1.61- 1.61
β=4.25	68.90-69.50	124.40-124.70	112.10-112.20	20.60- 20.60

The Edgeworth series as seen in Table 5.13 provides among the four samples, the best representation of the spreading function for the 85 and 109 nm samples. The results of applying eqn. (4.117) to these two samples are shown in Table 5.16. As expected, the calculations are insensitive to the value of β chosen. For β=2, the number average

diameter for both samples are remarkably on target; however, the higher diameter averages are slightly lower. Note that these calculations are based on parameters which have been estimated independently of the moment equations.

Table 5.16 Diameter Averages for Latex Particles Measured at 254 nm - Application of Mie Correction Factors

(Row 1, $\beta=2$; Row 2, $\beta=3$; Row 3, $\beta=4$)

Sample	D_n	D_s	D_v	D_{ss}	D_w	D_t
	86.2	83.7	81.9	78.4	77.2	77.0
85	85.0	82.7	81.1	78.0	77.0	76.9
	83.8	81.8	80.4	77.7	76.9	76.9
	108.6	104.2	101.1	95.2	93.1	92.6
109	106.2	102.3	99.6	94.5	92.9	92.5
	104.1	100.7	98.4	94.0	92.7	92.4

Two probable causes of error in the analysis are 1) the Edgeworth series does not adequately describe the tail ends of the spreading function. Consideration of additional coefficients A_n, $(n>6)$ when $kC\neq 0$ is impractical due to the complexity in deriving $Q_{n,k}$. 2) Error results from the use of $+\infty$ and $-\infty$ integration limits in the analysis, when in reality a species of mean retention volume y is dispersed between finite retention volume limits. The effect of this was investigated on the solution of

$$I_k(y) = \int_{-\infty}^{\infty} D(v)\, K^{k-2}(v)\, G(v-y)\, dv \qquad (4.85\&4.88)$$

$$\varepsilon = \int_{-\infty}^{\infty} D(v)\, K^{k-2}(v)\, G(v-y)\,dv \Big/ \int_{a}^{b} D(v)\, K^{k-2}(v) G(v-y)\,dv \qquad (5.12)$$

where a and b are the actual retention volume limits. The results are shown in Table 5.17. It is evident that significant error occurs for k=0 and 1 and that beyond k=6, the results become increasingly absurd.

Table 5.17 Estimation of ε [Eqn. (5.12)]

k	85 nm sample a=15.8 b=30.0 y=21.7	109 nm sample a=15.1 b=29.2 y=20.7	176 nm sample a=13.0 b=27.0 y=18.3	220 nm sample a=12.8 b=23.2 y=16.4
0	0.69	0.54	0.51	0.83
1	0.85	0.75	0.71	0.92
2	0.94	0.89	0.88	0.97
3	0.98	0.97	0.96	0.99
4	0.99	0.99	0.99	1.00
5	1.00	1.00	1.00	1.01
6	1.00	1.00	1.00	1.02
10	$0.45\ 10^{-4}$	$0.47\ 10^{-5}$	$0.06\ 10^{-5}$	$0.25\ 10^{-4}$
15	$4.7.10^{-4}$	$4.7.10^{-5}$	$1.5.10^{-5}$	$5.6.10^{-4}$

It is likely, that a good estimation of the lower diameter averages, results from the mutually compensating effects of errors 1 and 2. For the higher diameter averages, error 1 alone is the probable cause.

Consider now, the second case where the parameters of the spreading functions are calculated directly from the moment equations. The summation terms in eqn. (4.117) are linear in the coefficients, A_n.

If, therefore, a value of σ^2 is assumed, the term

$$\frac{M(c)_{(k+g_k)} \exp(R_k - R_0)}{M(c)_{g_0} \; M_k^{M}(uc)}$$

can be evaluated and hence, A_n obtained by solving a set of simultaneous linear equations. When the sum of squares of the deviations of the calculated diameter averages (from their known true values), attains a minimum, convergence occurs. When A_3 alone is considered, only one equation is solved using a value of k corresponding to $k+g_k = 0$. Thereafter, each additional parameter requires additional equations corresponding to $k+g_k = 1, 2 \ldots$etc. The calculation results are shown in Table 5.18 indicating excellent agreement with actual diameter averages of the samples. Note that the calculated parameter values differ significantly from the actual variance, skewness and kurtosis obtained by the numerical recovery of the spreading function.

5.3 CONCLUSIONS AND RECOMMENDATIONS FOR FURTHER STUDY

The experimental investigations discussed earlier, lead to the following conclusions.

1. It is advisable in choosing a train of columns, that each column be independently calibrated. The advantage of such a procedure is that it asseses each column independently, according to its resolution capability and the extent of sample loss that it will cause.

Table 5.18 Diameter Averages for Latex Particles Measured at 254 nm - Application of Mie Correction Factors (β=2)

Sample	σ^2	A_3	A_4	A_5	A_6	D_n	D_s	D_v	D_{ss}	D_w	D_t
85	3.2	4.72	0	0	0	86.4	87.1	86.9	86.3	82.5	83.4
	4.2	2.50	-2.15	0	0	85.2	85.2	84.6	83.6	81.1	82.0
	5.4	1.84	-3.51	2.12	0	85.2	85.4	85.2	84.9	83.0	83.9
	8.5	0.44	-2.53	4.16	-2.47	85.2	85.4	85.5	85.9	84.9	85.1
109	4.0	4.99	0	0	0	111.0	112.0	112.0	112.0	105.0	108.0
	5.0	2.61	-1.96	0	0	109.0	108.0	107.0	105.0	101.0	103.0
	6.7	1.76	-3.34	2.0	0	109.0	109.0	108.0	107.0	103.0	108.0
176	5.2	3.86	0	0	0	180.0	181.0	178.0	173.0	160.0	186.0
	6.0	2.53	-1.43	0	0	176.0	175.0	172.0	166.0	157.0	181.0
220	2.7	6.61	0	0	0	221.0	218.0	212.0	200.0	194.0	228.0
	5.1	1.70	-2.21	0	0	220.0	217.0	212.0	202.0	194.0	220.0

2. The response of the detector should be checked out to ensure linearity over the complete range of operation.
3. The available particle standards are not narrow enough, so that particle size analysis, using these as calibration standards, must take their size distribution into account.
4. Measured extinction coefficients for polystyrene latices deviate from theoretical calculations based on Mie theory for nonabsorbing spheres, due possibly to optical errors in the detector, polydispersity of latices, presence of styrene and oligomers within the particles and adsorbed emulsifier on the surface of the particle.
5. Particle recovery may easily be calculated as, the ratio of peak area measured during a normal chromatographic run to the peak area measured, when the packed columns are not included in the flow circuit. When very significant material loss occurs in a column, such a procedure may become invalid due to a time varying peak area.

In the particle size analysis presented earlier, extinction coefficients based either on Rayleigh or Mie theory were used in lieu of the actual coefficients. The discrepancy between the measured extinction coefficients and those based on theory will, therefore, be reflected in the values of the spreading function parameters. It might be tempting, therefore, to conclude that the simpler Rayleigh correction factors, be always used in preference to the more complex Mie correction factors. However, in a practical situation, the purpose of analysing

narrow distribution standards is to yield spreading function parameters, to be used as calibration constants for the analysis of unknown polydispersed samples. The success of size measurement of the latter will depend, in general, on whether or not the theoretical values of the extinction coefficients agree with the experimental values.

Table 3.1 indicates that when m ~ 1.26 (the value used at λ_o = 254 nm), Rayleigh theory underestimates the particle diameter by more than 10% for α ($=\pi D/\lambda$) equal to 1.2. This implies that for particles larger than 80 nm, error in excess of 10% could be expected for a turbidity measurement at 254 nm. However, comparison of the uncorrected diameter averages in Tables 5.4 and 5.10 indicate that, the upper diameter limit corresponding to a greater than 10% error may be much higher, depending upon the average diameter considered, the type of chromatogram and the calibration curve. In any given situation, it would be extremely useful to map out a region, well beyond the rigorous validity of Rayleigh theory, where errors resulting from its application are acceptable.

In general, latices are expected to be 'unclean' and also errors in turbidity measurement may exist. If a large number of narrow distribution standards are available, then their extinction coefficients may be measured to span the complete range of diameters. However, in a situation where the number of standards are limited, Mie theory may be applied to search for an imaginary part of the complex refractive index of the particle which best describes the measured data [Nagy (1979)]. This value is, then, used to calculate the extinction coefficients over the desired diameter range.

When peak broadening is not excessive and the spreading function is described by a single parameter σ^2, then the analytical Method 2 is the preferred method for analysis since, the variation of diameter averages across the chromatogram is also obtained. Otherwise Method 3 (Method 1 is a special case of Method 3) must be used. The parameters of the spreading function, in general, are retention volume dependent. When they are slowly varying functions, it may be permissible to use average parameter values in the analysis. An investigation of this effect is required.

When using packed columns, one will undoubtedly be confronted with the problem of material loss. Rather than be restricted to the range of particle sizes wherein recovery is total, it is conceivable that the chromatographic response of a broad polydispersed sample, containing colloids that would be significantly retained in the columns, can be suitably modified using a % recovery-particle size calibration curve, to yield a response that would be measured in the absence of particle loss.

Specific recommendations for future work with SEC are now made:

1. An extensive evaluation of various packing materials with differing pore geometry is required. This is necessary to minimize dispersion and particle loss in the columns. The optimum packing particle is probably one with a solid core and superficial surface pores.
2. Factors affecting particle loss such as a) ionic strength of eluant, b) use of ionic surfactant alone as opposed to a mixture

of surfactant and electrolyte,. c) effect of T_g (glass transition temperature) of particles, d) effect of packing type, e) effect of column temperature etc. need to be explored.

3. Colloid detection in the infra-red (IR) region was theoretically shown by Nagy (1979) to have some desirable features. An experimental evaluation of an IR detector is yet to be attempted.

4. The numerical treatment of chromatographic data hs been shown in this work to be rather inadequate. It is desirable to develop new improved methods for recovery of W(y).

5. It has been theoretically shown in this study, that, an absolute particle size detector based on turbidity spectra analysis has reasonable promise as an analytical tool for particle size measurement, requiring no prior calibration. An experimental evaluation of such a device could not be attempted due to unavailability of a detector capable of monitoring turbidity at several wavelengths simultaneously. It is hoped that in future this will become possible.

APPENDICES

A.1 DEFINITIONS OF IMPORTANT DIAMETER AVERAGES

The need for more than one definition for a diameter average arises from the fact that, different experimental techniques applied to polydispersed systems perceive the average properties of the population differently. The definition of some of the widely encountered averages are given below.

Number Average $$D_n = \int_0^\infty D\, f(D)dD \qquad (A.1)$$

Surface Average $$D_s = \{\int_0^\infty D^2\, f(D)\, dD\}^{1/2} \qquad (A.2)$$

Volume Average $$D_v = \{\int_0^\infty D^3\, f(D)\, dD\}^{1/3} \qquad (A.3)$$

Specific Surface Average $$D_{ss} = \int_0^\infty D^3\, f(D)dD / \int_0^\infty D^2 f(D)dD \qquad (A.4)$$

Weight Average $$D_w = \int_0^\infty D^4\, f(D)dD / \int_0^\infty D^3 f(D)dD \qquad (A.5)$$

Turbidity Average $$D_t = \{\int_0^\infty D^6\, f(D)dD / \int_0^\infty D^3 f(D)dD\}^{1/3} \qquad (A.6)$$

In terms of the chromatographic response, these definitions become

$$D_n(uc) = \int_0^\infty F(v)\, D^{-1}(v)\, K^{-1}(v)dv / \int_0^\infty F(v) D^{-2}(v)\, K^{-1}(v)dv \qquad (A.7)$$

$$D_s(uc) = \{\int_0^\infty F(v)\, K^{-1}(v)dv / \int_0^\infty F(v)\, D^{-2}(v)\, K^{-1}(v)dv\}^{1/2} \qquad (A.8)$$

$$D_v(uc) = \{\int_0^\infty F(v)\, D(v)\, K^{-1}(v)dv / \int_0^\infty F(v)\, D^{-2}(v)\, K^{-1}(v)dv\}^{1/3} \qquad (A.9)$$

$$D_{ss}(uc) = \int_0^\infty F(v)\, D(v)\, K^{-1}(v)dv / \int_0^\infty F(v)\, K^{-1}(v)dv \qquad (A.10)$$

$$D_w(uc) = \int_0^\infty F(v)\, D^2(v)\, K^{-1}(v)dv / \int_0^\infty F(v)\, D(v)\, K^{-1}(v)dv \qquad (A.11)$$

$$D_t(uc) = \{\int_0^\infty F(v)\, D^4(v)\, K^{-1}(v)dv / \int_0^\infty F(v)\, D(v)\, K^{-1}(v)dv\}^{1/3} \qquad (A.12)$$

(uc) denotes the uncorrected diameter averages. When Rayleigh theory is applicable, K(v) in the above equations is replaced by $D^4(v)$. The corrected diameter averages, denoted by the subscript (c), are obtained by replacing F(v) by the true chromatogram W(y) and the variable v by y.

A.2 CALCULATION OF SCATTERING COEFFICIENT FROM MIE THEORY

The scattering coefficient was calculated from Mie theory using a subroutine written by Dave (1968). The scattering coefficients for polystyrene spheres in aqueous media at three different wavelengths are

given in Table A.1. The refractive indices used in the computations are as follows:

Refractive index of polystyrene: 1.7246 (254), 1.6970 (280), 1.6506 (350)

Refractive index of water : 1.3712 (254), 1.3629 (280), 1.3489 (350)

The scattering coefficient for various values of the refractive index ratio, m, are given in Table A.2.

A.3 ELECTRON MICROSCOPY DATA OF DOW POLYSTYRENE LATICES

The electron microscopy data for Dow polystyrene latices are given in Table A.3. The samples 1 to 6 have designated sizes of 85, 109, 176, 220, 255 and 312 nm, respectively.

A.4 CHROMATOGRAPHIC DATA OF POLYSTYRENE LATICES

Two data sets were analysed. The second data set was supplied by Dr. T.H. MacRury (Union Carbide Corporation, South Charleston, W.Va)

Data Set 1

Calibration Curve	:	$D(v) = 2684 \exp(-0.05968v)$.
Samples 1, 2 and 3	:	85 nm Dow latex measured at 254, 280 and 350 nm, respectively.
Samples 4, 5 and 6	:	98 nm Polysciences latex measured at 254, 280 and 350 nm, respectively.
Samples 7, 8 and 9	:	109 nm Dow latex measured at 254, 280 and 350 nm, respectively.
Samples 10, 11 and 12	:	183 nm Polysciences latex measured at 254, 280 and 350 nm, respectively.

Table A.1 Scattering Coefficient of Polystyrene Spheres In Aqueous Media

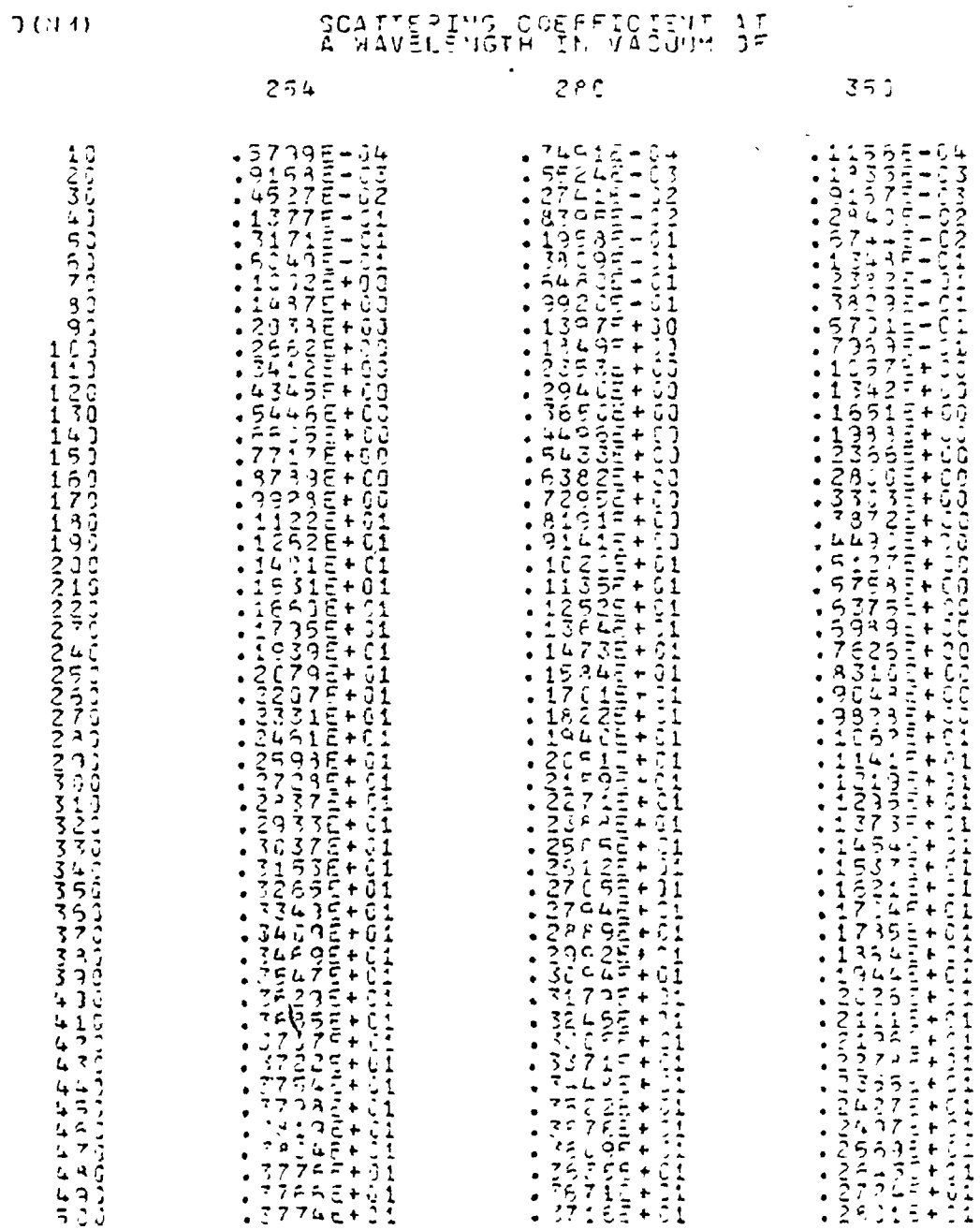

Table A.2 Scattering Coefficient of a Sphere Suspended in a Liquid Media

ALPHA	SCATTERING COEFFICIENT AT A REFRACTIVE INDEX RATIO OF						
	1.150	1.175	1.200	1.225	1.250	1.275	1.300
5.0	.1050E+01	.1397E+01	.1770E+01	.2157E+01	.2545E+01	.2918E+01	.3257E+01
5.1	.1099E+01	.1448E+01	.1832E+01	.2227E+01	.2619E+01	.2987E+01	.3311E+01
5.2	.1141E+01	.1500E+01	.1894E+01	.2295E+01	.2696E+01	.3046E+01	.3357E+01
5.3	.1173E+01	.1552E+01	.1954E+01	.2359E+01	.2743E+01	.3100E+01	.3402E+01
5.4	.1214E+01	.1604E+01	.2013E+01	.2420E+01	.2806E+01	.3154E+01	.3455E+01
5.5	.1256E+01	.1655E+01	.2069E+01	.2475E+01	.2864E+01	.3212E+01	.3519E+01
5.6	.1293E+01	.1704E+01	.2124E+01	.2536E+01	.2925E+01	.3277E+01	.3590E+01
5.7	.1339E+01	.1753E+01	.2179E+01	.2596E+01	.2991E+01	.3356E+01	.3658E+01
5.8	.1380E+01	.1803E+01	.2235E+01	.2666E+01	.3060E+01	.3413E+01	.3710E+01
5.9	.1421E+01	.1852E+01	.2293E+01	.2725E+01	.3128E+01	.3477E+01	.3741E+01
6.0	.1463E+01	.1903E+01	.2353E+01	.2790E+01	.3199E+01	.3552E+01	.3794E+01
6.1	.1505E+01	.1955E+01	.2413E+01	.2862E+01	.3241E+01	.3555E+01	.3798E+01
6.2	.1547E+01	.2008E+01	.2471E+01	.2908E+01	.3294E+01	.3574E+01	.3767E+01
6.3	.1591E+01	.2060E+01	.2527E+01	.2958E+01	.3322E+01	.3593E+01	.3796E+01
6.4	.1635E+01	.2112E+01	.2579E+01	.3004E+01	.3358E+01	.3632E+01	.3847E+01
6.5	.1679E+01	.2161E+01	.2629E+01	.3048E+01	.3399E+01	.3674E+01	.3871E+01
6.6	.1722E+01	.2209E+01	.2676E+01	.3095E+01	.3440E+01	.3722E+01	.3908E+01
6.7	.1765E+01	.2256E+01	.2725E+01	.3144E+01	.3487E+01	.3765E+01	.3922E+01
6.8	.1806E+01	.2303E+01	.2774E+01	.3190E+01	.3546E+01	.3797E+01	.3911E+01
6.9	.1844E+01	.2349E+01	.2825E+01	.3244E+01	.3558E+01	.3813E+01	.3982E+01
7.0	.1890E+01	.2397E+01	.2877E+01	.3295E+01	.3619E+01	.3869E+01	.3949E+01
7.1	.1932E+01	.2446E+01	.2927E+01	.3339E+01	.3645E+01	.3861E+01	.3925E+01
7.2	.1974E+01	.2494E+01	.2975E+01	.3375E+01	.3655E+01	.3797E+01	.3820E+01
7.3	.2017E+01	.2542E+01	.3020E+01	.3406E+01	.3666E+01	.3813E+01	.3852E+01
7.4	.2060E+01	.2588E+01	.3061E+01	.3435E+01	.3697E+01	.3826E+01	.3948E+01
7.5	.2102E+01	.2632E+01	.3093E+01	.3465E+01	.3711E+01	.3842E+01	.3944E+01
7.6	.2144E+01	.2675E+01	.3137E+01	.3497E+01	.3746E+01	.3867E+01	.3923E+01
7.7	.2186E+01	.2717E+01	.3170E+01	.3532E+01	.3760E+01	.3856E+01	.3771E+01
7.8	.2226E+01	.2756E+01	.3215E+01	.3565E+01	.3794E+01	.3835E+01	.3707E+01
7.9	.2266E+01	.2800E+01	.3255E+01	.3597E+01	.3796E+01	.3863E+01	.3847E+01
8.0	.2306E+01	.2842E+01	.3294E+01	.3622E+01	.3785E+01	.3788E+01	.3863E+01
8.1	.2346E+01	.2883E+01	.3330E+01	.3631E+01	.3770E+01	.3749E+01	.3883E+01
8.2	.2386E+01	.2924E+01	.3362E+01	.3651E+01	.3767E+01	.3725E+01	.3778E+01
8.3	.2426E+01	.2963E+01	.3390E+01	.3662E+01	.3765E+01	.3724E+01	.3776E+01
8.4	.2465E+01	.2998E+01	.3416E+01	.3674E+01	.3770E+01	.3723E+01	.3766E+01
8.5	.2534E+01	.3034E+01	.3441E+01	.3689E+01	.3778E+01	.3711E+01	.3673E+01
8.6	.2541E+01	.3069E+01	.3467E+01	.3708E+01	.3783E+01	.3741E+01	.3599E+01
8.7	.2578E+01	.3102E+01	.3494E+01	.3725E+01	.3776E+01	.3724E+01	.3700E+01
8.8	.2615E+01	.3137E+01	.3522E+01	.3734E+01	.3755E+01	.3664E+01	.3611E+01
8.9	.2651E+01	.3171E+01	.3548E+01	.3742E+01	.3735E+01	.3611E+01	.3604E+01
9.0	.2686E+01	.3205E+01	.3570E+01	.3739E+01	.3692E+01	.3469E+01	.3163E+01
9.1	.2724E+01	.3241E+01	.3587E+01	.3734E+01	.3663E+01	.3443E+01	.3154E+01
9.2	.2760E+01	.3267E+01	.3600E+01	.3721E+01	.3643E+01	.3431E+01	.3127E+01
9.3	.2795E+01	.3294E+01	.3611E+01	.3715E+01	.3615E+01	.3419E+01	.3067E+01
9.4	.2830E+01	.3320E+01	.3621E+01	.3714E+01	.3627E+01	.3382E+01	.3077E+01
9.5	.2862E+01	.3344E+01	.3632E+01	.3717E+01	.3614E+01	.3324E+01	.2977E+01
9.6	.2894E+01	.3367E+01	.3645E+01	.3719E+01	.3636E+01	.3295E+01	.2794E+01
9.7	.2925E+01	.3391E+01	.3660E+01	.3715E+01	.3594E+01	.3172E+01	.2711E+01
9.8	.2955E+01	.3415E+01	.3673E+01	.3702E+01	.3493E+01	.3104E+01	.2643E+01
9.9	.2986E+01	.3439E+01	.3682E+01	.3680E+01	.3440E+01	.3050E+01	.2577E+01
10.0	.3017E+01	.3462E+01	.3685E+01	.3653E+01	.3396E+01	.3035E+01	.2570E+01

Table A.2 (continued)

ALPHA	SCATTERING COEFFICIENT AT A REFRACTIVE INDEX RATIO OF						
	1.150	1.175	1.200	1.225	1.250	1.275	1.300
.1	.2506E-05	.3373E-05	.4354E-05	.5449E-05	.6638E-05	.7959E-05	.9515E-05
.2	.1981E-04	.5361E-04	.6926E-04	.8666E-04	.1057E-03	.1264E-03	.1486E-03
.3	.1996E-03	.2683E-03	.3471E-03	.4344E-03	.5311E-03	.6356E-03	.7480E-03
.4	.6179E-03	.8345E-03	.1081E-02	.1356E-02	.1659E-02	.1984E-02	.2334E-02
.5	.1474E-02	.1994E-02	.2598E-02	.3253E-02	.3988E-02	.4783E-02	.5654E-02
.6	.2967E-02	.4023E-02	.5233E-02	.6593E-02	.8098E-02	.9749E-02	.1155E-01
.7	.5302E-02	.7207E-02	.9336E-02	.1180E-01	.1461E-01	.1762E-01	.2089E-01
.8	.8855E-02	.1101E-01	.1543E-01	.1953E-01	.2409E-01	.2911E-01	.3461E-01
.9	.1320E-01	.1862E-01	.2360E-01	.2992E-01	.3699E-01	.4488E-01	.5354E-01
1.0	.1995E-01	.2596E-01	.3405E-01	.4326E-01	.5357E-01	.6499E-01	.7749E-01
1.1	.2902E-01	.3764E-01	.4808E-01	.5952E-01	.7378E-01	.8975E-01	.1069E+00
1.2	.3425E-01	.4693E-01	.6167E-01	.7848E-01	.9734E-01	.1182E+00	.1412E+00
1.3	.4552E-01	.5966E-01	.7846E-01	.9975E-01	.1237E+00	.1503E+00	.1794E+00
1.4	.5470E-01	.7358E-01	.9666E-01	.1229E+00	.1524E+00	.1854E+00	.2208E+00
1.5	.6461E-01	.8852E-01	.1162E+00	.1478E+00	.1831E+00	.2225E+00	.2652E+00
1.6	.7627E-01	.1044E+00	.1371E+00	.1742E+00	.2159E+00	.2622E+00	.3131E+00
1.7	.8865E-01	.1214E+00	.1594E+00	.2027E+00	.2511E+00	.3050E+00	.3642E+00
1.8	.1019E+00	.1397E+00	.1837E+00	.2341E+00	.2898E+00	.3519E+00	.4208E+00
1.9	.1164E+00	.1598E+00	.2107E+00	.2693E+00	.3331E+00	.4117E+00	.4927E+00
2.0	.1325E+00	.1822E+00	.2409E+00	.3091E+00	.3822E+00	.4761E+00	.5765E+00
2.1	.1500E+00	.2072E+00	.2748E+00	.3537E+00	.4445E+00	.5477E+00	.6644E+00
2.2	.1695E+00	.2348E+00	.3123E+00	.4027E+00	.5069E+00	.6246E+00	.7550E+00
2.3	.1908E+00	.2649E+00	.3526E+00	.4546E+00	.5716E+00	.7013E+00	.8446E+00
2.4	.2137E+00	.2966E+00	.3947E+00	.5078E+00	.6355E+00	.7760E+00	.9295E+00
2.5	.2377E+00	.3291E+00	.4374E+00	.5607E+00	.6983E+00	.8480E+00	.1009E+01
2.6	.2625E+00	.3630E+00	.4800E+00	.6126E+00	.7592E+00	.9182E+00	.1087E+01
2.7	.2875E+00	.3964E+00	.5222E+00	.6637E+00	.8194E+00	.9874E+00	.1168E+01
2.8	.3129E+00	.4298E+00	.5644E+00	.7152E+00	.8811E+00	.1061E+01	.1256E+01
2.9	.3382E+00	.4635E+00	.6073E+00	.7685E+00	.9465E+00	.1141E+01	.1352E+01
3.0	.3641E+00	.4981E+00	.6520E+00	.8253E+00	.1017E+01	.1228E+01	.1456E+01
3.1	.3909E+00	.5342E+00	.6992E+00	.8854E+00	.1092E+01	.1318E+01	.1564E+01
3.2	.4185E+00	.5722E+00	.7492E+00	.9491E+00	.1171E+01	.1414E+01	.1676E+01
3.3	.4475E+00	.6120E+00	.8016E+00	.1016E+01	.1256E+01	.1516E+01	.1794E+01
3.4	.4779E+00	.6536E+00	.8555E+00	.1086E+01	.1348E+01	.1628E+01	.1926E+01
3.5	.5095E+00	.6966E+00	.9107E+00	.1157E+01	.1440E+01	.1737E+01	.2054E+01
3.6	.5426E+00	.7398E+00	.9665E+00	.1232E+01	.1536E+01	.1851E+01	.2189E+01
3.7	.5751E+00	.7815E+00	.1018E+01	.1297E+01	.1619E+01	.1955E+01	.2312E+01
3.8	.6088E+00	.8274E+00	.1073E+01	.1364E+01	.1702E+01	.2053E+01	.2424E+01
3.9	.6427E+00	.8715E+00	.1127E+01	.1430E+01	.1781E+01	.2146E+01	.2528E+01
4.0	.6771E+00	.9163E+00	.1183E+01	.1497E+01	.1861E+01	.2240E+01	.2635E+01
4.1	.7125E+00	.9618E+00	.1240E+01	.1564E+01	.1942E+01	.2339E+01	.2750E+01
4.2	.7475E+00	.1008E+01	.1299E+01	.1636E+01	.2033E+01	.2449E+01	.2879E+01
4.3	.7837E+00	.1056E+01	.1358E+01	.1708E+01	.2120E+01	.2556E+01	.3004E+01
4.4	.8204E+00	.1104E+01	.1417E+01	.1780E+01	.2209E+01	.2663E+01	.3129E+01
4.5	.8578E+00	.1152E+01	.1475E+01	.1847E+01	.2296E+01	.2766E+01	.3249E+01
4.6	.8955E+00	.1200E+01	.1533E+01	.1882E+01	.2387E+01	.2878E+01	.3376E+01
4.7	.9335E+00	.1249E+01	.1591E+01	.1949E+01	.2511E+01	.2969E+01	.3496E+01
4.8	.9718E+00	.1297E+01	.1649E+01	.2016E+01	.2598E+01	.3095E+01	.3616E+01
4.9	.1011E+01	.1347E+01	.1709E+01	.2080E+01	.2687E+01	.3194E+01	.3748E+01

Table A.3 Electron Microscopy Data of Dow Polystyrene Latices.

SAMPLE NO. 1

D	75.2	78.2	81.3	[illegible]	87.3	90.3	93.3					
F(D)	13.0	6.0	18.0	8.0	16.0	39.0	2.0					

SAMPLE NO. 2

D	101.0	104.0	106.0	107.0	109.0	110.0	112.0	114.0	116.0	117.0	119.0	
F(D)	1.0	11.0	35.0	112.0	65.0	22.0	59.0	4.0	4.0	5.0	1.0	

SAMPLE NO. 3

D	169.0	171.0	172.0	174.0	175.0	176.0	177.0	178.0	179.0	180.0	182.0	
F(D)	1.0	7.0	15.0	82.0	72.0	16.0	15.0	35.0	3.0	25.0	1.0	

SAMPLE NO. 4

D	170.1	186.9	197.4	204.7	207.7	209.6	210.7	212.6	213.6	215.6	216.6	218.7
D	219.6	221.7	222.5	224.8	225.5	227.8	224.5					
F(D)	1.0	2.0	2.0	1.0	3.0	1.0	6.0	5.0	4.0	18.0	18.0	26.0
F(D)	30.0	27.0	54.0	33.0	4.0	26.0	2.0					

SAMPLE NO. 5

D	247.5	247.6	247.7	249.6	249.9	250.2	250.1	252.2	252.3	252.4	252.5	254.6
D	254.7	254.8	254.9	257.0	257.2	257.3	257.4	259.5	259.6	259.7	259.8	
F(D)	7.0	3.0	2.0	3.0	3.0	4.0	2.0	5.0	3.0	12.0	14.0	33.0
F(D)	18.0	82.0	79.0	13.0	20.0	24.0	11.0	1.0	2.0	3.0	1.0	

SAMPLE NO. 6

D	304.0	306.0	307.0	309.0	310.0	312.0	314.0	315.0	317.0
F(D)	1.0	2.0	4.0	30.0	7.0	112.0	12.0	7.0	10.0

Data Set 2

Calibration Curve : $D(v) = 3028.4 \exp(-0.1707v)$

Samples 1 to 8 are 85 nm Dow, 98 nm Polysciences, 109 nm Dow, 176 nm Dow, 209 nm Polysciences, 220 nm Dow, 255 nm Dow and 312 nm Dow latices, respectively. Samples 9 to 11 are mixtures of 109 and 312 nm latices in the weight ratio 3:1, 1:1 and 1:3, respectively.

These data were measured at 254 nm. They are given in Tables A.4 and A.5.

A.5 SOLUTION OF EQUATION (4.88)

Consider the solution of the integral

$$J_a = \int_{-\infty}^{\infty} \exp(-p\,x^2 + 2qx)\, x^a\, dx \qquad (A.13)$$

Let

$$x = \frac{q}{p} + \frac{y}{\sqrt{p}} \qquad (A.14)$$

Then

$$J_a = \frac{\exp(q^2/p)}{\sqrt{p}} \int_{-\infty}^{\infty} \exp(-y^2)\left(\frac{q}{p} + \frac{y}{\sqrt{p}}\right)^a dy$$

$$= \frac{\exp(q^2/p)}{\sqrt{p}} \int_{0}^{\infty} \exp(-y^2)\left(\frac{q}{p} + \frac{y}{\sqrt{p}}\right)^a dy +$$

$$\int_{0}^{\infty} \exp(-y^2)\left(\frac{q}{p} - \frac{y}{\sqrt{p}}\right)^a dy \qquad (A.15)$$

Table A.4 Chromatographic Data of Polystyrene Latices - Data Set #1

SAMPLE	1		2		3		4		5		6	
	V	F(V)	V	F(V)	V	F(V)	V	F(V)	V	F(V)	V	F(V)
	37.00	0	37.00	0	37.00	0	37.00	0	37.00	0	37.00	0
	38.00	0	38.00	0	38.00	0	38.00	0	38.00	0	38.00	0
	39.00	0	39.00	0	39.00	0	39.00	0	39.00	0	39.00	0
	40.00	0	40.00	0	40.00	0	40.00	0	40.00	0	40.00	0
	41.00	0	41.00	0	41.00	0	41.00	0	41.00	0	41.00	0
	42.00	0	42.00	0	42.00	0	42.00	0	42.00	0	42.00	0
	43.00	0	43.00	0	43.00	0	43.00	0	43.00	0	43.00	0
	44.00	0	44.00	0	44.00	0	44.00	0	44.00	0	44.00	0
	45.00	0	45.00	0	45.00	0	45.00	0	45.00	0	45.00	0
	46.00	0	46.00	0	46.00	0	46.00	10	46.00	5	46.00	5
	47.00	0	47.00	0	47.00	0	47.00	35	47.00	20	47.00	10
	48.00	5	48.00	0	48.00	0	48.00	85	48.00	70	48.00	25
	49.00	25	49.00	10	49.00	10	49.00	180	49.00	140	49.00	50
	50.00	60	50.00	40	50.00	20	50.00	325	50.00	270	50.00	95
	51.00	140	51.00	100	51.00	40	51.00	510	51.00	410	51.00	150
	52.00	280	52.00	210	52.00	70	52.00	710	52.00	575	52.00	210
	53.00	500	53.00	360	53.00	120	53.00	870	53.00	710	53.00	260
	54.00	770	54.00	560	54.00	190	54.00	980	54.00	900	54.00	235
	55.00	1040	55.00	730	55.00	260	55.00	1010	55.00	940	55.00	325
	56.00	1300	56.00	890	56.00	310	56.00	975	56.00	820	56.00	300
	57.00	1470	57.00	1000	57.00	350	57.00	875	57.00	735	57.00	270
	58.00	1520	58.00	1020	58.00	360	58.00	740	58.00	620	58.00	230
	59.00	1461	59.00	980	59.00	340	59.00	585	59.00	500	59.00	185
	60.00	1290	60.00	860	60.00	300	60.00	430	60.00	380	60.00	135
	61.00	1070	61.00	710	61.00	250	61.00	300	61.00	280	61.00	100
	62.00	840	62.00	560	62.00	200	62.00	200	62.00	190	62.00	70
	63.00	650	63.00	420	63.00	150	63.00	130	63.00	130	63.00	45
	64.00	430	64.00	300	64.00	100	64.00	90	64.00	85	64.00	30
	65.00	280	65.00	200	65.00	50	65.00	50	65.00	50	65.00	20
	66.00	170	66.00	130	66.00	40	66.00	25	66.00	40	66.00	10
	67.00	100	67.00	80	67.00	30	67.00	10	67.00	20	67.00	10
	68.00	60	68.00	50	68.00	20	68.00	0	68.00	10	68.00	5
	69.00	30	69.00	30	69.00	10	69.00	0	69.00	0	69.00	0
	70.00	15	70.00	20	70.00	0	70.00	0	70.00	0	70.00	0
	71.00	0	71.00	10	71.00	0	71.00	0	71.00	0	71.00	0

Table A.4 (continued)

SAMPLE	7		8		9		10		11		12	
	V	F(V)	V	F(V)	V	F(V)	V	F(V)	V	F(V)	V	F(V)
	37.00	0	37.00	0	37.00	0	37.00	0	37.00	0	37.00	0
	38.00	0	38.00	0	38.00	0	38.00	0	38.00	5	38.00	0
	39.00	0	39.00	0	39.00	0	39.00	15	39.00	20	39.00	10
	40.00	0	40.00	0	40.00	0	40.00	70	40.00	85	40.00	40
	41.00	0	41.00	0	41.00	0	41.00	190	41.00	210	41.00	105
	42.00	0	42.00	0	42.00	0	42.00	365	42.00	300	42.00	190
	43.00	5	43.00	5	43.00	0	43.00	540	43.00	550	43.00	270
	44.00	10	44.00	10	44.00	0	44.00	650	44.00	650	44.00	325
	45.00	25	45.00	20	45.00	10	45.00	680	45.00	680	45.00	340
	46.00	60	46.00	50	46.00	20	46.00	650	46.00	555	46.00	325
	47.00	140	47.00	120	47.00	45	47.00	565	47.00	575	47.00	285
	48.00	285	48.00	240	48.00	95	48.00	460	48.00	485	48.00	230
	49.00	520	49.00	420	49.00	170	49.00	350	49.00	330	49.00	180
	50.00	860	50.00	670	50.00	260	50.00	260	50.00	300	50.00	140
	51.00	1190	51.00	850	51.00	355	51.00	190	51.00	235	51.00	105
	52.00	1390	52.00	1050	52.00	435	52.00	140	52.00	180	52.00	80
	53.00	1505	53.00	1165	53.00	430	53.00	105	53.00	135	53.00	50
	54.00	1530	54.00	1190	54.00	500	54.00	80	54.00	105	54.00	45
	55.00	1455	55.00	1120	55.00	485	55.00	60	55.00	85	55.00	30
	56.00	1270	56.00	970	56.00	430	56.00	45	56.00	65	56.00	25
	57.00	1040	57.00	795	57.00	350	57.00	35	57.00	55	57.00	20
	58.00	820	58.00	630	58.00	280	58.00	30	58.00	45	58.00	15
	59.00	610	59.00	470	59.00	210	59.00	20	59.00	40	59.00	10
	60.00	435	60.00	335	60.00	150	60.00	15	60.00	40	60.00	5
	61.00	285	61.00	230	61.00	100	61.00	10	61.00	30	61.00	0
	62.00	185	62.00	150	62.00	70	62.00	5	62.00	30	62.00	0
	63.00	120	63.00	100	63.00	40	63.00	0	63.00	25	63.00	0
	64.00	75	64.00	60	64.00	25	64.00	0	64.00	20	64.00	0
	65.00	45	65.00	30	65.00	15	65.00	0	65.00	20	65.00	0
	66.00	30	66.00	20	66.00	10	66.00	0	66.00	15	66.00	0
	67.00	15	67.00	10	67.00	0	67.00	0	67.00	15	67.00	0
	68.00	10	68.00	5	68.00	0	68.00	0	68.00	15	68.00	0
	69.00	0	69.00	0	69.00	0	69.00	0	69.00	10	69.00	0
	70.00	0	70.00	0	70.00	0	70.00	0	70.00	10	70.00	0
	71.00	0	71.00	0	71.00	0	71.00	0	71.00	0	71.00	0

Table A.5 Chromatographic Data of Polystyrene Latices - Data Set #2

SAMPLE	1		2		3		4		5		6	
	V	F(V)	V	F(V)	V	F(V)	V	F(V)	V	F(V)	V	F(V)
	15.80	0	15.09	6	15.16	0	13.00	0	12.70	0	12.85	
	15.09	52	15.24	45	15.39	35	13.29	51	12.99	29	13.01	165
	15.39	124	15.56	79	15.68	210	13.57	145	13.24	317	13.22	337
	15.67	214	15.84	189	15.96	416	13.96	311	13.54	754	13.46	771
	15.96	340	16.13	359	16.25	627	14.14	534	13.87	1341	13.65	1226
	17.25	541	16.41	538	16.54	921	14.43	934	14.16	1956	13.96	1735
	17.54	747	16.66	757	16.83	1184	14.71	1352	14.45	2524	14.07	2273
	17.83	1036	16.97	1036	17.11	1542	15.00	1766	14.74	3070	14.29	2725
	18.12	1339	17.26	1373	17.43	1940	15.29	2138	15.03	3547	14.50	3048
	18.41	1682	17.53	1713	17.69	2327	15.57	2535	15.33	3816	14.71	3372
	18.70	2023	17.82	2056	17.98	2629	15.86	2946	15.62	3871	14.92	3492
	14.99	2349	18.11	2442	18.27	2933	16.14	3236	15.91	3968	15.13	3688
	13.28	2694	18.34	2745	18.55	3250	16.43	3453	16.26	3968	15.36	3932
	19.57	3062	18.66	3022	18.84	3371	16.71	3580	16.43	3795	15.56	3935
	19.86	3243	14.94	3254	19.13	3408	17.00	3615	16.73	3849	15.77	3932
	20.15	3423	19.22	3426	19.42	3486	17.29	3594	17.08	3970	15.98	3994
	20.44	3573	19.51	3515	19.70	3537	17.57	3445	17.37	3747	16.20	3958
	20.73	3630	19.79	3571	19.99	3479	17.86	3369	17.66	3443	16.41	3816
	21.02	3615	20.07	3524	20.23	3337	18.14	3196	17.95	3259	16.62	3[illegible]
	21.31	3550	20.36	3437	20.57	3258	18.43	3013	18.24	2850	16.83	3[illegible]
	21.60	3458	20.65	3305	20.86	3039	18.71	2774	18.54	2854	17.04	3[illegible]
	21.89	3336	20.91	3199	21.14	2802	19.00	2546	18.83	1620	17.26	3[illegible]
	22.18	3128	21.20	3027	21.43	2714	19.29	2315	19.12	1462	17.47	3[illegible]
	22.47	2931	21.49	2859	21.72	2634	19.57	2097	19.41	1269	17.68	3194
	22.76	2695	21.78	2622	22.01	2276	19.86	1873	19.70	1179	17.93	1[illegible]
	23.04	2493	22.04	2393	22.29	2156	20.14	1579	20.00	996	18.11	1771
	23.33	2264	22.32	2134	22.54	1837	20.43	1475	20.29	1[illegible]0	18.32	1[illegible]2
	23.62	2035	22.61	1909	22.87	1645	20.71	1203	20.59	7[illegible]1	18.53	1[illegible]6
	23.91	1825	22.19	1766	23.16	1449	21.00	1138	20.87	693	18.74	1441
	24.20	1602	27.17	1579	23.44	1235	21.23	972	21.16	550	18.96	1[illegible]4
	24.49	1391	23.46	1372	23.73	1129	21.57	946	21.46	4[illegible]	19.17	11[illegible]
	24.78	1224	23.73	1214	24.02	967	21.86	735	21.75	403	19.34	97[illegible]
	25.07	1079	24.01	1060	24.31	882	22.14	638	22.04	321	19.53	77[illegible]
	25.36	913	24.29	937	24.60	757	22.43	535	22.33	329	19.92	735
	25.65	788	24.58	864	24.89	671	22.71	459	22.62	264	20.32	733
	25.94	646	24.86	727	25.17	597	23.00	378	22.91	271	20.73	56[illegible]
	26.23	535	25.14	608	25.46	530	23.29	339	23.21	193	20.96	461
	26.52	421	25.42	561	25.75	468	23.57	244	23.50	195	21.65	472
	26.81	346	25.72	429	26.03	333	23.86	240	23.79	152	22.07	4[illegible]2
	27.10	271	25.98	366	26.32	272	24.14	205	24.08	130	22.[illegible]	3[illegible]5
	27.39	212	26.27	242	26.61	217	24.43	140	24.37	100	21.[illegible]	[illegible]
	27.68	157	26.56	197	26.90	153	24.71	131	24.67	121	21.55	[illegible]
	27.97	122	26.83	151	27.19	114	25.00	150	24.96	153	21.71	14[illegible]
	29.26	105	27.11	101	27.47	114	25.29	114	25.25	146	21.93	13[illegible]
	28.55	90	27.39	86	27.76	72	25.57	33	25.54	117	22.14	10[illegible]
	28.84	56	27.67	55	28.05	54	25.86	82	25.83	33	22.35	4[illegible]
	29.13	5	27.96	42	28.34	15	26.14	54	26.12	77	22.56	114
	29.42	0	28.24	43	28.62	22	26.43	51	26.42	29	22.79	93
	29.71	0	28.52	4	28.91	0	26.71	39	26.71	12	22.99	37
	30.00	0	28.80	0	29.20	0	27.00	0	27.00	0	23.20	0

Table A.5 (continued)

SAMPLE	7		8		9		10		11	
	V	F(V)	V	F(V)	V	F(V)	V	F(V)	V	F(V)
	12.40	0	11.90	0	12.60	0	12.00	0	12.40	0
	12.70	285	12.11	9	12.35	32	12.37	105	12.35	167
	13.00	907	12.23	46	12.74	759	12.73	947	12.60	992
	13.20	2014	12.35	231	13.11	1937	13.10	2457	13.00	2436
	13.50	2950	12.47	477	13.40	1942	13.47	3305	13.30	3567
	13.80	3766	12.59	916	13.86	1932	13.84	1178	13.70	2815
	14.10	3561	12.71	1605	14.23	489	14.20	913	14.00	1136
	14.40	3583	12.83	2197	14.60	293	14.57	511	14.35	511
	14.70	3484	12.95	2862	14.97	233	14.94	378	14.70	407
	15.00	3371	13.08	3423	15.34	174	15.31	314	15.10	329
	15.30	3183	13.20	3891	15.71	178	15.67	248	15.47	255
	15.64	3137	13.32	3536	16.09	142	16.04	243	15.82	206
	15.99	2436	13.44	3256	16.46	256	16.41	203	16.15	251
	16.27	2658	13.56	2758	16.83	336	16.79	332	16.51	145
	16.57	2458	13.68	2219	17.20	510	17.16	453	16.85	139
	16.87	2279	13.80	1749	17.57	458	17.51	746	17.20	293
	17.17	2193	13.92	1331	17.94	1237	17.89	1015	17.55	258
	17.47	1972	14.04	1033	18.31	1220	18.26	1372	17.90	512
	17.76	1822	14.16	851	18.68	2015	18.61	1715	18.24	859
	18.06	1674	14.28	652	19.06	2462	18.99	2035	18.61	695
	18.36	1552	14.40	529	19.43	2841	19.35	2404	18.96	539
	18.66	1411	14.52	401	19.80	3153	19.71	2704	19.28	484
	18.96	1257	14.64	326	20.17	3414	20.09	3033	19.59	555
	19.26	1164	14.76	350	20.54	3554	20.46	3172	19.89	719
	19.55	1111	14.88	319	20.91	3568	20.82	3241	20.33	756
	19.85	1049	15.01	274	21.29	3561	21.18	3221	20.57	773
	20.15	934	15.13	246	21.66	3409	21.55	3103	21.02	757
	20.46	886	15.25	235	22.03	3134	21.92	3017	21.37	650
	20.76	806	15.37	219	22.40	2752	22.28	2773	21.71	747
	21.04	733	15.49	194	22.77	2647	22.65	2510	22.05	615
	21.34	675	15.61	175	23.14	2413	23.02	2274	22.41	456
	21.64	617	15.73	151	23.51	2146	23.41	2025	22.75	387
	21.93	587	15.85	141	23.89	1842	23.76	1715	23.10	311
	22.23	506	15.97	143	24.26	1510	24.12	1438	23.46	256
	22.53	478	16.09	121	24.63	1421	24.49	1324	23.80	222
	22.83	415	16.21	109	25.00	1232	24.85	1133	24.14	195
	23.13	368	16.33	105	25.37	1051	25.22	993	24.44	215
	23.42	357	16.45	92	25.74	876	25.61	772	24.84	271
	23.72	317	16.57	79	26.11	708	25.98	627	25.19	222
	24.02	308	16.69	73	26.49	631	26.35	526	25.53	149
	24.32	286	16.81	61	26.86	543	26.69	351	25.83	122
	24.62	267	16.94	46	27.23	317	27.05	230	26.22	141
	24.91	249	17.06	44	27.60	230	27.43	202	26.57	121
	25.21	193	17.18	40	27.97	179	27.80	142	26.92	65
	25.51	164	17.30	40	28.34	143	28.16	95	27.27	48
	25.81	122	17.42	24	28.71	137	28.53	47	27.61	55
	26.11	112	17.54	26	29.09	71	28.90	54	27.96	20
	26.41	62	17.66	13	29.46	72	29.27	44	28.31	39
	26.71	24	17.78	11	29.83	36	29.64	41	28.65	21
	27.00	0	17.90	0	30.20	0	30.00	0	29.00	0

To solve eqn. (A.15), the following integral is required

$$I = \int_0^\infty x^m \exp(-b\, x^2)dx = \frac{\Gamma[(m+1)/2]}{2b^{(m+1)/2}} \tag{A.16}$$

where, the gamma function in the numerator is defined as

$$\Gamma(\tfrac{1}{2}) = \sqrt{\pi} \tag{A.17}$$

$$\Gamma(m+\tfrac{1}{2}) = \frac{1.3.5....(2m-1)}{2^m}\sqrt{\pi} \qquad m=1,2,3 \ldots \tag{A.18}$$

The solutions of equation (A.15) for a=1 ... 6 are given by

$$J_1 = \sqrt{(\frac{\pi}{p})}\, \exp(\frac{q}{p}^2)\, \frac{q}{p} \tag{A.19}$$

$$J_2 = \sqrt{(\frac{\pi}{p})}\, \exp(\frac{q}{p}^2)[(\frac{q}{p})^2 + \frac{1}{2p}] \tag{A.20}$$

$$J_3 = \sqrt{(\frac{\pi}{p})}\, \exp(\frac{q}{p}^2)[(\frac{q}{p})^3 + \frac{3}{2}\frac{q}{p^2}] \tag{A.21}$$

$$J_4 = \sqrt{(\frac{\pi}{p})}\, \exp(\frac{q}{p}^3)[(\frac{q}{p})^4 + 3\frac{q^2}{p^3} + \frac{3}{4}\frac{1}{p^2}] \tag{A.22}$$

$$J_5 = \sqrt{(\frac{\pi}{p})}\, \exp(\frac{q}{p}^2)[(\frac{q}{p})^5 + 5\frac{q^3}{p^4} + \frac{15}{4}\frac{q}{p^3}] \tag{A.23}$$

$$J_6 = \sqrt{(\frac{\pi}{p})}\, \exp(\frac{q}{p}^2)[(\frac{q}{p})^6 + \frac{15}{2}\frac{q^4}{p^5} + \frac{45}{4}\frac{q^2}{p^4} + \frac{15}{8}\frac{1}{p^3}] \tag{A.24}$$

REFERENCES

Allen, T., Particle Size Measurement, Chapman and Hall, London, 1975.

Berger, K.C., 'Gelchromatographische Refraktionierung, 1-Ein Verfahren zur Korrktur von Gelchromatogrammen', Makromol. Chem., 180, 1257, 1979.

Buffham, B.A., 'Model-Independent Aspects of Hydrodynamic Chromatography Theory', J. Coll. Int. Sci., 67, 1, 154, 1978.

Casassa, E.F., 'Theoretical Models for Peak Migration in Gel Permeation Chromatography', J. Phys. Chem., 75, 3929, 1972.

Coll, H., Fague, G.R. and Robillard, K.A., 'Exclusion Chromatography of Colloidal Dispersions', Unpublished Work, Eastman Kodak Co., Rochester, N.Y., 1975.

Dave, J.V., 'Subroutines for Computing the Parameters of the Electro-magnetic Radiation Scattered by a Sphere', IBM Report No. 320-3237, IBM Scientific Center, Palo Alto, Ca., 1968.

Figini, R.V. 'Relationship Between Apparent and True Molecular Weight in GPC 1. A New Analytical Solution of the Tung's Axial Spreading Integral', Poly. Bulletin, 1, 619, 1979.

Friis, N. and Hamielec, A.E. 'Gel Permeation Chromatography: A Review of Axial Dispersion Phenomena, Their Detection, and Correction', Adv. Chromat., 13, 41, 1975.

Gaylor, V.F. and James, H.L., Preprints, Pittsburgh Conference on Analytical Chemistry, Cleveland, March 1975.

Giddings, J.C. and Myers, M.N., 'Steric Field-Flow Fractionation: A New Method for Separating 1 to 100 nm Particles', Sep. Sci. Tech., 13, 8, 637, 1978.

Giddings, J.C., Myers, M.N. and Moellmer, J.F., 'Fine-Particle Separation and Characterization by Field-Flow Fractionation', J. Chrom., 149, 501, 1978.

Groves, M.J., 'Particle Size Analysis: Past, Present and Future', Analyst, 99, 959, 1974.

Groves, M.J., Particle Size Analysis, Heyden, London, 1978.

Groves, M.J. 'Particle Size Characterization in Dispersions', J. Dispersion Sci. Tech., 1(1), 97, 1980.

Groves, M.J. and Freshwater, D.C., J. Pharm. Sci., 57, 1273, 1968.

Groves, M.J. and Wyatt-Sargent, J.L., Particle Size Analysis, Soc. Analyt. Chem., London, 1972.

Grushka, E., Caldwell, K.D., Myers, M.N., and Giddings, J.C., 'Field Flow Fractionation', Sep. Purif. Methods, 2, 1, 127, 1973.

Hamielec, A.E., 'Chromatography of Suspensions: An Absolute Particle Size Detector Based on Turbidity Spectra Analysis', J. Liq. Chromat., 1, 555, 1978.

Hamielec, A.E. and Singh, S., 'Chromatography of Suspensions: An Experimental and Theoretical Investigation of Axial Dispersion Phenomena', J. Liq. Chromat., 1(2), 187, 1978.

Heller, W., 'Theoretical Investigations on the Light Scattering of Colloidal Spheres, III. Analytical Expressions for Turbidity Approximating the Performance of the Mie Equations Prior to the First Maximum', J. Chem. Phys., 26,5,1258, 1957.

Heller, W., 'Theoretical Investigations on the Light Scattering of Colloidal Spheres, XVI: Range of Practical Validity of the Rayleigh Theory', J. Chem. Phys., 42,5, 1609,1965.

Heller, W., 'Remarks on Refractive Index Mixture Rules', J. Phys. Chem., 69, 4, 1123, 1965.

Heller, W. and Pangonis, W.J., 'Theoretical Investigations on the Light Scattering of Colloidal Spheres, I: The Specific Turbidity', J. Chem. Phys., 26, 3, 498, 1957.

Heller, W. and Tabibian, R.M., 'Experimental Investigations on the Light Scattering of Colloidal Spheres II. Sources of Error in Turbidity Measurements', J. Coll. Sci., 12, 25, 1957.

Hiemenz, P.C., Principles of Colloid and Surface Chemistry, Marcel Dekker, Inc., 1977.

Ishige, T., Lee, S.I. and Hamielec, A.E., 'Solution of Tung's Axial Dispersion Equation by Numerical Techniques', J. Appl. Poly. Sci., 15, 1607, 1971.

Johnston, J.E., Cowherd, C.L. and MacRury, T.B., 'Size Exclusion Chromatography of Model Latices: A Feasibility Study', presented at ACS Meeting, Washington, 1979.

Kerker, M., The Scattering of Light and Other Electromagnetic Radiation, Academic Press, 1969.

Kirkland, J.J., 'High-Performance Size Exclusion Liquid Chromatography of Inorganic Colloids', J. Chromat., 185, 273, 1979.

Krebs, V.K.F. and Wunderlich, W., 'Die Ermittlung der TeilchengroBenverteilung von Polymer-Dispersionen durch Gelchromatographie', Die Ang. Makrom. Chem., 20(308), 203, 1971.

McHugh, A.J., Silebi, C., Poehlein, G.W. and Vanderhoff, J.W., 'Hydrodynamic Chromatography of Latex Particles', Coll Int. Sci., 4, 549, 1976.

Mie, G., Ann. Phys., 25, 377, 1908

Nagy, D.J., Column Chromatography of Polymer Latexes, Ph.D. Thesis, Lehigh U., 1979.

Nakagaki, M. and Heller, W., 'Effect of Light Scattering Upon the Refractive Index of Dispersed Colloidal Spheres', J. Appl. Phys., 27, 9, 1956.

Noel, R.J., Gooding, K.M., Regnier, F.E., Ball, D.M., Orr, C. and Mullins, M.E., 'Capillary Hydrodynamic Chromatography', J. Chromat., 166, 373, 1978.

Oliver, D.R., 'Influence of Particle Rotation on Radial Migration in the Poiseuille Flow of Suspensions', Nature, 194, 1269, 1962.

Prieve, D.C. and Hoysan, P.M., 'Role of Colloidal Forces in Hydrodynamic Chromatography', J. Coll. Int. Sci., 64, 201, 1978.

Provder, T. and Rosen, E.M., 'The Instrument Spreading Correction in GPC', Sep. Sci., 5(4), 437, 1970 ; 5(4), 485, 1970.

Rayleigh, L., Phil Mag., 12, 81, 1881.

Ruckenstein, E. and Prieve, D.C., 'Adsorption and Desorption of Particles and Their Chromatographic Separation', A.I.Ch.E. J., 22, 276, 1976.

Segre, G. and Silberberg, A., 'Behaviour of Macroscopic Rigid Spheres in Poiseuille Flow', J. Fluid Mech., 14, 136, 1962.

Shull, B., private communication, Dow Research Centre, Indianapolis, 1979.

Silebi, C.A. and McHugh, A.J., 'An Analysis of Flow Separation in Hydrodynamic Chromatography of Polymer Latexes', A.I.Ch.E. J., 24, 2, 204, 1978.

Silebi, C.A. and McHugh, A.J., 'The Determination of Particle Size Distributions by Hydrodynamic Chromatography. An Analysis of Dispersion and Methods for Improved Signal Resolution', J. Appl. Poly. Sci., 23, 1699, 1979.

Singh, S. and Hamielec, A.E., 'Liquid Exclusion Chromatography: A Technique for Monitoring the Growth of Polymer Particles in Emulsion Polymerization', J. Appl. Polym. Sci., 22, 577, 1978.

Small, H., 'Hydrodynamic Chromatograph: A Technique for Size Analysis of Colloidal Particles', J. Coll. Int. Sci., 48, 1, 147, 1974.

Small, H., 'Hydrodynamic Chromatography and Flow Induced Separations', Adv. Chromat., 15, 113, 1977.

Small, H., Saunders, F.L. and Solc, J., 'Hydrodynamic Chromatography: A New Approach to Particle Size Analysis', Adv. Coll. Int. Sci., 6, 237, 1976.

Stoisits, F.R., Poehlein, G.W. and Vanderhoff, J.W., 'Mathematical Modelling of Hydrodynamic Chromatography', J. Coll. Int. Sci., 57, 2, 1976.

Tung, L.H., 'Correction of Instrument Spreading in Gel Permeation Chromatography', J. Appl. Poly. Sci., 13, 775, 1969.

Tung, L.H., Moore, J.C. and Knight, G.W., 'Method of Calculating Molecular Weight Distribution Function from Gel Permeation Chromatograms. II. Evaluation of the Method by Experiments', J. Appl. Poly. Sci., 10, 1261, 1966.

Tung, L.H. and Runyon, J.R., 'Calibration of Instrumental Spreading for GPC', J. Appl. Polym. Sci., 13, 2397, 1969.

Walz, D. and Grun, F., 'The Radial Velocity of Spherical Particles in Tubular Pinch Effect Experiments', J. Coll. Sci., 45, 467, 1973.

Yau, W.W., Stoklosa, H.J. and Bly, D.D., 'Calibration and Molecular Weight Calculations in GPC Using a New Practical Method for Dispersion Correction: GPCV2', J. Appl. Poly. Sci., 21, 1911, 1977.

Zimm, H.B. and Dandliker, W.B., 'Theory of Light Scattering and Refractive Index of Solutions of Large Colloidal Particles', J. Phy. Chem., 58, 644, 1954.

Zollars, R.L., 'Turbidimetric Method for On-Line Determination of Latex Particle Number and Particle Size Distribution', J. Coll. Int. Sci., 74, 1, 163, 1980.